Analytical Approaches to Dynamic Issues Related to High-Speed Railway Bridge-Train Interaction System

何, 興文

(Degree)
博士（工学）

(Date of Degree)
2007-03-25

(Date of Publication)
2009-07-13

(Resource Type)
doctoral thesis

(Report Number)
甲3956

(URL)
https://hdl.handle.net/20.500.14094/D1003956

Doctoral Dissertation

Analytical Approaches to Dynamic Issues Related to High-Speed Railway Bridge-Train Interaction System

（高速鉄道高架橋－列車連成系の動的問題に関する解析的研究）

January 2007

Graduate School of Science and Technology
Kobe University, Japan

Xingwen HE

Summary

Japan's high-speed railway system, the Shinkansen, serves a vital role in the transportation network that connects its major cities. The high-speed railway's main lines usually pass directly over densely populated urban areas, where the railway structure mainly comprises elevated bridges. Considering the extremely high speed of the bullet train, the bridge vibration caused by running trains is concerned. The severe vibration over a long term may cause deterioration of the bridge structures, such as the cracking or exfoliation of concrete. On the other hand, the bridge vibration caused by running trains propagates to the ambient ground via footing and pile structures, thereby causing some environmental problems. Those vibrations can influence precision instruments in hospitals and laboratories or people who are studying or resting in schools, hospitals and residences, etc. Along with further urbanization and more rapid transport facilities, there is rising public concern about the environmental problems in modern Japan. Another dynamic issue related to the high-speed railway bridge-train interaction system is its earthquake-poof capacity. Japan is located in an earthquake-prone region. Therefore, the earthquake-proof capacity of the Shinkansen system is always a concern considering the extremely high-speed of the bullet train.

In this study, analytical approaches to simulate the dynamic issues related to high-speed railway bridge-train interaction system: the traffic-induced bridge vibration problem, the site vibration problem caused by bullet trains and the seismic performance of the bridge-train interaction system are established.

As the first objective, an analytical procedure to simulate the bridge-train coupled vibration problem considering their interaction as well as the effect of ground properties is established. Dynamic responses of the high-speed railway viaducts under moving bullet trains are analyzed in consideration of the wheel-track interaction including the rail surface roughness. The viaducts including the track structure are modeled as 3-D beam elements and simultaneous dynamic differential equations of the bridge are derived using modal analysis. The elastic effect of ground springs at the pier bottoms and the connection effect of the sleepers and ballast between the track and deck slab are modeled with double nodes connected by springs. A 3-D bullet train model as dynamic system that can appropriately express the lateral, vertical and rotational motions of the car body and bogies is developed for the analyses. Newmark's β direct numerical integration method is applied to solve the dynamic differential equations.

For the validation of the developed 3-D bullet train models, the dynamic response analysis of the bridge-train interaction system was carried out and the analytical results were compared with experimental ones. Based on the simulation of bridge-train interaction, the dynamic

characteristics of the viaducts including the fact where predominant vibration occurs are clarified. Then the countermeasures to allay the undesirable vibration are discussed. In this study, from the dynamic response analysis results, the fact that the excessive vibration occurs at the hanging parts of the viaducts, which is coincident with the experimental results, is confirmed. Consequently, countermeasures against the predominant vibration are proposed by reinforcing the hanging parts. The effect of the proposed countermeasures is demonstrated through both numerical analysis and actual construction case.

Based on the developed analytical procedure for bridge-train interaction system, an approach to simulate site vibration around the viaducts of the high-speed railway is established, in which the dynamic interactions between the train and track and between the foundation and ground are considered. The bridge-train interaction models established previously are conveniently used in this analysis. The entire train-bridge-ground interaction system is divided into two subsystems: train-bridge interaction and foundation-ground interaction. In the stage of the train-bridge interaction problem, the dynamic responses of viaducts are simulated to obtain the dynamic reaction forces at the pier bottoms. Then, applying those reaction forces as input excitation forces in the foundation-ground interaction problem, the site vibration around the viaducts is simulated and evaluated using a general-purpose program named SASSI2000. The effect of countermeasures against predominant bridge vibration on reduction of the environmental vibration is also confirmed.

For the seismic performance of the bridge-train interaction system in this study, as the first effort, assuming that the structures remain in elastic domain during a moderate earthquake, an analytical procedure to simulate the dynamic response of the high-speed railway bridge-train-earthquake interaction system is established. The bridge-train interaction models established previously are also conveniently used in this stage. The ground motions defined in seismic design codes and also actual measured ones downloaded from the Kyoshin Network (K-NET) of National Research Institute for Earth Science and Disaster Prevention in Japan (NIED) are adopted as the seismic load. Newmark's β method is also adopted here to solve the coupled differential equations of the bridge-train-earthquake interaction system. The accuracy of the seismic analysis algorithm is validated in comparison with a general program named MIDAS. The dynamic responses of the bridge and the train are then simulated and evaluated. The seismic performance of the bridge is investigated by examining the cross-sectional forces of the pier with respect to the strength limits. To examine the running safety of the bullet train, the derailment coefficient defined as the lateral wheel load to the vertical one is simulated and examined.

CONTENTS

Chapter 1

Introduction

1.1 Backgrounds

Japan's high-speed railway system, the Shinkansen, serves a vital role in the transportation network that connects its major cities. It has contributed importantly to the economic and social development of Japanese society since 1964. To this day, the transportation capacities of the high-speed railway system have been continually augmented through the use of new train models and improved equipment along with the increased number of trains. Especially in recent years, the speed-up process of bullet trains has been executed in JR companies and remarkable progress has been achieved. In October 2003, along with the inauguration of the new Shinagawa station, all Tokaido Shinkansen trains are upgraded into models with top speed of 270 km/h and efforts on further speed-up are in progress.

The high-speed railway's main lines usually pass directly over densely populated urban areas, where the railway structure mainly comprises elevated bridges. Such as in Tokaido Shinkansen, standard structure in urban area is mainly composed of viaducts of reinforced concrete in the form of a portal rigid frame. These viaducts are built with 24 m-length bridge blocks which are separated from each other and connected only by rail structure at adjacent ends. Each block consists of three 6 m-length center spans and two 3 m cantilever girders at each end. Regular inspections of the soundness and maintenance of the concrete structures are very important tasks. In 2001, a standard specification on maintenance of concrete structures [1] was drawn up by the Japan Society of Civil Engineers (JSCE), summarizing up-to-date concepts and technologies on prediction and diagnosis of deterioration as well as reinforcement of structures. Considering the extremely high speed of bullet trains, the bridge vibration caused by running trains is concerned. The severe vibration over a long term may cause deterioration of the bridge structures, such as the cracking or exfoliation of concrete.

An important feature of the railway bridges distinguished from the highway bridges is that the live load of train takes a high ratio in the design loads. Moreover, the displacement limit of railway structures regarding the runnabilities of the trains is far stricter than that in highway. In the new design standard for railway concrete structures [2] published in 2004, the concept of performance-based design is adopted. However, the live load of the train is merely treated as subordinate variable load (additional mass) to bridge structures but not dynamic system. This is partially due to the complexities of using bridge-train interaction analytical approach

for engineers in practical design, and also because such approach is still under research and not available to be handily used. It is obviously not completely reasonable to treat the train load as only additional mass because the train is a complicated vibrational system and its dynamic effect can not be simply presumed. If a handy approach to simulate the bridge-train interaction problem is available, it is possible to achieve more reliable and economical structures under the system of performance-based design. On the other hand, the runnability of the trains is another important issue of railway bridge design. In 2006, the Design Standard for Railway Structures regarding displacement limits [3] is published, in which the displacement limits of structures are designated to ensure the train's riding comfort in normal operation and running safety under earthquakes. To discuss such problem, it is necessary to clarify the bridge-train interaction. However, although the codes recommend the usage of dynamic analytical approach, it still could not definitely designate such an approach as the demanded method in design due to its complexities.

To perform effective prediction and diagnosis on the soundness of viaducts subjected to train-induced vibration, and also to examine the performance of the bridge under moving trains as well as the runnabilities of the trains, it is necessary to elucidate the phenomenon of bridge-train interaction. Not to mention it is important to investigate the vibration characteristics of the viaducts under moving trains by means of field tests. However, the phenomenon of running train-induced bridge vibration is so complicated, because it involves the dynamic train systems, the track, bridge and foundation structures, the ground conditions, and their dynamic interactions. In some cases, it is difficult to grasp the essential characteristics of the bridge vibration through only filed tests. Moreover, it needs enormous labors and costs and is impossible to carry out field tests on all viaducts. Therefore it will be desirable if there is a reliable and effective analytical approach to simulate the bridge vibration caused by running trains. Such approach can offer convenient predictions and diagnoses on the vibration of either existing bridges or those in the planning stage.

On the other hand, the bridge vibration caused by running trains propagates to the ambient ground via footing and pile structures, thereby causing some environmental problems. Those vibrations can influence precision instruments in hospitals and laboratories or people who are studying or resting in schools, hospitals and residences, etc. Along with further urbanization and more rapid transport facilities, there is rising public concern about the environmental problems in modern Japan [4]. Its vibration regulation law legislated in 1976 was the first one concerning the environmental vibration problems in the world. Almost concurrently, recommendations for countermeasures against vibration problems of the Shinkansen railway [5] were also proposed, in which a vibration acceleration level limit was specified to allay the environmental impacts of train-induced vibration on important facilities surrounding the main

lines.

The importance and urgency of environmental problems have already been recognized, and numerous efforts have been made to solve the problems. However, only a few solutions against the wayside vibration have been practically developed, such as to lighten the train's axial load and to soften the rail spring support like rubber-coated sleepers or ballast mats, etc. To find out more effective countermeasures against the traffic-induced environmental vibration problems, it is necessary to clarify the development and propagation mechanism of the site vibration caused particularly by running vehicles on viaducts. Nevertheless, such site vibration phenomenon remains unclear because of its complicated nature. Without a clear grasp of the site vibration mechanism through analytical studies, environmental vibration problems are traditionally evaluated and predicted based on field test data [6] [7]. The efficiency of such a process is limited to particular cases. For more general cases, essential information and reliable evaluation of site vibrations are necessary to perform accurate predictions and develop effective countermeasures. For that purpose, a corresponding analytical approach to simulate the environmental vibration problems is anticipated.

Another dynamic issue related to the high-speed railway bridge-train interaction system is its earthquake-poof capacity. Japan is located in an earthquake-prone region. Therefore, the earthquake-proof capacity of the Shinkansen system is always a concern considering the extremely high-speed of the bullet trains.

The Niigata earthquake, which occurred on Oct. 23, 2004 and was the strongest since the Kobe earthquake, brought severe damage in the Chuetsu region of Japan's Niigata Prefecture. In that earthquake disaster, the Shinkansen system was also damaged over a wide range and the first derailment accident of the bullet train occurred. Although fortunately no human lives were lost, the running safety of the bullet trains on bridges subjected to seismic load was recognized anew after this accident. After the Kobe earthquake and this Niigata earthquake, it came to be recognized that a high possibility exists to encounter an earthquake during rush hour. Therefore, it has become increasingly important to investigate and evaluate dynamic responses of bullet trains running on bridges under earthquake to ensure the train system's running safety. Nevertheless, discussion of the running safety of bullet trains on viaducts under Level-2 (L2) earthquake motion (earthquakes with low probability of occurrence during the service life of the structure, but which strike with high intensity) is not prescribed because of the complicated nature of its phenomenon, whereas that is designated for Level-1 (L1) earthquake motion (an earthquake of moderate intensity with recurrence probability of a few times during the service life of the structure) in the design standards for railway structures [3] [8]. Even without the danger of derailment, it is still necessary to evaluate the running characteristics and riding serviceability of the bullet train during an earthquake.

In both the Kobe earthquake and the Niigata earthquake, the bridge structures, especially the piers, were severely damaged over large distances. Although the live load of trains is considered in the Seismic Design Codes for Railway Structures [8] in Japan, the trains are merely attached as an additional mass to the bridge structure. Nevertheless, it is not rational to treat the train merely as an additional mass because the train is a complicated dynamic system. To satisfy both safety and economy demands in seismic design, the dynamic effect of trains on the bridge structures subjected to ground motion should be investigated further. Therefore, a reliable and effective analytical procedure to simulate the dynamic response of the high-speed railway bridge-train-earthquake interaction system is expected.

Cave-in of viaducts in Kobe earthquake

Derailment accident in Niigata earthquake

1.2 Objectives

The dynamic issues related to high-speed railway bridge-train interaction system: the traffic-induced bridge vibration problem, the environmental vibration problem caused by bullet trains and the seismic performance of the bridge-train interaction system, as described in previous Section 1.1, have been seriously concerned and need urgent resolution. Although efforts have been devoted by many researchers until today, it is still far from clarifying the phenomena by reason of the complicated nature of these problems. A common feature of these issues is that they all involves the train as dynamic system, the track, bridge and foundation structures, the ground conditions, and their dynamic interactions.

The dynamic interaction problems between the train, bridge as well as between the foundation and ground have been important topics in the filed of structural dynamics. Nevertheless, no research has been able to handle the problem by treating the train, bridge structure, foundation and ambient soil as an integrated system considering their exact dynamic interaction. This is because of not only the complexities of the whole interaction system but also the enormous computational capacities it requires of the computer. Therefore in this study, to simulate the bullet train-induced vibration problem, related environmental vibration problem and the seismic performance of the bridge-train interaction system, endeavors are devoted to solve the problems by dividing the whole interaction system into two subsystems: the bridge-train interaction and the foundation-ground interaction; and the two subsystems are connected with idealized ground springs. Thus the effect of ground properties on bridge-train interaction subsystem can be approximately expressed by ground springs, and correspondingly the dynamic response output form the bridge-train interaction analysis can be employed as input excitations in the foundation-ground interaction subsystem. The methodology adopted here can set a foundation for further research of this topic. It is possible to integrate the two subsystems into one complete interaction system including the train, structure, foundation and the ground with the further advancement of the theoretical research as well as the improvement of the computational capacities and methods.

To perform effective prediction and diagnosis on the soundness of bridge structures, and also to examine the performance of the bridge under moving trains as well as the runnabilities of the trains, it is necessary to establish a reliable approach to simulated the bridge-train interaction numerically. In this study, as the first objective, an analytical procedure to simulate the bridge-train coupled vibration problem considering their interaction as well as the effect of ground properties is established. Dynamic responses of the high-speed railway viaducts under moving bullet trains are analyzed in consideration of the wheel-track interaction including the rail surface roughness. The viaducts including the track structure are modeled as 3-D beam

elements and simultaneous dynamic differential equations of the bridge are derived using modal analysis. The elastic effect of ground springs at the pier bottoms and the connection effect of the sleepers and ballast between the track and the deck slab are modeled with double nodes connected by springs. A 3-D bullet train model as dynamic system that can appropriately express the lateral, vertical and rotational motions of the car body and bogies is developed for the analyses. Newmark's β-method for direct numerical integration is applied to solve the dynamic differential equations.

Confirming the reliability of the developed analytical approach is another important objective in this study. The analytical procedure is a numerical simulation of the practical engineering problem and must produce proper accuracy to reveal the essential characteristics of the problem. To demonstrate the validity of the finite element bridge model, eigenvalue analysis is carried out and the basic natural frequency is compared with experimental value. For the validation of the developed 3-D bullet train models, the dynamic response analysis of the bridge-train interaction system was carried out and the analytical results were compared with experimental ones.

Based on the simulation of bridge-train interaction, the dynamic characteristics of the viaducts including the fact where predominant vibration occurs are clarified. Then the countermeasures to allay the undesirable vibration of the bridge are discussed. In this study, from the analytical dynamic responses, the fact that the excessive vibration occurs at the hanging parts of the elevated bridge, which is coincident with the experimental results, is confirmed. Consequently, countermeasures against the predominant vibration are proposed by reinforcing the hanging parts. The effect of the proposed countermeasures is demonstrated through both numerical analysis and actual construction case.

As described previously, the environmental problems caused by traffic-induced bridge vibration have been increasingly concerned and need proper solution. In addition to empirical knowledge based on field test data, a corresponding analytical approach to simulate the environmental vibration problems is anticipated. Though some efforts were paid to simulate the site vibration, few can appropriately handle the dynamic excitation on the foundation because the input motion is resulted from the running vehicles on bridge structures. In this study, an approach to simulate site vibration around the viaducts of the high-speed railway is established, in which the dynamic interactions between the train and track and between the foundation and ground are considered. The bridge-train interaction models established previously are conveniently used in this analysis. The entire train-bridge-ground interaction system is divided into two subsystems: train-bridge interaction and foundation-ground interaction. In the stage of the train-bridge interaction problem, the dynamic responses of viaducts are simulated to obtain the dynamic reaction forces at the pier bottoms. Then,

applying those reaction forces as input excitation forces in the foundation-ground interaction problem, the site vibration around the viaducts is simulated and evaluated using a general-purpose program named SASSI2000. The effect of countermeasures against predominant bridge vibration on reduction of the environmental vibration is also confirmed.

The seismic analysis of bridge-train interaction is an important and difficult topic in bridge engineering. Especially for the seismic performance of the bridge-train interaction system under violent earthquakes, analytical researches are still in its early stage. In this study, as the first effort, assuming that the structures remain in elastic domain during a moderate earthquake, an analytical procedure to simulate the dynamic response of the high-speed railway bridge-train-earthquake interaction system is established. In this state of the analytical approach, considering the intensity of the ground motion and its complexity, the relative motion between the wheels and the track structure is neglected and the movement of the wheels is presumed dependent on the displacement of tracks.

The bridge-train interaction models established previously are also conveniently used in this stage. The ground motions defined in seismic design codes and also actual measured ones downloaded from the Kyoshin Network (K-NET) of National Research Institute for Earth Science and Disaster Prevention in Japan (NIED) are adopted as the seismic load. Newmark's β-method is also adopted here to solve the coupled differential equations of the bridge-train-earthquake interaction system. The accuracy of the seismic analysis algorithm is validated in comparison with a general program named MIDAS. The dynamic responses of the bridge and the train are then simulated and evaluated. The seismic performance of the bridge is investigated by examining the cross-sectional forces of the pier with respect to the strength limits. To examine the running safety of the bullet train, the derailment coefficient defined as the lateral wheel load to the vertical one is simulated and examined.

To simulate the seismic performance of the bridge-train system subjected to violent earthquakes, it is necessary to establish the non-linear models of the bridge as well as the train, and the interaction between the bridge and train become extremely complicated. Some efforts are devoted to such simulations by RTRI [9], in which the structures are only treated as very simple non-linear systems. In this study, based on the results in the development of the linear bridge-train-earthquake interaction analysis, preparations to simulate the seismic performance of bridge-train system subjected to strong ground motion are also undertaken. The progress of the development is also included in this thesis.

1.3 State of the art

1.3.1 Traffic-induced vibration problem of bridges

The earliest awareness of bridge-vehicle interaction phenomena can date back to early 19th century after the advent of railway system. The first milestone was the accident at the Dee railway bridge in Chester, England on May 24th, 1847. One of the girders was broken as the train passed over; four people were killed on the spot and several others were seriously injured. Every catastrophic accident brought people lessons to advance in the struggle against nature. The importance of research on bridge-train interaction is fully recognized through this accident. The earliest landmark efforts were devoted by Willis [10] [11], who carried out an entire series of laboratory experiments and also some field tests on bridge-vehicle interaction within the framework of a commission investigated by the English queen. Based on the results of these tests, Willis formulated the differential equation for the trajectory of a mass of constant magnitude traversing a massless beam as a function of the speed of the mass. As Willis only gave an approximate solution of this problem, Stokes [12] who worked with Willis at Cambridge found the exact numerical solution by series method and discussed the reason for the collapse of the Dee railway bridge. Waddell [13] [14] also achieved remarkable results in the research of bridge-vehicle interaction and its application in bridge design.

Over the next decades, research on bridge dynamics were mainly focused on developing analytical solutions for simple cases of moving forces or moving masses on bridges. In 1934, based on numerous field test results, Inglis [15] formulated the bridge-vehicle interaction problem considering the mass of both the bridge and the vehicle, in which the vehicle is simplified as moving periodic force or inertia. In 1953, Former Soviet researcher Muchnikov [16] performed more strict analyses on such problem employing integral equation method. In these researches, the moving force model, in which a vehicle is modeled as a force, is the simplest model whereby researchers can capture the basic dynamic characteristics of a bridge under moving load, but the interaction between the vehicle and bridge is ignored. In the case that inertia of the vehicle cannot be neglected, a moving mass model, in which a vehicle is modeled as a mass with inertia, is often adopted instead. However, the moving mass model suffers from its inability to consider the bouncing effect of the mass, which is significant in the presence of rail/road surface irregularities or for vehicles running with high speed.

From the 1950s, with the spread of application of the electronic computer, the theoretical research based on numerical computation had significantly progressed. Digital computers introduced a new level of detail in bridge dynamics research because the complexities of the bridge and vehicle system could be modeled. Notable numerical simulation researches

together with field tests were carried out by Biggs et al [17], Wen et al [18] [19] and Veletsos et al [20] in MIT, in which the vehicles were modeled as two-axle sprung mass system. The two-axle model can express the bouncing and pitching movements of the vehicle body, which is considered more realistic and can reveal more essential characteristics of the bridge-vehicle interaction system. However, compared with the more complicated dynamic mechanism of vehicles, such model is still too simple and can not express more accurate motions of the vehicle including the motions of the bogies/axles and wheels.

With the significant progress of the computational techniques as well as the hardware capacities of computers from the late 1960s up to today, the bridge-vehicle interaction problems have been prosperously researched by many researchers and remarkable progress in modeling the dynamic vehicle systems and the bridge structures as well as their interaction has been achieved. A series of renowned researches on bridge-vehicle interaction problem are accomplished by Prof. Frýba [21~25], and were applied to many actual engineering problems. Notable studies are also carried out by Diana et al [26~28], Xia et al [29~32] and Yang et al [33~35]. These researches had begun to treat the vehicles as well as the structures as three-dimensional (3-D) models and their interaction was relatively accurately considered.

In Japan, the earliest researches on bridge-train interaction problem were initiated from the late 1960s and were systematically integrated by Matsuura [36] [37], in which the car and bridge are idealized as relatively simple models of two dimensions. Subsequently based on the researches initiated by Matsuura, Wakui and Matsuura et al [38~41] developed the analytical approach for bridge-train interaction problem and elaborated more detailed analytical models, in which the trains and structures were treated as 3-D models and their interaction was relatively appropriately simulated though simplified presumptions were still made in modeling the contacting problem between the wheels and rail treads. The results of these studies are mainly applied in design work or practical cases conducted by Railway Technical Research Institute (RTRI). At the same time, efforts to clarify the bridge-train interaction problems are also devoted by many other researchers. Yasoshima et al [42] developed a dynamic response analysis of a suspension bridge under freight cars. In order to investigate the running stability of the train, the freight car is modeled as a two-axle model. Modal analysis is applied to the dynamic analysis of the specific two-hinged suspension bridges. Tanabe et al [43] carried out an analysis employing 3-D finite element method to simulate the interaction of track structures and trains.

Almost concurrently, the researches on dynamic characteristics of highway bridges due to traveling vehicles were also prosperously carried out in Japan. Investigations of the impact effect of moving vehicles on highway bridges are summarized by Honda et al [44] and Kawatani et al [45~47]. In Kawatanis' researches, the dynamic response analytical approach

for the bridge-vehicle interaction system was established using ether simple two-degree-of-freedom (two-DOF) sprung-mass vehicle model or 3-D vehicle model with eight-DOF, considering bouncing, pitching and rolling of the vehicle body, parallel hop and axle tramp of the front axle, parallel hop, axle windup motion and axle tramp of the rear axles, and is applied on various highway bridge-vehicle interaction problems [48] [49]. Recently, based on the results of the highway bridge dynamic analysis, Kawatani and He et al [50~54] established an analytical approach to simulate the bridge-train interaction of high-speed railway system, and the procedure is further developed to cope with the site vibration problem and seismic analysis of the bridge-train interaction system.

Although enormous efforts have been devoted and significant progress has been achieved towards elucidating the bridge-vehicle interaction problems, challenges still remain for researchers because the complicated nature of the phenomena. For instance, bridge-train interaction considering the exact contact between wheels and rail/road surface is still difficult to be accurately solved, since it needs multidisciplinary cooperation and also high capacity of computers. Also, how to treat the vehicles as dynamic vibrational systems in the bridge design codes is either an interest of many researchers. Moreover, researches on the non-linear bridge-train interaction problem such as caused by strong ground motions are still in the early stage and need urgent progress. With the further advancements of the theoretical research as well as the improvements of the computational capacities and methods, it is desirable to analyze the train, bridge structure, foundation and ambient soil as an integrated system considering their exact dynamic interaction.

1.3.2 Environmental vibration problem caused by bullet trains

Along with the rapid urban development and economical growth in many areas of modern Japan, there has been a significant increase in numbers of new infrastructures including viaducts. Since Japan is a densely populated country, in urban areas the elevated bridge structures, e.g. the Shinkansen lines, are often so adjacent to private buildings or important facilities such as residences, schools, hospitals and laboratories. The bridge vibration caused by running trains propagates to the ambient ground via footing and pile structures, thereby causing some environmental vibration problems, such as influences to precision instruments or people who are studying or resting. With further progress of transport facilities, there is rising public concern about the environmental problems [4].

Although the importance and urgency of environmental problems have been recognized, the development and propagation mechanism of site vibration caused particularly by running

vehicles on viaducts remains unclear because of its complicated nature. Without a clear grasp of the site-vibration mechanism through analytical studies, environ-mental vibration problems are traditionally evaluated and predicted based on field test data[6] [7]. The efficiency of such a process is limited to particular cases.

In recent years, a great deal of effort has been devoted to analytical studies of site vibrations induced by trains moving on the ground surface. Fujikake [55] proposed a predictive method for vibration levels of the surrounding environment. Takemiya [56] conducted a simulation of track-ground vibrations caused by a high-speed train for predicting train-track and nearby ground-borne vibrations. Yang et al [57] also examined train-induced wave propagation in layered soils using a 2.5-D finite/infinite element approach. Nonetheless, little is known about the ground vibration caused by trains moving over viaducts because of its complicated nature: vibrations are transmitted to the ground via piers, footings and piles. Recently, Xia et al [58] evaluated the vibration-related effects of light-rail train-viaduct system on the surrounding environment using a 2-D interaction model of a "train-bridge" system for obtaining the dynamic loads of moving trains on bridge piers and a 2-D dynamic model of "pier-foundation-ground" system for analyzing vibration responses of the ground. Wu et al [59] [60] attempted to establish a semi-analytical approach to deal with ground vibration induced by trains moving over viaducts. Hara et al [61] attempted to clarify the site vibration around Shinkansen viaducts by both experiments and analytical procedure, but in their analyses, the excitations of the trains are only treated as simple equivalent moving force based on the measured results. Such approach not only cannot directly take consideration of the interaction between the bridge and train, but is incapable to set the wheel loads without experimental results. Yoshida and Seki [62] indicated the necessities to consider the bridge-train interaction when discussing the environmental vibration problem around Shinkansen viaducts. Based on the results [50~54] in traffic-induced vibration analyses, Kawatani and He et al [63~68] have recently developed an approach to simulate the ground vibrations around high-speed railway viaducts employing a general site vibration analytical program, in which the effect of bridge-train interaction on the response of ground is to a certain extent accurately considered. Nonetheless, the phenomena of the train-induced site vibration problem around viaducts still remain unclear especially in the case of complicated ground conditions. Moreover, with the progress of computational techniques, it is desirable to analyze the bridge-train-foundation-ground interaction as a integrated system.

1.3.3 Seismic analysis of the bridge-train interaction system

Japan is located in an earthquake-prone region. Therefore, the earthquake-proof capacity of the Shinkansen system is always a concern considering the extremely high-speed of the bullet trains. The devastating damages brought by either the Niigata earthquake or the Kobe earthquake gave people tragic lessons. The running safety of the bullet trains on bridges subjected to seismic load and the earthquake-proof capacities of the bridge structures have to be further investigated and urgently improved. However, for the discussions it is difficult to reproduce the seismic responses of the bridge-train interaction system through experiments. Therefore, a reliable and effective analytical procedure to simulate the dynamic response of the high-speed railway bridge-train-earthquake interaction system is expected.

To establish a procedure like that described above, it is first important to accurately simulate the dynamic response of the bridge-train system considering their exact interaction. As introduced previously, researches on traffic-induced bridge vibration problems have been prosperously carried out. However, until recently, little effort has been made towards clarifying the dynamic characteristics of the bridge-train interaction system subjected to seismic load. One study, by Yasoshima et al. [69], included some experiments to investigate the running stability of the train on the vibrating tracks. Miura [70] carried out a study to simulate the track and structure displacement as well as the damage of trains under earthquake motion, rather than specifically examining the train's running safety. Miyamoto et al [71] examined the running safety of trains employing a simple 3-D car model, but it subsumes that the train is stationary on the track. Han et al [72] simulated the dynamic behavior of a coupled-cable-stayed bridge-train system under an earthquake. Yang and Wu [73] evaluated the running stability of trains on bridges subjected to an earthquake taking advantage of a simply supported bridge model and a 3-D train model. Recently, Kim et al [74] established an analytical procedure to simulate the dynamic responses of a monorail bridge-train interaction system under earthquake. For the Shinkansen high-speed railway system, efforts have been undertaken by the Railway Technical Research Institute to investigate the running safety of the high-speed bullet train [9] [75]. He and Kawatani et al [76] [77] also attempted recently to establish an approach to simulate the seismic response of the Shinkansen bridge-train interaction system. Nevertheless, it is still far from clarifying the bridge-train-earthquake interaction system because of the complicated nature of the problem.

1.4 Brief review of this study

This dissertation is composed of six chapters, and the contents of each chapter are organized as follows:

The first chapter introduces the backgrounds of this study, including three dynamic issues related to high-speed railway bridge-train interaction system: the traffic-induced bridge vibration problem, the environmental vibration problem caused by running trains and the seismic performance of the bridge-train interaction system. Then the main objectives of this research work related to the above-mentioned dynamic issues are described. A brief historical review regarding these topics is also introduced.

The analytical procedures of the traffic-induced bridge vibration analysis, the site vibration analysis, and the seismic analysis of the bridge-train interaction system are described in Chapter 2. The bridge structures are modeled with finite elements and the trains are idealized as sprung-mass dynamic systems. The developed governing dynamic differential equations for the bullet train-bridge interaction system are derived based on D'Alembert's Principle and modal analytical method is applied to the bridge system. The numerical integration method used in dynamic analysis is also introduced.

In Chapter 3, the phenomena of bridge vibration caused by running trains are clarified. Natural modes and analytical dynamic responses of the bridge are compared with experimental ones to demonstrate the validity of the analytical procedure. Then, the dynamic characteristics of the viaducts are revealed. Further investigations are performed to examine the influences of different train models and different speed of trains on analytical results. According to analytical investigations, countermeasures against predominant vibration of the bridge are proposed and simulated. Efforts are also made to improve the analytical efficiency by developing a one-block model of the bridge.

Chapter 4 contains the analyses of the environmental vibration problem caused by bullet train-induced bridge vibration. Dynamic reaction forces at the pier bottoms are simulated by previously established bridge-train interaction analytical approach using influence matrix of the reaction force. Then, applying those reaction forces as input excitation forces in the foundation-ground interaction problem, the site vibration around the viaducts is simulated and evaluated using a general-purpose program named SASSI2000. Analytical results of the site vibration are also compared with experimental ones to validate the analytical procedure. Then the evaluations of the bullet train-induced environmental vibration are performed and the effect of countermeasures against predominant bridge vibration on reduction of the environmental vibration is also confirmed.

In Chapter 5, based on the bridge-train interaction analytical approach, an analytical procedure to simulate the linear response of the high-speed railway bridge-train-earthquake interaction system is established. The ground motions are considered as inertia force simultaneously acting on all the degree-of-freedoms of the bridge-train system. Newmark's β-method is also adopted here to solve the coupled equations of the bridge-train-earthquake interaction system. The accuracy of the seismic analysis algorithm is validated in comparison with the results of a general program named MIDAS. The dynamic responses of the bridge and the train are then simulated and evaluated. The seismic performance of the bridge is investigated by examining the cross-sectional forces of the pier with respect to the strength limits. To examine the running safety of the bullet train, the derailment coefficient defined as the lateral wheel load to the vertical one is simulated and examined.

Main conclusions obtained through this research are summarized and future works are indicated in Chapter 6.

References

[1] Japan Society of Civil Engineers: Standard Specifications for Concrete Structures-2001, Maintenance, MARUZEN Co., Ltd., January 2001. (*in Japanese*)

[2] Railway Technical Research Institute: Design standard for railway structures (Concrete structures), MARUZEN Co., Ltd.: Tokyo, Japan, 2004. (*in Japanese*)

[3] Railway Technical Research Institute: Design standard for railway structures (Displacement limits), MARUZEN Co., Ltd.: Tokyo, Japan, 2006. (*in Japanese*)

[4] Seki, M., Inoue, Y. and Naganuma, Y.: Reduction of subgrade vibration and track maintenance for Tokaido Shinkansen, *WCRR'97*, Vol. E, 1997.

[5] The Minister of the Environment: Recommendations for countermeasures against urgent vibration problems of the Shinkansen railway, March 1976. (*in Japanese*)

[6] Yoshioka, O. and Ashiya, K.: Dependence of Shinkansen-induced ground vibration upon their influence factors, *QR of RTRI*, Vol. 29, No. 4, pp.176–183, 1988.

[7] Yoshioka, O.: A Dynamic Model for Generation and Propagation of Shinkansen-Induced Ground Vibrations and Its Applications to Vibration Reduction Measures, *RTRI Report*, Special No.30, Oct. 1999. (*in Japanese*)

[8] Railway Technical Research Institute: Seismic design codes for railway structures, MARUZEN Co., Ltd.: Tokyo, Japan, 1999. (*in Japanese*)

[9] Matsumoto, N., Sogabe, M., Wakui, H. and Tanabe, M.: Running safety snalysis of vehicles on structures subjected to earthquake motion. *QR of RTRI*, Vol. 45, No. 3, pp. 116-122, 2004.

[10] Willis, R.: Appendix of the report of commissioners appointed to inquire application of iron to railway structures, *Report of His Majesty's Stationary Office*, London, 1849.

[11] Willis, R.: An essay on the effects produced by causing weights to travel over elastic bars, Extracted from the report of the commissioners, published as an Addendum in: Barlow, P., A treatise on the strength of timber, Cast and Malleable Iron, John Weale, London, 1851.

[12] Stokes, G. G.: Discussion of a differential equation relating to the breaking of railway bridges, *Trans*, *of the Cambridge Philosophical Society*, 8, Part V, No. LII, pp. 707, 1849.

[13] Waddell, J. A. L.: The designing of ordinary iron highway bridges, New York, J. Wiley, 1884.

[14] Waddell, J. A. L.: New impact formulas needed in designing bridges of various type, *Engineering New-Record 81*, No. 21, 1918.

[15] Inglis, C. E.: A Mathematical treatise on vibrations in railway bridges, Cambridge

University Press, London, England, 1934.

[16] Muchikov, V. M.: Some methods of computing vibration of elastic systems subjected to moving loads, Gosstroiizdat, Moscow, 1953.

[17] Biggs, J. M., Suer, H. S. and Louw, J. M.: The vibration of simple span highway bridges, *J. of Struc. Div.*, *Proc. of ASCE*, Vol. 83, No. ST2, pp. 1186/1-32, March, 1957.

[18] Wen, R. K.: Dynamic response of beams traversed by two-axle loads, *Journal of the Engineering Mechanics Division*, *ASCE*, Vol. 86, No. EM5, pp. 91-111, Oct., 1960.

[19] Wen, R. K. and Toridis, T.: Dynamic behavior of cantilever bridges, *Journal of the Engineering Mechanics Division*, *ASCE*, Vol. 88, No. EM4, pp. 27-43, Aug., 1962.

[20] Veletsos, A. S. and Haung, T.: Analysis of dynamic response of highway bridges, *Journal of the Engineering Mechanics Division*, *ASCE*, Vol. 96, No. EM5, pp. 593-620, Oct., 1970.

[21] Fryba, L.: Vibration of solids and structures under moving load, *Noordhoff International*, 1972.

[22] Fryba, L.: Nonstationary response of a beam to moving random force, J. of Sound & Vibration, Vol. 46, pp. 323-338, 1976.

[23] Fryba, L.: Dynamics of railway bridges, Thomas Telford, London, 1996.

[24] Fryba, L.: Vibration of solids and structures under moving loads, Thomas Telford, London, 1999.

[25] Fryba, L.: Dynamic behaviour of bridges due to high speed trains, *Proc. of Workshop: Bridges for High Speed Railways*, pp. 137-158, Porto, June 2004.

[26] Diana, G., et al.: A numerical method to define the dynamic behavior of a train running on a deformable structure, *MECCANICA*, Special Issue, pp. 27-42, 1988.

[27] Diana, G. and Cheli, F.: Dynamic interaction of railway systems with large bridges, *Vehicle System Dynamics*, Vol. 18(1-3), pp. 71-106, 1989.

[28] Diana, G., Cheli, F. and Bruni, S.: Railway runnablility and train-track interaction in long span cable supported bridges, *Advances in structural dynamics*, Vol. 1, pp. 43-54. Elsevier Science Ltd., 2000.

[29] Xia, H., G. Roeck, D., Zhang, H. R. and Zhang, N.: Dynamic analysis of train-bridge system and its application in steel girder reinforcement, *Computers and Structures*, Vol. 79, pp. 1851-1860, 2001.

[30] Xia, H., G. Roeck, D., Zhang, N. and Maeck, J.: Dynamic analysis of high speed railway bridge under articulated trains, *Computers & Structures*, Vol. 81, pp. 2467-2478, 2003.

[31] Xu, Y. L. and Xia H.: Dynamic response of suspension bridge to high wind and running train, *Journal of Bridge Engineering*, ASCE, Vol. 8, pp. 46-55, 2003.

[32] Xia, H. and Zhang, N.: Experimental analysis of railway bridge under high speed trains,

Journal of Sound & Vibration, Vol. 280, pp. 1233-1242, 2005.

[33] Yang, Y. B. et al.: Vehicle-bridge interaction analysis by dynamic condensation method, *Journal of Structural Engineering*, ASCE, Vol. 121(11), pp. 1636-1643, 1995.

[34] Yang, Y. B. et al.: Vehicle-bridge interaction element for dynamic analysis, *Journal of Structural Engineering*, ASCE, Vol. 123(11), pp. 1512-1518, 1997.

[35] Yang, Y. B. et al.: Vibration of simple beams due to trains moving at high speeds, *Journal of Engineering Structures*, Vol. 19, Issue 11, pp. 936-944, 1997.

[36] Matsuura, A.: A study of dynamic behavior of bridge girder for high speed railway, *Railway Technical Research Report*, No. 1074, Mar., 1978. (*in Japanese*)

[37] Matsuura, A.: A study of dynamic behavior of bridge girder for high speed railway, *Proceedings of the Japan Society of Civil Engineers*, No. 256, Dec., 1978. (*in Japanese*)

[38] Wakui, H.: Allowable Bent-angle of long-spanned suspension bridges determined by running property of Shinkansen car, *Railway Technical Research Report*, No. 1087, Jul., 1978. (*in Japanese*)

[39] Matsuura, A. and Wakui, H.: Allowable Bent-angle of long-spanned suspension bridges determined by running property of railway car, *Proceedings of the Japan Society of Civil Engineers*, No. 291, Dec., 1979. (*in Japanese*)

[40] Wakui, H., Matsumoto, N. and Tanabe, M.: A study on dynamic interaction analysis for railway vehicles and structures —Mechanical model and practical analysis method—, *RTRI Report*, Vol. 7, No. 4, Apr., 1993. (*in Japanese*)

[41] Wakui, H., Matsumoto, N., Matsuura, A. and Tanabe, M.: Dynamic interaction analysis for railway vehicles and structures, *Journal of Structural and Earthquake Engineering*, JSCE, Vol. I-31, No. 513, pp.129-138, Apr., 1995. (*in Japanese*)

[42] Yasoshima Y, Matsumoto Y, Nishioka T.: Studies on the running stability of railway vehicles on suspension bridges. *Journal of the Faculty of Engineering*, the University of Tokyo; XXXVI/1: 99-232, 1981.

[43] Tanabe M, Wakui H, Matsumoto N.: The finite element analysis of dynamic interactions of high-speed Shinkansen, rail, and bridge. *ASME Computers in Engineering*; G0813A: 17-22, 1993.

[44] Honda, H., Kobori, T. and Yamada, Y.: Dynamic factor of highway steel girder bridges, *IABSE PROCEEDINGS*, P-98/86, pp. 57-75, 1986.

[45] Kawatani, M., Nishiyama, S. and Yamada, Y.: Dynamic response analysis of highway girder bridges under moving vehicles, *Technology Reports of the Osaka University*, Vol. 43, No. 2137, pp. 109-118, 1993.

[46] Kawatani, M. and Nishiyama, S.: Dynamic response characteristics of highway bridges with roadway roughness under moving vehicles, *Journal of Structural Engineering*,

JSCE, Vol.39A, pp. 733-740, Mar., 1993. (*in Japanese*)

[47] Kawatani, M., Yamada, Y. and Dakeshita, Y.: Dynamic response analysis of plate girder bridge due to 3-dimensional vehicle model, *Journal of Structural and Earthquake Engineering*, JSCE, Vol. I-42, No. 584, pp.79-86, Jan., 1998. (*in Japanese*)

[48] Kawatani, M. and Kim, C. W.: Computer simulation for dynamic wheel loads of heavy vehicles," *Structural Engineering and Mechanics*, Vol. 12, No. 4, pp. 409-428, 2001.

[49] Kim, C. W. and Kawatani, M.: A Comparative Study on Dynamic Wheel Loads of Multi-Axle Vehicle and Bridge Responses, *Proc. ASME International 2001 Design Engineering Technical Conferences, Symposium on Dynamics and Control of Moving Load Problems*, Pittsburgh, USA, September 9-12, 2001.

[50] Kawatani, M., He, X., Sobukawa, R., Masaki, S. and Nishiyama, S.: Dynamic Ground Reaction Forces at Pier Bottoms due to Running Trains on Viaducts, Proc. of Annual Conference of Civil Engineers 2003, JSCE Kansai Chapter, I-50, May 2003. (*in Japanese*)

[51] Kawatani, M., He, X., Sobukawa, R., Masaki, S. and Nishiyama, S.: Dynamic Ground Reaction Forces at Pier Bottoms due to Running Trains on Viaducts and Improvement of Analytical Efficiency, Proceedings of the 58th Annual Conference of the Japan Society of Civil Engineers, I-748, Sep., 2003. (*in Japanese*)

[52] Kawatani, M., He, X., Sobukawa, R. and Nishiyama, S.: Dynamic Response Analysis of Elevated Railway Bridges due to Shinkansen Trains and Influence of Train models, Proc. of International Workshop on Structural Health Monitoring Bridges/Colloquium on Bridge Vibration, pp.249-256, Kitami, Japan, Sept. 2003.

[53] Kawatani, M., He, X., Sobukawa, R. and Nishiyama, S.: Traffic-induced dynamic response analysis of high-speed railway bridges. *Proceedings of the Third Asian-Pacific Symposium on Structural Reliability and Its Applications*, Seoul, Korea, pp. 569-580, 2004.

[54] Kawatani, M., He, X., Shiraga, R., Masaki, S., Nishiyama, S. and Yoshida, K.: Dynamic response analysis of elevated railway bridges due to Shinkansen trains, *Journal of Structural and Earthquake Engineering (Doboku Gakkai Ronbunshuu A)*, JSCE, Vol. 62, No. 3, pp.509-519, 2006. (*in Japanese*)

[55] Fujikake, T. A.: A prediction method for the propagation of ground vibration from railway trains, *Journal of Sound and Vibration*, Vol. 111, Issue 2, pp.289–297, 1986.

[56] Takemiya, H.: Simulation of track-ground vibrations due to a high-speed train: the case of X-2000 at ledsgard, *Journal of Sound and Vibration*, Vol. 261, Issue 3, pp.503–526, 2003.

[57] Yang, Y. B., Hung, H. H. and Chang, D. W.: Train-induced wave propagation in layered soils using finite/infinite element simulation, *Soil Dynamics and Earthquake*

Engineering, Vol. 23, No. 4, pp.263–278, 2003.

[58] Xia, H., Cao, Y. M., Zhang, N. and Qu, J. J.: Vibration effects of light-rail train-viaduct system on surrounding environment, *International Journal of Structural Stability and Dynamics*, Vol. 2, No. 2, pp.227–240, 2002.

[59] Wu, Y. S., Hsu, L. C. and Yang, Y. B.: Ground vibrations induced by trains moving over series of elevated bridge, *Proc. of the 10th Sound and Vibration Conference*, Taipei, Taiwan, pp.1–7, 2002.

[60] Wu, Y. S. and Yang, Y. B.: A semi-analytical approach for analyzing ground vibrations caused by trains moving over elevated bridges, *International Journal of Soil Dynamics and Earthquake Engineering*, Vol. 24, Issue 12, pp. 949-962 2004.

[61] Hara, T., Yoshioka, O., Kanda, H., Funabashi, H., Negishi, H., Fujino, Y. and Yoshida K.: Development of a new method to reduce Shinkansen-induced wayside vibrations applicable to rigid frame bridges: bridge-end reinforcing method, *Journal of Structural and Earthquake Engineering (Doboku Gakkai Ronbunshuu A)*, JSCE, Vol. 68, No. 766, pp.325-338, July 2004. (*in Japanese*)

[62] Yoshida, K. and Seiki, M.: Influence of improved rigidity in railway viaducts on the environmental ground vibration, *Journal of Structural Engineering*, JSCE, Vol. 50A, pp. 403-412, 2004. (*in Japanese*)

[63] Kawatani, M., He, X., Sobukawa, R., Masaki, S., Nishiyama, S. and Sasakawa, T.: Analysis of Site Vibration around Shinkansen Viaducts due to Running Trains, Proc. of Annual Conference of Civil Engineers 2004, JSCE Kansai Chapter, I-73, May 2004. (*in Japanese*)

[64] Kawatani, M., He, X., Sobukawa, R., Masaki, S., Nishiyama, S. and Sasakawa, T.: Evaluation on Ground Vibration around Shinkansen Viaducts due to Running Trains, Proceedings of the 59th Annual Conference of the Japan Society of Civil Engineers, I-431, Sep., 2004. (*in Japanese*)

[65] Kawatani, M., He, X., Yoshida, K., Sobukawa, R., Nishiyama, S. and Yamaguchi, S.: Countermeasures on Reducing Ground Vibration around Shinkansen Viaducts by means of Stiffening Rail Structure, Proc. of Annual Conference of Civil Engineers 2005, JSCE Kansai Chapter, I-35, May 2005. (*in Japanese*)

[66] Kawatani, M., Yoshida, K., He, X., Sobukawa, R. and Yamaguchi, S.: Analytical Evaluation of Effect on Reducing Site Vibration around Shinkansen Viaducts by Reinforcing Hanging Parts of Bridges, Proceedings of the 60th Annual Conference of the Japan Society of Civil Engineers, I-562, Sep., 2005. (*in Japanese*)

[67] Kawatani, M., He, X., Yoshida, K., Yamaguchi, S. and Nishiyama, S.: Soundness Investigation of Shinkansen Viaducts by means of analysis on ambient site vibration

caused by bullet trains, Proc. of Annual Conference of Civil Engineers 2006, JSCE Kansai Chapter, I-65, Jun., 2005. (*in Japanese*)

[68] He, X., Kawatani, M., Yamaguchi, S. and Nishiyama, S.: Evaluation of Site Vibration around Shinkansen Viaducts under Bullet Train, Proc. of 2nd International Symposium on Environmental Vibrations (ISEV2005), Okayama, Japan, Sep. 20-22, 2005.

[69] Yasoshima, Y., Matsumoto, Y. and Nishioka, T.: Experimental study for derailment on vibration tracks, *Proc. of JSCE*, Vol. 164, pp. 71-76, 1969.

[70] Miura, S.: Deformation of track and safety of train in earthquake. *QR of RTRI*, Vol. 37, No.3, pp. 139-147, 1969.

[71] Miyamoto, T., Ishida, H. and Matsuo, M.: Running safety of railway vehicle as earthquake occurs, *QR of RTRI*, Vol. 38, No. 3, pp. 117-122, 1997.

[72] Han, Y., Xia, H., Guo, W. and Zhang, N.: Dynamic analysis of cable-stayed bridge subjected to running trains and earthquakes, *Environmental Vibration*, Beijing: China Communications Press, pp. 242-251, 2003.

[73] Yang, Y. B. and Wu, Y. S.: Dynamic stability of trains moving over bridges shaken by earthquakes, *J. of Sound and Vibration*, Vol. 258, No. 1, pp. 65-94, 2002.

[74] Kim, C. W. and Kawatani, M.: Effect of train dynamics on seismic response of steel monorail bridges under moderate ground motion, *Earthquake Engineering & Structural Dynamics*, DOI: 10.1002/eqe.580, 2006.

[75] Miyamoto, T., Sogabe, M., Shimomura, T., Nishiyama, Y., Matsumoto, N. and Matsuo, M.: Real-size experiment and numerical simulation of dynamic behavior of railway vehicle against track vibration, *RTRI Report,* Vol. 17, No. 9, pp. 39-44, 2004. (*in Japanese*)

[76] He, X., Kawatani, M., Sobukawa, R. and Nishiyama, S.: Dynamic response analysis of Shinkansen train-bridge interaction system subjected to seismic load, *Proc. of 4th International Conference on Current and Future Trends in Bridge Design, Construction and Maintenance*, Kuala Lumpur, Malaysia, pp. 1-12, 2005 (CD-ROM).

[77] Kawatani, M., He, X., Nishiyama, S., Yoshida, K. and Yamaguchi, S.: Dynamic Response Analysis of Shinkansen Train-Bridge Interaction System Subjected to Moderate Earthquake, Proceedings of the 61st Annual Conference of the Japan Society of Civil Engineers, I-502，2006.9. (*in Japanese*)

Chapter 2

Analytical procedures

2.1 Introduction

This chapter is to introduce the theoretical procedures used in this research to develop the analytical approaches. For the dynamic interaction problems between the bridge, train, foundation, ground as well as earthquake motion, currently it is difficult to handle the problem by treating all these factors as an integrated system considering their exact dynamic interaction, because of not only the complexities of the whole interaction system but also the enormous computational capacities it requires of the computer. Therefore in this study, to simulate the bullet train-induced bridge vibration problem, related environmental vibration problem and the seismic performance of the bridge-train interaction system, endeavors are devoted to solve the problems by dividing the whole interaction system into two subsystems: the bridge-train interaction (including seismic loads) and the foundation-ground interaction; and the two subsystems are connected with idealized ground springs.

In the first stage, the analytical procedure [1] to simulate the traffic-induced bridge vibration problem is established. Dynamic responses of the high-speed railway viaducts under moving bullet trains are analyzed in consideration of the wheel-track interaction with the rail surface roughness. The finite element (FE) method is applied to idealize the bridge structures. The viaducts including the track structure are modeled as 3-D beam elements. For the linear response analysis, simultaneous dynamic differential equations of the bridge are simplified using modal analytical approach. The elastic effect of ground springs at the pier bottoms and the connection effect of the sleepers and ballast between the track and the deck slab are model with double nodes connected by springs. A 3-D bullet train model as dynamic system that can appropriately express the lateral, vertical and rotational motions of the car body and bogies is developed for the analyses. Newmark's β-method for direct numerical integration is applied to solve the dynamic differential equations. Furthermore, the dynamic reaction forces at the pier bottoms are simulated based on the dynamic responses of viaducts using influence value matrix.

Then, applying the reaction forces obtained in bridge-train interaction analysis as input excitation forces in the foundation-ground interaction problem, the site vibration around the viaducts is simulated and evaluated [2] using a general-purpose program named SASSI2000. The foundation structures including footings and piles are modeled with finite elements and

the ground are modeled with 3-D thin layer elements. A brief introduction to the analytical theory of foundation-ground interaction employed in SASSI2000 is described in Chapter 4.

For the seismic performance of the bridge-train system in this study, as the first effort, assuming that the structures remain in elastic domain during a moderate earthquake, an analytical procedure [3] to simulate the bridge-train-earthquake interaction system is established. The bridge-train interaction models established in traffic-induced bridge vibration analysis are conveniently used in this stage. The seismic load is applied as inertia force simultaneously acting on all the DOFs of the bridge and train models. Newmark's β-method is also adopted to solve the coupled differential equations of the bridge-train-earthquake interaction system. In the case of seismic analysis considering strong ground motions, because the response of the bridge-train system is non-linear, modal analysis is no longer able to be applied. The dynamic differential equations should be solved by direct integration method. In this study, the efforts to formulize of the bridge-train-earthquake interaction by direct integration approach are devoted at first.

2.2 Finite element approach for dynamic response analysis [4~9]

2.2.1 Stiffness matrix of beam element

The whole bridge structures are modeled as three-dimensional beam elements. The geometric configuration of the beam element is depicted in **Fig. 2.2.1**. Constant cross-section is assumed for the beam element. The general static stiffness matrix for the beam element, which is composed of components of axial force, shear force, bending moment and torsional force, is represented as Eq. (2.2.1), where $\boldsymbol{f_e}$, $\boldsymbol{K_e}$ and $\boldsymbol{w_e}$ denote the nodal force vector, the stiffness matrix and the nodal displacement vector of the beam element, respectively.

$$\boldsymbol{f_e} = \boldsymbol{K_e} \cdot \boldsymbol{w_e} \tag{2.2.1}$$

where,

$$\boldsymbol{f_e} = \{F_{xL}, F_{yL}, F_{zL}, M_{xL}, M_{yL}, M_{zL}, F_{xR}, F_{yR}, F_{zR}, M_{xR}, M_{yR}, M_{zR}\}$$

$$\boldsymbol{w_e} = \{u_L, v_L, w_L, \theta_{xL}, \theta_{yL}, \theta_{zL}, u_R, v_R, w_R, \theta_{xR}, \theta_{yR}, \theta_{zR}\}$$

$$\boldsymbol{K_e} = \begin{bmatrix}
\frac{EA}{l} & & & & & & & & & & & \\
0 & \frac{12EI_z}{l^3} & & & & & & & & & & \\
0 & 0 & \frac{12EI_y}{l^3} & & & & & & & & & \\
0 & 0 & 0 & \frac{GK}{l} & & & & & & & & \\
0 & 0 & -\frac{6EI_y}{l^2} & 0 & \frac{4EI_y}{l} & & & & & & & \\
0 & \frac{6EI_z}{l^2} & 0 & 0 & 0 & \frac{4EI_z}{l} & & & & & & \\
-\frac{EA}{l} & 0 & 0 & 0 & 0 & 0 & \frac{EA}{l} & & & & & \\
0 & -\frac{12EI_z}{l^3} & 0 & 0 & 0 & -\frac{6EI_z}{l^2} & 0 & \frac{12EI_z}{l^3} & & & & \\
0 & 0 & -\frac{12EI_y}{l^3} & 0 & \frac{6EI_y}{l^2} & 0 & 0 & 0 & \frac{12EI_y}{l^3} & & & \\
0 & 0 & 0 & -\frac{GK}{l} & 0 & 0 & 0 & 0 & 0 & \frac{GK}{l} & & \\
0 & 0 & -\frac{6EI_y}{l^2} & 0 & \frac{2EI_y}{l} & 0 & 0 & 0 & \frac{6EI_y}{l^2} & 0 & \frac{4EI_y}{l} & \\
0 & \frac{6EI_z}{l^2} & 0 & 0 & 0 & \frac{2EI_z}{l} & 0 & -\frac{6EI_z}{l^2} & 0 & 0 & 0 & \frac{4EI_z}{l}
\end{bmatrix} \quad sym.$$

(2.2.2)

where, A, E and l indicate the cross sectional area of the beam element, Young's modulus and length of the beam element, respectively; I_y and I_z indicate the moment of inertia about y- and z-axis, respectively; G is the shear modulus and K is the Saint-Venan's torsional constant.

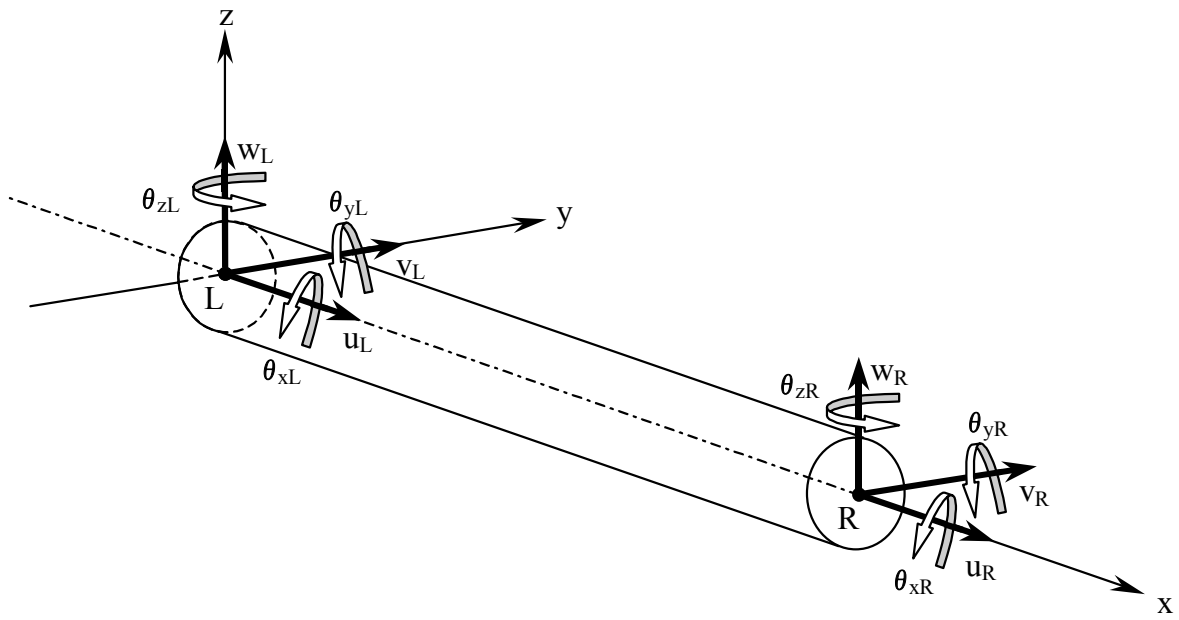

Fig. 2.2.1 Coordinate of member element

2.2.2 Mass matrix of beam element

To form the mass matrix of the beam element, consistent mass matrix and lumped mass matrix are available. The consistent mass matrix demands more arrays in the program compared with that of the lumped mass matrix, though it simulates the inertia effects of the beam element more accurately. The lumped mass matrix is considered having adequate accuracy and suitable one for its economical efficiency while dealing with a large number of elements. In this study, the lumped mass matrix is adopted for the beam element and is shown in Eq. (2.2.3).

$$\boldsymbol{M}_{l,e}=\frac{\gamma AL}{2g}\begin{bmatrix}
1 & & & & & & & & & & & \\
0 & 1 & & & & & & & & & & \\
0 & 0 & 1 & & & & & & & sym. & & \\
0 & 0 & 0 & I_\theta/A & & & & & & & & \\
0 & 0 & 0 & 0 & 0 & & & & & & & \\
0 & 0 & 0 & 0 & 0 & 0 & & & & & & \\
0 & 0 & 0 & 0 & 0 & 0 & 1 & & & & & \\
0 & 0 & 0 & 0 & 0 & 0 & 0 & 1 & & & & \\
0 & 0 & 0 & 0 & 0 & 0 & 0 & 0 & 1 & & & \\
0 & 0 & 0 & 0 & 0 & 0 & 0 & 0 & 0 & I_\theta/A & & \\
0 & 0 & 0 & 0 & 0 & 0 & 0 & 0 & 0 & 0 & 0 & \\
0 & 0 & 0 & 0 & 0 & 0 & 0 & 0 & 0 & 0 & 0 & 0
\end{bmatrix} \tag{2.2.3}$$

where, A, L and γ indicate cross sectional area, length and unit weight of the beam element; g is the acceleration of gravity and I_θ denote the polar moment of inertia.

2.2.3 Double nodes

For structures such as pin connection, roller and rubber bearing, etc., the beam element cannot be considered rigidly connected to the adjacent node or joint at either ends. In this study, double nodes defined as two nodes of independence sharing the same coordinate are adopted to simulate the effect of hinge or elastic support, e.g. for pin structure, moment will not be deliver to each other in the double notes and for rubber bearing structure, appropriate spring constant will be added to double notes.

For pin structure, two nodes i and j are connected to each other with a pin as shown in **Fig. 2.2.2(a)**, the external forces acts on the pin structure are p= (p_x, p_y, p_z) and the moments are m_i, and m_j. Dividing the structure into to two independent structures as shown in **Fig 2.2.2 (b)**, the general stiffness matrix of the pin structure in the global stiffness matrix can be represented as Eq. (2.2.4). q= (q_x, q_y, q_z) denotes the unknown force simultaneously acting on nodes i and j.

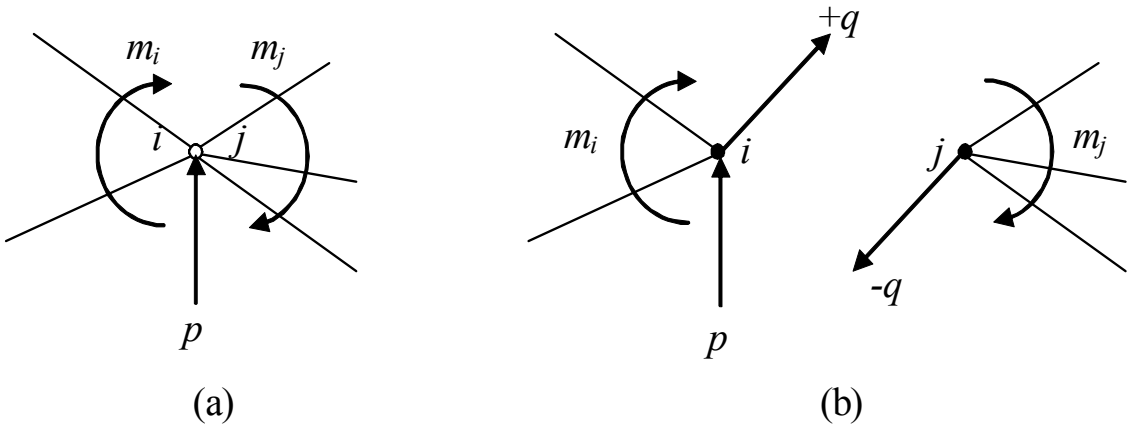

Fig. 2.2.2 Double nodes

$$\begin{matrix} i^{th}\ \ Row \\ (i+1)^{th}\ \ Row \\ j^{th}\ \ Row \\ (j+1)^{th}\ \ Row \end{matrix} \begin{Bmatrix} \vdots \\ p+q \\ m_i \\ -q \\ m_j \\ \vdots \end{Bmatrix} = \begin{bmatrix} \vdots & \vdots & \vdots & \vdots & \vdots & \vdots \\ \vdots & K_{iw1} & K_{i\theta 1} & 0 & 0 & \vdots \\ \vdots & K_{iw2} & K_{i\theta 2} & 0 & 0 & \vdots \\ \vdots & 0 & 0 & K_{jw1} & K_{j\theta 1} & \vdots \\ \vdots & 0 & 0 & K_{jw2} & K_{j\theta 2} & \vdots \\ \vdots & \vdots & \vdots & \vdots & \vdots & \vdots \end{bmatrix} \begin{Bmatrix} \vdots \\ w_i \\ \theta_i \\ w_j \\ \theta_j \\ \vdots \end{Bmatrix} \tag{2.2.4}$$

Adding the j^{th} row to the i^{th} row of the Eq. (2.2.4) and considering the condition of compatibility of w_i=w_j, the unknown force q can be deleted. Consequently the general stiffness matrix of the pin structure in the global stiffness matrix can be written as Eq. (2.2.5).

$$\boldsymbol{K} = \begin{bmatrix} \vdots & \vdots & \vdots & \vdots & \vdots & \vdots \\ \vdots & K_{iw1}+K_{jw1} & K_{i\theta 1} & 0 & K_{j\theta 1} & \vdots \\ \vdots & K_{iw2} & K_{i\theta 2} & 0 & 0 & \vdots \\ \vdots & 0 & 0 & 1 & 0 & \vdots \\ \vdots & K_{jw2} & 0 & 0 & K_{j\theta 2} & \vdots \\ \vdots & \vdots & \vdots & \vdots & \vdots & \vdots \end{bmatrix} \tag{2.2.5}$$

In the case of elastic support such as two nodes connected with each other by rubber bearing, the stiffness matrix of the rubber spring is expressed as Eq. (2.2.6). By applying this stiffness matrix to the double notes, such elastic support can be simulated numerically.

$$\boldsymbol{K}_{sp.}=\begin{bmatrix} k_x & & & & & & & & & & & \\ 0 & k_y & & & & & & & & & & \\ 0 & 0 & k_z & & & & & & & sym. & & \\ 0 & 0 & 0 & k_{\theta x} & & & & & & & & \\ 0 & 0 & 0 & 0 & k_{\theta y} & & & & & & & \\ 0 & 0 & 0 & 0 & 0 & k_{\theta z} & & & & & & \\ -k_x & 0 & 0 & 0 & 0 & 0 & k_x & & & & & \\ 0 & -k_y & 0 & 0 & 0 & 0 & 0 & k_y & & & & \\ 0 & 0 & -k_z & 0 & 0 & 0 & 0 & 0 & k_z & & & \\ 0 & 0 & 0 & -k_{\theta x} & 0 & 0 & 0 & 0 & 0 & k_{\theta x} & & \\ 0 & 0 & 0 & 0 & -k_{\theta y} & 0 & 0 & 0 & 0 & 0 & k_{\theta y} & \\ 0 & 0 & 0 & 0 & 0 & -k_{\theta z} & 0 & 0 & 0 & 0 & 0 & k_{\theta z} \end{bmatrix} \tag{2.2.6}$$

where, k_x, k_y and k_z denote the Spring constants of elastic support in x, y and z directions, respectively. $k_{\theta x}$,$k_{\theta y}$ and $k_{\theta z}$ indicate the rotational spring constant in x, y and z directions, respectively.

2.2.4 Transformation of coordinates

If local axes for a finite element are not parallel to the global axes for the whole structure, rotation-of-axes transformations must be used for nodal loads, displacements, accelerations, stiffnesses, and consistent masses. Thus, when the elements are assembled, the resulting equations of motion will pertain to the global directions at each node. The concept of rotation of axes applies to a force, a moment, a translation, a small rotation, velocities, accelerations, orthogonal coordinates, and so on.

Assume that unit vectors of the local and global axes are represented as Eq. (2.2.7), respectively.

$$\bar{\boldsymbol{e}}=\begin{bmatrix} \bar{\boldsymbol{i}}_{\mathrm{x}} \\ \bar{\boldsymbol{i}}_{\mathrm{y}} \\ \bar{\boldsymbol{i}}_{\mathrm{z}} \end{bmatrix}, \quad \boldsymbol{e}=\begin{bmatrix} \boldsymbol{i}_{\mathrm{x}} \\ \boldsymbol{i}_{\mathrm{y}} \\ \boldsymbol{i}_{\mathrm{z}} \end{bmatrix} \tag{2.2.7}$$

The transformation of coordinates from local system to global system using rotation matrix $\boldsymbol{T}$ can be represented as Eq. (2.2.8)

$$\bar{\boldsymbol{e}}=\boldsymbol{T}\cdot\boldsymbol{e} \tag{2.2.8}$$

where,

$$\boldsymbol{T} = \begin{bmatrix} l_{11} & l_{12} & l_{13} \\ l_{21} & l_{22} & l_{23} \\ l_{31} & l_{32} & l_{33} \end{bmatrix} \tag{2.2.9}$$

Herein, $\{l_{11} \quad l_{12} \quad l_{13}\}$, $\{l_{21} \quad l_{22} \quad l_{23}\}$ and $\{l_{31} \quad l_{32} \quad l_{33}\}$ denote the vectors of direction cosines of the local axes to the global axes.

2.2.5 Matrix condensation [7]

The concept of matrix condensation [10] [11] is a well-known procedure for reducing the number of unknown displacements in a statics problem. With such applications no loss of accuracy results from the reduction process, because the method is simply Gaussian elimination of displacements in matrix form. For dynamic analysis, a similar type of condensation was introduced by Guyan [12], which brings in an additional approximation.

Starting with static reduction, the static equations of equilibrium of the global system can be written as follows:

$$\boldsymbol{F} = \boldsymbol{K}_{\mathrm{T}} \cdot \boldsymbol{W} \tag{2.2.10}$$

where, $\boldsymbol{F}$, $\boldsymbol{K}_{\mathrm{T}}$ and $\boldsymbol{W}$ denote the external force vector at nodal points, stiffness matrix and nodal displacements of the whole global system.

Simply assuming that no displacements occur at the freedoms of nodal points restrained (The displacements of restrained freedoms can also be set as known quantities), the action equations of equilibrium can be written in the partitioned form as follows:

$$\begin{Bmatrix} \boldsymbol{f} \\ \boldsymbol{m} \\ \boldsymbol{f}_{\mathrm{R}} \\ \boldsymbol{m}_{\mathrm{R}} \end{Bmatrix} = \begin{bmatrix} \boldsymbol{K}_{11} & \boldsymbol{K}_{12} & \boldsymbol{K}_{13} & \boldsymbol{K}_{14} \\ \boldsymbol{K}_{21} & \boldsymbol{K}_{22} & \boldsymbol{K}_{23} & \boldsymbol{K}_{24} \\ \boldsymbol{K}_{31} & \boldsymbol{K}_{32} & \boldsymbol{K}_{33} & \boldsymbol{K}_{34} \\ \boldsymbol{K}_{41} & \boldsymbol{K}_{42} & \boldsymbol{K}_{43} & \boldsymbol{K}_{44} \end{bmatrix} \begin{Bmatrix} \boldsymbol{w} \\ \boldsymbol{\theta} \\ \boldsymbol{0} \\ \boldsymbol{0} \end{Bmatrix} \tag{2.2.11}$$

where,

$$\boldsymbol{w} = \begin{Bmatrix} \boldsymbol{w}_x \\ \boldsymbol{w}_y \\ \boldsymbol{w}_z \end{Bmatrix}, \quad \boldsymbol{\theta} = \begin{Bmatrix} \boldsymbol{\theta}_x \\ \boldsymbol{\theta}_y \\ \boldsymbol{\theta}_z \end{Bmatrix}, \quad \boldsymbol{f} = \begin{Bmatrix} \boldsymbol{f}_x \\ \boldsymbol{f}_y \\ \boldsymbol{f}_z \end{Bmatrix}, \quad \boldsymbol{m} = \begin{Bmatrix} \boldsymbol{m}_x \\ \boldsymbol{m}_y \\ \boldsymbol{m}_z \end{Bmatrix}, \quad \boldsymbol{f}_R = \begin{Bmatrix} \boldsymbol{f}_{\mathrm{R}x} \\ \boldsymbol{f}_{\mathrm{R}y} \\ \boldsymbol{f}_{\mathrm{R}z} \end{Bmatrix}, \quad \boldsymbol{m}_R = \begin{Bmatrix} \boldsymbol{m}_{\mathrm{R}x} \\ \boldsymbol{m}_{\mathrm{R}y} \\ \boldsymbol{m}_{\mathrm{R}z} \end{Bmatrix}.$$

Herein, $\boldsymbol{w}$ and $\boldsymbol{\theta}$ denote the free displacement and angular displacement vectors; $\boldsymbol{f}$ and $\boldsymbol{m}$ indicate the external force and moment vectors; $\boldsymbol{f}_{\mathrm{R}}$ and $\boldsymbol{m}_{\mathrm{R}}$ are the reaction force and reaction moment vectors acting on the restrained nodal points, respectively. Subscripts of x, y and z indicate the axes in the Cartesian coordinates.

Considering that the restrained displacements are known, the reaction forces can be derived if the unknown free displacements are obtained, which will be explained in the next subsection. The equations of equilibrium for solving the unknown displacements can be written as follows:

$$\begin{Bmatrix} \boldsymbol{f} \\ \boldsymbol{m} \end{Bmatrix} = \begin{bmatrix} \boldsymbol{K}_{11} & \boldsymbol{K}_{12} \\ \boldsymbol{K}_{21} & \boldsymbol{K}_{22} \end{bmatrix} \begin{Bmatrix} \boldsymbol{w} \\ \boldsymbol{\theta} \end{Bmatrix} \tag{2.2.12}$$

To reduce the matrix size, the finite-element theme of “master” and “slave” displacements can be introduced. In the framed structures, rotations at the joints of beams, plane frames, grids, and space frames are usually chosen as the dependent set of displacements. Moreover, this method can be used in a much more general manner for various discretized continua. However, the trouble with this generality is that a good choice of “master” and “slave” displacements is not always obvious. Even with framed structures there are cases when joint rotations are important than translations and should not be eliminated.

Here, choosing the rotational displacements as “slave” ones, the following relations can be derived,

$$\boldsymbol{K}_{21}\boldsymbol{w} + \boldsymbol{K}_{22}\boldsymbol{\theta} = \boldsymbol{m} \tag{2.2.13}$$

and

$$\boldsymbol{\theta} = \boldsymbol{K}_{22}^{-1}\left(\boldsymbol{m} - \boldsymbol{K}_{21}\boldsymbol{w}\right) \tag{2.2.14}$$

Substituting Eqs. (2.2.13) and (2.2.14) into Eq. (2.2.12), the equations of equilibrium can be obtained as follows:

$$\boldsymbol{f} - \boldsymbol{K}_{12}\boldsymbol{K}_{22}^{-1}\boldsymbol{m} = \left(\boldsymbol{K}_{11} - \boldsymbol{K}_{12}\boldsymbol{K}_{22}^{-1}\boldsymbol{K}_{21}\right)\boldsymbol{w} \tag{2.2.15}$$

Assuming $\boldsymbol{f}_b = \boldsymbol{f} - \boldsymbol{K}_{12}\boldsymbol{K}_{22}^{-1}\boldsymbol{m}$, the new equations of equilibrium can be written as:

$$\boldsymbol{f}_b = \boldsymbol{K}_b \cdot \boldsymbol{w} \tag{2.2.16}$$

where, $\boldsymbol{K}_b$ is called reduced stiffness matrix and represented as follows:

$$\boldsymbol{K}_b = \boldsymbol{K}_{11} - \boldsymbol{K}_{12}\boldsymbol{K}_{22}^{-1}\boldsymbol{K}_{21} \tag{2.2.17}$$

If external moments are not applied, and then $\boldsymbol{m}$ is the zero vector, the equations can be further simplified.

Turning next to dynamic reduction, the damped equations of motion for free displacements can be written as follows:

$$\boldsymbol{M}\ddot{\boldsymbol{X}} + \boldsymbol{C}\dot{\boldsymbol{X}} + \boldsymbol{K}\boldsymbol{X} = \boldsymbol{S} \tag{2.2.18}$$

where, $\boldsymbol{M}$, $\boldsymbol{C}$ and $\boldsymbol{K}$ are respectively the mass, damping and stiffness matrices with respect to the free freedoms, and

$$\boldsymbol{X} = \begin{Bmatrix} \boldsymbol{w} \\ \boldsymbol{\theta} \end{Bmatrix}, \text{ and } \quad \boldsymbol{S} = \begin{Bmatrix} \boldsymbol{f} \\ \boldsymbol{m} \end{Bmatrix}$$

Thus the damped equations of motion for free displacements can be also written in the partitioned form as follows:

$$\begin{bmatrix} \boldsymbol{M}_{11} & \boldsymbol{M}_{12} \\ \boldsymbol{M}_{21} & \boldsymbol{M}_{22} \end{bmatrix} \begin{Bmatrix} \ddot{\boldsymbol{w}} \\ \ddot{\boldsymbol{\theta}} \end{Bmatrix} + \begin{bmatrix} \boldsymbol{C}_{11} & \boldsymbol{C}_{12} \\ \boldsymbol{C}_{21} & \boldsymbol{C}_{22} \end{bmatrix} \begin{Bmatrix} \dot{\boldsymbol{w}} \\ \dot{\boldsymbol{\theta}} \end{Bmatrix} + \begin{bmatrix} \boldsymbol{K}_{11} & \boldsymbol{K}_{12} \\ \boldsymbol{K}_{21} & \boldsymbol{K}_{22} \end{bmatrix} \begin{Bmatrix} \boldsymbol{w} \\ \boldsymbol{\theta} \end{Bmatrix} = \begin{Bmatrix} \boldsymbol{f} \\ \boldsymbol{m} \end{Bmatrix} \tag{2.2.19}$$

Then assume as a new approximation that the displacements of $\boldsymbol{\theta}$ are dependent on those of $\boldsymbol{w}$, as follows:

$$\boldsymbol{\theta} = \boldsymbol{K}_{\mathrm{A}}\boldsymbol{w} \tag{2.2.20}$$

where

$$\boldsymbol{K}_{\mathrm{A}} = -\boldsymbol{K}_{22}^{-1}\boldsymbol{K}_{21} \tag{2.2.21}$$

Even for static analysis, this relationship is correct only when actions of $\boldsymbol{m}$ do not exist. Differentiating Eq. (2.2.20) once and twice with respect to time respectively produces

$$\dot{\boldsymbol{\theta}} = \boldsymbol{K}_{\mathrm{A}}\dot{\boldsymbol{w}} \tag{2.2.22}$$

$$\ddot{\boldsymbol{\theta}} = \boldsymbol{K}_{\mathrm{A}}\ddot{\boldsymbol{w}} \tag{2.2.23}$$

For the purpose of reducing the equations of motion to a smaller set, the transformation operator can be formed as follows:

$$\boldsymbol{T} = \begin{bmatrix} \boldsymbol{I} \\ \boldsymbol{K}_{\mathrm{A}} \end{bmatrix} \tag{2.2.24}$$

in which $\boldsymbol{I}$ is an identity matrix of the same order as $\boldsymbol{K}_{11}$. Substituting Eqs. (2.2.20), (2.2.22) and (2.2.23) into Eq. (2.2.19) and premultiplying the latter by $\boldsymbol{T}^{\mathrm{T}}$ gives

$$\boldsymbol{M}_b \ddot{\boldsymbol{w}} + \boldsymbol{C}_b \dot{\boldsymbol{w}} + \boldsymbol{K}_b \boldsymbol{w} = \boldsymbol{f}_b \tag{2.2.25}$$

Herein, the matrices $\boldsymbol{K}_b$ and $\boldsymbol{f}_b$ have the definitions given previously. The reduced mass and damping matrices $\boldsymbol{M}_b$ and $\boldsymbol{C}_b$ are respectively as

$$\boldsymbol{M}_b = \boldsymbol{M}_{11} + \boldsymbol{K}_{\mathrm{A}}^{\mathrm{T}} \boldsymbol{M}_{21} + \boldsymbol{M}_{12} \boldsymbol{K}_{\mathrm{A}} + \boldsymbol{K}_{\mathrm{A}}^{\mathrm{T}} \boldsymbol{M}_{22} \boldsymbol{K}_{\mathrm{A}} \tag{2.2.26}$$

$$\boldsymbol{C}_b = \boldsymbol{C}_{11} + \boldsymbol{K}_{\mathrm{A}}^{\mathrm{T}} \boldsymbol{C}_{21} + \boldsymbol{C}_{12} \boldsymbol{K}_{\mathrm{A}} + \boldsymbol{K}_{\mathrm{A}}^{\mathrm{T}} \boldsymbol{C}_{22} \boldsymbol{K}_{\mathrm{A}} \tag{2.2.27}$$

2.2.6 Simulation of reaction force of piers

In order to investigate environmental problems by means of simulating the site vibration, the accurate reaction forces of the piers of elevated bridges, which will be used as input external excitations in the future analysis of site vibration problems, are demanded. The reaction forces of piers cannot be obtained accurately in modal analysis by means of calculating the shear forces at the end of the piers due to the gibbs phenomenon [13] [14]. Therefore in this study, reaction forces of the piers are calculated using the influence value matrix of reaction force.

For static problems, simply rewrite Eq. (2.2.11) as

$$\begin{Bmatrix} \boldsymbol{S} \\ \boldsymbol{R} \end{Bmatrix} = \begin{bmatrix} \boldsymbol{K}_{\mathrm{S}} & \boldsymbol{K}_{\mathrm{SR}} \\ \boldsymbol{K}_{\mathrm{RS}} & \boldsymbol{K}_{\mathrm{R}} \end{bmatrix} \begin{Bmatrix} \boldsymbol{X} \\ \boldsymbol{\theta} \end{Bmatrix} \tag{2.2.28}$$

where $\boldsymbol{S} = \begin{Bmatrix} \boldsymbol{f} \\ \boldsymbol{m} \end{Bmatrix}$, $\boldsymbol{R} = \begin{Bmatrix} \boldsymbol{f}_{\mathrm{R}} \\ \boldsymbol{m}_{\mathrm{R}} \end{Bmatrix}$, $\boldsymbol{X} = \begin{Bmatrix} \boldsymbol{w} \\ \boldsymbol{\theta} \end{Bmatrix}$

From Eq. (2.2.28) the following relationship can be obtained

$$\boldsymbol{X} = \boldsymbol{K}_S^{-1}\boldsymbol{S} \tag{2.2.29}$$

Then the reaction forces acting on the restrained nodes are

$$\boldsymbol{R} = \boldsymbol{K}_{\mathrm{RS}}\boldsymbol{X} = \boldsymbol{K}_{\mathrm{RS}}\boldsymbol{K}_S^{-1}\boldsymbol{S} = \boldsymbol{K}_{\mathrm{RF}}\boldsymbol{S} \tag{2.2.30}$$

In particular, for the case that no moment forces acting on the nodal points, i.e. $\boldsymbol{m} = \boldsymbol{0}$, according to Eq. (2.2.11), Eq. (2.2.14), (2.2.15) and Eq. (2.2.16), the reaction forces can be expressed separately by only the translational displacements as follows:

$$\boldsymbol{f}_{\mathrm{R}} = \left(\boldsymbol{K}_{31} - \boldsymbol{K}_{32}\boldsymbol{K}_{22}^{-1}\boldsymbol{K}_{21}\right)\boldsymbol{w} \tag{2.2.31}$$

and

$$\boldsymbol{w} = \boldsymbol{K}_b^{-1}\boldsymbol{f} = \left(\boldsymbol{K}_{11} - \boldsymbol{K}_{12}\boldsymbol{K}_{22}^{-1}\boldsymbol{K}_{21}\right)^{-1}\boldsymbol{f} \tag{2.2.32}$$

then

$$\boldsymbol{f}_{\mathrm{R}} = \left(\boldsymbol{K}_{31} - \boldsymbol{K}_{32}\boldsymbol{K}_{22}^{-1}\boldsymbol{K}_{21}\right)\left(\boldsymbol{K}_{11} - \boldsymbol{K}_{12}\boldsymbol{K}_{22}^{-1}\boldsymbol{K}_{21}\right)^{-1}\boldsymbol{f} = \boldsymbol{K}_{\mathrm{RF}}\boldsymbol{f} \tag{2.2.33}$$

similarly

$$\boldsymbol{m}_{\mathrm{R}} = \left(\boldsymbol{K}_{41} - \boldsymbol{K}_{42}\boldsymbol{K}_{22}^{-1}\boldsymbol{K}_{21}\right)\left(\boldsymbol{K}_{11} - \boldsymbol{K}_{12}\boldsymbol{K}_{22}^{-1}\boldsymbol{K}_{21}\right)^{-1}\boldsymbol{f} = \boldsymbol{K}_{\mathrm{RF}}^{*}\boldsymbol{f} \tag{2.2.34}$$

The matrix $\boldsymbol{K}_{\mathrm{RF}}$ or $\boldsymbol{K}^{*}_{\mathrm{RF}}$ is called the influence value matrix of reaction force.

In this study, the dynamic reaction forces at the pier bottoms of the bridge are calculated using the following equation,

$$\boldsymbol{R}(t) = \boldsymbol{K}_{\mathrm{RF}}\left\{\boldsymbol{P}_{vst}(t) + \boldsymbol{P}_{vdy}(t) + \boldsymbol{P}_{sdy}(t)\right\} \tag{2.2.35}$$

Herein, $\boldsymbol{R}(t)$ denotes the reaction force vector. $\boldsymbol{P}_{vst}(t)$, $\boldsymbol{P}_{vdy}(t)$, and $\boldsymbol{P}_{sdy}(t)$, respectively denote vectors of the static components of the wheel loads, the dynamic components of the wheel loads and the inertia force of the structural nodes.

2.3 Eigenvalue analysis [15]

Dynamic equation of the free vibration that neglects the damping effect can be represented as Eq. (2.3.1),

$$\boldsymbol{M}_b \ddot{\boldsymbol{w}}_b + \boldsymbol{K}_b \boldsymbol{w}_b = \boldsymbol{0} \tag{2. 3.1}$$

where, $\boldsymbol{M}_b$ and $\boldsymbol{K}_\mathbf{b}$ are the mass matrix and stiffness matrix of the bridge, respectively. The symbol · indicates the partial differential of time.

Assuming $\boldsymbol{w}_b = e^{jnt}\boldsymbol{\varphi}$, then $\ddot{\boldsymbol{w}}_b = -\boldsymbol{n}^2 \boldsymbol{\varphi} e^{jnt}$ is derived, herein $\boldsymbol{\varphi}$ and $\boldsymbol{n}$ are the vector of natural mode and frequency of the bridge, respectively. Substituting these relations into Eq. (2. 3.1), Eq. (2. 3.2) can be obtained as follows:

$$(\boldsymbol{K}_b - n^2 \boldsymbol{M}_b)\boldsymbol{\varphi} = \boldsymbol{0} \tag{2. 3.2}$$

Consequently, if the natural frequency vector can be calculate through the relationship of $\left|\boldsymbol{K}_b - \boldsymbol{n}^2\ \boldsymbol{M}_b\right| = \boldsymbol{0}$, then the natural mode vector $\boldsymbol{\varphi}$ can be obtained according to Eq. (2. 3.2).

In this study, the eigenvalue analysis is performed using QR method [16] [17]. This method was first pubished in 1961 by J. G. F. Francis and it has since been the subject of intense investigation. The QR method is quite complex in both its theory and application. The detailed description of the method can be found in references.

2.4 Formulization of the bridge-train-earthquake interaction system

In this section, the formulization of the bridge-train-earthquake interaction system will be established, based on which the analytical programs are developed. Cars of the train are idealized as either 2-D or 3-D sprung-mass vibrational systems, assuming that the car body and the bogies are rigid bodies and that they are connected three-dimensionally by scalar spring and damper elements. The viaducts together with the rail structures are modeled as 3-D beam elements and then formulized by finite element approach. Then the coupled dynamic differential equations of bridge-train system subjected to seismic load are derived in consideration of the wheel-track interaction including the rail surface roughness.

2.4.1 Idealization of the bullet train

The interaction problem of the bridge-train system is directly due to the interaction between the moving wheels and rail [18] [19]. To obtain accurate solutions, it is necessary to model the bridge-train system as in detail as possible, such as using detailed train and structural models as well as accurate contact model of the wheel-track interaction. However, such problems are very complicated and need enormous computing capacities, which are still under research. For example, in the filed of vehicle engineering [20], to investigate the exact motion and dynamic characteristics of the train, car models with tens of DOFs are often used. On the other hand, in many cases it is not realistic or necessary to use such detailed models in the filed of civil engineering. The analytical models should be determined considering not only the accuracy demanded but also the analytical efficiency and cost.

In this research, in the cases focusing on the dynamic responses of the viaducts and related site vibration, it has been found that the predominant components are owing to the responses in vertical direction [21] [22]. Therefore it is conceivable that the train model with the DOFs that contribute to the vertical response will be sufficient. In Kawatani et al's researches [23] [24], to investigate the dynamic responses of plate girder bridges, a vehicle model with eight DOFs considering the bouncing, pitching and rolling motions of the body and axles is employed. It was indicated that such a simple vehicle model is sufficient to evaluate the vertical bridge vibration.

On the other hand, in detailed discussion of bridge-train interaction, it is desirable to employ the contact model of wheel-track interaction [25], which is rather complicated and needs proper presumptions. However, the mass of the wheel-sets takes only a small proportion in the whole train system, and it is reported [26] that the variation of the wheel loads was not notable while the train running over a straight-line section under regular

maintenances. Therefore in such cases the variation of the dynamic response of the bridge-train interaction system caused by the motions of wheel-sets can be neglected and the enormous work of modeling the wheel-track contact problem can be avoided. In this research, considering the complexities of modeling the wheel-track interaction and the efficiency of the analysis, the motion of the wheel set is attached to the rail structure. The relative motion between the wheel and the track is assumed small for normal running even under a moderate earthquake. Dynamic interaction between the bridge and train system is considered via calculating momentary wheel loads of the train.

In this study, based on Kawatani et al's vehicle model [23], car models so called two-, six-, nine- and 15-DOF car models (see **Fig. 2.4.1－2.4.4**) are developed for analysis. The two- and six-DOF models are only plane 2-D ones. In the two-DOF model, only the motion of the car body is considered, while the motions of the bogies are also taken into account in the six-DOF model. These models are used to investigate the influence of the bogies' motions on the dynamic response of the bridge, because the mass of the bogies take a considerable proportion in the whole train system and their dynamic effect is considered to be notable. Furthermore, the rolling motions of the car body and the bogies also have significant influence on the dynamic bridge response in vertical direction and should be taken into account. Thus a nine-DOF car model is developed based on Kawatani et al's eight-DOF vehicle model to fully consider the three-dimensional effect of the train dynamics on the vertical response of the bridge. The difference of the bridge response due to the different train models will be discussed in this study to find the rational one [1].

On the other hand, in the case of simulating the horizontal site vibration around the viaducts, it is desirable to use the horizontal dynamic reaction forces of the bridge simultaneously with the vertical ones. The horizontal response of the bridge may affect the site vibration especially in the ambient area around the viaducts. Therefore in this research, a 15-DOF car model is developed [2] based on the former described nine-DOF model by further taking account of the lateral translation and the yawing motion of the car body and bogies. This model can properly simulate not only the vertical motions but also the horizontal vibrations of the train, thus to obtain the lateral response of the bridge.

Furthermore, in the analysis of bridge-train-earthquake interaction analysis, the horizontal responses of both the bridge and the train become the critical ones and the lateral vibrations of the bridge-train system should be simulated appropriately. In this research, for preliminary discussions of the seismic performance of the bridge-train system, the 15-DOf train model is used. Though the relative motion between the wheels and track is considered to be notable under seismic load, the 15-DOF train model still can express the reasonable lateral vibrations of the train [3] provided that the derailment does not occur. In this case, the running safety of

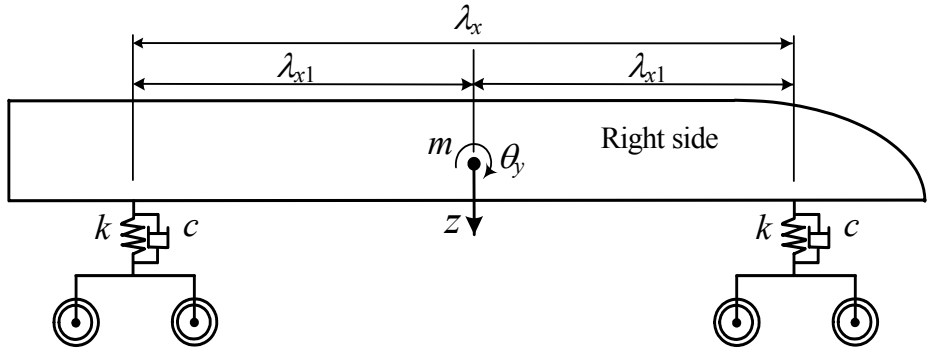

Fig. 2.4.1 two-DOF car model

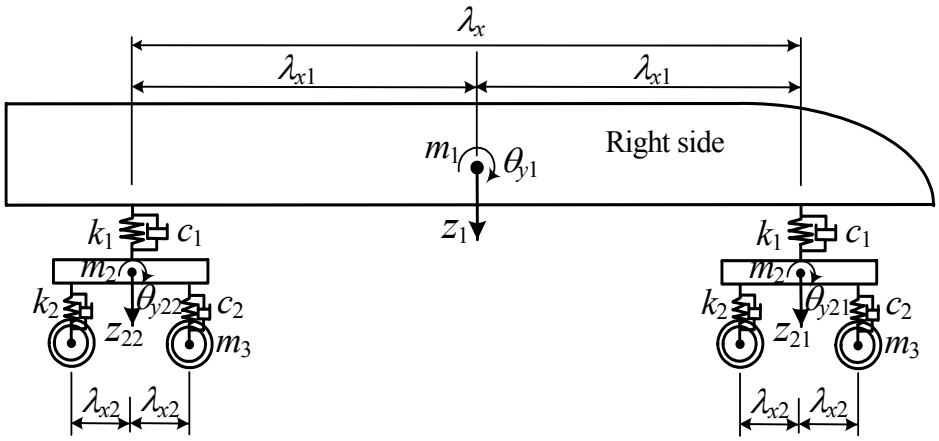

Fig. 2.4.2 six-DOF car model

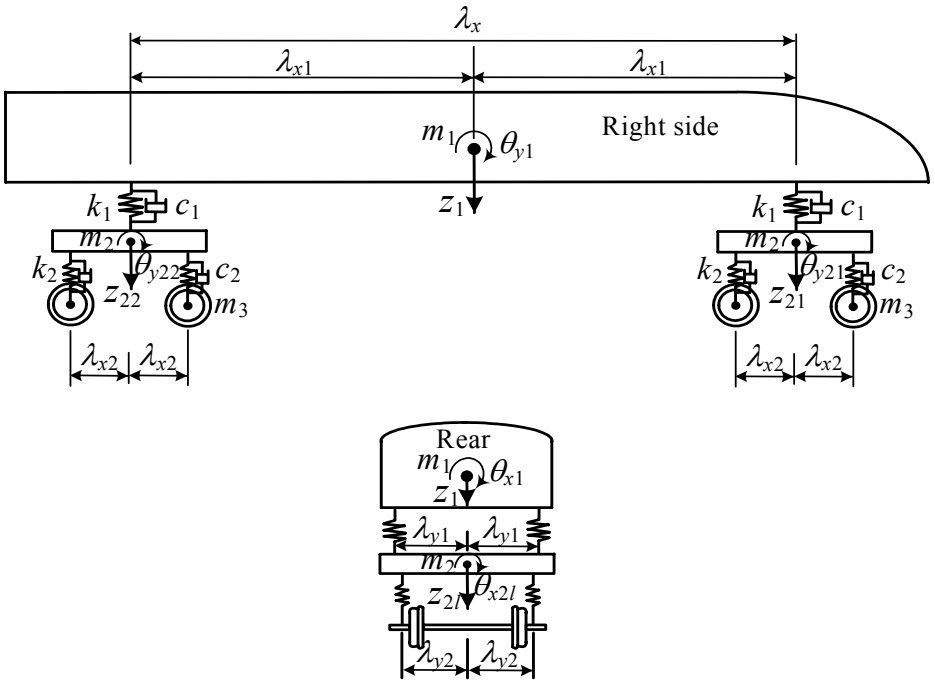

Fig. 2.4.3 nine-DOF car model

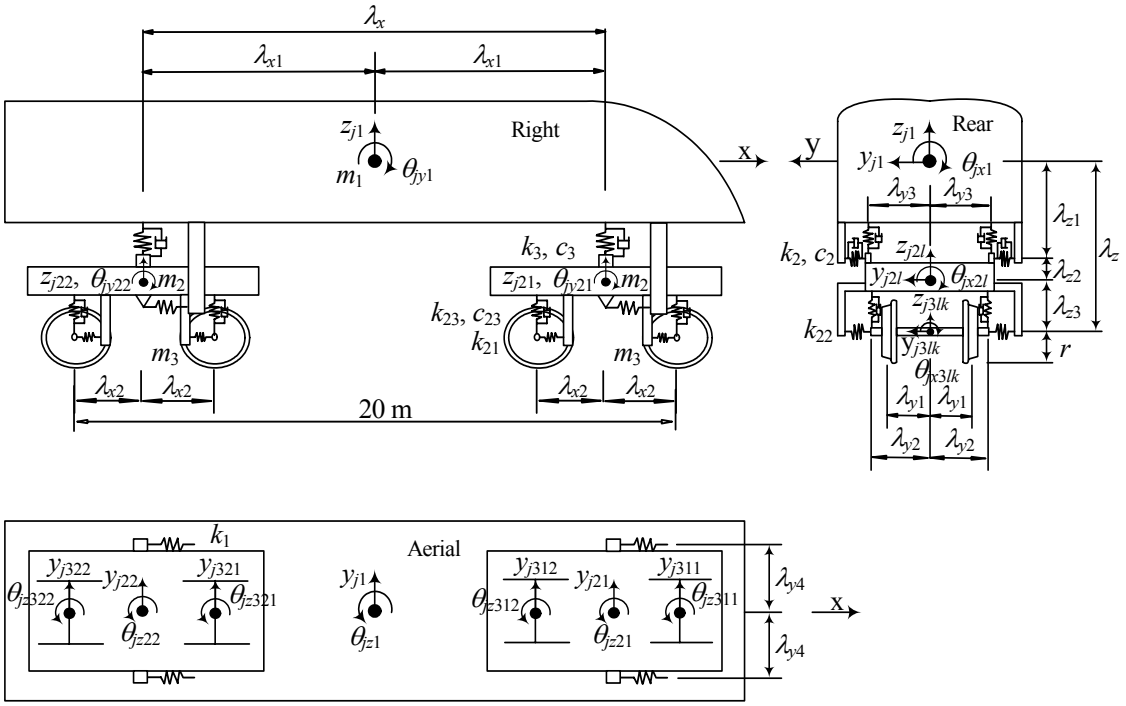

Fig. 2.4.4 15-DOF car model

Table 2.4.1 Variants employed in train system

Definition	Notation
Lateral translation of car body	y_{j1}
Sway of bogie	y_{j2l}
Lateral displacement of wheelset	y_{j3lk}
Bouncing of car body	z_{j1}
Parallel hop of bogie	z_{j2l}
Vertical displacement of wheelset	z_{j3lk}
Rolling of car body	θ_{jx1}
Axle tramp of bogie	θ_{jx2l}
Rolling of wheelset	θ_{jx3lk}
Pitching of car body	θ_{jy1}
Windup of bogie	θ_{jy2l}
Yawing of car body	θ_{jz1}
Yawing of bogie	θ_{jz2l}
Yawing of wheelset	θ_{jz3lk}

Note: j: jth car of train; l = 1, 2: front and rear bogies; k = 1, 2: front and rear wheelsets.

Table 2.4.2 Properties of bullet train

Definition		Notation
Weight	car body	w_1
	bogie	w_2
	wheelset	w_3
Mass moment of inertia	car body	I_{x1}
		I_{y1}
		I_{z1}
	bogie	I_{x2}
		I_{y2}
		I_{z2}
	wheelset	I_{x3}
		I_{z3}
Spring constant	upper	k_1
		k_2
		k_3
	lower	k_{21}
		k_{22}
		k_{23}
Damping coefficient	lateral upper	c_2
	vertical upper	c_3
	vertical lower	c_{23}

Table 2.4.3 Dimension of bullet train

1/2 length of car body in x-direction	λ_c
Distance of centers of bogies in x-direction	λ_x
1/2 distance of centers of bogies in x-direction	λ_{x1}
1/2 distance of axes in x-direction	λ_{x2}
1/2 width of track gauge	λ_{y1}
1/2 distance of vertical lower springs in y-direction	λ_{y2}
1/2 distance of vertical upper springs in y-direction	λ_{y3}
1/2 distance of longitudinal upper springs in y-direction	λ_{y4}
Distance from centroid of body to axis in z-direction	λ_z
Distance from centroid of body to lateral upper spring in z-direction	λ_{z1}
Distance from centroid of bogie to lateral upper spring in z-direction	λ_{z2}
Distance from centroid of bogie to lateral lower spring in z-direction	λ_{z3}
Radius of wheel	r

the train can be examined by derailment coefficient which will be introduced later. The seismic responses of the bridge can be even more rational because the dynamic effect of the car body and bogies is to some extent appropriately considered. However, for more accurate investigations, especially when discussing the derailment phenomenon caused by strong ground motion, it is necessary to simulate the bridge-train interaction with more detailed models [27] such as introducing the wheel-track contact model.

2.4.2 Formulization of the train model

Since the formulizations of two-, six- and nine-DOF car models can be obtained by simplifying the 15-DOF car model, herein only the equations of the 15-DOF car model will be described.

Figure 2.4.4 shows one car of the train modeled as a 15-DOF system. In this model, the sway, bouncing, pitching, rolling and yawing motions of the car body, and the sway, parallel hop, axle windup, axle tramp and yawing motions of the front and rear bogies are considered. The variants employed in the car model are shown in **Table 2.4.1**. The notations of the train properties are indicated in **Table 2.4.2**. The dimension of the car is shown in **Table 2.4.3**.

The formulization of the 15-DOF model is expressed by Eq. (2.4.1) through Eq. (2.4.33).

a) Dynamic differential equations of the car body

y_{j1}--- Lateral translation of the car body

$$m_1\ddot{y}_{j1} - \sum_{l=1}^{2}\sum_{m=1}^{2}(-1)^m v_{jylm}(t) = 0 \tag{2.4.1}$$

z_{j1}--- Bouncing of the car body

$$m_1\ddot{z}_{j1} + \sum_{l=1}^{2}\sum_{m=1}^{2} v_{jzlm}(t) = 0 \tag{2.4.2}$$

θ_{jx1}--- Rolling of the car body

$$I_{x1}\ddot{\theta}_{jx1} - \sum_{l=1}^{2}\sum_{m=1}^{2}(-1)^m \lambda_{y3} v_{jzlm}(t) - \sum_{l=1}^{2}\sum_{m=1}^{2}(-1)^m \lambda_{z1} v_{jylm}(t) = 0 \tag{2.4.3}$$

θ_{jy1}--- Pitching of the car body

$$I_{y1}\ddot{\theta}_{jy1} + \sum_{l=1}^{2}\sum_{m=1}^{2}(-1)^l \lambda_{x1} v_{jzlm}(t) = 0 \tag{2.4.4}$$

θ_{jz1}--- Yawing of the car body

$$I_{z1}\ddot{\theta}_{jz1}+\sum_{l=1}^{2}\sum_{m=1}^{2}(-1)^{l+m}\lambda_{x1}v_{jylm}(t)+\sum_{l=1}^{2}\sum_{m=1}^{2}(-1)^{m}\lambda_{y4}v_{jxlm}(t)=0 \tag{2.4.5}$$

where,

$$v_{jxlm}(t)=k_1\left\{(-1)^{m}\lambda_{y4}\left(\theta_{jz1}-\theta_{jz2l}\right)\right\} \tag{2.4.6}$$

$$\begin{aligned}v_{jylm}(t)=&k_2\left\{-(-1)^{m}y_{j1}-(-1)^{m}\lambda_{z1}\theta_{jx1}+(-1)^{l+m}\lambda_{x1}\theta_{jz1}+(-1)^{m}y_{j2l}-(-1)^{m}\lambda_{z2}\theta_{jx2l}\right\}\\&+c_2\left\{-(-1)^{m}\dot{y}_{j1}-(-1)^{m}\lambda_{z1}\dot{\theta}_{jx1}+(-1)^{l+m}\lambda_{x1}\dot{\theta}_{jz1}+(-1)^{m}\dot{y}_{j2l}-(-1)^{m}\lambda_{z2}\dot{\theta}_{jx2l}\right\}\end{aligned} \tag{2.4.7}$$

$$\begin{aligned}v_{jzlm}(t)=&k_3\left\{z_{j1}+(-1)^{l}\lambda_{x1}\theta_{jy1}-(-1)^{m}\lambda_{y3}\theta_{jx1}-z_{j2l}+(-1)^{m}\lambda_{y3}\theta_{jx2l}\right\}\\&+c_3\left\{\dot{z}_{j1}+(-1)^{l}\lambda_{x1}\dot{\theta}_{jy1}-(-1)^{m}\lambda_{y3}\dot{\theta}_{jx1}-\dot{z}_{j2l}+(-1)^{m}\lambda_{y3}\dot{\theta}_{jx2l}\right\}\end{aligned} \tag{2.4.8}$$

Herein, the subscripts relative to the motion of the car body are described as: l=1, 2 respectively indicate the front and rear bogies; m=1, 2 respectively indicate the left and right sides of the train. j is the sequence number of the car. $v_{jxlm}(t)$, $v_{jylm}(t)$ and $v_{jzlm}(t)$ denote the forces caused by the extension of the upper springs in relative directions, respectively.

b) Dynamic differential equations of the bogies

y_{j2l}--- Sway of the bogie

$$m_2\ddot{y}_{j2l}+\sum_{m=1}^{2}(-1)^{m}v_{jylm}(t)-\sum_{k=1}^{2}\sum_{m=1}^{2}(-1)^{m}v_{jylkm}(t)=0 \tag{2.4.9}$$

z_{j2l} --- Parallel hop of the bogie

$$m_2\ddot{z}_{j2l}-\sum_{m=1}^{2}v_{jzlm}(t)+\sum_{k=1}^{2}\sum_{m=1}^{2}v_{jzlkm}(t)=0 \tag{2.4.10}$$

θ_{jx2l} --- Axle tramp of the bogie

$$\begin{aligned}&I_{x2}\ddot{\theta}_{jx2l}-\sum_{m=1}^{2}(-1)^{m}\lambda_{z2}v_{jylm}(t)+\sum_{m=1}^{2}(-1)^{m}\lambda_{y3}v_{jzlm}(t)\\&-\sum_{k=1}^{2}\sum_{m=1}^{2}(-1)^{m}\lambda_{z3}v_{jylkm}(t)-\sum_{k=1}^{2}\sum_{m=1}^{2}(-1)^{m}\lambda_{y2}v_{jzlkm}(t)=0\end{aligned} \tag{2.4.11}$$

θ_{jy2l} --- Windup motion of the bogie

$$I_{y2}\ddot{\theta}_{jy2l}+\sum_{k=1}^{2}\sum_{m=1}^{2}(-1)^{k}\lambda_{x2}v_{jzlkm}(t)=0 \tag{2.4.12}$$

θ_{jz2l} --- Yawing of the bogie

$$I_{z2}\ddot{\theta}_{jz2l} - \sum_{m=1}^{2}(-1)^m \lambda_{y4} v_{jxlm}(t) + \sum_{k=1}^{2}\sum_{m=1}^{2}(-1)^{k+m} \lambda_{y2} v_{jxlkm}(t) + \sum_{k=1}^{2}\sum_{m=1}^{2}(-1)^{k+m} \lambda_{x2} v_{jylkm}(t) = 0 \tag{2.4.13}$$

where,

$$v_{jxlkm}(t) = k_{21}\left\{(-1)^{k+m} \lambda_{y2}\left(\theta_{jz2l} - \theta_{jz3lk}\right)\right\} \tag{2.4.14}$$

$$v_{jylkm}(t) = k_{22}\left\{-(-1)^m y_{j2l} - (-1)^m \lambda_{z3}\theta_{jx2l} + (-1)^{k+m}\lambda_{x2}\theta_{jz2l} + (-1)^m y_{j3lk}\right\} \tag{2.4.15}$$

$$\begin{aligned} v_{jzlkm}(t) = {} & k_{23}\left\{z_{j2l} - (-1)^m \lambda_{y2}\theta_{jx2l} + (-1)^k \lambda_{x2}\theta_{jy2l} - z_{j3lk} + (-1)^m \lambda_{y2}\theta_{jx3lk}\right\} \\ & + c_{23}\left\{\dot{z}_{j2l} - (-1)^m \lambda_{y2}\dot{\theta}_{jx2l} + (-1)^k \lambda_{x2}\dot{\theta}_{jy2l} - \dot{z}_{j3lk} + (-1)^m \lambda_{y2}\dot{\theta}_{jx3lk}\right\} \end{aligned} \tag{2.4.16}$$

Herein, the subscripts relative to the motion of the bogies are described as: k=1, 2 respectively indicate the front and rear axles of the rear bogie, m=1, 2 respectively indicate the left and right sides of the bogie. $v_{jxlkm}(t)$, $v_{jylkm}(t)$ and $v_{jzlkm}(t)$ denote the forces caused by the extension of the lower springs in relative directions, respectively.

c) Dynamic differential equations of the wheelsets

y_{j3lk}--- Lateral displacement of the wheelset

$$m_3\ddot{y}_{j3lk} + \sum_{m=1}^{2}(-1)^m v_{jylkm}(t) = -\sum_{m=1}^{2} P_{jylkm}(t) \tag{2.4.17}$$

z_{j3lk} --- Vertical displacement of the wheelset

$$m_3\ddot{z}_{j3lk} - \sum_{m=1}^{2} v_{jzlkm}(t) = -\sum_{m=1}^{2} P_{jzlkm}(t) \tag{2.4.18}$$

θ_{jx3lk} --- Rolling of the wheelset

$$I_{x3}\ddot{\theta}_{jx3lk} + \sum_{m=1}^{2}(-1)^m \lambda_{y2} v_{jzlkm}(t) = -r\sum_{m=1}^{2} P_{jylkm}(t) + (-1)^m \lambda_{y1}\sum_{m=1}^{2} P_{jzlkm}(t) \tag{2.4.19}$$

θ_{jz3lk} --- Yawing of the wheelset

$$I_{z3}\ddot{\theta}_{jz3lk} - \sum_{m=1}^{2}(-1)^{k+m} \lambda_{y2} v_{jxlkm}(t) = -(-1)^m \sum_{m=1}^{2} P_{jxlkm}(t) \tag{2.4.20}$$

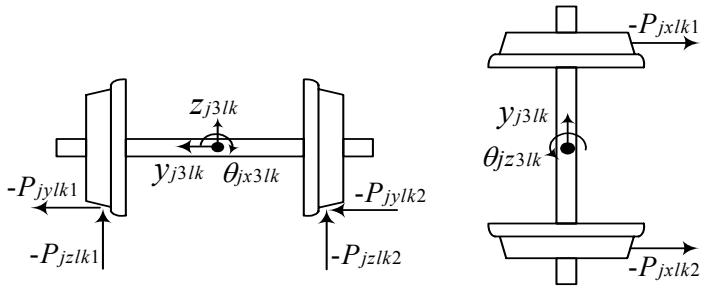

Fig. 2.4.5 Contact forces acting on the wheelset

Herein, $P_{jxlkm}(t)$, $P_{jylkm}(t)$ and $P_{jzlkm}(t)$ respectively represent the dynamic wheel loads acting on the structure in horizontal, vertical and longitudinal directions. The depiction of the reaction forces from the rail treads acting on a wheelset is shown in **Fig. 2.4.5**

Actually, $P_{jxlkm}(t)$ is the creeping force in longitudinal direction between the wheel and rail tread; $P_{jzlkm}(t)$ is the normal contact force; $P_{jylkm}(t)$ is the combination of the horizontal creeping force between the wheel and rail tread and the lateral force due to the contact of wheel flange and track, respectively. $P_{jxlkm}(t)$, $P_{jylkm}(t)$ and $P_{jzlkm}(t)$ can be calculated following the contact theory between the wheel and rail treads, which leads to a complicated simulation process [25].

In the present idealization of the train-bridge interaction system, because of its complication, instead of calculating the contact forces between the wheel and track structure, the motions of the wheelset are determined according to its compatibility with the displacements of the structure at the contact points. Herein, the yawing motion of the wheelset can be ignored (θ_{jz3lk}= 0). The motions of the wheelset are represented as follows.

$$y_{j3lk} = \frac{1}{2}\sum_{m=1}^{2} w_{jylkm} \tag{2.4.21}$$

$$z_{j3lk} = \frac{1}{2}\sum_{m=1}^{2} w_{jzlkm} \tag{2.4.22}$$

$$\theta_{jx3lk} = -(-1)^m \frac{1}{2\lambda_{y1}}\sum_{m=1}^{2} w_{jzlkm} \tag{2.4.23}$$

The variables w_{jylkm} and w_{jzlkm} denote the sum of the displacement and surface roughness of the rail in y and z-direction, respectively.

$$w_{jylkm} = w_y(t, x_{jlkm}) + z_{0y}(x_{jlkm}) \tag{2.4.24}$$

$$w_{jzlkm} = w_z(t, x_{jlkm}) + z_{0z}(x_{jlkm}) \tag{2.4.25}$$

where, $w_y(t, x_{jlkm})$ and $w_z(t, x_{jlkm})$ are the displacements of the rail at the contact points of the wheel and the rail in y and z-direction, respectively; and $z_{0y}(x_{jlkm})$ and $z_{0z}(x_{jlkm})$ represent the rail surface roughness in y and z-direction, respectively.

$$w_y\left(t, x_{jlkm}\right) = \boldsymbol{\Psi}_{jylkm}^T(t)\boldsymbol{w}_b \tag{2.4.26}$$

$$w_z\left(t, x_{jlkm}\right) = \boldsymbol{\Psi}_{jzlkm}^T(t)\boldsymbol{w}_b \tag{2.4.27}$$

Herein, $\boldsymbol{\Psi}_{jylkm}(t)$ and $\boldsymbol{\Psi}_{jzlkm}(t)$ respectively represent the distribution vectors of y and z-directions that distribute the wheel loads to the ends of the beam elements, and $\boldsymbol{w}_b$ denotes the nodal displacement vector of the finite element bridge model.

$$\boldsymbol{\Psi}_{jylkm}(t) = \left\{0;\cdots;0;\psi_{p,jlkm};\psi_{p+1,jlkm};0;\cdots;0\right\}^T \tag{2.4.28}$$

$$\boldsymbol{\Psi}_{jzlkm}(t) = \left\{0;\cdots;0;\psi_{q,jlkm};\psi_{q+1,jlkm};0;\cdots;0\right\}^T \tag{2.4.29}$$

Expanding the equations described above, the differential equations of the train system can be expressed in matrix form as Eq. (2.4.30), without considering the earthquake load.

$$\boldsymbol{M}_v\ddot{\boldsymbol{w}}_v + \boldsymbol{C}_v\dot{\boldsymbol{w}}_v + \boldsymbol{K}_v\boldsymbol{w}_v = \boldsymbol{f}_v \tag{2.4.30}$$

Therein, $\boldsymbol{M}_v$, $\boldsymbol{C}_v$, $\boldsymbol{K}_v$ and $\boldsymbol{f}_v$ respectively denote the mass, damping, stiffness matrices and the external force vector of the train system.

Assuming the ground acceleration vector acting on all DOFs of the train model as $\ddot{\boldsymbol{\Delta}}_v$, the equation of the bridge system subjected to seismic load can be represented as follows:

$$\boldsymbol{M}_v\ddot{\boldsymbol{w}}_v + \boldsymbol{C}_v\dot{\boldsymbol{w}}_v + \boldsymbol{K}_v\boldsymbol{w}_v = \boldsymbol{f}_v - \boldsymbol{M}_v\ddot{\boldsymbol{\Delta}}_v \tag{2.4.31}$$

Assuming the ground acceleration in y and z-directions, respectively as $\ddot{\delta}_y(t)$ and $\ddot{\delta}_z(t)$, the wheel loads acting on the bridge, $P_{jylkm}(t)$ and $P_{jzlkm}(t)$, are represented as follows:

$$P_{jylkm}(t) = -\frac{1}{2}m_3\ddot{w}_{jylkm} - \frac{1}{2}m_3\ddot{\delta}_y(t) - (-1)^m v_{jylkm}(t) \tag{2.4.32}$$

$$P_{jzlkm}(t) = -\left(\frac{1}{8}m_1 g + \frac{1}{4}m_2 g + \frac{1}{2}m_3 g\right) - \frac{1}{2}m_3\ddot{w}_{jzlkm} - \frac{1}{2}m_3\ddot{\delta}_z(t) + v_{jzlkm}(t) \tag{2.4.33}$$

2.4.3 Modal analytical procedure for the bridge system

Assuming the ground acceleration vector acting on all DOFs of the bridge model as $\ddot{\boldsymbol{\Delta}}_b$, the differential equation of the bridge is derived as follows, based on D'Alembert's Principle.

$$\boldsymbol{M}_b\ddot{\boldsymbol{w}}_b + \boldsymbol{C}_b\dot{\boldsymbol{w}}_b + \boldsymbol{K}_b\boldsymbol{w}_b = \boldsymbol{f}_b - \boldsymbol{M}_b\ddot{\boldsymbol{\Delta}}_b \tag{2.4.34}$$

where, $\boldsymbol{M}_b$, $\boldsymbol{C}_b$ and $\boldsymbol{K}_b$ denote mass, damping and stiffness matrices of the bridge system, respectively.

Herein, the damping matrix of bridge $\boldsymbol{C}_b$ is assumed to be calculated by the linear relation between mass and stiffness matrices [28] as follows:

$$\boldsymbol{C}_b = p_1\boldsymbol{M}_b + p_2\boldsymbol{K}_b \tag{2.4.35}$$

where, p_1 and p_2 are the ratio coefficients.

$$p_1 = \frac{2\omega_{b1}\omega_{b2}\left(h_{b1}\omega_{b2} - h_{b2}\omega_{b1}\right)}{\omega_{b2}^2 - \omega_{b1}^2} \tag{2.4.36}$$

$$p_2 = \frac{2\left(h_{b2}\omega_{b2} - h_{b1}\omega_{b1}\right)}{\omega_{b2}^2 - \omega_{b1}^2} \tag{2.4.37}$$

Herein, ω_{b1} and ω_{b2} respectively denote the first and second natural circular frequencies of the bridge model; h_{b1} and h_{b2} is the damping constants corresponding to ω_{b1} and ω_{b2}, respectively.

Assuming the total number of cars as h, the external force vector $\boldsymbol{f}_b$ can be represented as follows:

$$\boldsymbol{f_b} = \sum_{j=1}^{h}\sum_{l=1}^{2}\sum_{k=1}^{2}\sum_{m=1}^{2}\left\{\boldsymbol{\Psi}_{jylkm}(t)P_{jylkm}(t) + \boldsymbol{\Psi}_{jzlkm}(t)P_{jzlkm}(t)\right\} \tag{2.4.38}$$

where, $P_{jylkm}(t)$ and $P_{jzlkm}(t)$ are the wheel loads of the train and $\boldsymbol{\Psi}_{jylkm}(t)$ and $\boldsymbol{\Psi}_{jzlkm}(t)$ are the distribution vectors.

The vector of nodal displacement of the bridge, $\boldsymbol{w}_b$, is derived from modal analysis method and represented as follows.

$$\boldsymbol{w}_b = \sum_{i=1}^{n}\boldsymbol{\varphi}_i q_i = \boldsymbol{\Phi}\cdot\boldsymbol{q} \tag{2.4.39}$$

where, $\boldsymbol{q}$ is the generalized coordinate vector of the bridge and $\boldsymbol{\Phi}$ is the modal matrix composed of the natural modal vector of the bridge $\boldsymbol{\varphi}_i$.

$$\boldsymbol{q} = \{q_1 \quad q_2 \quad \cdots \quad q_n\}^T \tag{2.4.40}$$

$$\boldsymbol{\Phi} = \{\boldsymbol{\varphi}_1, \quad \boldsymbol{\varphi}_2, \quad \cdots, \quad \boldsymbol{\varphi}_n\} = \begin{bmatrix} \phi_{11} & \phi_{12} & \cdots & \phi_{1n} \\ \phi_{21} & \ddots & & \vdots \\ \vdots & & \ddots & \vdots \\ \phi_{m1} & \cdots & \cdots & \phi_{mn} \end{bmatrix} \tag{2.4.41}$$

Herein, the subscript m indicates the number of freedoms of the bridge finite element model after matrix condensation, and n denotes the highest mode number considered in the analysis.

Substituting $\boldsymbol{w}_b$ into Eq. (2.4.34), the following equation can be derived,

$$\boldsymbol{M}_b\boldsymbol{\Phi}\ddot{\boldsymbol{q}} + \boldsymbol{C}_b\boldsymbol{\Phi}\dot{\boldsymbol{q}} + \boldsymbol{K}_b\boldsymbol{\Phi}\boldsymbol{q} = \boldsymbol{f}_b - \boldsymbol{M}_b\ddot{\boldsymbol{\Delta}}_b \tag{2.4.42}$$

Multiplying both sides by $\boldsymbol{\Phi}^T$, the following equation is derived,

$$\boldsymbol{\Phi}^T\boldsymbol{M}_b\boldsymbol{\Phi}\ddot{\boldsymbol{q}} + \boldsymbol{\Phi}^T\boldsymbol{C}_b\boldsymbol{\Phi}\dot{\boldsymbol{q}} + \boldsymbol{\Phi}^T\boldsymbol{K}_b\boldsymbol{\Phi}\boldsymbol{q} = \boldsymbol{\Phi}^T\boldsymbol{f}_b - \boldsymbol{\Phi}^T\boldsymbol{M}_b\ddot{\boldsymbol{\Delta}}_b \tag{2.4.43}$$

Herein,

$$\boldsymbol{\Phi}^T = \begin{Bmatrix} \boldsymbol{\varphi}_1 \\ \boldsymbol{\varphi}_2 \\ \vdots \\ \boldsymbol{\varphi}_n \end{Bmatrix} = \begin{bmatrix} \phi_{11} & \phi_{21} & \cdots & \phi_{m1} \\ \phi_{12} & \ddots & & \vdots \\ \vdots & & \ddots & \vdots \\ \phi_{1n} & \cdots & \cdots & \phi_{mn} \end{bmatrix} \tag{2.4.44}$$

According to the orthogonality of the normal modal vectors, and that $\boldsymbol{C}_b$ is linearly composed of $\boldsymbol{M}_b$ and $\boldsymbol{K}_b$,

while $i \neq j$,

$$\boldsymbol{\varphi}_i^T\boldsymbol{M}_b\boldsymbol{\varphi}_i = 0, \qquad \boldsymbol{\varphi}_i^T\boldsymbol{K}_b\boldsymbol{\varphi}_i = 0, \qquad \boldsymbol{\varphi}_i^T\boldsymbol{C}_b\boldsymbol{\varphi}_i = 0$$

while $i = j$,

$$\boldsymbol{\varphi}_i^T\boldsymbol{M}_b\boldsymbol{\varphi}_i = M_i, \qquad \boldsymbol{\varphi}_i^T\boldsymbol{K}_b\boldsymbol{\varphi}_i = K_i, \qquad \boldsymbol{\varphi}_i^T\boldsymbol{C}_b\boldsymbol{\varphi}_i = C_i$$

Assuming $\boldsymbol{\Phi}^T\boldsymbol{f}_b - \boldsymbol{\Phi}^T\boldsymbol{M}_b\ddot{\boldsymbol{\Delta}}_b = f_i$, the dynamic differential equation of the elevated bridge with respect to generalized coordinate can be developed as follows:

$$M_i\ddot{q}_i + C_i\dot{q}_i + K_iq_i = f_i \tag{2.4.45}$$

2.4.4 Coupled equation of bridge-train-earthquake system in matrix form

Based on the formulization developed in Section 2.2.2 and Section 2.2.3, the coupled equation of bridge-train interaction system can be expressed in matrix form as follows. Herein, to simplify the problem, the wheel inertia is ignored.

$$\begin{bmatrix} \boldsymbol{M}_b^* & \boldsymbol{0} \\ Sym. & \boldsymbol{M}_v \end{bmatrix} \begin{Bmatrix} \ddot{\boldsymbol{q}}_b \\ \ddot{\boldsymbol{w}}_v \end{Bmatrix} + \begin{bmatrix} \boldsymbol{C}_b^* & \boldsymbol{C}_{bv} \\ Sym. & \boldsymbol{C}_v \end{bmatrix} \begin{Bmatrix} \dot{\boldsymbol{q}}_b \\ \dot{\boldsymbol{w}}_v \end{Bmatrix} + \begin{bmatrix} \boldsymbol{K}_b^* & \boldsymbol{K}_{bv} \\ Sym. & \boldsymbol{K}_v \end{bmatrix} \begin{Bmatrix} \boldsymbol{q}_b \\ \boldsymbol{w}_v \end{Bmatrix} = \begin{Bmatrix} \boldsymbol{F}_b \\ \boldsymbol{F}_v \end{Bmatrix} \tag{2.4.46}$$

where, $\boldsymbol{M}_b^*$, $\boldsymbol{C}_b^*$ and $\boldsymbol{K}_b^*$, respectively denote the mass, damping and stiffness components corresponding to the generalized coordinate of the bridge system; $\boldsymbol{M}_v$, $\boldsymbol{C}_v$ and $\boldsymbol{K}_v$, respectively denote the mass, damping and stiffness components corresponding to the DOF of the train system; $\boldsymbol{C}_{bv}$ and $\boldsymbol{K}_{bv}$, respectively denote the coupled damping and stiffness components between the bridge and train systems.

$$\boldsymbol{M}_b^* = \begin{bmatrix} m_{b1} & & & & \boldsymbol{0} \\ & \ddots & & & \\ & & m_{bi} & & \\ & & & \ddots & \\ \boldsymbol{0} & & & & m_{bn} \end{bmatrix}, \qquad \boldsymbol{C}_b^* = \begin{bmatrix} c_{11} & \cdots & c_{1g} & \cdots & c_{1n} \\ \vdots & \ddots & \vdots & & \vdots \\ c_{i1} & \cdots & c_{ig} & \cdots & c_{in} \\ \vdots & & \vdots & \ddots & \vdots \\ c_{n1} & \cdots & c_{ng} & \cdots & c_{nn} \end{bmatrix}$$

$$\boldsymbol{K}_b^* = \begin{bmatrix} k_{11} & \cdots & k_{1g} & \cdots & k_{1n} \\ \vdots & \ddots & \vdots & & \vdots \\ k_{i1} & \cdots & k_{ig} & \cdots & k_{in} \\ \vdots & & \vdots & \ddots & \vdots \\ k_{n1} & \cdots & k_{ng} & \cdots & k_{nn} \end{bmatrix}, \qquad \boldsymbol{q}_b = \begin{Bmatrix} q_1 \\ \vdots \\ q_i \\ \vdots \\ q_n \end{Bmatrix}, \qquad \boldsymbol{F}_b = \begin{Bmatrix} f_1 \\ \vdots \\ f_i \\ \vdots \\ f_n \end{Bmatrix}$$

$$\boldsymbol{M}_v = \begin{bmatrix} \boldsymbol{M}_{v1} & & & & \boldsymbol{0} \\ & \ddots & & & \\ & & \boldsymbol{M}_{vj} & & \\ & & & \ddots & \\ \boldsymbol{0} & & & & \boldsymbol{M}_{vh} \end{bmatrix}, \qquad \boldsymbol{C}_v = \begin{bmatrix} \boldsymbol{C}_{v1} & & & & \boldsymbol{0} \\ & \ddots & & & \\ & & \boldsymbol{C}_{vj} & & \\ & & & \ddots & \\ \boldsymbol{0} & & & & \boldsymbol{C}_{vh} \end{bmatrix}$$

$$\boldsymbol{K}_v = \begin{bmatrix} \boldsymbol{K}_{v1} & & & \widetilde{\boldsymbol{0}} \\ & \ddots & & \\ & & \boldsymbol{K}_{vj} & \\ & & & \ddots \\ \widetilde{\boldsymbol{0}} & & & \boldsymbol{K}_{vh} \end{bmatrix}, \qquad \boldsymbol{w}_v = \begin{Bmatrix} \boldsymbol{w}_{v1} \\ \vdots \\ \boldsymbol{w}_{vj} \\ \vdots \\ \boldsymbol{w}_{vh} \end{Bmatrix}, \qquad \boldsymbol{F}_v = \begin{Bmatrix} \boldsymbol{F}_{v1} \\ \vdots \\ \boldsymbol{F}_{vj} \\ \vdots \\ \boldsymbol{F}_{vh} \end{Bmatrix}$$

$$\boldsymbol{C}_{bv} = \begin{bmatrix} c_{1A1} & \cdots & c_{iA1} & \cdots & c_{nA1} \\ \vdots & & \vdots & & \vdots \\ c_{1Aj} & \cdots & c_{iAj} & \cdots & c_{nAj} \\ c_{1Bj} & \cdots & c_{iBj} & \cdots & c_{nBj} \\ c_{1Cj} & \cdots & c_{iCj} & \cdots & c_{nCj} \\ c_{1Dj} & \cdots & c_{iDj} & \cdots & c_{nDj} \\ c_{1Ej} & \cdots & c_{iEj} & \cdots & c_{nEj} \\ c_{1Fj} & \cdots & c_{iFj} & \cdots & c_{nFj} \\ c_{1Gj} & \cdots & c_{iGj} & \cdots & c_{nGj} \\ c_{1Hj} & \cdots & c_{iHj} & \cdots & c_{nHj} \\ c_{1Ij} & \cdots & c_{iIj} & \cdots & c_{nIj} \\ c_{1Jj} & \cdots & c_{iJj} & \cdots & c_{nJj} \\ c_{1Kj} & \cdots & c_{iKj} & \cdots & c_{nKj} \\ c_{1Lj} & \cdots & c_{iLj} & \cdots & c_{nLj} \\ c_{1Mj} & \cdots & c_{iMj} & \cdots & c_{nMj} \\ c_{1Nj} & \cdots & c_{iNj} & \cdots & c_{nNj} \\ c_{1Oj} & \cdots & c_{iOj} & \cdots & c_{nOj} \\ \vdots & & \vdots & & \vdots \\ c_{1Oh} & \cdots & c_{iOh} & \cdots & c_{nOh} \end{bmatrix}^T$$

$$\boldsymbol{K}_{bv} = \begin{bmatrix} k_{1A1} & \cdots & k_{iA1} & \cdots & k_{nA1} \\ \vdots & & \vdots & & \vdots \\ k_{1Aj} & \cdots & k_{iAj} & \cdots & k_{nAj} \\ k_{1Bj} & \cdots & k_{iBj} & \cdots & k_{nBj} \\ k_{1Cj} & \cdots & k_{iCj} & \cdots & k_{nCj} \\ k_{1Dj} & \cdots & k_{iDj} & \cdots & k_{nDj} \\ k_{1Ej} & \cdots & k_{iEj} & \cdots & k_{nEj} \\ k_{1Fj} & \cdots & k_{iFj} & \cdots & k_{nFj} \\ k_{1Gj} & \cdots & k_{iGj} & \cdots & k_{nGj} \\ k_{1Hj} & \cdots & k_{iHj} & \cdots & k_{nHj} \\ k_{1Ij} & \cdots & k_{iIj} & \cdots & k_{nIj} \\ k_{1Jj} & \cdots & k_{iJj} & \cdots & k_{nJj} \\ k_{1Kj} & \cdots & k_{iKj} & \cdots & k_{nKj} \\ k_{1Lj} & \cdots & k_{iLj} & \cdots & k_{nLj} \\ k_{1Mj} & \cdots & k_{iMj} & \cdots & k_{nMj} \\ k_{1Nj} & \cdots & k_{iNj} & \cdots & k_{nNj} \\ k_{1Oj} & \cdots & k_{iOj} & \cdots & k_{nOj} \\ \vdots & & \vdots & & \vdots \\ k_{1Oh} & \cdots & k_{iOh} & \cdots & k_{nOh} \end{bmatrix}^T$$

Herein,

$$\boldsymbol{w}_{vj}{}^T = \left\{ y_{j1} \quad z_{j1} \quad \theta_{jx1} \quad \theta_{jy1} \quad \theta_{jz1} \quad y_{j21} \quad z_{j21} \quad \theta_{jx21} \quad \theta_{jy21} \quad \theta_{jz21} \quad y_{j22} \quad z_{j22} \quad \theta_{jx22} \quad \theta_{jy22} \quad \theta_{jz22} \right\}$$

$$\boldsymbol{F}_{vj}{}^T = \left\{ f_{Aj} \quad f_{Bj} \quad f_{Cj} \quad f_{Dj} \quad f_{Ej} \quad f_{Fj} \quad f_{Gj} \quad f_{Hj} \quad f_{Ij} \quad f_{Jj} \quad f_{Kj} \quad f_{Lj} \quad f_{Mj} \quad f_{Nj} \quad f_{Oj} \right\}$$

$$\boldsymbol{M}_{vj} = \begin{bmatrix} m_{Aj} & & & & & & & & & & & & & \\ & m_{Bj} & & & & & & & & & & & & \\ & & m_{Cj} & & & & & & & & & & & \\ & & & m_{Dj} & & & & & & & & & & \\ & & & & m_{Ej} & & & & & & & & & \\ & & & & & m_{Fj} & & & & & & & & \\ & & & & & & m_{Gj} & & & & & & & \\ & & & & & & & m_{Hj} & & & & & & \\ & & & & & & & & m_{Ij} & & & & & \\ & & & & & & & & & m_{Jj} & & & & \\ & & & & & & & & & & m_{Kj} & & & \\ & & & & & & & & & & & m_{Lj} & & \\ & & & & & & & & & & & & m_{Mj} & \\ & & & & & & & & & & & & & m_{Nj} \\ & & & & & & & & & & & & & & m_{Oj} \end{bmatrix}$$

$$\boldsymbol{C}_{vj} = \begin{bmatrix} c_{AAj} & c_{ABj} & c_{ACj} & c_{ADj} & c_{AEj} & c_{AFj} & c_{AGj} & c_{AHj} & c_{AIj} & c_{AJj} & c_{AKj} & c_{ALj} & c_{AMj} & c_{ANj} & c_{AOj} \\ & c_{BBj} & c_{BCj} & c_{BDj} & c_{BEj} & c_{BFj} & c_{BGj} & c_{BHj} & c_{BIj} & c_{BJj} & c_{BKj} & c_{BLj} & c_{BMj} & c_{BNj} & c_{BOj} \\ & & c_{CCj} & c_{CDj} & c_{CEj} & c_{CFj} & c_{CGj} & c_{CHj} & c_{CIj} & c_{CJj} & c_{CKj} & c_{CLj} & c_{CMj} & c_{CNj} & c_{COj} \\ & & & c_{DDj} & c_{DEj} & c_{DFj} & c_{DGj} & c_{DHj} & c_{DIj} & c_{DJj} & c_{DKj} & c_{DLj} & c_{DMj} & c_{DNj} & c_{DOj} \\ & & & & c_{EEj} & c_{EFj} & c_{EGj} & c_{EHj} & c_{EIj} & c_{EJj} & c_{EKj} & c_{ELj} & c_{EMj} & c_{ENj} & c_{EOj} \\ & & & & & c_{FFj} & c_{FGj} & c_{FHj} & c_{FIj} & c_{FJj} & c_{FKj} & c_{FLj} & c_{FMj} & c_{FNj} & c_{FOj} \\ & & & & & & c_{GGj} & c_{GHj} & c_{GIj} & c_{GJj} & c_{GKj} & c_{GLj} & c_{GMj} & c_{GNj} & c_{GOj} \\ & & & & & & & c_{HHj} & c_{HIj} & c_{HJj} & c_{HKj} & c_{HLj} & c_{HMj} & c_{HNj} & c_{HOj} \\ & & & & & & & & c_{IIj} & c_{IJj} & c_{IKj} & c_{ILj} & c_{IMj} & c_{INj} & c_{IOj} \\ & & & & & & & & & c_{JJj} & c_{JKj} & c_{JLj} & c_{JMj} & c_{JNj} & c_{JOj} \\ & & & Sym & & & & & & & c_{KKj} & c_{KLj} & c_{KMj} & c_{KNj} & c_{KOj} \\ & & & & & & & & & & & c_{LLj} & c_{LMj} & c_{LNj} & c_{LOj} \\ & & & & & & & & & & & & c_{MMj} & c_{MNj} & c_{MOj} \\ & & & & & & & & & & & & & c_{NNj} & c_{NOj} \\ & & & & & & & & & & & & & & c_{OOj} \end{bmatrix}$$

$$\boldsymbol{K}_{vj} = \begin{bmatrix} k_{AAj} & k_{ABj} & k_{ACj} & k_{ADj} & k_{AEj} & k_{AFj} & k_{AGj} & k_{AHj} & k_{AIj} & k_{AJj} & k_{AKj} & k_{ALj} & k_{AMj} & k_{ANj} & k_{AOj} \\ & k_{BBj} & k_{BCj} & k_{BDj} & k_{BEj} & k_{BFj} & k_{BGj} & k_{BHj} & k_{BIj} & k_{BJj} & k_{BKj} & k_{BLj} & k_{BMj} & k_{BNj} & k_{BOj} \\ & & k_{CCj} & k_{CDj} & k_{CEj} & k_{CFj} & k_{CGj} & k_{CHj} & k_{CIj} & k_{CJj} & k_{CKj} & k_{CLj} & k_{CMj} & k_{CNj} & k_{COj} \\ & & & k_{DDj} & k_{DEj} & k_{DFj} & k_{DGj} & k_{DHj} & k_{DIj} & k_{DJj} & k_{DKj} & k_{DLj} & k_{DMj} & k_{DNj} & k_{DOj} \\ & & & & k_{EEj} & k_{EFj} & k_{EGj} & k_{EHj} & k_{EIj} & k_{EJj} & k_{EKj} & k_{ELj} & k_{EMj} & k_{ENj} & k_{EOj} \\ & & & & & k_{FFj} & k_{FGj} & k_{FHj} & k_{FIj} & k_{FJj} & k_{FKj} & k_{FLj} & k_{FMj} & k_{FNj} & k_{FOj} \\ & & & & & & k_{GGj} & k_{GHj} & k_{GIj} & k_{GJj} & k_{GKj} & k_{GLj} & k_{GMj} & k_{GNj} & k_{GOj} \\ & & & & & & & k_{HHj} & k_{HIj} & k_{HJj} & k_{HKj} & k_{HLj} & k_{HMj} & k_{HNj} & k_{HOj} \\ & & & & & & & & k_{IIj} & k_{IJj} & k_{IKj} & k_{ILj} & k_{IMj} & k_{INj} & k_{IOj} \\ & & & & & & & & & k_{JJj} & k_{JKj} & k_{JLj} & k_{JMj} & k_{JNj} & k_{JOj} \\ & & & Sym & & & & & & & k_{KKj} & k_{KLj} & k_{KMj} & k_{KNj} & k_{KOj} \\ & & & & & & & & & & & k_{LLj} & k_{LMj} & k_{LNj} & k_{LOj} \\ & & & & & & & & & & & & k_{MMj} & k_{MNj} & k_{MOj} \\ & & & & & & & & & & & & & k_{NNj} & k_{NOj} \\ & & & & & & & & & & & & & & k_{OOj} \end{bmatrix}$$

2.4.5 Direct integration procedure for the bridge system

For strong ground motions, because the response of the bridge-train system is non-linear, modal analysis is no longer able to be applied. The dynamic differential equations should be solved by direct integration method. Moreover, in each integral time interval, convergent calculation is required because unbalance force occurs due to the non-linearity of the structural stiffness. Therefore, it is necessary to treat the train and the bridge as separated systems, while it is possible to treat the bridge and the train as an integrated system in linear analysis. In this study, for the direct integration approach, the independence of the train and the bridge systems is realized by considering their effects on each other as external forces.

Based on the formulization developed in Section 2.4.4, the bridge-train interaction can be derived as follows for direct integration approach, by eliminating the modal expressions.

The dynamic differential equation of elevated bridge is derived as follows:

$$\boldsymbol{M}_b\ddot{\boldsymbol{w}}_b + \boldsymbol{C}_b^{*}\dot{\boldsymbol{w}}_b + \boldsymbol{K}_b^{*}\boldsymbol{w}_b = \boldsymbol{F}_b \tag{2.4.46}$$

where,

$$\boldsymbol{C}_b^{*} = \boldsymbol{C}_b + \sum_{j=1}^{h}\sum_{l=1}^{2}\sum_{k=1}^{2}\sum_{m=1}^{2}\boldsymbol{\Psi}_{jzlkm}(t)c_{23}\boldsymbol{\Psi}_{jzlkm}^{T}(t)$$

$$\boldsymbol{K}_b^{*} = \boldsymbol{K}_b + \sum_{j=1}^{h}\sum_{l=1}^{2}\sum_{k=1}^{2}\sum_{m=1}^{2}\left[\boldsymbol{\Psi}_{jylkm}(t)k_{22}\boldsymbol{\Psi}_{jylkm}^{T}(t) + \boldsymbol{\Psi}_{jzlkm}(t)k_{23}\boldsymbol{\Psi}_{jzlkm}^{T}(t)\right]$$

$$\begin{aligned}
\boldsymbol{F}_b = {} & -\boldsymbol{M}_b\ddot{\boldsymbol{\Delta}}_b - \sum_{j=1}^{h}\sum_{l=1}^{2}\sum_{k=1}^{2}\sum_{m=1}^{2}\boldsymbol{\Psi}_{jzlkm}(t)\left(\frac{1}{8}m_1g + \frac{1}{4}m_2g + \frac{1}{2}m_3g\right) \\
& - \sum_{j=1}^{h}\sum_{l=1}^{2}\sum_{k=1}^{2}\sum_{m=1}^{2}\boldsymbol{\Psi}_{jylkm}(t)\frac{1}{2}m_3\ddot{z}_{0y}(x_{jlkm}) - \sum_{j=1}^{h}\sum_{l=1}^{2}\sum_{k=1}^{2}\sum_{m=1}^{2}\boldsymbol{\Psi}_{jylkm}(t)\frac{1}{2}m_3\ddot{\delta}_y(t) - \sum_{j=1}^{h}\sum_{l=1}^{2}\sum_{k=1}^{2}\sum_{m=1}^{2}\boldsymbol{\Psi}_{jzlkm}(t)\frac{1}{2}m_3\ddot{\delta}_z(t) \\
& - \sum_{j=1}^{h}\sum_{l=1}^{2}\sum_{k=1}^{2}\sum_{m=1}^{2}\boldsymbol{\Psi}_{jylkm}(t)k_{22}z_{0y}(x_{jlkm}) - \sum_{j=1}^{h}\sum_{l=1}^{2}\sum_{k=1}^{2}\sum_{m=1}^{2}\boldsymbol{\Psi}_{jzlkm}(t)k_{23}z_{0z}(x_{jlkm}) - \sum_{j=1}^{h}\sum_{l=1}^{2}\sum_{k=1}^{2}\sum_{m=1}^{2}\boldsymbol{\Psi}_{jzlkm}(t)c_{23}\dot{z}_{0z}(x_{jlkm}) \\
& + \sum_{j=1}^{h}\sum_{l=1}^{2}\sum_{k=1}^{2}\sum_{m=1}^{2}\boldsymbol{\Psi}_{jylkm}(t)k_{22}y_{j2l} + \sum_{j=1}^{h}\sum_{l=1}^{2}\sum_{k=1}^{2}\sum_{m=1}^{2}\boldsymbol{\Psi}_{jzlkm}(t)k_{23}z_{j2l} - \sum_{j=1}^{h}\sum_{l=1}^{2}\sum_{k=1}^{2}\sum_{m=1}^{2}\left\{(-1)^m\boldsymbol{\Psi}_{jzlkm}(t)k_{23}\lambda_{y2} - \boldsymbol{\Psi}_{jylkm}(t)k_{22}\lambda_{z3}\right\}\theta_{jx2l} \\
& + \sum_{j=1}^{h}\sum_{l=1}^{2}\sum_{k=1}^{2}\sum_{m=1}^{2}\boldsymbol{\Psi}_{jzlkm}(t)(-1)^k k_{23}\lambda_{x2}\theta_{jy2l} - \sum_{j=1}^{h}\sum_{l=1}^{2}\sum_{k=1}^{2}\sum_{m=1}^{2}\boldsymbol{\Psi}_{jylkm}(t)(-1)^{k+2m}k_{22}\lambda_{x2}\theta_{jz2l} \\
& + \sum_{j=1}^{h}\sum_{l=1}^{2}\sum_{k=1}^{2}\sum_{m=1}^{2}\boldsymbol{\Psi}_{jzlkm}(t)c_{23}\dot{z}_{j2l} - \sum_{j=1}^{h}\sum_{l=1}^{2}\sum_{k=1}^{2}\sum_{m=1}^{2}\boldsymbol{\Psi}_{jzlkm}(t)(-1)^m c_{23}\lambda_{y2}\dot{\theta}_{jx2l} + \sum_{j=1}^{h}\sum_{l=1}^{2}\sum_{k=1}^{2}\sum_{m=1}^{2}\boldsymbol{\Psi}_{jzlkm}(t)(-1)^k c_{23}\lambda_{x2}\dot{\theta}_{jy2l}
\end{aligned}$$

Assuming total number of cars as h, the equation of the bridge system subjected to seismic load can be represented as follows:

$$\boldsymbol{M}_v\ddot{\boldsymbol{w}}_v + \boldsymbol{C}_v\dot{\boldsymbol{w}}_v + \boldsymbol{K}_v\boldsymbol{w}_v = \boldsymbol{F}_v \qquad \left(= \boldsymbol{f}_v - \boldsymbol{M}_v\ddot{\boldsymbol{\Delta}}_v\right) \tag{2.4.47}$$

where,

$$\boldsymbol{M}_v = \begin{bmatrix} \boldsymbol{M}_{v1} & & & \boldsymbol{0} \\ & \ddots & & \\ & & \boldsymbol{M}_{vj} & \\ & & & \ddots \\ \boldsymbol{0} & & & \boldsymbol{M}_{vh} \end{bmatrix}, \quad \boldsymbol{C}_v = \begin{bmatrix} \boldsymbol{C}_{v1} & & & \boldsymbol{0} \\ & \ddots & & \\ & & \boldsymbol{C}_{vj} & \\ & & & \ddots \\ \boldsymbol{0} & & & \boldsymbol{C}_{vh} \end{bmatrix}, \quad \boldsymbol{K}_v = \begin{bmatrix} \boldsymbol{K}_{v1} & & & \tilde{\boldsymbol{0}} \\ & \ddots & & \\ & & \boldsymbol{K}_{vj} & \\ & & & \ddots \\ \tilde{\boldsymbol{0}} & & & \boldsymbol{K}_{vh} \end{bmatrix},$$

$$\boldsymbol{w}_v = \begin{Bmatrix} \boldsymbol{w}_{v1} \\ \vdots \\ \boldsymbol{w}_{vj} \\ \vdots \\ \boldsymbol{w}_{vh} \end{Bmatrix}, \qquad \boldsymbol{F}_v = \begin{Bmatrix} \boldsymbol{F}_{v1} \\ \vdots \\ \boldsymbol{F}_{vj} \\ \vdots \\ \boldsymbol{F}_{vh} \end{Bmatrix}$$

$$\boldsymbol{w}_{vj}{}^T = \left\{ y_{j1} \quad z_{j1} \quad \theta_{jx1} \quad \theta_{jy1} \quad \theta_{jz1} \quad y_{j21} \quad z_{j21} \quad \theta_{jx21} \quad \theta_{jy21} \quad \theta_{jz21} \quad y_{j22} \quad z_{j22} \quad \theta_{jx22} \quad \theta_{jy22} \quad \theta_{jz22} \right\}$$

$$\boldsymbol{F}_{vj}{}^T = \left\{ f_{Aj} \quad f_{Bj} \quad f_{Cj} \quad f_{Dj} \quad f_{Ej} \quad f_{Fj} \quad f_{Gj} \quad f_{Hj} \quad f_{Ij} \quad f_{Jj} \quad f_{Kj} \quad f_{Lj} \quad f_{Mj} \quad f_{Nj} \quad f_{Oj} \right\}$$

The components of $\boldsymbol{M}_{vj}$, $\boldsymbol{C}_{vj}$ and $\boldsymbol{K}_{vj}$ are respectively the same as those in Section 1.4.4.

2.5 Numerical integration

The simultaneous differential equations derived in subsection 2.4.4 and 2.4.5 are non-stationary dynamic problems because the coefficient matrices or the external vectors in the equations vary according to the train position. Such problems can be solved by step-by-step direct numerical integration methods, in which the changed components are updated at each time step.

2.5.1 Discussion of direct numerical integration methods

Various step-by-step integration methods [29－48] to solve the equations of structural dynamics have been developed. The central-difference method used in References [31－35] was a widely used explicit two-step formula for solving the structural dynamics problems. However, the expressions of this type have a rather critical time step, above which the solution becomes numerically unstable and diverges [31]. In complicated finite element structural models, containing slender members exhibiting bending effects, such restriction is a stringent one and often entails using time steps which are much smaller than those needed for accuracy. For many cases only low-mode responses are of interest and a rather larger time step is desired. High-mode responses of complicated finite element models often cannot express the reasonable motions of the actual structures and should be eliminated. Therefore it is often advantageous for an algorithm to possess some form of numerical dissipation to damp out any spurious participation of the higher modes.

For those reasons, unconditionally stable algorithms which achieve the optimal balance between effective numerical dissipation and loss of accuracy compared with trapezoidal rule are generally preferred. Although there is no universal consensus, it is generally agreed [47] that for a method to be competitive, it should possess the following attributes:

1) Unconditional stability
2) No more than one set of implicit equations
3) Second-order accuracy
4) Controllable algorithmic dissipation in the higher modes
5) Self-starting

The Newmark family of algorithms enjoys wide use in structural dynamics. In his 1959 paper [30], Newmark generalized certain direct numerical integration methods that had been in use up to that time. For the damped equation of motion of a single degree-of-freedom (SDOF) system, he presented equations for approximating the velocity and displacement at time step t_{j+1} as Eqs. (2.5.1) and (2.5.2) as follows:

$$\dot{x}^{j+1} = \dot{x}^{j} + \left\{(1-\gamma)\ddot{x}^{j} + \gamma\ddot{x}^{j+1}\right\}\Delta t \tag{2.5.1}$$

$$x^{j+1} = x^{j} + \dot{x}^{j}\Delta t + \left\{\left(\frac{1}{2} - \beta\right)\ddot{x}^{j} + \beta\ddot{x}^{j+1}\right\}(\Delta t)^2 \tag{2.5.2}$$

$$m\ddot{x}^{j+1} + c\dot{x}^{j+1} + kx^{j+1} = f^{j+1} \tag{2.5.3}$$

Here, x denotes the displacement and superposed dots indicate time differentiation. m, c, k and f are respectively mass, damping coefficient, stiffness and external force of the SDOF system. j is the sequence number of time step and Δt represents the time interval. Actually the time interval can be set to vary at each step, whereas for most cases it is convenient to set the time interval constant.

The Newmark family of methods, so called Newmark's β method (or Newmark's generalized acceleration method), allows the amount of numerical (or algorithmic) damping to be continuously controlled by the parameter γ in Eq. (2.5.1) other than time step. If γ is taken to be less than 1/2, an artificial negative damping results. This will involve a self-excited vibration arising solely from the numerical procedure and should be absolutely avoided. On the contrary, if γ is greater than 1/2, such damping is positive. For example, set $\beta = (\gamma + 1/2)^2/4$ and $\gamma > 1/2$; then the amount of dissipation for a fixed time step is increased by increasing γ. The positive damping will reduce the magnitude of the response even without real damping. To avoid numerical damping altogether, the value of γ must be equal to 1/2; and Eq. (2.5.1) becomes the trapezoidal rule.

On the other hand, the parameter β in Eq. (2.5.2) controls the variation of acceleration within the time step. For example, while $\beta = 0$, 1/4 and 1/6, the formula respectively become the constant-acceleration method, average-acceleration method and linear-acceleration method. It is well-known that the linear-acceleration method is somewhat more accurate than the average-acceleration method [41]. However, it has been shown [30] that the former technique is only conditionally stable and requires a critical time step. On the other hand, the average-acceleration method is unconditionally stable, although less accurate.

It should be noted that for the Newmark family of methods, the attributes 3) and 4) enumerated previously cannot exist simultaneously (Second-order accuracy requires $\gamma = 1/2$ which precludes numerical damping) [46]. Furthermore, the dissipative properties of this family of algorithms are considered to be inferior to both the Houbolt [29] and the Wilson [39] methods, since the lower modes are affected too strongly. (It seems all of these algorithms adequately damp the highest modes [40].)

In 1968 Wilson developed the first method, so called Wilson-θ method [39], which essentially satisfied attributes 1)－5), by extending the linear-acceleration method in a manner

that makes it numerically stable. The basic assumption of the Wilson-θ approach is that the acceleration $\ddot{x}$ varies linearly over an extended time step $\Delta t^{\theta} = \theta \Delta t$. During that time step the acceleration is $\ddot{x}^{j+\theta} = \ddot{x}^{j} + \theta\left(\ddot{x}^{j+1} - \ddot{x}^{j}\right)$. Not to explain, while $\theta = 1.0$ the Whilson-θ method is identical with the linear-acceleration method. The Wilson-θ method for solving a SDOF system can be represented as follows:

$$\dot{x}^{j+\theta} = \dot{x}^{j} + \frac{1}{2}\left(\ddot{x}^{j} + \ddot{x}^{j+\theta}\right)\Delta t^{\theta} \tag{2.5.4}$$

$$x^{j+\theta} = x^{j} + \dot{x}^{j}\Delta t^{\theta} + \frac{1}{2}\ddot{x}^{j}\left(\Delta t^{\theta}\right)^{2} + \frac{1}{6}\left\{\ddot{x}^{j+\theta} - \ddot{x}^{j}\right\}\left(\Delta t^{\theta}\right)^{2} \tag{2.5.5}$$

$$m\ddot{x}^{j+\theta} + c\dot{x}^{j+\theta} + kx^{j+\theta} = f^{j+\theta} \tag{2.5.6}$$

where,

$$f^{j+\theta} = f^{j} + \theta\left(f^{j+1} - f^{j}\right) \tag{2.5.7}$$

Then the differential equation can be solved at time $t_{j+\theta}$ by the above formula just like the procedure of Newmark's β method. While $\ddot{x}^{j+\theta}$ is obtained, the acceleration at time t_{j+1} can be derived with Eq. (2.5.8). Note here that the velocity and displacement responses at time t_{j+1} should be further calculated with Eqs. (2.5.4) and (2.5.5) by setting $\theta = 1.0$.

$$\ddot{x}^{j+1} = \ddot{x}^{j} + \frac{1}{\theta}\left(\ddot{x}^{j+\theta} - \ddot{x}^{j}\right) \tag{2.5.8}$$

In the Wilson method, θ must be selected greater than or equal to 1.37 to maintain unconditional stability. It is recommended [40] that $\theta = 1.4$ be employed as the optimum value since further increasing θ reduces accuracy and further increases dissipation. However, even for $\theta = 1.4$ the Wilson method was pointed out [46] to possess excessive low-mode dissipation (i.e. loss of accuracy), and requires a time step to be taken that is smaller than that needed for accuracy. Another peculiar property of the Wilson method was shown numerically by Goudreau and Taylor [36] and Argyris et al [38]. When large time steps are employed, the Wilson method has a tendency to overshoot significantly exact solutions to initial value problems in the early response, especially for applications involving impact or suddenly applied loads. Incidentally, the Houbolt's method [29] is even more highly dissipative than Wilson's method and does not permit parametric control over the amount of dissipation.

Considering the drawbacks possessed by the above described algorithms, Hilber et al [46] developed an approach, so called Hilber-α method, to enhance the Newmark family of methods by employing a parameter α to improve control of numerical damping. The Hilber-α approach can be described as Eq. (2.5.9) by introducing the parameter α into the equation of motion of a SDOF system. The rules for calculation of displacement and velocity responses are the same as those in Newark's method.

$$m\ddot{x}^{j+1} + c\dot{x}^{j+1} + (1+\alpha)kx^{j+1} - \alpha kx^{j} = f^{j+1} \tag{2.5.9}$$

In the Hilber method, it is recommended [7] that the optimum selection of parameters is to let α = -0.1, β = 0.3025, and γ = 0.6.

The errors introduced by numerical integration methods mainly attribute to amplitude suppression and period elongation [7] [46] [47]. Generally the effect of amplitude suppression is considered more important. Here, to compare the significant differences of the approaches introduced previously, assuming T as the period of a SDOF system the diagram for the damping ratios h vs Δt/T of those methods are indicated in Fig. 2.5.1 [46] (It is only an extraction from the references and the values indicated in the diagram are approximations.)

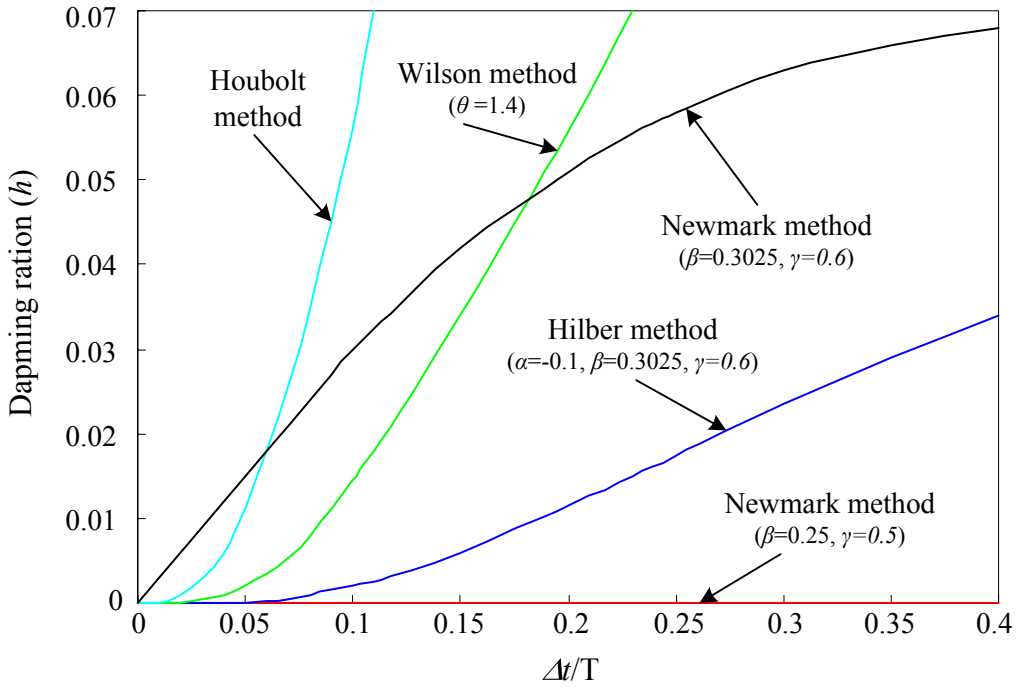

Fig. 2.5.1 Damping ratio *vs* Δt/T for various numerical methods

Desirable properties for an algorithmic damping ratio graph to possess are a zero tangent at the origin and subsequently a controlled turn upward. This ensures adequate dissipation in the higher modes and at the same time guarantees that the lower modes are not affected too strongly. In Fig. 2.5.1, the dissipation ratio curve of the Newmark method with γ-damping has positive slope at the origin. This is why the Newmark family is felt to possess ineffective numerical dissipation. In the rest methods, the Houbolt method has the strongest dissipative property but affects lower modes too strongly. Compared with the Wilson method, the Hilber method seems to be the most accurate one in the lower modes. However, if the time step can be set sufficiently short, the Wilson method may be more effective to damp out the higher modes. Figure 2.5.1 also indicates the criterion to set the time interval if the highest mode to be considered is determined in a complicated structure.

According to the discussion above, in the case of numerical damping is desired, the Hilber method or the Wilson method should be used. If large time step is preferred, the Hilber method seems to be the best choice. However, it is difficult to conclude that the Hilber method is superior to the Wilson method in all cases. On the other hand, though the Newmark method of the trapezoidal rule (γ = 1/2) offers no damping effect, it is considered the most accurate one if without the influence of higher modes. Therefore, for cases that the effect of higher modes can be eliminated, such as using modal analytical approach or viscous damping, the linear acceleration method or the average acceleration method may lead to more accurate results.

Incidentally, to ensure the stability and accuracy of numerical analysis in structural dynamics, some researchers continue to suggest that the viscous damping term, e.g. Rayleigh damping, be used to suppress higher modes [49]. The viscous damping is expected to have the same effect as the numerical damping. However, some researches indicated that the interaction between the viscous damping and typical implicit integrators results in virtually no dissipation in the higher modes [40] [43] [44].

2.5.2 Integrated numerical integration formula

In this study, taking advantage of their analogous basic feature, the Newmark's β method, the Wilson-θ method and the Hilber-α method are implemented in an integrated algorithm. The algorithm can be controlled by the parameters α, β, γ, and θ to execute either of the methods. Therefore, the comparison of these approaches can be conducted and the most appropriate one can be selected for particular case.

For the algorithm of these methods, it is possible to carry out the procedure by its implicit form or explicit form [7]. The implicit form is also called the predictor-corrector method [35]

[41]. For linear analysis, such an iterative procedure is not required since explicit form can be used. The implicit form formula as the iterative procedure can be used in nonlinear problems where physical properties can change in each cycle of iteration. On the other hand, we can formulate either the total-response or incremental-response algorithms. The incremental technique applies to both linear and nonlinear problems.

In this study, the integrated numerical procedure in implicit form of total-response is developed first, and then it is represented in explicit form of incremental-response. Also for generality the algorithms will be developed in matrix form corresponding to multiple degree-of-freedom (MDOF) dynamic system.

a) Implicit form of total-response algorithm

The integrated formula of the Newmark's β method, the Wilson-θ method and the Hilber-α method described previously can be represented as follows in the matrix form:

$$\dot{\boldsymbol{X}}^{j+\theta} = \dot{\boldsymbol{X}}^{j} + \left\{(1-\gamma)\ddot{\boldsymbol{X}}^{j} + \gamma\ddot{\boldsymbol{X}}^{j+\theta}\right\}\Delta t^{\theta} \tag{2.5.10}$$

$$\boldsymbol{X}^{j+\theta} = \boldsymbol{X}^{j} + \dot{\boldsymbol{X}}^{j}\Delta t^{\theta} + \left\{\left(\frac{1}{2}-\beta\right)\ddot{\boldsymbol{X}}^{j} + \beta\ddot{\boldsymbol{X}}^{j+\theta}\right\}\left(\Delta t^{\theta}\right)^{2} \tag{2.5.11}$$

$$\boldsymbol{M}\ddot{\boldsymbol{X}}^{j+\theta} + \boldsymbol{C}\dot{\boldsymbol{X}}^{j+\theta} + (1+\alpha)\boldsymbol{K}\boldsymbol{X}^{j+\theta} - \alpha\boldsymbol{K}\boldsymbol{X}^{j} = \boldsymbol{F}^{j+\theta} \tag{2.5.12}$$

where, if $\theta \neq 1.0$

$$\boldsymbol{F}^{j+\theta} = \boldsymbol{F}^{j} + \theta\left(\boldsymbol{F}^{j+1} - \boldsymbol{F}^{j}\right) \tag{2.5.13}$$

Here, $\boldsymbol{X}$ denotes the displacement vector. $\boldsymbol{M}$, $\boldsymbol{C}$, $\boldsymbol{K}$ and $\boldsymbol{F}$ are respectively mass, damping coefficient, stiffness matrices and external force vector of the MDOF system.

Because the values of $\ddot{\boldsymbol{X}}^{j+\theta}$ in Eqs. (2.5.10) and (2.5.11) are not known in advance, the approximation is said to be implicit, so the solution must be iterative within each time step. The following recurrence equations represent the Nth iteration of the $(j+\theta)$th time step.

$$\left(\dot{\boldsymbol{X}}^{j+\theta}\right)_{N} = \dot{\boldsymbol{X}}^{j} + \left\{(1-\gamma)\ddot{\boldsymbol{X}}^{j} + \gamma\left(\ddot{\boldsymbol{X}}^{j+\theta}\right)_{N-1}\right\}\Delta t^{\theta} \tag{2.5.14}$$

$$\left(\boldsymbol{X}^{j+\theta}\right)_{N} = \boldsymbol{X}^{j} + \dot{\boldsymbol{X}}^{j}\Delta t^{\theta} + \left\{\left(\frac{1}{2}-\beta\right)\ddot{\boldsymbol{X}}^{j} + \beta\left(\ddot{\boldsymbol{X}}^{j+\theta}\right)_{N-1}\right\}\left(\Delta t^{\theta}\right)^{2} \tag{2.5.15}$$

$$\left(\ddot{\boldsymbol{X}}^{j+\theta}\right)_{N} = \boldsymbol{M}^{-1}\left\{\boldsymbol{F}^{j+\theta} - \boldsymbol{C}\left(\dot{\boldsymbol{X}}^{j+\theta}\right)_{N} - (1+\alpha)\boldsymbol{K}\left(\boldsymbol{X}^{j+\theta}\right)_{N} + \alpha\boldsymbol{K}\boldsymbol{X}^{j}\right\} \tag{2.5.16}$$

To start the iterative process of the (j+θ)th time step, the acceleration vector $\left(\ddot{\boldsymbol{X}}^{j+\theta}\right)_0$ is assumed to possess the same values of that of the converged previous time interval $\ddot{\boldsymbol{X}}^{j}$. For the first time step, knowing the initial condition of the system, i.e. the values of $\dot{\boldsymbol{X}}^{0}$ and $\boldsymbol{X}^{0}$, the acceleration vector $\left(\ddot{\boldsymbol{X}}^{\theta}\right)_0$ can be obtained as follows:

$$\left(\ddot{\boldsymbol{X}}^{\theta}\right)_0 = \ddot{\boldsymbol{X}}^{0} = \boldsymbol{M}^{-1}\left\{\boldsymbol{F}^{0} - \boldsymbol{C}\dot{\boldsymbol{X}}^{0} - \boldsymbol{K}\boldsymbol{X}^{0}\right\} \tag{2.5.17}$$

An iterative type of solution requires some criterion for stopping or changing the step size, such as a limit on the number of iterations. A convenient method for measuring the rate of convergence is to control the number of significant figures in $\boldsymbol{X}^{j+\theta}$ as follows:

$$\left\|\left(\boldsymbol{X}^{j+\theta}\right)_N - \left(\boldsymbol{X}^{j+\theta}\right)_{N-1}\right\| < \varepsilon\left\|\left(\boldsymbol{X}^{j+\theta}\right)_N\right\| \tag{2.5.18}$$

where ε is some small number selected by the analyst. For example, an accuracy of approximately three digits may be specified by taking ε = 0.001. For the MDOF structure, the length of the vector in Eq. (2.5.18), which is equal to the square root of the sum of the squares of its components, can be used; or simply judge on the each component of the vector.

The process can be iterated until it is judged to reach convergence. In most cases, an upper limit of iterative number N should be designated. If the process does not converge until the upper limit number, then the time step should be further divided into smaller one or just stop the calculation.

In the case of using Wilson-θ method, i.e. $\theta \neq 1.0$, once the convergence is confirmed, the acceleration response at time step t_{j+1} can be obtained linearly as follows:

$$\ddot{\boldsymbol{X}}^{j+1} = \ddot{\boldsymbol{X}}^{j} + \frac{1}{\theta}\left(\ddot{\boldsymbol{X}}^{j+\theta} - \ddot{\boldsymbol{X}}^{j}\right) \tag{2.5.19}$$

and the velocity and displacement responses should be further calculated as follows:

$$\dot{\boldsymbol{X}}^{j+1} = \dot{\boldsymbol{X}}^{j} + \frac{1}{2}\left\{\ddot{\boldsymbol{X}}^{j} + \ddot{\boldsymbol{X}}^{j+1}\right\}\Delta t \tag{2.5.20}$$

$$\boldsymbol{X}^{j+1} = \boldsymbol{X}^{j} + \dot{\boldsymbol{X}}^{j}\Delta t + \frac{1}{2}\ddot{\boldsymbol{X}}^{j}(\Delta t)^2 + \frac{1}{6}\left\{\ddot{\boldsymbol{X}}^{j+1} - \ddot{\boldsymbol{X}}^{j}\right\}(\Delta t)^2 \tag{2.5.21}$$

b) Explicit form of incremental-response algorithm

In this subsection, the explicit form of incremental-response integrated formula will be developed. It is feasible to set up simultaneous equations for incremental accelerations, velocities, or displacements. Here the incremental displacements as unknowns will be adopted, so to solve a pseudo-static problem for each time step.

At time t_j, the damped equations of motion with α-damping for a MDOF structure are

$$\boldsymbol{M}\ddot{\boldsymbol{X}}^{j} + \boldsymbol{C}\dot{\boldsymbol{X}}^{j} + (1+\alpha)\boldsymbol{K}\boldsymbol{X}^{j} - \alpha\boldsymbol{K}\boldsymbol{X}^{j-1} = \boldsymbol{F}^{j} \tag{2.5.22}$$

Similarly, at time $t_{j+1} = t_j + \Delta t$, the equations of motion become

$$\begin{aligned} &\boldsymbol{M}\left(\ddot{\boldsymbol{X}}^{j} + \Delta\ddot{\boldsymbol{X}}^{j}\right) + \boldsymbol{C}\left(\dot{\boldsymbol{X}}^{j} + \Delta\dot{\boldsymbol{X}}^{j}\right) \\ &+ (1+\alpha)\boldsymbol{K}\left(\boldsymbol{X}^{j} + \Delta\boldsymbol{X}^{j}\right) - \alpha\boldsymbol{K}\left(\boldsymbol{X}^{j-1} + \Delta\boldsymbol{X}^{j-1}\right) = \boldsymbol{F}^{j} + \Delta\boldsymbol{F}^{j} \end{aligned} \tag{2.5.23}$$

Subtraction of Eq. (2.5.22) from Eq. (2.5.23) produces the incremental equations of motion as

$$\boldsymbol{M}\Delta\ddot{\boldsymbol{X}}^{j} + \boldsymbol{C}\Delta\dot{\boldsymbol{X}}^{j} + (1+\alpha)\boldsymbol{K}\Delta\boldsymbol{X}^{j} - \alpha\boldsymbol{K}\Delta\boldsymbol{X}^{j-1} = \Delta\boldsymbol{F}^{j} \tag{2.5.24}$$

These equations will be used for the integrated formula developed in the following descriptions.

For the integrated formula, the incremental velocity and displacement vectors at time $t_{j+\theta}$ can be derived from Eqs. (2.5.10) and (2.5.11) as follows:

$$\Delta\dot{\boldsymbol{X}}^{\theta} = \ddot{\boldsymbol{X}}^{j}\Delta t^{\theta} + \gamma\Delta\ddot{\boldsymbol{X}}^{\theta}\Delta t^{\theta} \tag{2.5.25}$$

$$\Delta\boldsymbol{X}^{\theta} = \dot{\boldsymbol{X}}^{j}\Delta t^{\theta} + \frac{1}{2}\ddot{\boldsymbol{X}}^{j}\left(\Delta t^{\theta}\right)^{2} + \beta\Delta\ddot{\boldsymbol{X}}^{\theta}\left(\Delta t^{\theta}\right)^{2} \tag{2.5.26}$$

Solving for $\Delta\ddot{\boldsymbol{X}}^{\theta}$ in Eq. (2.5.26) produces

$$\Delta\ddot{\boldsymbol{X}}^{\theta} = \frac{1}{\beta\left(\Delta t^{\theta}\right)^{2}}\Delta\boldsymbol{X}^{\theta} - \frac{1}{\beta\Delta t^{\theta}}\dot{\boldsymbol{X}}^{j} - \frac{1}{2\beta}\ddot{\boldsymbol{X}}^{j} \tag{2.5.27}$$

Substitution of Eq. (2.5.27) into Eq. (2.5.25) yields

$$\Delta\dot{\boldsymbol{X}}^{\theta} = \frac{\gamma}{\beta\Delta t^{\theta}}\Delta\boldsymbol{X}^{\theta} - \frac{\gamma}{\beta}\dot{\boldsymbol{X}}^{j} - \left(\frac{\gamma}{2\beta} - 1\right)\Delta t^{\theta}\ddot{\boldsymbol{X}}^{j} \tag{2.5.28}$$

Then substituting Eqs. (2.5.27) and (2.5.28) into the incremental equations of motion, the pseudo-static equations can be obtained as follows:

$$\begin{aligned}&\left\{(1+\alpha)\boldsymbol{K}+\frac{1}{\beta(\Delta t^{\theta})^{2}}\boldsymbol{M}+\frac{\gamma}{\beta\Delta t^{\theta}}\boldsymbol{C}\right\}\Delta\boldsymbol{X}^{\theta}\\&=\Delta\boldsymbol{F}^{\theta}+\boldsymbol{M}\left\{\frac{1}{\beta\Delta t^{\theta}}\dot{\boldsymbol{X}}^{j}+\frac{1}{2\beta}\ddot{\boldsymbol{X}}^{j}\right\}+\boldsymbol{C}\left\{\frac{\gamma}{\beta}\dot{\boldsymbol{X}}^{j}+\left(\frac{\gamma}{2\beta}-1\right)\Delta t^{\theta}\ddot{\boldsymbol{X}}^{j}\right\}+\alpha\boldsymbol{K}\Delta\boldsymbol{X}^{j-1}\end{aligned}\tag{2.5.29}$$

where, if $\theta \neq 1.0$

$$\Delta\boldsymbol{F}^{\theta}=\theta\Delta\boldsymbol{F}^{j}\tag{2.5.30}$$

For the first time step, $\Delta\boldsymbol{X}^{j-1}$ can be taken as zero vector.

Through solving the pseudo-static equation (2.5.29), the incremental displacement response $\Delta\boldsymbol{X}^{\theta}$ can be obtained. Then the incremental velocity and acceleration responses $\Delta\dot{\boldsymbol{X}}^{\theta}$ and $\Delta\ddot{\boldsymbol{X}}^{\theta}$ can be calculated by Eqs. (2.5.27) and (2.5.28).

In the case of using Wilson-θ method, i.e. $\theta \neq 1.0$, once the acceleration response $\Delta\ddot{\boldsymbol{X}}^{\theta}$ is obtained, then the incremental acceleration response $\Delta\ddot{\boldsymbol{X}}^{j}$ can be obtained linearly as follows:

$$\Delta\ddot{\boldsymbol{X}}^{j}=\frac{1}{\theta}\Delta\ddot{\boldsymbol{X}}^{\theta}\tag{2.5.31}$$

Furthermore, the incremental velocity and acceleration responses $\Delta\dot{\boldsymbol{X}}^{j}$ and $\Delta\ddot{\boldsymbol{X}}^{j}$ should be further calculated as follows:

$$\Delta\dot{\boldsymbol{X}}^{j}=\ddot{\boldsymbol{X}}^{j}\Delta t+\frac{1}{2}\Delta\ddot{\boldsymbol{X}}^{j}\Delta t\tag{2.5.32}$$

$$\Delta\boldsymbol{X}^{j}=\dot{\boldsymbol{X}}^{j}\Delta t+\frac{1}{2}\ddot{\boldsymbol{X}}^{j}(\Delta t)^{2}+\frac{1}{6}\Delta\ddot{\boldsymbol{X}}^{j}(\Delta t)^{2}\tag{2.5.33}$$

Finally, the total values of $\boldsymbol{X}^{j+1}$, $\dot{\boldsymbol{X}}^{j+1}$ and $\ddot{\boldsymbol{X}}^{j+1}$ can be derived as follows:

$$\boldsymbol{X}^{j+1}=\boldsymbol{X}^{j}+\Delta\boldsymbol{X}^{j}\tag{2.5.34}$$

$$\dot{\boldsymbol{X}}^{j+1}=\dot{\boldsymbol{X}}^{j}+\Delta\dot{\boldsymbol{X}}^{j}\tag{2.5.35}$$

$$\ddot{\boldsymbol{X}}^{j+1}=\ddot{\boldsymbol{X}}^{j}+\Delta\ddot{\boldsymbol{X}}^{j}\tag{2.5.36}$$

For the integrated formula developed above, the reasonable combinations of the parameters are listed as follows:

1) $\alpha = 0.0$, $\beta = 1/4$, $\gamma = 1/2$, $\theta = 1.0$ (Average-acceleration method)

2) $\alpha = 0.0$, $\beta = 1/6$, $\gamma = 1/2$, $\theta = 1.0$ (Linear-acceleration method)

3) $\alpha = 0.0$, $\beta = 1/6$, $\gamma = 1/2$, $\theta \geq 1.37$ (Wilson-θ method)

4) $\alpha < 0.0$, $\beta = (\gamma + 1/2)^2/4$, $\gamma > 1/2$, $\theta = 1.0$ (Hilber-α method)

The numerical errors caused by both the amplitude suppression and the period elongation may be made negligible by using sufficiently small time steps. For the Newmark's β method, Newmark [30] recommended a time step of duration equal to 1/5 or 1/6 of T_n, which is the smallest period of a MDOF structure. However, a more commonly used time step is $\Delta t = T_n/10$. For the Wilson-θ method or the Hilber-α method, the time interval can be determined according to the highest mode to be considered.

References

[1] Kawatani, M., He, X., Shiraga, R., Masaki, S., Nishiyama, S. and Yoshida, K.: Dynamic response analysis of elevated railway bridges due to Shinkansen trains, *Journal of Struc-tural and Earthquake Engineering (Doboku Gakkai Ron-bunshuu A)*, JSCE, Vol. 62, No. 3, pp.509-519, 2006. (*in Japanese*)

[2] He, X., Kawatani, M., Yamaguchi, S. and Nishiyama, S.: Evaluation of Site Vibration around Shinkansen Viaducts under Bullet Train, Proc. of 2nd International Symposium on Environmental Vibrations (ISEV2005), Okayama, Japan, Sep. 20-22, 2005.

[3] He, X., Kawatani, M., Sobukawa, R. and Nishiyama, S.: Dynamic response analysis of Shinkansen train-bridge interaction system subjected to seismic load, *Proc. of 4th International Conference on Current and Future Trends in Bridge Design, Construction and Maintenance*, Kuala Lumpur, Malaysia, pp. 1-12, 2005 (CD-ROM).

[4] Washidu, K., Miyamoto, H., Yamada, Y., Yamamoto, Y. and Kawai, T.: A handbook of finite element method · I Theory, BAIFUKAN, 1981. (*in Japanese*)

[5] Washidu, K., Miyamoto, H., Yamada, Y., Yamamoto, Y. and Kawai, T.: A handbook of finite element method · II Application, BAIFUKAN, 1981. (*in Japanese*)

[6] Ray W. Clough and Joseph Penzien: Dynamics of Structures, McGraw-Hill, Inc., 1975.

[7] William Weaver, Jr. and Paul R. Johnston: Structural Dynamics by Finite Elements, Prentice-Hall, Inc., 1987.

[8] Kawatani, M., Kobayashi, Y. and Kawaki, H.: Influence of Elastomeric Bearings on Traffic-Induced Vibration of Highway Bridges, *Transportation Research Record*, No.1696, Vol.2, pp.76-82, 2000 (5th International Bridge Engineering Conference, Tampa, USA, April 3-5, 2000).

[9] Bathe, K. J.: Finite element procedures in engineering analysis, Prentice-Hall, Englewood Cliffs, N. J., 1982.

[10] Weaver, W., Jr. and Gere, J. M.: Matrix analysis of framed structures, 2nd ed., Van Nostrand Reinhold, New York, 1980.

[11] Weaver, W., Jr. and Johnston, P. R.: Finite-element for structural analysis, Prentice-Hall, Inc., Englewood Cliffs, New Jersey, 1984.

[12] Guyan, R. J.: Reduction of Stiffness and Mass Matrices, *AIAA J.*, 3(2), 380, 1965.

[13] Gibbs, J. W.: Fourier Series, *Nature*, Vol. 59, pp. 606, 1899.

[14] Antoni Zygmund: Trigonometrical series, Dover publications, 1955.

[15] TOGAWA, Hayato: Vibration Analysis by Finite Element Method, SAIENSU-SHA Co., Ltd. Oct., 1975. (*in Japanese*)

[16] Wilkinson, J. and Reinsch, C., Eds.: Linear Algebra, Srpinger-Verlag, New York, 1971.

[17] Atkinson, Kendall E.: An introduction to numerical analysis, Second Ediong, John Wiley & Sons, New York, 1989.

[18] Maruyama, H. and Fukazawa, Y.: Railway engineering for civil engineers, MARUZEN Co., Ltd., Nov., 1981. (*in Japanese*)

[19] Maruyama, H. and Kageyama, N.: Railway engineering for civil engineers, MARUZEN Co., Ltd., Oct., 1981. (*in Japanese*)

[20] The Japan Society of Mechanical Engineers: Dynamics of railway vehicles—Up to date technologies on trucks—, DENKISHAKENKYUKAI, Dec., 1994. (*in Japanese*)

[21] Ejima, A.: Site vibration and countermeasure, pp. 146-154, YOSHIISHOTEN, June 1979. (*in Japanese*)

[22] Yoshioka, O.: A Dynamic Model for Generation and Propagation of Shinkansen-Induced Ground Vibrations and Its Applications to Vibration Reduction Measures, *RTRI Report*, Special No.30, Oct. 1999. (*in Japanese*)

[23] Kawatani,M., Yamada, Y. and Dakeshita, Y.: Dynamic response analysis of plate girder bridge due to 3-dimensional vehicle model, *Journal of Structural and Earthquake Engineering*, JSCE, Vol. I-42, No. 584, pp.79-86, Jan., 1998. (*in Japanese*)

[24] Kawatani, M., Kobayashi, Y. and Kawaki, H.: Influence of Elastomeric Bearings on Traffic-Induced Vibration of Highway Bridges, *Transportation Research Record*, No.1696, Vol.2, pp. 76-82, 2000 (5th International Bridge Engineering Conference, Tampa, USA, April 3-5, 2000).

[25] Wakui, H., Matsumoto, N., Matsuura, A. and Tanabe, M.: Dynamic interaction analysis for railway vehicles and structures, *Journal of Structural and Earthquake Engineering*, JSCE, Vol. I-31, No. 513, pp.129-138, Apr., 1995. (*in Japanese*)

[26] Shoji, T., Yito, Y. and Seki, M.: Research on axle load distribution of high-speed train and stress distribution of steel girder, Proceedings of the 59th Annual Conference of the Japan Society of Civil Engineers, I-078， Sep., 2004. (*in Japanese*)

[27] Matsumoto, N., Sogabe, M., Wakui, H. and Tanabe, M.: Running safety snalysis of vehicles on structures subjected to earthquake motion. *QR of RTRI*, Vol. 45, No. 3, pp. 116-122, 2004.

[28] Agabein M.E.: The effect of various damping assumptions on the dynamic response of structure, Bulletin of International Institute of Seismology and Earthquake Eng., Vol. 8, pp. 217-236, 1971.

[29] Houbolt, J. C.: A recurrence matrix solution for the dynamic response of elastic aircraft, *Journal of Aeronautical Sciences* (A predecessor of *AIAA Journal*), Vol. 17, pp. 540-550, 1950.

[30] Newmark, N. M.: A Method of Computation for Structural Dynamics, *Journal of the*

Engineering Mechanics Division, *ASCE*, Vol. 85, No. EM3, pp. 67-94, 1959.

[31] Dahlquist, G. G.: A special stability problem for linear multistep methods, *Nord. Tidskr. Inf. behandling*, Vol. 3, pp. 27-43, 1963.

[32] krieg, R. D.: Unconditional stability in numerical time integration methods, *Journal of applied mechanics*, Vol. 40, No. 2, pp. 417-421, 1973.

[33] Krieg, R. D., and Key, S. W.: Transient shell response by numerical time integration, *International Journal for Numerical Methods in Engineering*, Vol. 7, No. 3, pp. 273-286, 1973.

[34] Key, S. W.: A finite element procedure for the large deformation dynamic response of axisymmetric solids, *Computer Methods in Applied Mechanics and Engineering*, Vol. 4, No. 2, pp. 195-218, 1974.

[35] Morino, L., Leech, J. W. and Witmer, E. A.: Optimal predictor-corrector method for systems of second-order differential equations, *AIAA Journal*, Vol. 12, No. 10, pp. 1343-1347, 1974.

[36] Goudreau, G. L. and Taylor, R. L.: Evaluation of numerical integration methods in elastodynamics, *Computer Methods in Applied Mechanics and Engineering*, Vol. 2, pp. 69-97, 1972.

[37] Argyris, J. H., Dunne, P. C. and Angelopoulos, T.: Dynamic response by large step integration, *Earthquake Engineering & Structural Dynamics*, Vol. 2, pp. 185-203, 1973.

[38] Argyris, J. H., Dunne, P. C. and Angelopoulos, T.: Non-linear oscillations using the finite element technique, *Computer Methods in Applied Mechanics and Engineering*, Vol. 2, pp. 203-250, 1973.

[39] Wilson, E. L., Farhoomand, I. and Bathe, K. J.: Nonlinear dynamic analysis of complex structures, *Earthquake Engineering & Structural Dynamics*, Vol. 1, No. 3, pp. 241-252, 1973.

[40] Bathe, K. J., and Wilson, E. L.: Stability and accuracy analysis of direct integration methods, *Earthquake Engineering & Structural Dynamics*, Vol. 1, No. 3, pp. 283-291, 1973.

[41] Timoshenko, S. P., Young, D. H. and Weaver, W., Jr.: Vibration problems in engineering, 4th ed., Wiley, New York, 1974.

[42] Belytschko, T. and Schoeberle, D. F.: On the unconditional stability of an implicit algorithm for nonlinear structural dynamics, *Journal of applied mechanics*, Vol. 42, pp. 865-869, 1975.

[43] Hilber, H. M.: Analysis and design of numerical integration methods in structural dynamics, *Ph.D. Dissertation*, Division of Structural Engineering and Structural Mechanics, Univ. of California, Berkeley, 1976.

[44] Hughes, T. J. R.: Stability, convergence and growth and decay of energy of the average acceleration method in nonlinear structural dynamics, *Computers and Structures*, Vol. 6, pp. 313-324, 1976.

[45] Hughes, T. J. R.: A note on the stability of Newmark's algorithm in nonlinear structural dynamics, *International Journal for Numerical Methods in Engineering*, Vol. 11, pp. 383-386, 1977.

[46] Hilber, H. M., Hughes, T. J. R., and Taylor, R. L.; "Improved Numerical dissipation for Time Integration Algorithms in Structural Mechanics," *Earthquake Engineering & Structural Dynamics*, Vol. 5, No. 3, pp. 283-292, 1977.

[47] Hilber, H. M. and Hughes, T. J. R.: Collocation, Dissipation, and 'Overshoot' for Time Integration Schemes in Structural Dynamics, *Earthquake Engineering & Structural Dynamics*, Vol. 6, No. 1, pp. 99-117, Sep., 1978.

[48] Shing, P. B., Vannan, M. T. and Cater, E.: Implicit time integration for pseudo dynamic tests, *Earthquake Engineering & Structural Dynamics*, Vol. 20, pp. 551-576, 1991.

[49] JSCE: Evaluation on checking approaches to earthquake performance of concrete structures based on damage investigation in Hanshin Awaji Great Earthquake, CONCRETE ENGINEERING SERIES 49, Dec., 2002. (*in Japanese*)

Appendices

A. Detailed components of matrices in Section 2.4.4

The detailed components of the matrices shown in Section 2.4.4 can be given as follows.

$$m_{bi} = \tilde{\boldsymbol{\phi}}_i^T \tilde{\boldsymbol{M}}_b \tilde{\boldsymbol{\phi}}_i = M_i$$

$$k_{ig} = \sum_{j=1}^{h}\sum_{l=1}^{2}\sum_{k=1}^{2}\sum_{m=1}^{2} \tilde{\phi}_i^T \left\{ \tilde{\boldsymbol{\Psi}}_{jzlkm}(t)\tilde{\boldsymbol{\Psi}}_{jzlkm}^T(t)k_{23} + \tilde{\boldsymbol{\Psi}}_{jylkm}(t)\tilde{\boldsymbol{\Psi}}_{jylkm}^T(t)k_{22} \right\} \tilde{\phi}_g \qquad (i \neq g)$$

$$= \sum_{j=1}^{h}\sum_{l=1}^{2}\sum_{k=1}^{2}\sum_{m=1}^{2} \tilde{\phi}_i^T \left\{ \tilde{\boldsymbol{\Psi}}_{jzlkm}(t)\tilde{\boldsymbol{\Psi}}_{jzlkm}^T(t)k_{23} + \tilde{\boldsymbol{\Psi}}_{jylkm}(t)\tilde{\boldsymbol{\Psi}}_{jylkm}^T(t)k_{22} \right\} \tilde{\phi}_g + \omega^2{}_i M_i \qquad (i = g)$$

$$c_{ig} = \sum_{j=1}^{h}\sum_{l=1}^{2}\sum_{k=1}^{2}\sum_{m=1}^{2} \tilde{\phi}_i^T \tilde{\boldsymbol{\Psi}}_{jzlkm}(t)c_{23}\tilde{\boldsymbol{\Psi}}_{jzlkm}^T(t)\tilde{\phi}_g \qquad (i \neq g)$$

$$= \sum_{j=1}^{h}\sum_{l=1}^{2}\sum_{k=1}^{2}\sum_{m=1}^{2} \tilde{\phi}_i^T \tilde{\boldsymbol{\Psi}}_{jzlkm}(t)c_{23}\tilde{\boldsymbol{\Psi}}_{jzlkm}^T(t)\tilde{\phi}_g + 2h_i\omega_i M_i \qquad (i = g)$$

$$k_{iAj} = k_{iBj} = k_{iCj} = k_{iDj} = k_{iEj} = 0$$

$$k_{iFj} = k_{iKj} = -\sum_{k=1}^{2}\sum_{m=1}^{2} \tilde{\phi}_i^T \tilde{\boldsymbol{\Psi}}_{jylkm}(t)k_{22}$$

$$k_{iGj} = k_{iLj} = -\sum_{k=1}^{2}\sum_{m=1}^{2} \tilde{\phi}_i^T \tilde{\boldsymbol{\Psi}}_{jzlkm}(t)k_{23}$$

$$k_{iHj} = k_{iMj} = \sum_{k=1}^{2}\sum_{m=1}^{2} \tilde{\phi}_i^T \left\{ (-1)^m \tilde{\boldsymbol{\Psi}}_{jzlkm}(t)k_{23}\lambda_{y2} - \tilde{\boldsymbol{\Psi}}_{jylkm}(t)k_{22}\lambda_{z3} \right\}$$

$$k_{iIj} = k_{iNj} = -\sum_{k=1}^{2}\sum_{m=1}^{2} \tilde{\phi}_i^T \tilde{\boldsymbol{\Psi}}_{jzlkm}(t)(-1)^k k_{23}\lambda_{x2}$$

$$k_{iJj} = k_{iOj} = \sum_{k=1}^{2}\sum_{m=1}^{2} \tilde{\phi}_i^T \tilde{\boldsymbol{\Psi}}_{jylkm}(t)(-1)^{k+2m} k_{22}\lambda_{x2}$$

$$c_{iAj} = c_{iBj} = c_{iCj} = c_{iDj} = c_{iEj} = 0$$

$$c_{iFj} = c_{iKj} = 0$$

$$c_{iGj} = c_{iLj} = -\sum_{k=1}^{2}\sum_{m=1}^{2} \tilde{\phi}_i^T \tilde{\boldsymbol{\Psi}}_{jzlkm}(t)c_{23}$$

$$c_{iHj} = c_{iMj} = \sum_{k=1}^{2}\sum_{m=1}^{2} \tilde{\phi}_i^T \tilde{\boldsymbol{\Psi}}_{jzlkm}(t)(-1)^m c_{23}\lambda_{y2}$$

$$c_{iIj} = c_{iNj} = -\sum_{k=1}^{2}\sum_{m=1}^{2} \tilde{\phi}_i^T \tilde{\boldsymbol{\Psi}}_{jzlkm}(t)(-1)^k c_{23}\lambda_{x2}$$

$$c_{iJj} = c_{iOj} = 0$$

$$m_{Aj} = m_1 \qquad m_{Bj} = m_1 \qquad m_{Cj} = I_{x1} \qquad m_{Dj} = I_{y1} \qquad m_{Ej} = I_{z1}$$

$$m_{Fj} = m_{Kj} = m_2 \qquad m_{Gj} = m_{Lj} = m_2 \qquad m_{Hj} = m_{Mj} = I_{x2} \qquad m_{Ij} = m_{Nj} = I_{y2} \qquad m_{Jj} = m_{Oj} = I_{z2}$$

$k_{AAj}=\sum_{l=1}^{2}\sum_{m=1}^{2}k_2$	$c_{AAj}=\sum_{l=1}^{2}\sum_{m=1}^{2}c_2$
$k_{ABj}=0$	$c_{ABj}=0$
$k_{ACj}=\sum_{l=1}^{2}\sum_{m=1}^{2}k_2\lambda_{z1}$	$c_{ACj}=\sum_{l=1}^{2}\sum_{m=1}^{2}c_2\lambda_{z1}$
$k_{ADj}=0$	$c_{ADj}=0$
$k_{AEj}=-\sum_{l=1}^{2}\sum_{m=1}^{2}(-1)^{l+2m}k_2\lambda_{x1}$	$c_{AEj}=-\sum_{l=1}^{2}\sum_{m=1}^{2}(-1)^{l+2m}c_2\lambda_{x1}$
$k_{AFj}=k_{AKj}=-\sum_{m=1}^{2}k_2$	$c_{AFj}=c_{AKj}=-\sum_{m=1}^{2}c_2$
$k_{AGj}=k_{ALj}=0$	$c_{AGj}=c_{ALj}=0$
$k_{AHj}=k_{AMj}=\sum_{m=1}^{2}k_2\lambda_{z2}$	$c_{AHj}=c_{AMj}=\sum_{m=1}^{2}c_2\lambda_{z2}$
$k_{AIj}=k_{ANj}=0$	$c_{AIj}=c_{ANj}=0$
$k_{AJj}=k_{AOj}=0$	$c_{AJj}=c_{AOj}=0$
$k_{BBj}=\sum_{l=1}^{2}\sum_{m=1}^{2}k_3$	$c_{BBj}=\sum_{l=1}^{2}\sum_{m=1}^{2}c_3$
$k_{BCj}=-\sum_{l=1}^{2}\sum_{m=1}^{2}(-1)^{m}k_3\lambda_{y3}$	$c_{BCj}=-\sum_{l=1}^{2}\sum_{m=1}^{2}(-1)^{m}c_3\lambda_{y3}$
$k_{BDj}=\sum_{l=1}^{2}\sum_{m=1}^{2}(-1)^{l}k_3\lambda_{x1}$	$c_{BDj}=\sum_{l=1}^{2}\sum_{m=1}^{2}(-1)^{l}c_3\lambda_{x1}$
$k_{BEj}=0$	$c_{BEj}=0$
$k_{BFj}=k_{BKj}=0$	$c_{BFj}=c_{BKj}=0$
$k_{BGj}=k_{BLj}=-\sum_{m=1}^{2}k_3$	$c_{BGj}=c_{BLj}=-\sum_{m=1}^{2}c_3$
$k_{BHj}=k_{BMj}=\sum_{m=1}^{2}(-1)^{m}k_3\lambda_{y3}$	$c_{BHj}=c_{BMj}=\sum_{m=1}^{2}(-1)^{m}c_3\lambda_{y3}$
$k_{BIj}=k_{BNj}=0$	$c_{BIj}=c_{BNj}=0$
$k_{BJj}=k_{BOj}=0$	$c_{BJj}=c_{BOj}=0$

$$k_{CCj} = \sum_{l=1}^{2}\sum_{m=1}^{2}\{k_2\lambda^2{}_{z1} + k_3\lambda^2{}_{y3}\}$$

$$k_{CDj} = -\sum_{l=1}^{2}\sum_{m=1}^{2}(-1)^{l+m}k_3\lambda_{y3}\lambda_{x1}$$

$$k_{CEj} = -\sum_{l=1}^{2}\sum_{m=1}^{2}(-1)^{l+2m}k_2\lambda_{z1}\lambda_{x1}$$

$$k_{CFj} = k_{CKj} = -\sum_{m=1}^{2}k_2\lambda_{z1}$$

$$k_{CGj} = k_{CLj} = \sum_{m=1}^{2}(-1)^{m}k_3\lambda_{y3}$$

$$k_{CHj} = k_{CMj} = \sum_{m=1}^{2}\{k_2\lambda_{z1}\lambda_{z2} - k_3\lambda^2{}_{y3}\}$$

$$k_{CIj} = k_{CNj} = 0 \qquad k_{CJj} = k_{COj} = 0$$

$$k_{DDj} = \sum_{l=1}^{2}\sum_{m=1}^{2}k_3\lambda^2{}_{x1}$$

$$k_{DEj} = 0$$

$$k_{DFj} = k_{DKj} = 0$$

$$k_{DGj} = k_{DLj} = -\sum_{m=1}^{2}(-1)^{l}k_3\lambda_{x1}$$

$$k_{DHj} = k_{DMj} = \sum_{m=1}^{2}(-1)^{l+m}k_3\lambda_{x1}\lambda_{y3}$$

$$k_{DIj} = k_{DNj} = 0 \qquad k_{DJj} = k_{DOj} = 0$$

$$k_{EEj} = \sum_{l=1}^{2}\sum_{m=1}^{2}\{k_2\lambda^2{}_{x1} + k_1\lambda^2{}_{y4}\}$$

$$k_{EFj} = k_{EKj} = \sum_{m=1}^{2}(-1)^{l+2m}k_2\lambda_{x1}$$

$$k_{EGj} = k_{ELj} = 0$$

$$k_{EHj} = k_{EMj} = -\sum_{m=1}^{2}(-1)^{l+2m}k_2\lambda_{x1}\lambda_{z2}$$

$$k_{EIj} = k_{ENj} = 0$$

$$k_{EJj} = k_{EOj} = -\sum_{m=1}^{2}k_1\lambda^2{}_{y4}$$

$$c_{CCj} = \sum_{l=1}^{2}\sum_{m=1}^{2}\{c_2\lambda^2{}_{z1} + c_3\lambda^2{}_{y3}\}$$

$$c_{CDj} = -\sum_{l=1}^{2}\sum_{m=1}^{2}(-1)^{l+m}c_3\lambda_{y3}\lambda_{x1}$$

$$c_{CEj} = -\sum_{l=1}^{2}\sum_{m=1}^{2}(-1)^{l+2m}c_2\lambda_{z1}\lambda_{x1}$$

$$c_{CFj} = c_{CKj} = -\sum_{m=1}^{2}c_2\lambda_{z1}$$

$$c_{CGj} = c_{CLj} = \sum_{m=1}^{2}(-1)^{m}c_3\lambda_{y3}$$

$$c_{CHj} = c_{CMj} = \sum_{m=1}^{2}\{c_2\lambda_{z1}\lambda_{z2} - c_3\lambda^2{}_{y3}\}$$

$$c_{CIj} = c_{CNj} = 0 \qquad c_{CJj} = c_{COj} = 0$$

$$c_{DDj} = \sum_{l=1}^{2}\sum_{m=1}^{2}c_3\lambda^2{}_{x1}$$

$$c_{DEj} = 0$$

$$c_{DFj} = c_{DKj} = 0$$

$$c_{DGj} = c_{DLj} = -\sum_{m=1}^{2}(-1)^{l}c_3\lambda_{x1}$$

$$c_{DHj} = c_{DMj} = \sum_{m=1}^{2}(-1)^{l+m}c_3\lambda_{x1}\lambda_{y3}$$

$$c_{DIj} = c_{DNj} = 0 \qquad c_{DJj} = c_{DOj} = 0$$

$$c_{EEj} = \sum_{l=1}^{2}\sum_{m=1}^{2}c_2\lambda^2{}_{x1}$$

$$c_{EFj} = c_{EKj} = \sum_{m=1}^{2}(-1)^{l+2m}c_2\lambda_{x1}$$

$$c_{EGj} = c_{ELj} = 0$$

$$c_{EHj} = c_{EMj} = -\sum_{m=1}^{2}(-1)^{l+2m}c_2\lambda_{x1}\lambda_{z2}$$

$$c_{EIj} = c_{ENj} = 0$$

$$c_{EJj} = c_{EOj} = 0$$

$$k_{FFj} = \sum_{m=1}^{2} k_2 + \sum_{k=1}^{2}\sum_{m=1}^{2} k_{22}$$

$$k_{FGj} = 0$$

$$k_{FHj} = \sum_{k=1}^{2}\sum_{m=1}^{2} k_{22}\lambda_{z3} - \sum_{m=1}^{2} k_2\lambda_{z2}$$

$$k_{FIj} = 0$$

$$k_{FJj} = -\sum_{k=1}^{2}\sum_{m=1}^{2} (-1)^{k+2m} k_{22}\lambda_{x2}$$

$$k_{FKj} = k_{FLj} = k_{FMj} = k_{FNj} = k_{FOj} = 0$$

$$c_{FFj} = \sum_{m=1}^{2} c_2$$

$$c_{FGj} = 0$$

$$c_{FHj} = -\sum_{m=1}^{2} c_2\lambda_{z2}$$

$$c_{FIj} = 0$$

$$c_{FJj} = 0$$

$$c_{FKj} = c_{FLj} = c_{FMj} = c_{FNj} = c_{FOj} = 0$$

$$k_{GGj} = \sum_{m=1}^{2} k_3 + \sum_{k=1}^{2}\sum_{m=1}^{2} k_{23}$$

$$k_{GHj} = -\sum_{m=1}^{2} (-1)^m k_3\lambda_{y3} - \sum_{k=1}^{2}\sum_{m=1}^{2} (-1)^m k_{23}\lambda_{y2}$$

$$k_{GIj} = \sum_{k=1}^{2}\sum_{m=1}^{2} (-1)^k k_{23}\lambda_{x2}$$

$$k_{GJj} = 0$$

$$k_{GKj} = k_{GLj} = k_{GMj} = k_{GNj} = k_{GOj} = 0$$

$$c_{GGj} = \sum_{m=1}^{2} c_3 + \sum_{k=1}^{2}\sum_{m=1}^{2} c_{23}$$

$$c_{GHj} = -\sum_{m=1}^{2} (-1)^m c_3\lambda_{y3} - \sum_{k=1}^{2}\sum_{m=1}^{2} (-1)^m c_{23}\lambda_{y2}$$

$$c_{GIj} = \sum_{k=1}^{2}\sum_{m=1}^{2} (-1)^k c_{23}\lambda_{x2}$$

$$c_{GJj} = 0$$

$$c_{GKj} = c_{GLj} = c_{GMj} = c_{GNj} = c_{GOj} = 0$$

$$k_{HHj} = \sum_{m=1}^{2} k_2\lambda^2_{z2} + \sum_{m=1}^{2} k_3\lambda^2_{y3} + \sum_{k=1}^{2}\sum_{m=1}^{2} k_{22}\lambda^2_{z3} + \sum_{k=1}^{2}\sum_{m=1}^{2} k_{23}\lambda^2_{y2}$$

$$k_{HIj} = -\sum_{k=1}^{2}\sum_{m=1}^{2} (-1)^{k+m} k_{23}\lambda_{y2}\lambda_{x2}$$

$$k_{HJj} = -\sum_{k=1}^{2}\sum_{m=1}^{2} (-1)^{k+2m} k_{22}\lambda_{z3}\lambda_{x2}$$

$$k_{HKj} = k_{HLj} = k_{HMj} = k_{HNj} = k_{HOj} = 0$$

$$c_{HHj} = \sum_{m=1}^{2} c_2\lambda^2_{z2} + \sum_{m=1}^{2} c_3\lambda^2_{y3} + \sum_{k=1}^{2}\sum_{m=1}^{2} c_{23}\lambda^2_{y2}$$

$$c_{HIj} = -\sum_{k=1}^{2}\sum_{m=1}^{2} (-1)^{k+m} c_{23}\lambda_{y2}\lambda_{x2}$$

$$c_{HJj} = 0$$

$$c_{HKj} = c_{HLj} = c_{HMj} = c_{HNj} = c_{HOj} = 0$$

$$k_{IIj} = \sum_{k=1}^{2}\sum_{m=1}^{2} k_{23}\lambda^2_{x2}$$

$$k_{IJj} = 0$$

$$k_{IKj} = k_{ILj} = k_{IMj} = k_{INj} = k_{IOj} = 0$$

$$c_{IIj} = \sum_{k=1}^{2}\sum_{m=1}^{2} c_{23}\lambda^2_{x2}$$

$$c_{IJj} = 0$$

$$c_{IKj} = c_{ILj} = c_{IMj} = c_{INj} = c_{IOj} = 0$$

$$k_{JJj} = \sum_{m=1}^{2} k_1 \lambda^2_{y4} + \sum_{k=1}^{2}\sum_{m=1}^{2} k_{21} \lambda^2_{y2} + \sum_{k=1}^{2}\sum_{m=1}^{2} k_{22} \lambda^2_{x2}$$

$$k_{JKj} = k_{JLj} = k_{JMj} = k_{JNj} = k_{JOj} = 0$$

$$k_{KKj} = \sum_{m=1}^{2} k_2 + \sum_{k=1}^{2}\sum_{m=1}^{2} k_{22}$$

$$k_{KLj} = 0$$

$$k_{KMj} = \sum_{k=1}^{2}\sum_{m=1}^{2} k_{22} \lambda_{z3} - \sum_{m=1}^{2} k_2 \lambda_{z2}$$

$$k_{KNj} = 0$$

$$k_{KOj} = -\sum_{k=1}^{2}\sum_{m=1}^{2} (-1)^{k+2m} k_{22} \lambda_{x2}$$

$$k_{LLj} = \sum_{m=1}^{2} k_3 + \sum_{k=1}^{2}\sum_{m=1}^{2} k_{23}$$

$$k_{LMj} = -\sum_{m=1}^{2} (-1)^m k_3 \lambda_{y3} - \sum_{k=1}^{2}\sum_{m=1}^{2} (-1)^m k_{23} \lambda_{y2}$$

$$k_{LNj} = \sum_{k=1}^{2}\sum_{m=1}^{2} (-1)^k k_{23} \lambda_{x2}$$

$$k_{LOj} = 0$$

$$k_{MMj} = \sum_{m=1}^{2} k_2 \lambda^2_{z2} + \sum_{m=1}^{2} k_3 \lambda^2_{y3} + \sum_{k=1}^{2}\sum_{m=1}^{2} k_{22} \lambda^2_{z3} + \sum_{k=1}^{2}\sum_{m=1}^{2} k_{23} \lambda^2_{y2}$$

$$k_{MNj} = -\sum_{k=1}^{2}\sum_{m=1}^{2} (-1)^{k+m} k_{23} \lambda_{y2} \lambda_{x2}$$

$$k_{MOj} = -\sum_{k=1}^{2}\sum_{m=1}^{2} (-1)^{k+2m} k_{22} \lambda_{z3} \lambda_{x2}$$

$$k_{NNj} = \sum_{k=1}^{2}\sum_{m=1}^{2} k_{23} \lambda^2_{x2}$$

$$k_{NOj} = 0$$

$$k_{OOj} = \sum_{m=1}^{2} k_1 \lambda^2_{y4} + \sum_{k=1}^{2}\sum_{m=1}^{2} k_{21} \lambda^2_{y2} + \sum_{k=1}^{2}\sum_{m=1}^{2} k_{22} \lambda^2_{x2}$$

$$c_{JJj} = 0$$

$$c_{JKj} = c_{JLj} = c_{JMj} = c_{JNj} = c_{JOj} = 0$$

$$c_{KKj} = \sum_{m=1}^{2} c_2$$

$$c_{KLj} = 0$$

$$c_{KMj} = -\sum_{m=1}^{2} c_2 \lambda_{z2}$$

$$c_{KNj} = 0$$

$$c_{KOj} = 0$$

$$c_{LLj} = \sum_{m=1}^{2} c_3 + \sum_{k=1}^{2}\sum_{m=1}^{2} c_{23}$$

$$c_{LMj} = -\sum_{m=1}^{2} (-1)^m c_3 \lambda_{y3} - \sum_{k=1}^{2}\sum_{m=1}^{2} (-1)^m c_{23} \lambda_{y2}$$

$$c_{LNIj} = \sum_{k=1}^{2}\sum_{m=1}^{2} (-1)^k c_{23} \lambda_{x2}$$

$$c_{LOj} = 0$$

$$c_{MMj} = \sum_{m=1}^{2} c_2 \lambda^2_{z2} + \sum_{m=1}^{2} c_3 \lambda^2_{y3} + \sum_{k=1}^{2}\sum_{m=1}^{2} c_{23} \lambda^2_{y2}$$

$$c_{MNj} = -\sum_{k=1}^{2}\sum_{m=1}^{2} (-1)^{k+m} c_{23} \lambda_{y2} \lambda_{x2}$$

$$c_{MOj} = 0$$

$$c_{NNj} = \sum_{k=1}^{2}\sum_{m=1}^{2} c_{23} \lambda^2_{x2}$$

$$c_{NOj} = 0$$

$$c_{OOj} = 0$$

$$f_i = -\sum_{j=1}^{h}\sum_{l=1}^{2}\sum_{k=1}^{2}\sum_{m=1}^{2}\tilde{\phi}_i^T\tilde{\boldsymbol{\Psi}}_{jzlkm}(t)\left(\frac{1}{8}m_1 g+\frac{1}{4}m_2 g+\frac{1}{2}m_3 g\right)$$
$$-\sum_{j=1}^{h}\sum_{l=1}^{2}\sum_{k=1}^{2}\sum_{m=1}^{2}\tilde{\phi}_i^T\tilde{\boldsymbol{\Psi}}_{jylkm}(t)\frac{1}{2}m_3\left\{\ddot{z}_{0y}\left(x_{jlkm}\right)+\ddot{\delta}_y(t)\right\}-\sum_{j=1}^{h}\sum_{l=1}^{2}\sum_{k=1}^{2}\sum_{m=1}^{2}\tilde{\phi}_i^T\tilde{\boldsymbol{\Psi}}_{jzlkm}(t)\frac{1}{2}m_3\left\{\ddot{z}_{0z}\left(x_{jlkm}\right)+\ddot{\delta}_z(t)\right\}$$
$$-\sum_{j=1}^{h}\sum_{l=1}^{2}\sum_{k=1}^{2}\sum_{m=1}^{2}\tilde{\phi}_i^T\tilde{\boldsymbol{\Psi}}_{jylkm}(t)k_{22}z_{0y}\left(x_{jlkm}\right)-\sum_{j=1}^{h}\sum_{l=1}^{2}\sum_{k=1}^{2}\sum_{m=1}^{2}\tilde{\phi}_i^T\tilde{\boldsymbol{\Psi}}_{jzlkm}(t)\left\{c_{23}\dot{z}_{0z}\left(x_{jlkm}\right)+k_{23}z_{0z}\left(x_{jlkm}\right)\right\}$$

$$f_{Aj} = -m_1\ddot{\delta}_y(t) \qquad f_{Bj} = -m_1\ddot{\delta}_z(t) \qquad f_{Cj} = f_{Dj} = f_{Ej} = 0$$

$$f_{Fj} = f_{Kj} = -m_2\ddot{\delta}_y(t)+\sum_{k=1}^{2}\sum_{m=1}^{2}k_{22}z_{0y}\left(x_{jlkm}\right)$$

$$f_{Gj} = f_{Lj} = -m_2\ddot{\delta}_z(t)+\sum_{k=1}^{2}\sum_{m=1}^{2}k_{23}z_{0z}\left(x_{jlkm}\right)+\sum_{k=1}^{2}\sum_{m=1}^{2}c_{23}\dot{z}_{0z}\left(x_{jlkm}\right)$$

$$f_{Hj} = f_{Mj} = \sum_{k=1}^{2}\sum_{m=1}^{2}\left\{k_{22}\lambda_{z3}z_{0y}\left(x_{jlkm}\right)-(-1)^m k_{23}\lambda_{y2}z_{0z}\left(x_{jlkm}\right)\right\}-\sum_{k=1}^{2}\sum_{m=1}^{2}(-1)^m c_{23}\lambda_{y2}\dot{z}_{0z}\left(x_{jlkm}\right)$$

$$f_{Ij} = f_{Nj} = \sum_{k=1}^{2}\sum_{m=1}^{2}(-1)^k k_{23}\lambda_{x2}z_{0z}\left(x_{jlkm}\right)+\sum_{k=1}^{2}\sum_{m=1}^{2}(-1)^k c_{23}\lambda_{x2}\dot{z}_{0z}\left(x_{jlkm}\right)$$

$$f_{Jj} = f_{Oj} = -\sum_{k=1}^{2}\sum_{m=1}^{2}(-1)^{k+2m}k_{22}\lambda_{x2}z_{0y}\left(x_{jlkm}\right)$$

B. Detailed components of matrices in Section 2.4.5

The components of $\boldsymbol{M}_v$, $\boldsymbol{C}_v$ and $\boldsymbol{K}_v$ are respectively the same with those in Section 2.4.4. The components of $\boldsymbol{F}_v$ can be given as follows.

$$f_{Aj} = -m_1\ddot{\delta}_y(t) \qquad f_{Bj} = -m_1\ddot{\delta}_z(t) \qquad f_{Cj} = f_{Dj} = f_{Ej} = 0$$

$$f_{Fj} = f_{Kj} = -m_2\ddot{\delta}_y(t)+\sum_{k=1}^{2}\sum_{m=1}^{2}k_{22}z_{0y}\left(x_{jlkm}\right)+\sum_{k=1}^{2}\sum_{m=1}^{2}k_{22}\boldsymbol{\Psi}_{jylkm}^T(t)\boldsymbol{w}_b$$

$$f_{Gj} = f_{Lj} = -m_2\ddot{\delta}_z(t)+\sum_{k=1}^{2}\sum_{m=1}^{2}k_{23}z_{0z}(x_{jlkm})+\sum_{k=1}^{2}\sum_{m=1}^{2}c_{23}\dot{z}_{0z}(x_{jlkm})+\sum_{k=1}^{2}\sum_{m=1}^{2}k_{23}\boldsymbol{\Psi}_{jzlkm}^T(t)\boldsymbol{w}_b+\sum_{k=1}^{2}\sum_{m=1}^{2}c_{23}\boldsymbol{\Psi}_{jzlkm}^T(t)\dot{\boldsymbol{w}}_b$$

$$f_{Hj} = f_{Mj} = \sum_{k=1}^{2}\sum_{m=1}^{2}\{k_{22}\lambda_{z3}z_{0y}(x_{jlkm})-(-1)^m k_{23}\lambda_{y2}z_{0z}(x_{jlkm})\}-\sum_{k=1}^{2}\sum_{m=1}^{2}(-1)^m c_{23}\lambda_{y2}\dot{z}_{0z}(x_{jlkm})$$
$$+\sum_{k=1}^{2}\sum_{m=1}^{2}\{k_{22}\lambda_{z3}\boldsymbol{\Psi}_{jylkm}^T(t)-(-1)^m k_{23}\lambda_{y2}\boldsymbol{\Psi}_{jzlkm}^T(t)\}\boldsymbol{w}_b-\sum_{k=1}^{2}\sum_{m=1}^{2}(-1)^m c_{23}\lambda_{y2}\boldsymbol{\Psi}_{jzlkm}^T(t)\dot{\boldsymbol{w}}_b$$

$$f_{Ij} = f_{Nj} = \sum_{k=1}^{2}\sum_{m=1}^{2}(-1)^k k_{23}\lambda_{x2}z_{0z}(x_{jlkm})+\sum_{k=1}^{2}\sum_{m=1}^{2}(-1)^k c_{23}\lambda_{x2}\dot{z}_{0z}(x_{jlkm})$$
$$+\sum_{k=1}^{2}\sum_{m=1}^{2}(-1)^k k_{23}\lambda_{x2}\boldsymbol{\Psi}_{jzlkm}^T(t)\boldsymbol{w}_b+\sum_{k=1}^{2}\sum_{m=1}^{2}(-1)^k c_{23}\lambda_{x2}\boldsymbol{\Psi}_{jzlkm}^T(t)\dot{\boldsymbol{w}}_b$$

$$f_{Jj} = f_{Oj} = -\sum_{k=1}^{2}\sum_{m=1}^{2}(-1)^{k+2m}k_{22}\lambda_{x2}z_{0y}(x_{jlkm})-\sum_{k=1}^{2}\sum_{m=1}^{2}(-1)^{k+2m}k_{22}\lambda_{x2}\boldsymbol{\Psi}_{jylkm}^T(t)\boldsymbol{w}_b$$

Chapter 3

Train-induced vibration of high-speed railway viaducts

3.1 Introduction

The running-train induced bridge vibration problem has been an interest of many researchers since a long time ago and numerous efforts have been made. For the high-speed railway system in Japan, considering the extremely high speed of bullet trains, the bridge vibration caused by bullet trains is concerned. The severe vibration over a long term may cause deterioration of the bridge structures, such as the cracking or exfoliation of concrete. In addition to the investigation on the vibration characteristics of the viaducts by means of field tests, it is necessary to establish a reliable and effective analytical approach to simulate the bridge vibration caused by running trains. Such approach can offer convenient predictions and diagnoses to the vibration of either existing bridges or those in the planning stage, therefore effective countermeasures can be proposed.

In this chapter, focusing on a standard type of elevated bridge in Tokaido Shinkansen, which is built with reinforced concrete in the form of a portal rigid frame, an analytical procedure [1~5] to simulate the bridge-train coupled vibration problem considering their interaction as well as the effect of ground properties is established. Dynamic responses of the high-speed railway viaducts under moving bullet trains are analyzed in consideration of the wheel-track interaction with the rail surface roughness, based on the analytical theory described in Chapter 2. The viaducts including the track structure are modeled as 3-D beam elements and simultaneous dynamic differential equations of the bridge are derived using modal analysis. The elastic effect of ground springs at the pier bottoms and the connection effect of the sleepers and ballast between the track and the deck slab are model with double nodes connected by springs. Bullet train models of two-, six- and nine-DOF dynamic systems are developed for the analyses and the differences between these models are discussed. To demonstrate the validity of the finite element bridge model, eigenvalue analysis is carried out and the basic natural frequency is compared with experimental value. For the validation of the developed bullet train models, the dynamic response analysis of the bridge-train interaction system was carried out and the analytical results were compared with experimental ones.

Based on the simulation of bridge-train interaction, the dynamic characteristics of the viaducts including the fact where predominant vibration occurs are clarified. Influences of train models on the dynamic responses of viaducts are discussed. The predominant

acceleration responses and frequencies of the bridge vibration are investigated. The effect of train speed on bridge response is also examined. The reaction forces at the pier bottoms, which can be used in further analysis of site vibration, are calculated using its influence value matrix. Then the countermeasures against to allay the undesirable vibration of the bridge are proposed. In this study, form the dynamic response analysis results, the fact that the excessive vibration occurs at the hanging parts of the elevated bridge, which is coincident with the experimental results, is confirmed. Consequently, countermeasures against the predominant vibration are proposed by reinforcing the hanging parts. The effect of the proposed countermeasures is demonstrated through dynamic analysis as well as the results from actual construction case. At last, the efforts are also made to improve the analytical efficiency by developing a one-block model of the bridge.

3.2 Analytical models

3.2.1 Bridge model

A typical high-speed railway reinforced concrete viaduct in the form of a rigid portal frame shown in **Fig. 3.2.1** is adopted in this analysis. Field test was carried out on such an elevated bridge of Shinkansen railway and the dynamic responses of the viaducts caused by running bullet train are recorded [5] [6]. The viaducts are built with 24 m-length bridge blocks which are separated with each other and connected only by rail structure at adjacent ends. Each block consists of three 6 m-length center spans and two 3 m cantilever girders, so called hanging parts, at each end. Considering the boundary condition of the bridge, three blocks (72 m) of the bridge with 24 m-length of each block are adopted as the analytical model. Only the dynamic response of the middle block will be examined, thus the influence of train entering or quitting can be considered and the connection effect of rail structure can be taken into account. The unit weights and Young's moduli of the structures are shown in **Table 3.2.1**.

Fig. 3.2.2 shows that the three-block bridge is modeled as 3-D beam elements with 6 DOF at each node. The lumped mass system is adopted for the bridge beam elements. Mass of the ballast is also incorporated. Hanging parts also exist on both sides of the superstructure in the traverse direction as shown in **Fig. 3.2.1**. The mass of these parts are attached to the nodes at the most outside line in the finite element model. The ground condition of the site where the field tests are conducted is measured to be Dense to Soft Soil that is defined in seismic design codes [7]. Double nodes defined as two independent nodes sharing the same coordinate are adopted at the bottoms of the piers to simulate the effect of ground springs [8]. The ground springs are calculated according the design codes [9], including the effect of the footing and pile structures. The ground spring constants are shown in **Table 3.2.2**. Rayleigh damping [10] is adopted for the structural model. A damping constant of 0.03 is assumed for the first and second natural modes of the structure [11].

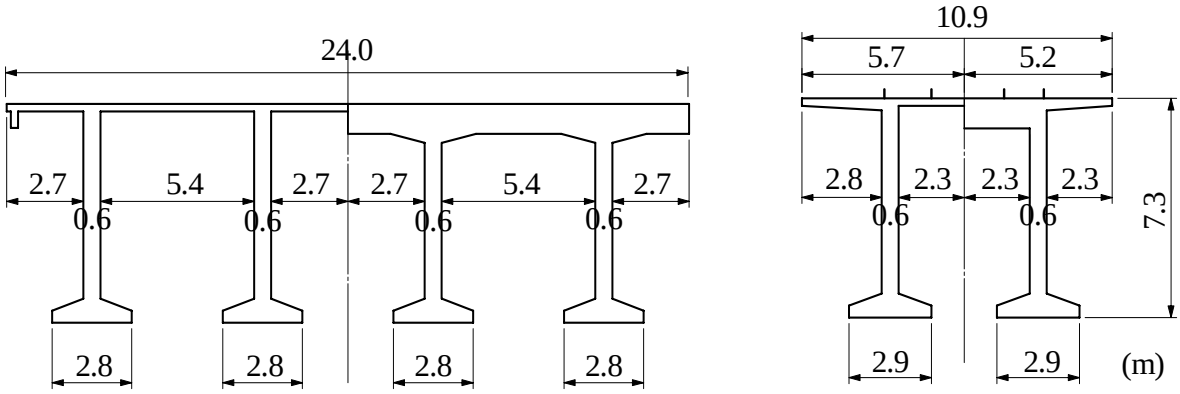

Fig. 3.2.1 Dimension of the bridge

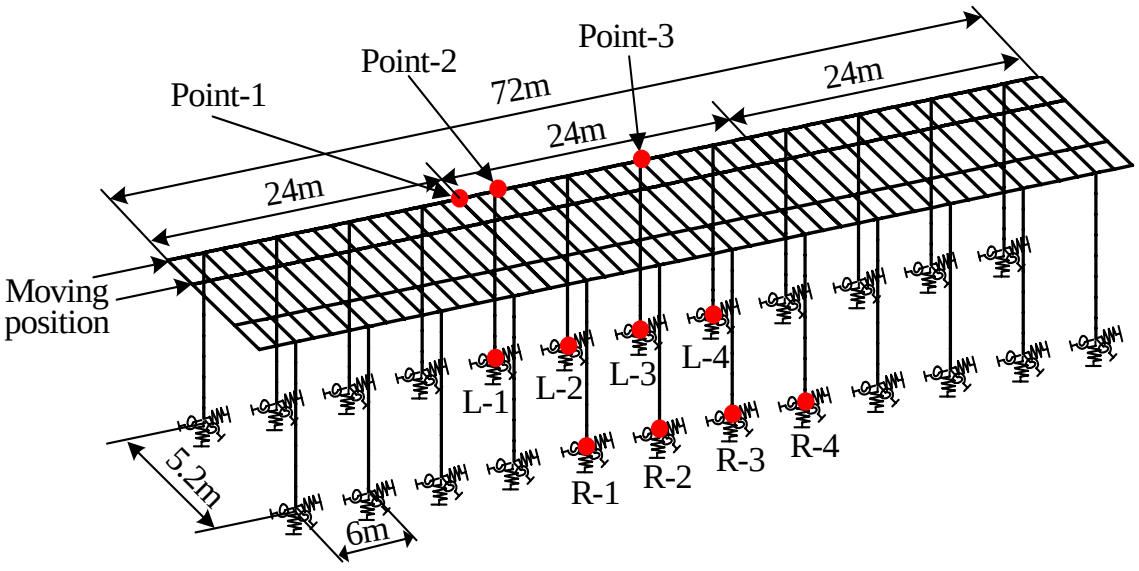

Fig. 3.2.2 Finite element model of the bridge

Table 3.2.1 Unit weight

	Weight (tf/m^3)	Young's moduli E (N/cm^2)
Reinforced concrete	2.5	2.45×10^6
Track skeleton	0.75	2.06×10^7
Ballast	1.9	—

Table 3.2.2 Ground spring constants

Sort of spring	Longitudinal	Transverse
Vertical spring of pile top (kN/m)	3.86×10^6	
Rotating spring of pile top (kN·m/rad)	3.64×10^6	2.42×10^6
Horizontal spring of footing (kN/m)	4.84×10^3	4.72×10^3
Horizontal spring of pile top (kN/m)	8.22×10^4	8.08×10^4

Table 3.2.3 Property of rail

Area (m^2)	7.75×10^{-3}
Mass (t/m)	0.0608
Moment of inertia (m^4)	3.09×10^{-5}
Spring constant of track (MN/m)	70

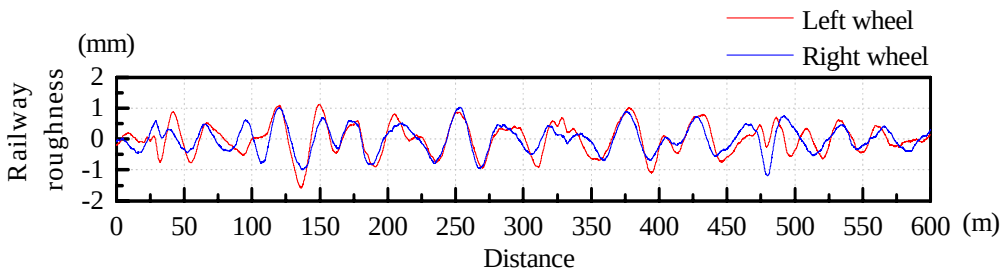

Fig. 3.2.3 Surveyed value of rail surface roughness

3.2.2 Rail model

The rail structure is also modeled as 3D beam elements with 6 DOF at each node. Double nodes are also defined here to simulate the elastic effect of sleepers and ballast at the positions of sleepers. Properties of the rail and the spring constant of the track are shown in **Table 3.2.3**. The vertical spring constant of the track is derived from the ratio of the wheel load to the rail's displacement in the vertical direction. The horizontal spring constant of the track is assumed to be 1/3 of the value in the vertical direction [12]. Only roughness in the vertical direction of the rail is taken into account. The surveyed values of railway roughness are shown in **Fig. 3.2.3**

3.2.3 Train models

In the field of vehicle engineering, vehicle model often comprises dozens of DOFs in order to evaluate the dynamic responses of the vehicle. In this study, considering the focuses of the analysis and also the analytical efficiency, the DOFs of the car model are limited to the ones that contribute to the vertical vibration of the bridge. Presuming that the variable dynamic load caused by the wheelset is negligible, the motions of the wheelsets are assumed to be compatible with the rail structure. More detailed discussion about the train model has been performed in Reference [6].

In order to investigate the influence of train models on the dynamic responses of elevated bridges, each car of the train is modeled as two-, six-, and nine-DOF models which are idealized in Chapter 2. The dimensions of the train models are shown in **Fig. 3.2.4**. As described in Chapter 2, the two-DOF plane train model does not take account of the mass of axles, while the six-DOF plane train model and the nine-DOF 3-D train model consider the motions of the axle masses. The train is assumed to be composed of 16 cars according to the actual operational case. **Table 3.2.4** and **Table 3.2.5** respectively show the values of the dimensions and the dynamic properties of the train. The train velocity is assumed to be 270 km/h, referring to the actual Shinkansen operational speed.

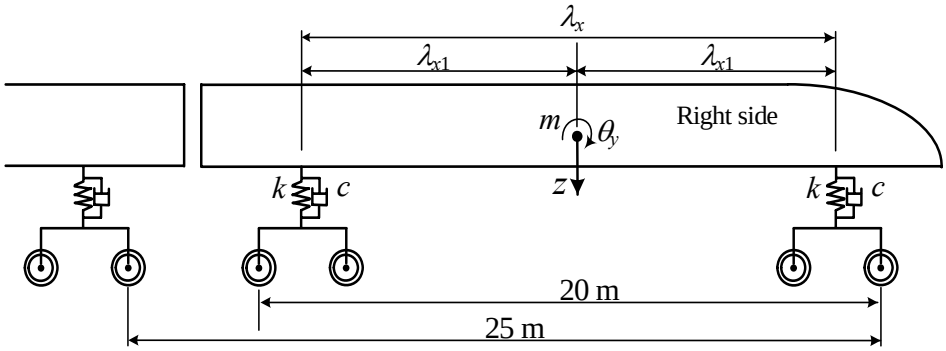

Fig. 3.2.4 (a) two-DOF vehicle model

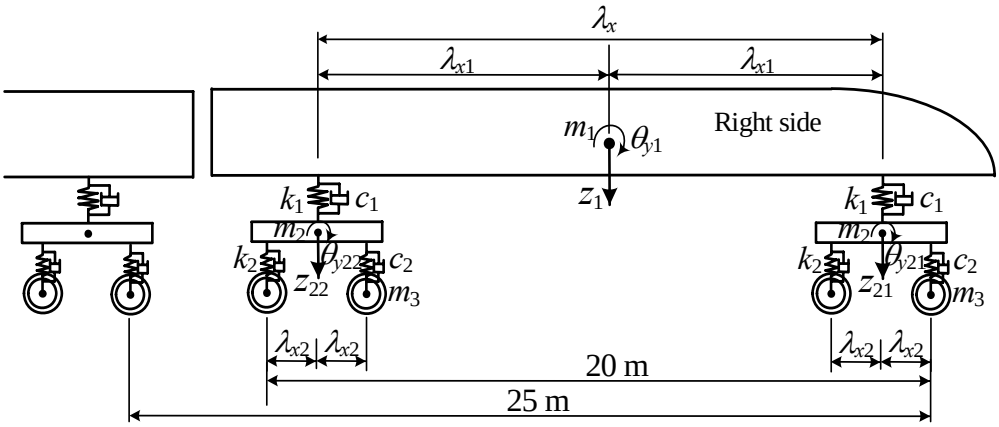

Fig. 3.2.4 (b) six-DOF vehicle model

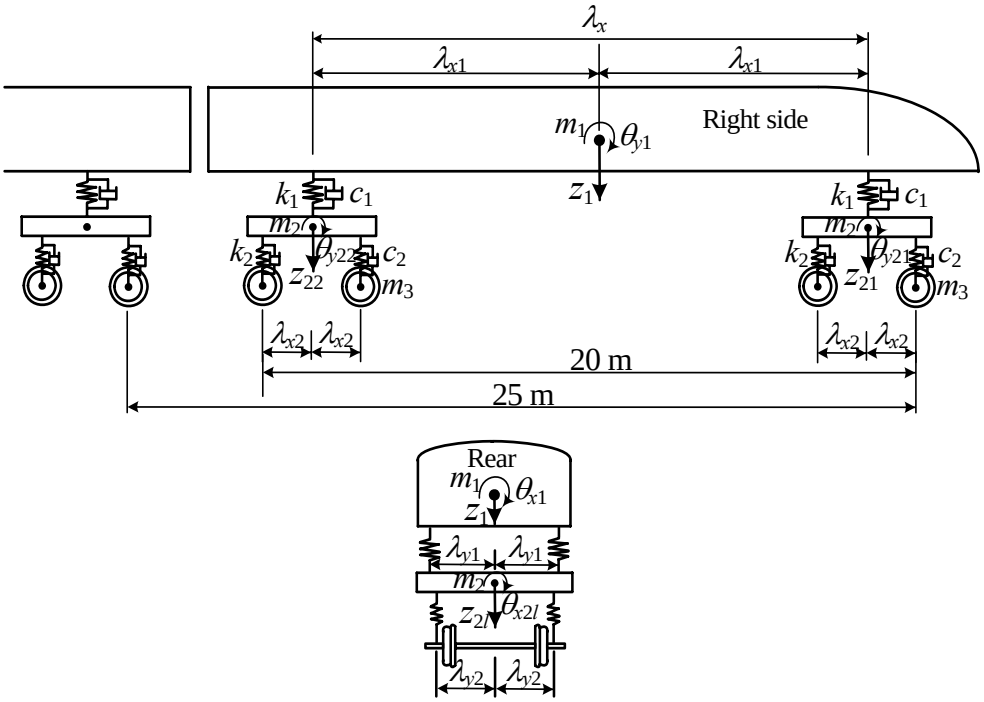

Fig. 3.2.4 (c) nine-DOF vehicle model

Table 3.2.4 Dimension of bullet train

Distance of centers of bogies	λ_x	17.50 m
1/2 distance of bogie centers	λ_{x1}	8.75 m
1/2 distance of axes	λ_{x2}	1.25 m
1/2 distance of upper springs	λ_{y1}	1.23 m
1/2 distance of lower springs	λ_{y2}	1.00 m

Table 3.2.5 Properties of moving train

Definition	Notation	Value
Weight of car body	w_1	321.616 kN
Weight of bogie	w_2	25.862 kN
Weight of wheel	w_3	17.689 kN
Mass moment of inertia of car body	I_{x1}	49.248 kN·s^2·m
	I_{y1}	2512.628 kN·s^2·m
Mass moment of inertia of bogie	I_{x2}	2.909 kN·s^2·m
	I_{y2}	4.123 kN·s^2·m
Spring constant	k_1	443.0 kN/m
	k_2	1209.81 kN/m
Damping coefficient	c_1	21.6 kN·s/m
	c_2	19.6 kN·s /m

3.3 Natural modes and frequencies

Eigenvalue analysis of the bridge model is performed and the mode shapes are shown in **Fig. 3.3.1**. The first through the ninth modes indicate the vibration in horizontal direction of the bridge. The predominant frequency of the horizontal natural mode is observed to be 2.20 Hz, showing good agreement with the value of filed test which is 2.19 Hz. Therefore, the validity of the bridge model can be confirmed. Predominant frequencies of vertical bending natural mode and torsional mode are about 11.9 Hz and 13.9 Hz, respectively. The highest frequency taken into account in this analysis is about 102 Hz corresponding to the 277th natural mode. The predominant frequencies of the rail mode are larger than 200 Hz, but it is considered that the influence of the rail vibration on the structures can be neglected.

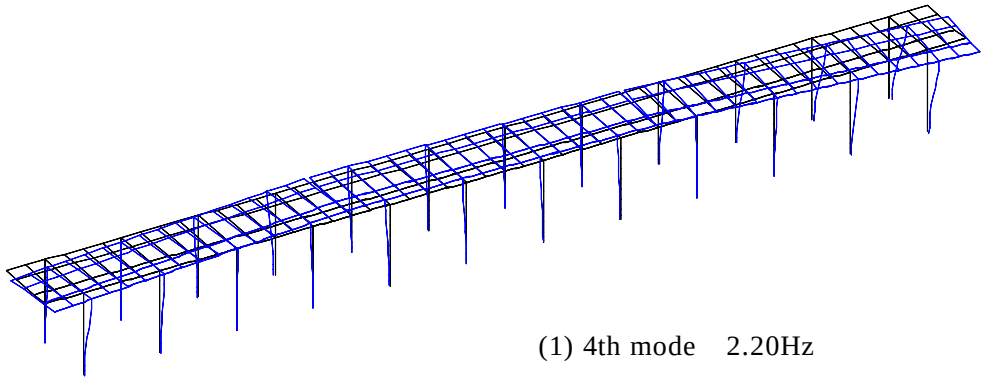

(1) 4th mode　2.20Hz

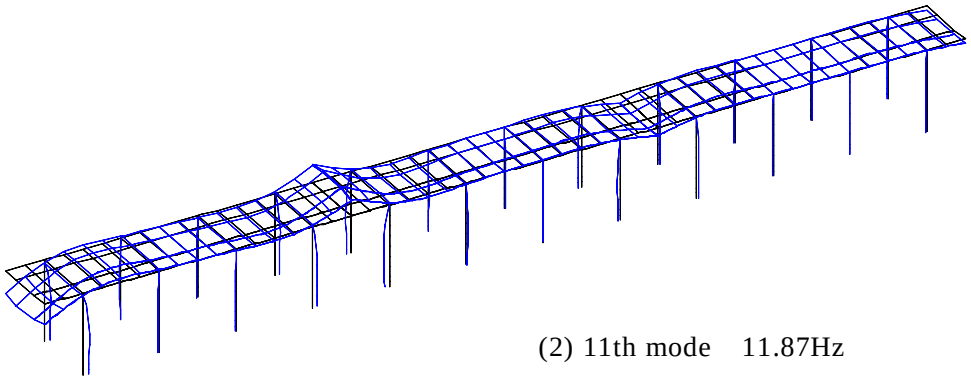

(2) 11th mode　11.87Hz

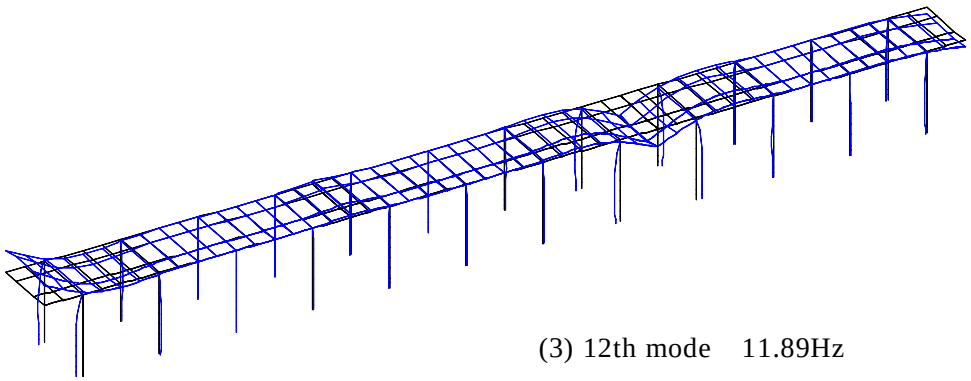

(3) 12th mode　11.89Hz

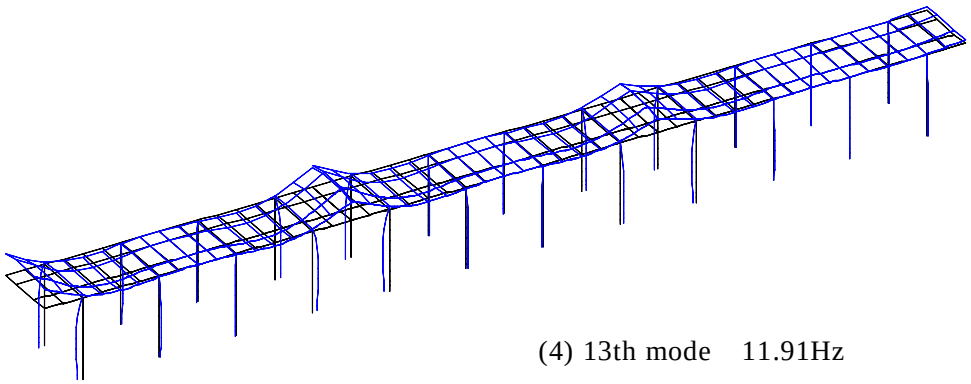

(4) 13th mode　11.91Hz

Fig. 3.3.1 (1)　Natural mode shapes and Natural frequencies of bridge

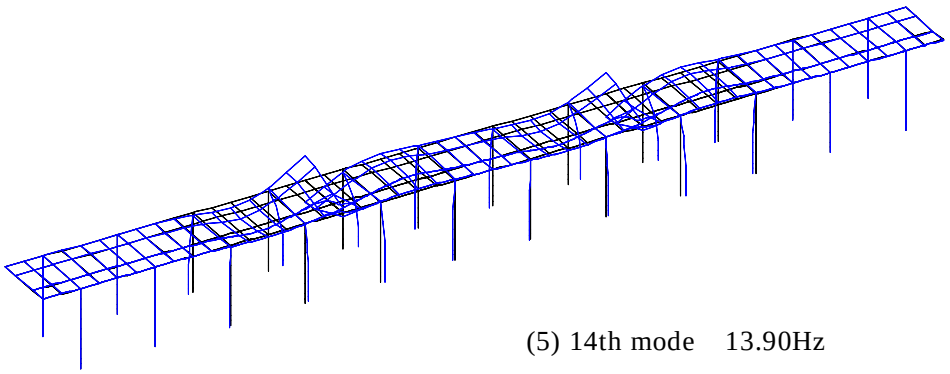

(5) 14th mode　13.90Hz

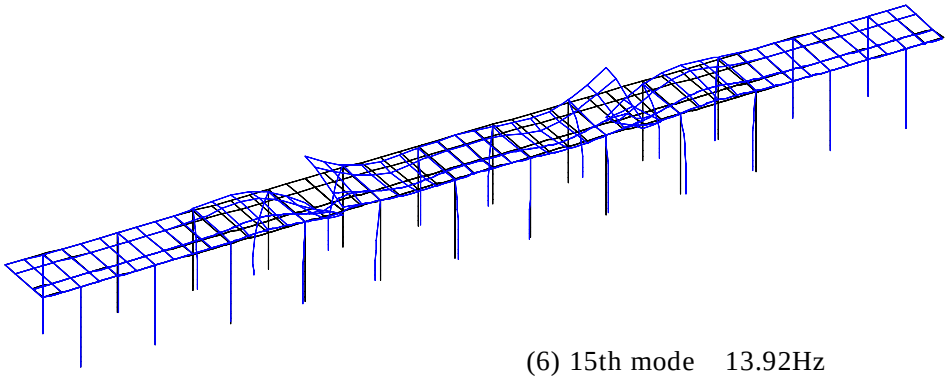

(6) 15th mode　13.92Hz

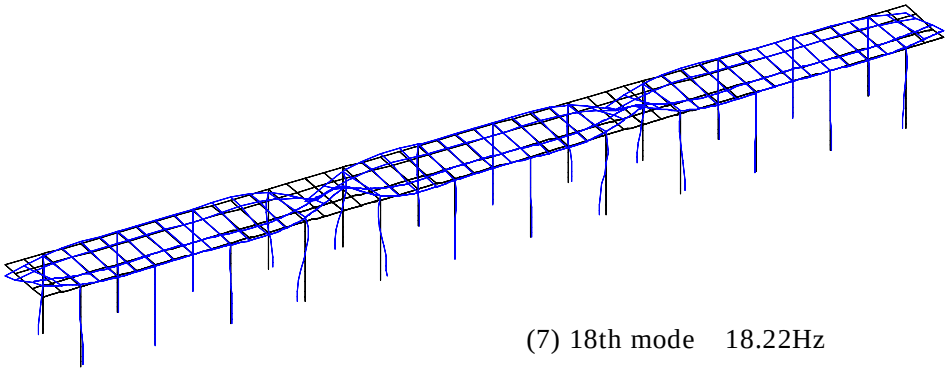

(7) 18th mode　18.22Hz

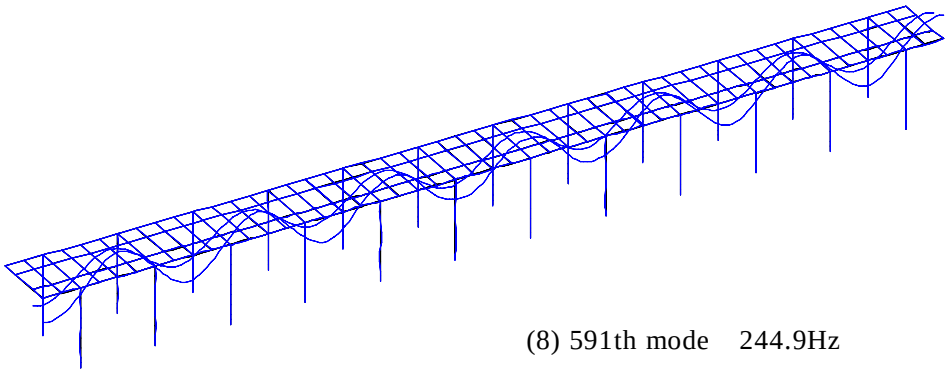

(8) 591th mode　244.9Hz

Fig. 3.3.1 (2)　Natural mode shapes and Natural frequencies of bridge

3.4 Validation of train model

In the previous section, the bridge model is validated through confirming its natural frequency. In order to discuss the dynamic responses of the bridge-train interaction system using the train models established in Chapter 2, it is also necessary to confirm the validity of the analytical train model. In this study, since no experimental data of the dynamic responses of the train itself are available, the validity of the train model will be demonstrated by comparing the analytical and experimental bridge responses subjected to the running train. Since the two- and six-DOF models are only simplifications of the nine-DOF model, herein only the validity of the nine-DOF train model will be discussed.

The actual field test [6] to measure the vibration of Shinkensen viaduct was conducted at the No. 1 Arasaki Viaduct of the Tokaido Shinkansen located in Ogaki, Gifu on November 1, 1999. Bullet trains composed of sixteen cars were running through the viaduct with its actual operational speeds of 270 km/h or 220 km/h. The bridge vibration was measured at different points of the viaduct during the bullet trains' passage using accelerometers. Then the acceleration responses of the viaduct were recorded on the data recorder from the accelerometers after being processed by amplifiers. The sampling rate of the data was 512 Hz. In this analysis, the bridge vibration recorded at point-1 through point-3 of the viaducts indicated in **Fig. 3.2.2** will be examined. Herein, point-1, point-2, and point-3 respectively indicate the point of the end of the cantilever beam (referred to as the hanging part), the top of the first pier and the top of the third pier of the middle block of the three-block viaduct model, with respect to the direction that the train runs towards.

Based on the conditions of the field test described above and the actual properties of the viaduct and the bullet train, the analytical conditions were determined and the analysis was carried out with the developed analytical program. Since there are still many uncertainties in modeling either the bullet train or the viaduct, it is difficult to reproduce the completely accurate responses of the bridge vibration by numerical approaches. However, for actual discussion in civil engineering filed, in most cases it is sufficient if the amplitudes and main vibrational components can be expressed.

The analytical acceleration responses and the experimental ones in the vertical direction, of point-1 through point-3 of the viaducts indicated in **Fig. 3.2.2**, are shown respectively in **Fig. 3.4.1** with Fourier spectra under the speed of 270 km/h. The features of this analytical case are that the stiffness of the viaduct is relatively high and the train was running with an extremely high speed. Thus the high frequencies of the bridge vibration should be sufficiently considered. On the other hand, the highest frequency interested in environmental vibration problems is less than 100 Hz. Therefore in this study, the highest frequency taken into account

in the analysis is set as 100 Hz and the components above 100 Hz will be filtered by a low-pass filter. As shown in **Fig. 3.4.1**, analytical results using the nine-DOF train model indicate relatively good agreement with the experimental results, especially for the amplitudes. The main components of frequencies can also considered to some extent acceptable for discussing the interested structural or environmental vibration problems. Thereby the bullet train model established here and the analytical procedure developed can be considered valid and effective. Therefore, it is possible to investigate various problems related the traffic-induced bridge vibration using the developed analytical procedure.

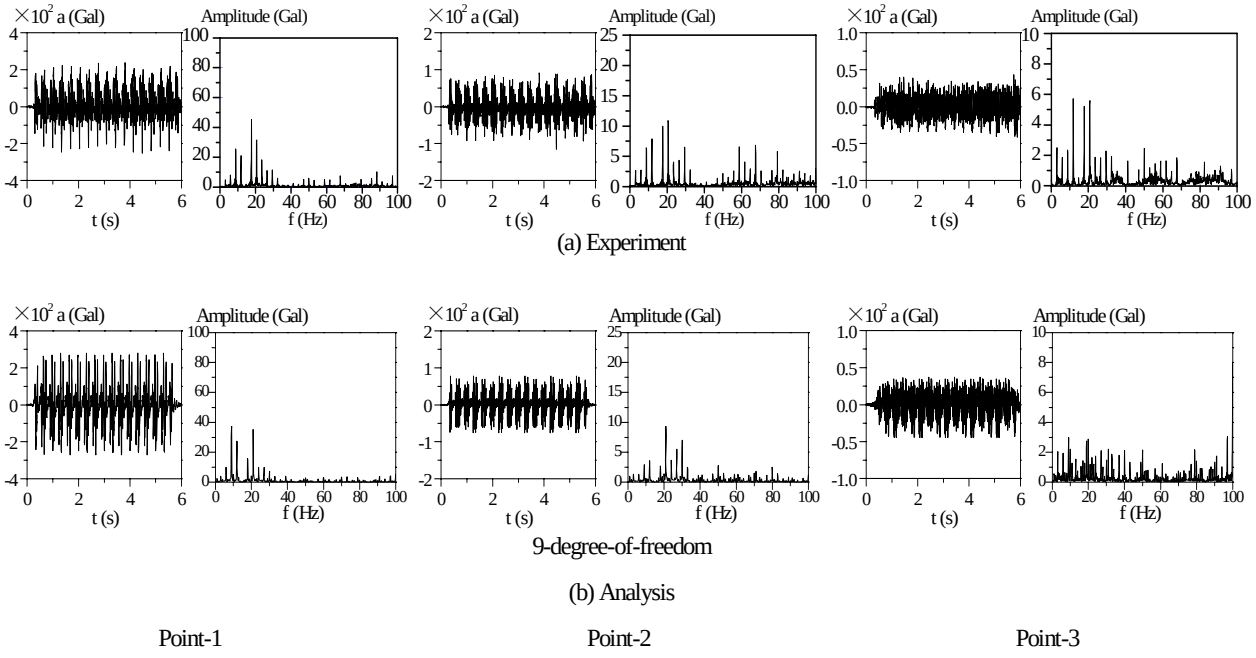

Fig. 3.4.1 Bridge acceleration response under moving train

3.5 Dynamic responses of viaducts

3.5.1 Influence of train models on acceleration response

In this subsection, the analytical values compared with experimental ones at the point-1 through point-3 of the viaducts indicated in **Fig. 3.2.2**, referring to the velocity of 270 km/h of the train, are investigated to examine the influence of different train models. The experimental values and analytical acceleration responses simultaneously with the Fourier spectra at point-1 through point-3 in vertical direction, referring to two-, six-, nine-degree-of-freedom train models, are shown in **Fig. 3.5.1**, respectively. Here, the response component above 100 Hz is also filtered for both analytical and experimental values. The maximum acceleration responses and root-mean-square (rms) values corresponding to experiment and analysis are shown in **Tables 3.5.1** and **3.5.2**, respectively. The errors of the analytical results compared with experimental values are also indicated in the parentheses in both **Tables 3.5.1** and **3.5.2**.

We can see from **Fig. 3.5.1** that the experimental acceleration responses indicate the tendency of Point-1>Point-2>Point3. For all points, the acceleration responses are predominant at around 10 Hz and 20 Hz. These features can be also seen in the analytical results of either two-, or six-, or nine-DOF train model.

By comparing the maximum and rms values in **Tables 3.5.1** and **3.5.2**, we can say that the analytical results due to the six- and nine-DOF train models considering the mass of the axles show better agreement with the experimental ones than those of the two-DOF model. In particular for the rms values, the results due to two-DOF model introduced errors about 50% at Point-1 and 40% at Point-3. On the other hand, for the frequency components above 50 Hz expressed by the six- and nine-DOF models at Point-2 and Point-3 cannot be seen in the results of two-DOF model. This phenomenon indicates that, without considering the mass of the axles which have higher natural frequencies than the car body, the two-DOF model can’t reproduce the vibrational components in the high frequencies.

For the predominant components at around 10 Hz and 20 Hz indicated in the experimental values, the results due to two- and six-DOF models show too large Fourier amplitudes of about 1.5 times those of the experimental ones. On the contrary, the results due to the nine-DOF model indicate good coincidence with the experimental values. This is inferred because of the effect of the rolling motions of the car body and the bogies in nine-DOF model. The amplitudes in the results of the nine-DOF model decreased compared with those of the six-DOF model. The reason is also considered due to the effect of the rolling motions, because in the nine-DOF model the motions of the train are three-dimensional and the wheel loads are distributed compared with the two-dimensional model, so that the excessive impact

effect on the bridge is allayed.

According to the discussion above, we can conclude that the analytical results of six- and nine-DOF train models are showing better agreement with the experimental values, compared with the results of two-DOF model. Furthermore, the analytical results of nine-DOF model are considered indicating the best coincidence with the experimental ones, because it can take account of all the main factors that contribute to the vertical vibration of the bridge-train interaction system. Therefore for more accurate investigation, it is desirable to use the nine-DOF train model while the six-DOF model can used in preliminary discussions.

3.5.2 Predominant acceleration responses and frequencies

As known from the discussion in the preceding subsection, the analytical results of the nine-DOF train model indicate the best agreement with the experimental values. In the followings, only the analytical results by the nine-DOF train model will be used for discussion.

As shown in **Fig. 3.5.1**., the analytical acceleration responses by the nine-DOF train model displayed larger amplitudes, 16.7% of the maximum value and 33.5% of the rms value, compared with experimental values at point-1. Moreover, the analytical results are predominant at the lower parts of frequencies around 10 Hz. The main reason is considered as that the hanging parts of the viaducts are connected with neighboring ones by rail and ballast in the actual structures, but only the effects of the rail can be taken into account in the analysis, i.e. the damping effect of the ballast cannot be considered. Furthermore, there should be errors in modeling the structure and the train, and also approximate properties of the bullet train have been used (Since exact properties are not available). Despite of these uncertainties, the analytical results by the nine-DOF train model are considered with sufficient accuracy to discuss the actual engineering problems. For the maximum acceleration responses and rms values as respectively shown in **Tables 3.5.1** and **3.5.2**, both indicate the largest values at point-1, and the maximum acceleration response at Point-2 that is close to the hanging part showed larger value, compared with the values of point-3. The reason is considered as that the predominant vibration affect the adjacent Pint-2 more seriously than the separated Point-3. The high-frequency components, in the range of about 60Hz to 100Hz, are relatively important in responses of the tops of piers, compared with the response of the hanging part.

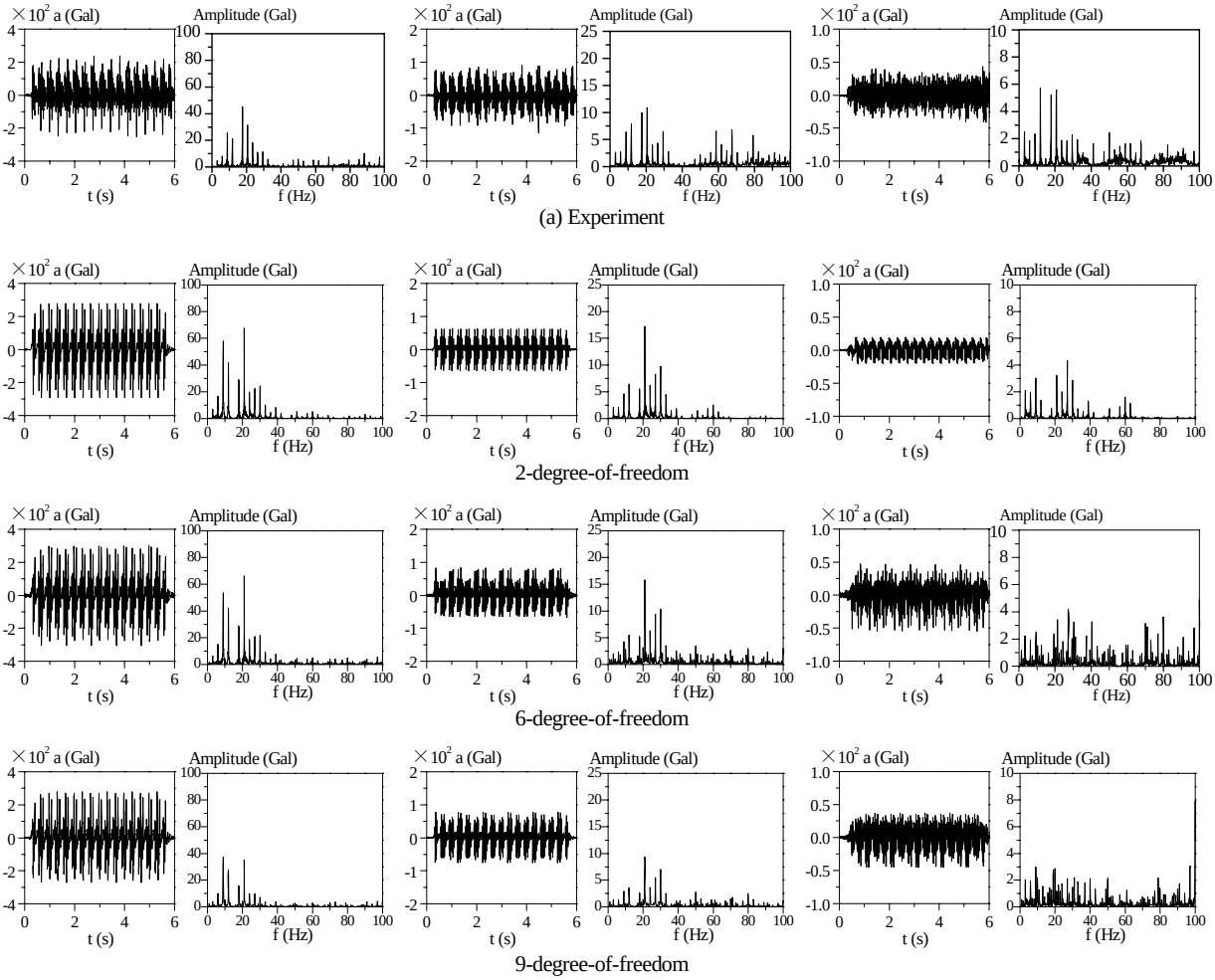

Fig. 3.5.1 Acceleration responses of bridge

Table 3.5.1 Maximum acceleration (v=270km/h)

Point No.	Maximum acceleration (Gal)			
	Experiment	Analysis (error)		
		2 DOF	6 DOF	9 DOF
Point-1	239.4	293.3 (+22.5%)	305.4 (+27.6%)	279.4 (+16.7%)
Point-2	91.4	65.8 (-28.0%)	83.5 (-8.6%)	78.3 (-14.3%)
Point-3	43.1	21.2 (-50.8%)	55.2 (-28.1%)	44.9 (+4.2%)

Table 3.5.2 rms values (v=270km/h)

Point No.	rms value (Gal)			
	Experiment	Analysis (error)		
		2 DOF	6 DOF	9 DOF
Point-1	79.8	119.7 (+50.0%)	116.1 (+45.5%)	106.5 (+33.5%)
Point-2	29.0	26.9 (-7.2%)	28.6 (-1.4%)	26.8 (-7.6%)
Point-3	14.9	8.8 (-40.9%)	14.6 (-2.0%)	14.8 (-0.7%)

3.5.3 Responses under different velocities of train

Analysis with the train speed of 220 km/h is also carried out to investigate the influence of velocity. At first, the analytical responses of acceleration and Fourier spectra are also compared with experimental values to validate the analytical procedure. Then the analytical results are compared with the ones under the train with the speed of 270 km/h..

As shown in **Fig. 3.5.2**, the analytical results also indicate good agreement with the experimental values. Responses of the bridge display similar characteristics with the case under the train with the velocity of 270 km/h.

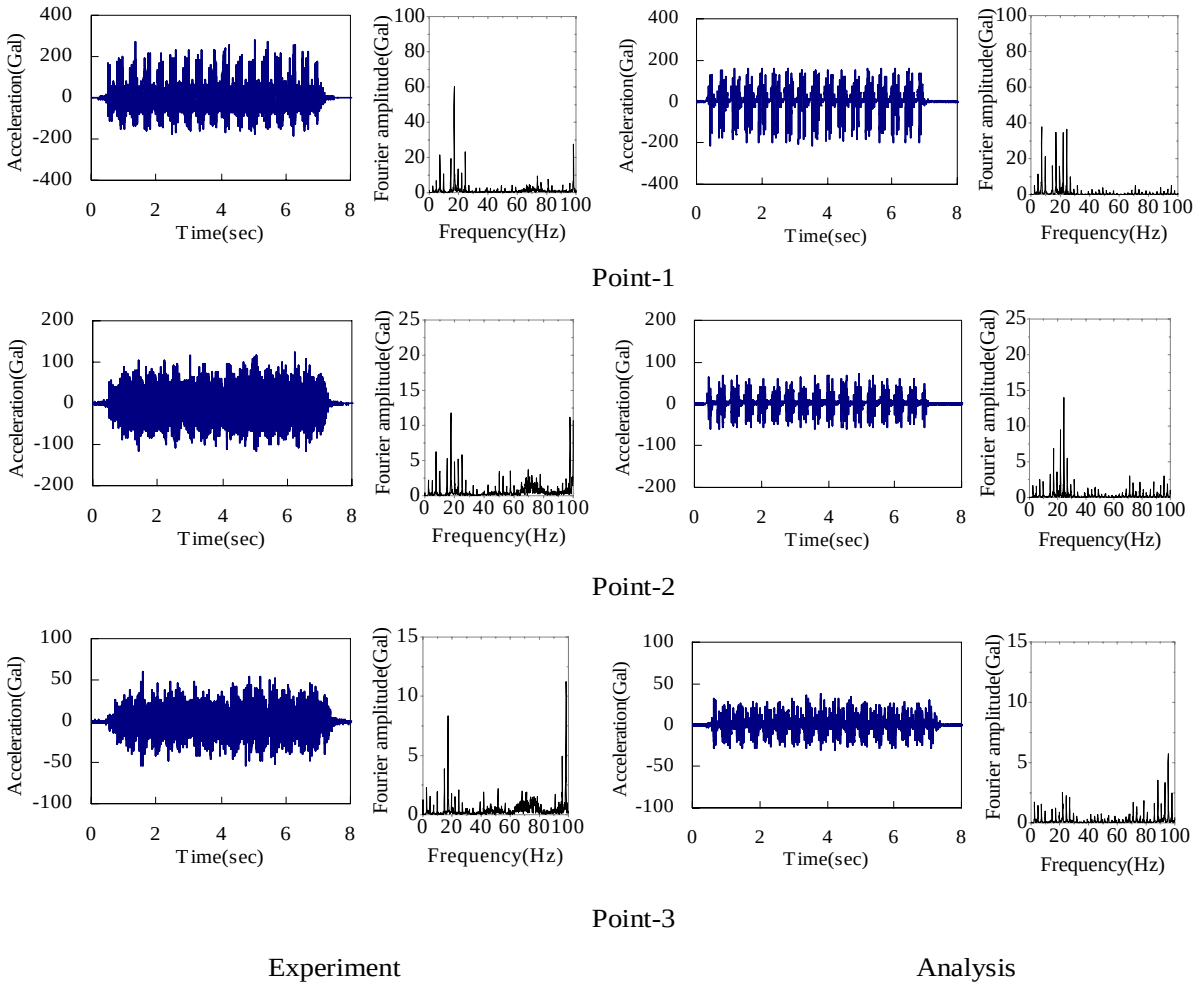

Fig. 3.5.2 Acceleration of Bridge (220km/h)

Comparison of the analytical responses by different speeds of train is shown in **Fig. 3.5.3**. As known form the comparison, the responses of 270 km/h indicate larger amplitudes than that of 220 km/h, especially for the hanging part of the bridge, which can be predicted since the train's impact effect of 270 km/h on the structure excels that of 220 km/h.

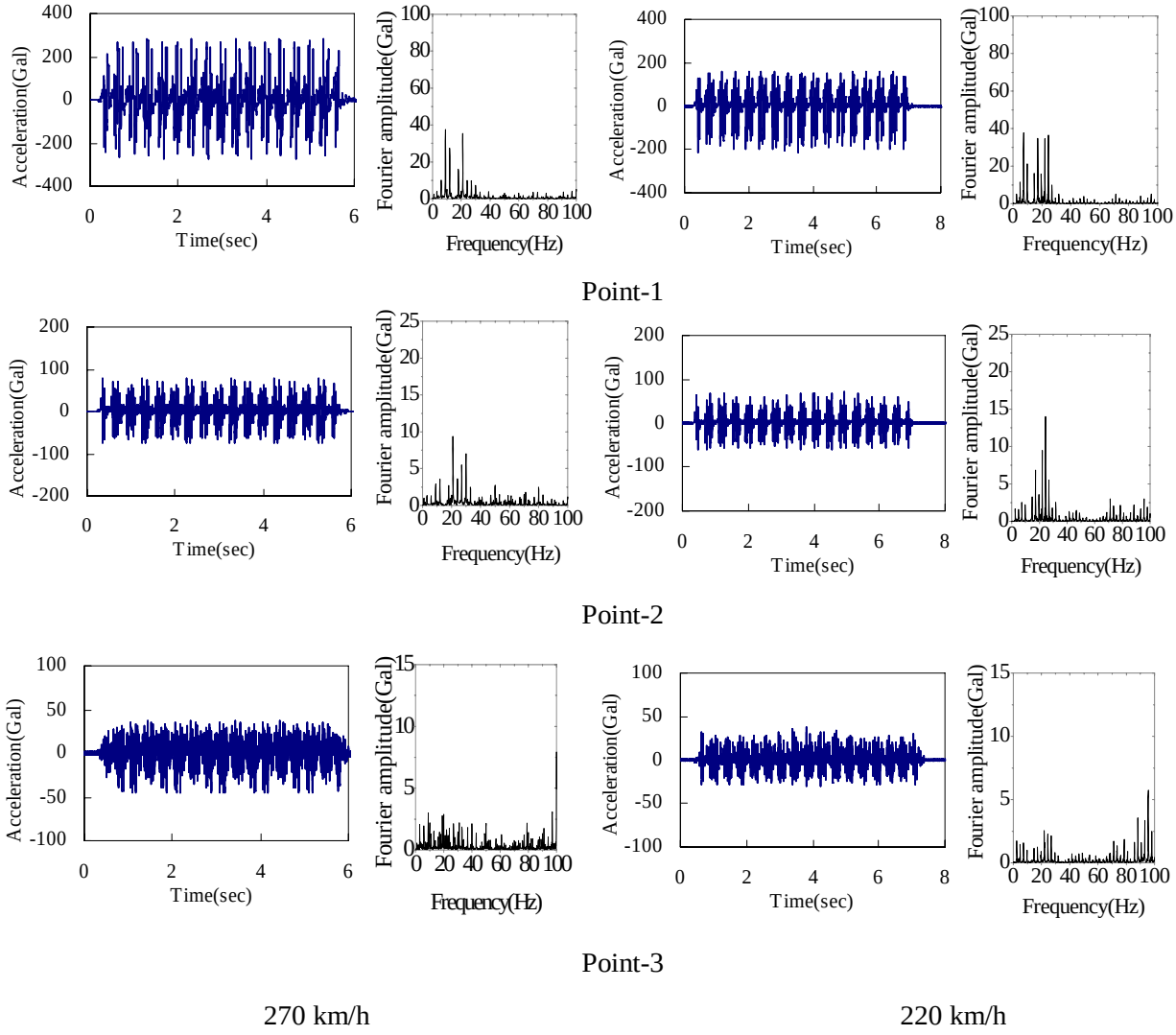

Fig. 3.5.3 Responses of different speed of train

3.5.4 Reaction force of piers

Reaction forces of the piers in vertical direction are calculated using the theory described in chapter 2 and the results are partly shown in **Fig. 3.5.4**. Herein, as depicted in **Fig. 3.2.2**, L-1 to L-4 and R-1 to R-4 respectively indicate the piers on the left and right side of the middle block of the bridge, with respect to the direction that the train runs towards. The reaction forces of the piers on the left side are predominant compared with the ones on the right side since the trains are assumed running along the left side of the bridges. In particular, as shown in **Fig. 3.5.4**, the amplitude of L-1 is observed to some extent larger compared with that of L-2. The reason is considered as that the maximum acceleration response, which leads to a larger inertia force, is appearing at the hanging part of the bridge as shown in **Fig. 3.5.1**.The reaction forces of the piers obtained in this study can be used as input external excitations in the future analysis of site vibration problems.

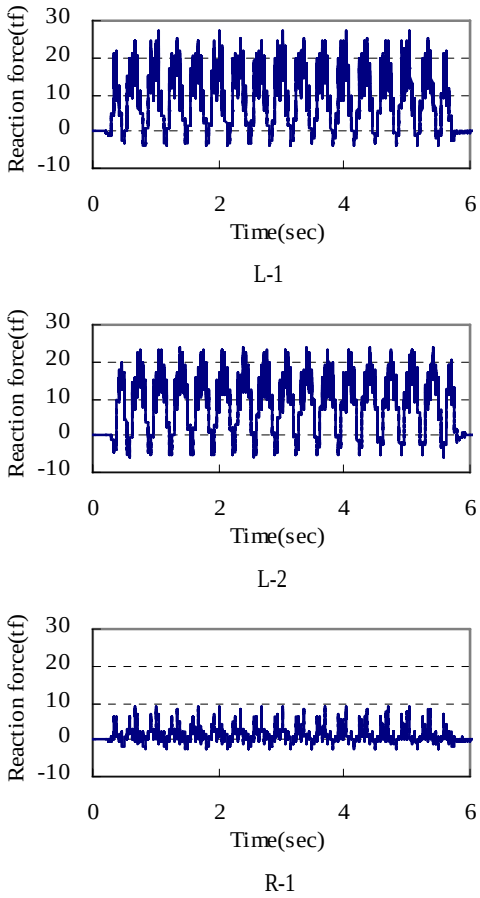

Fig. 3.5.4 Reaction force of piers (270 km/h)

Reaction forces of piers under the speed of 220 km/h of train are shown in **Fig. 3.5.5**. The reaction forces of 220 km/h are showing similar characteristics with those of 270 km/h, while the responses show smaller amplitudes. The reason is considered that the acceleration responses of bridge are smaller as discussed in previous section and also that the dynamic wheel loads of the train decrease according to speed.

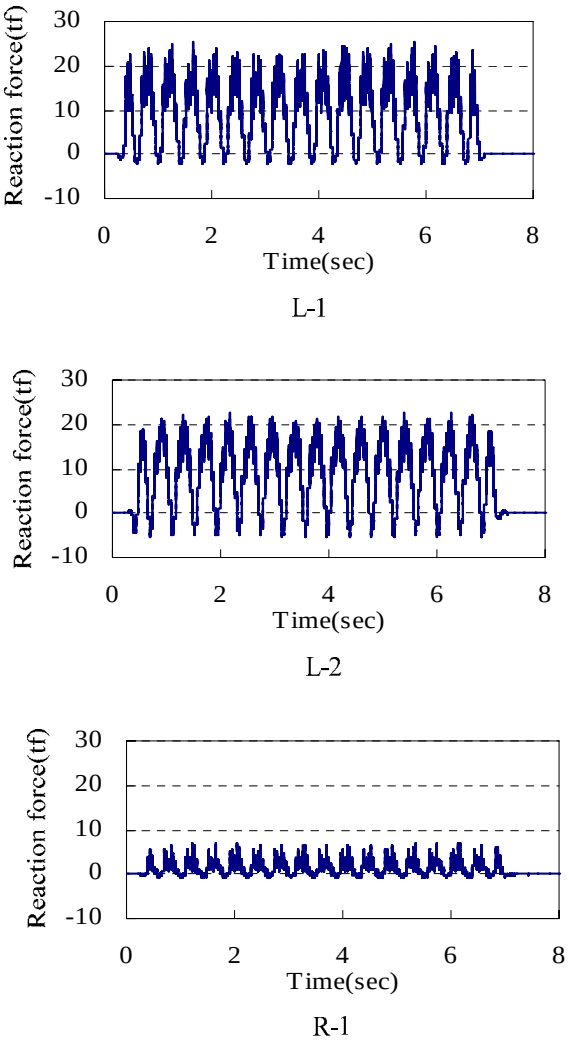

Fig. 3.5.5 Reaction force of piers (220 km/h)

3.6 Countermeasures against predominant vibration

Dynamic characteristics of the high-speed railway elevated bridge due to bullet train are clarified in the previous sections. Countermeasures against predominant vibration of the bridge are proposed and simulated in this section, considering such dynamic characteristics. Since the predominant vibrations occur at the hanging parts of the elevated bridge, it is considered effective to decrease the vibration by reinforcing the hanging parts. Two proposals are considered. One is to connect the neighboring hanging parts rigidly and the other arranges to raise the stiffness of the hanging parts by supporting them with H steel.

Proposal of reinforcing the hanging parts by H steels is depicted in **Fig. 3.6.1**. The reinforcing material i.e. H steel is assumed to have 1/2 stiffness of the piers and is arranged to connect to the hanging part at one end and to the middle of the pier at the other end. The other analytical conditions, including the 9-DOF train model, are assumed the same with the previous analysis under the speed of 270 km/h.

Eigenvalue analyses of both proposals are performed and the natural modal shapes simultaneously with the natural frequencies of bridge are shown in **Fig. 3.6.2**. In the case of reinforcing with H steel, the predominant frequency of bending mode of the hanging part is observed to be 12.87 Hz that is about 1 Hz higher compared with that before reinforcement, and the predominant frequency of torsion is 14.09 Hz. In the case of reinforcing by connect the hanging parts rigidly, the predominant frequency of bending mode of the hanging part is observed to be 17.86 Hz that is even higher than the case of reinforcing with H steel.

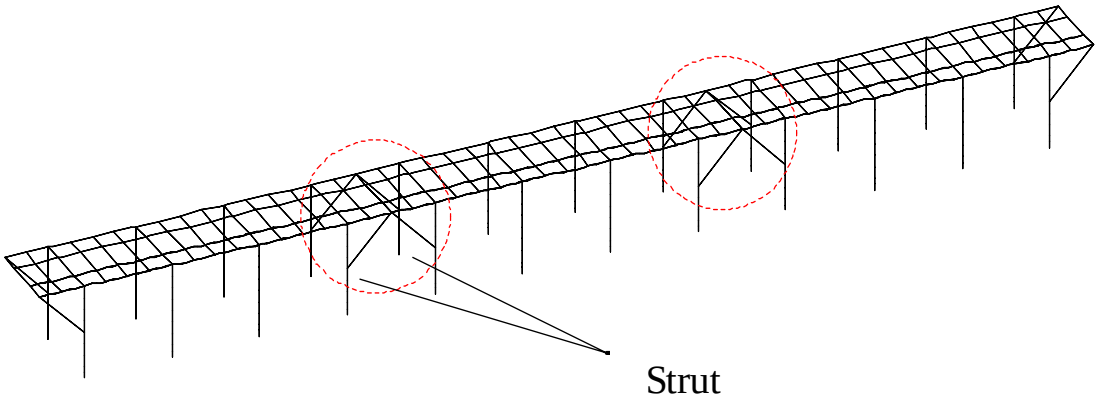

Fig. 3.6.1 Analytical model of bridge with strut

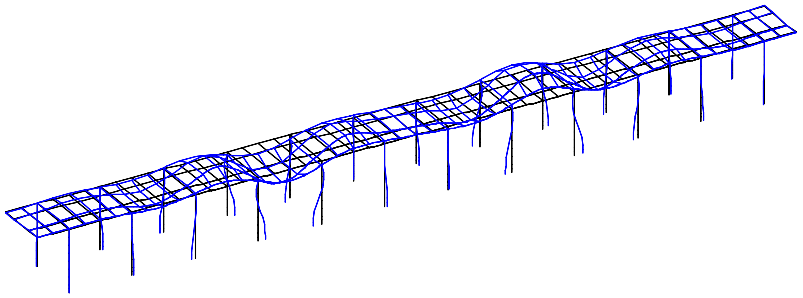

(1) Rigid joint　12th mode　17.86Hz

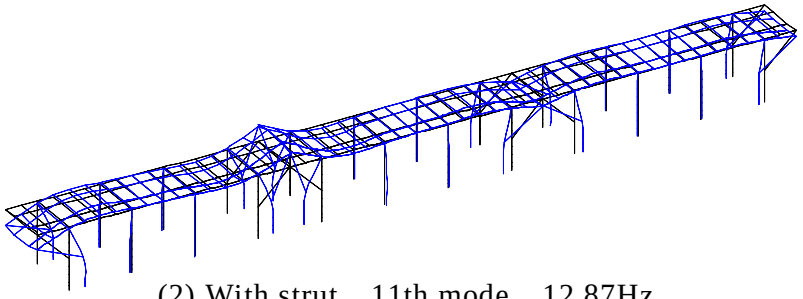

(2) With strut　11th mode　12.87Hz

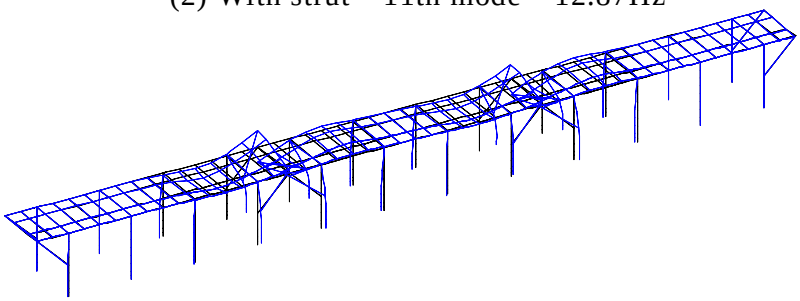

(3) With strut　14th mode　14.09Hz

Fig. 3.6.2 Natural mode shapes and frequencies of bridge

The analytical results in vertical direction of the cases of H steel reinforcement and rigid joint simultaneously with those before reinforcement are shown in **Fig. 3.6.3**. As known from the comparison, at hanging parts of the bridge the acceleration responses are remarkably decreased after reinforcement either in the case of reinforcement by H steel or rigid connection. From the Fourier spectra of acceleration responses, the low frequency components from 10 Hz to 30 Hz are observed extremely reduced, which is predicted to influence the site vibration caused by the bridge vibration. Influenced by the vibration of hanging part, the response of point-2 is also observed to some extent reduced. On the other hand, the response of point-3 which is far from the hanging part indicates no notable change after reinforcement. According to the discussion above, the effect on reducing bridge vibration of both reinforcement proposals can be expected. In addition, the effect of connection reinforcement is obviously conspicuous than that of H steel reinforcement, though it may bring some additional structural problems.

The maximum and rms values are shown in **Table 3.6.1** and **Table 3.6.2**.

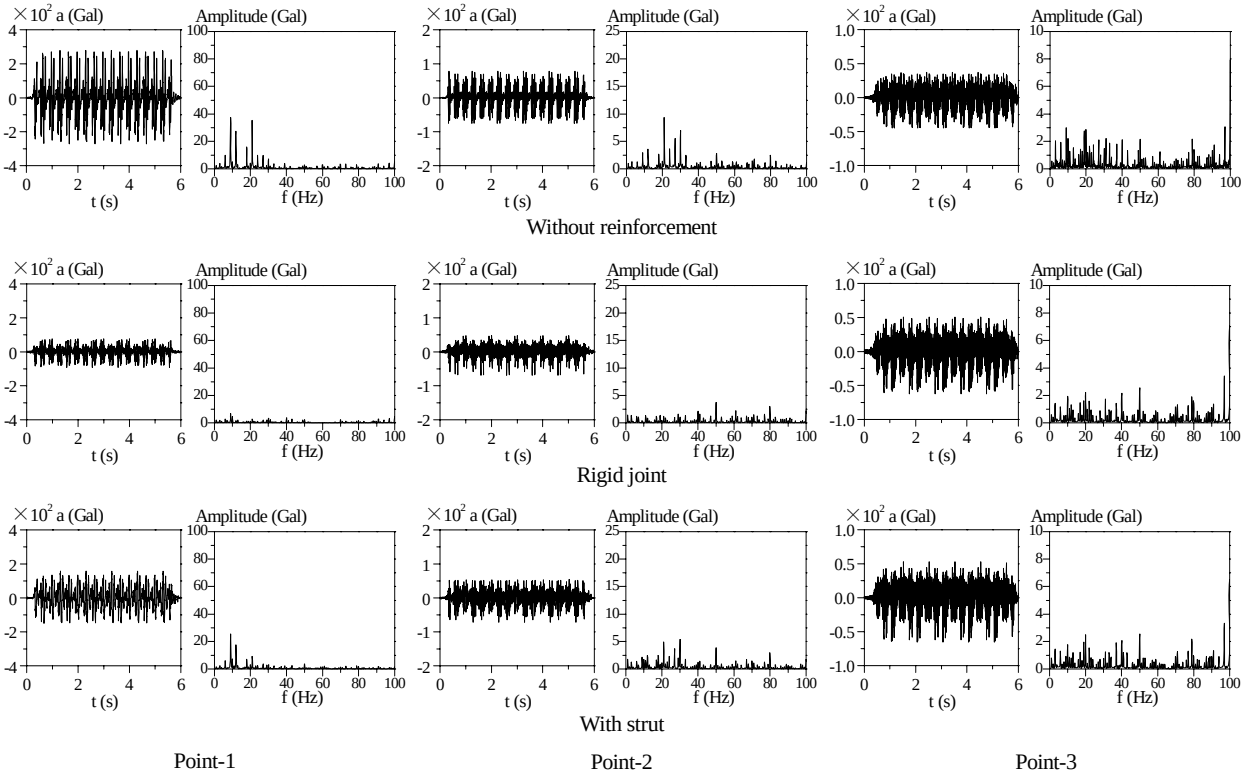

Fig. 3.6.3 Acceleration of bridge (Train speed 270 km/h)

Table 3.6.1 Maximum acceleration of bridge (Gal)

	Point-1	Point-2	Point-3
Without reinforcement	279.4	78.3	44.9
Rigid joint	93.1	65.8	62.4
With strut	157.2	72.0	65.4

Table 3.6.2 rms value of bridge (Gal)

	Point-1	Point-2	Point-3
Without reinforcement	106.5	26.8	14.8
Rigid joint	24.5	14.5	17.0
With strut	55.4	20.1	16.6

Reaction forces of piers after reinforcement are also simulated and compared with the ones before reinforcement, as shown in **Fig. 3.6.4**. The responses of piers L-1 and R-1 that is close to the hanging part are to some extent reduced, thus the effect of reinforcement can be confirmed. Reaction forces of piers L-2 and L-3 are observed no apparent change due to reinforcement since they are difficult to be influenced by the response of hanging part.

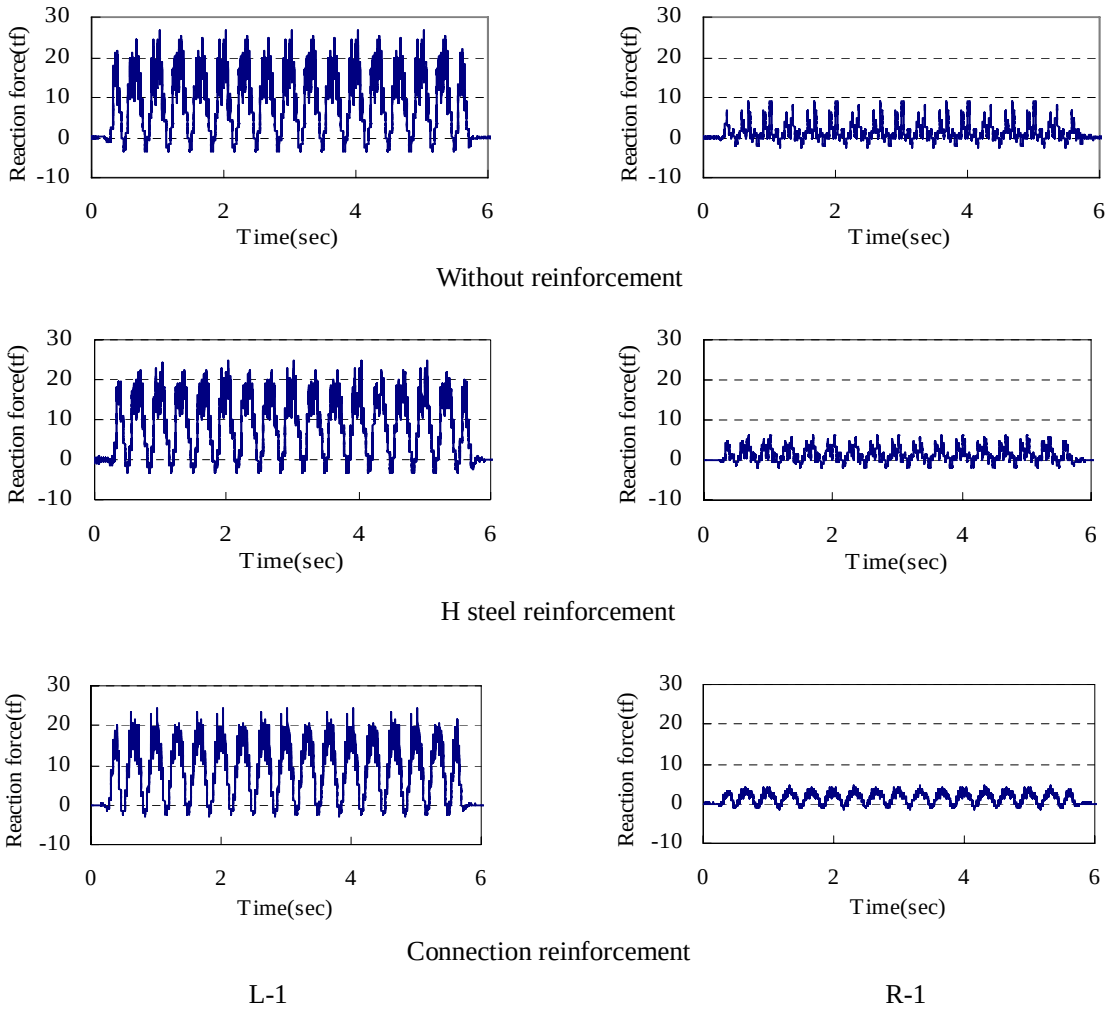

Fig. 3.6.4 (a) comparison of reaction force of piers

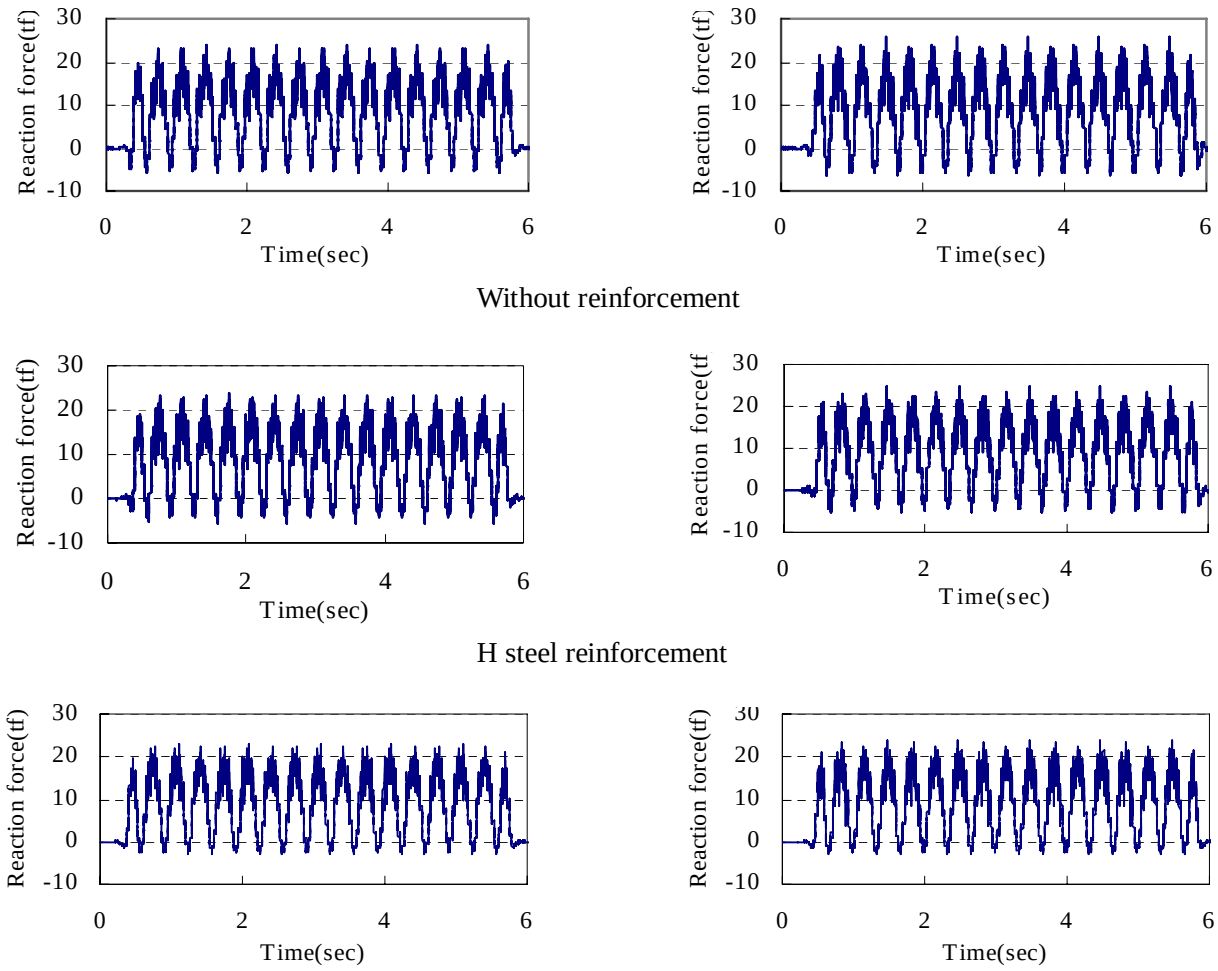

Fig. 3.6.4 (b) comparison of reaction force of piers

3.7 Analytical evaluation on actual countermeasure

An actual constructed countermeasure to reduce the bridge vibration by Hara et al [13] is examined using the developed analytical procedure. The outline of the reinforcement is shown in **Fig. 3.7.1**. Here, the bridge model is established according to the information extracted from Reference [13]. The properties of the bridge are almost the same as those of the previous model except that the height of the bridge is 6.2 m. The ground conditions are also different and shown in **Table 3.7.1.**

To confirm the validity of the analysis, the analytical results and the experimental values (only those of Point-2 are available) are compared with each other as shown in **Fig. 3.7.2**. As observed in the figure, the analytical results indicated good agreement with the experimental ones. Then, the analytical results before and after reinforcement is shown in **Fig. 3.7.3**, and corresponding maximum and rms values are shown in **Table 3.7.2**. From the results, the effect of the reinforcement on the bridge can be confirmed.

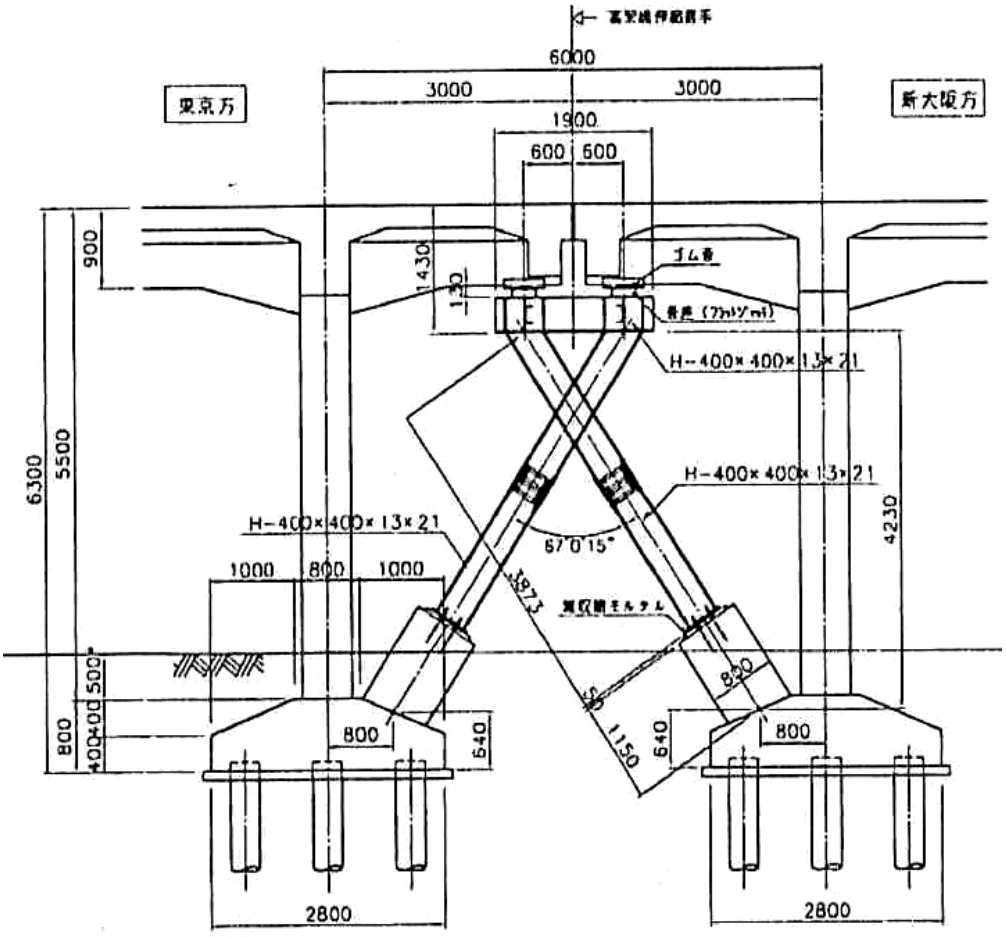

Fig. 3.7.1 Outline of X-shape strut

Table 3.7.1 Ground spring constant

Sort of spring	Longitudinal	Transverse
Vertical spring of pile top (kN/m)	9.25×10^5	
Rotating spring of pile top (kN·m/rad)	5.88×10^5	
Horizontal spring of footing (kN/m)	1.34×10^4	
Horizontal spring of pile top (kN/m)	7.47×10^4	

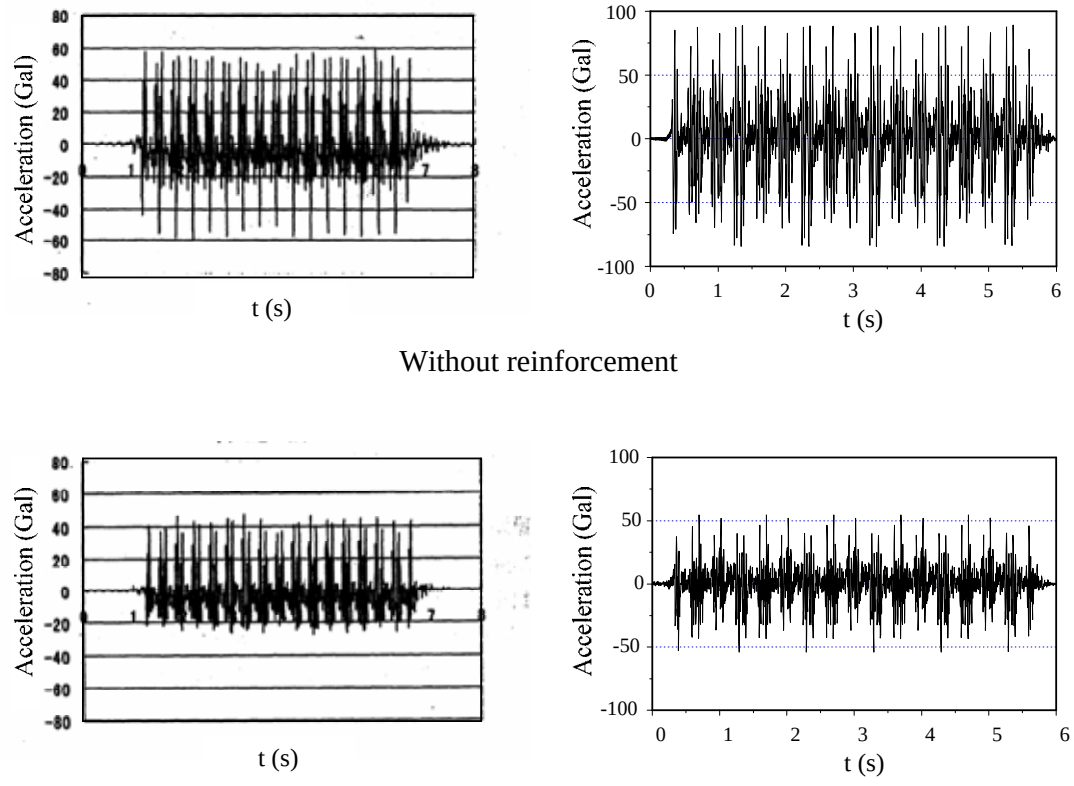

Fig. 3.7.2 Comparison of acceleration responses (Point-2)

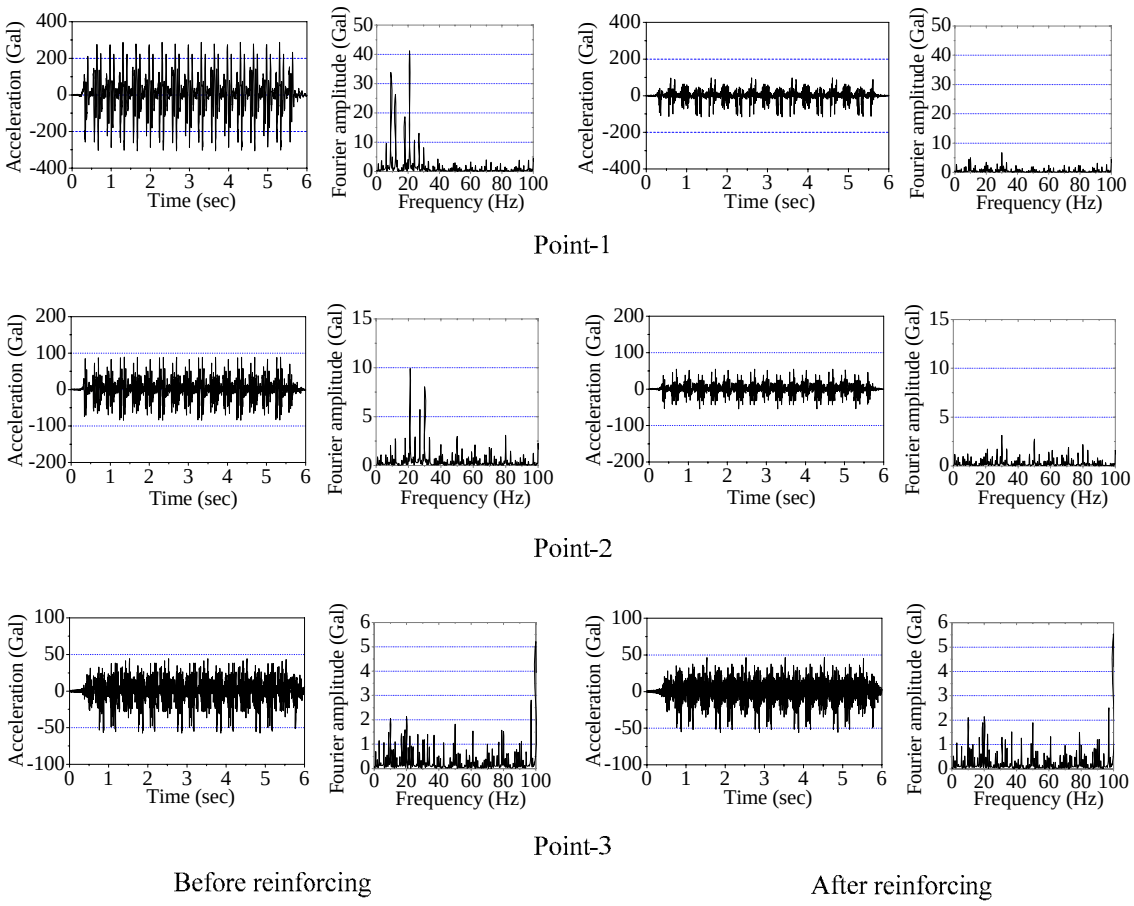

Fig. 3.7.3 Comparison of analytical responses before and after reinforcement

Table 3.7.2 Maximum and rms values of responses before and after reinforcement (Gal)

Point No.	Maximum acceleration (Gal)		rms value (Gal)	
	Before reinforcement	After reinforcement	Before reinforcement	After reinforcement
Point-1	296.82	106.23	111.15	28.23
Point-2	86.69	54.22	28.66	14.49
Point-3	50.79	51.05	15.86	15.34

3.8 Improvement of analytical efficiency

In previous sections, the analysis using a 3-blcok bridge model demands high capability of the computer and a long computational time, which leads to a high cost. In this section, attempt to improve efficiency of the analysis are made by developing a 1-block bridge model, which can also consider the influence of the train's entering and quitting.

The 1-block bridge model with 24 m length is depicted in **Fig. 3.8.1**. To express the actual structure of hanging part, double notes are set up at the hanging parts to simulate the effects of rail and ballast. The illustration of this technique is shown in **Fig. 3.8.2**. The spring constants defined in the double notes are adjusted according to the response of the bridge. The computational conditions including train model and properties of the bridge are assumed the same with the previous analysis under the speed of 270 km/h of the train.

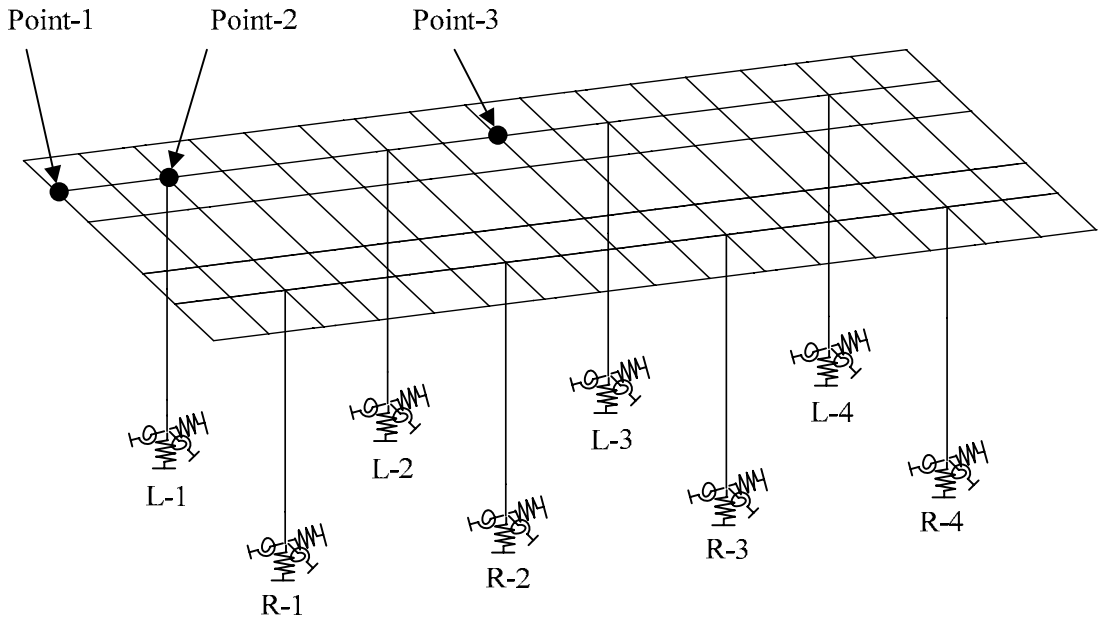

Fig. 3.8.1 1-block bridge model

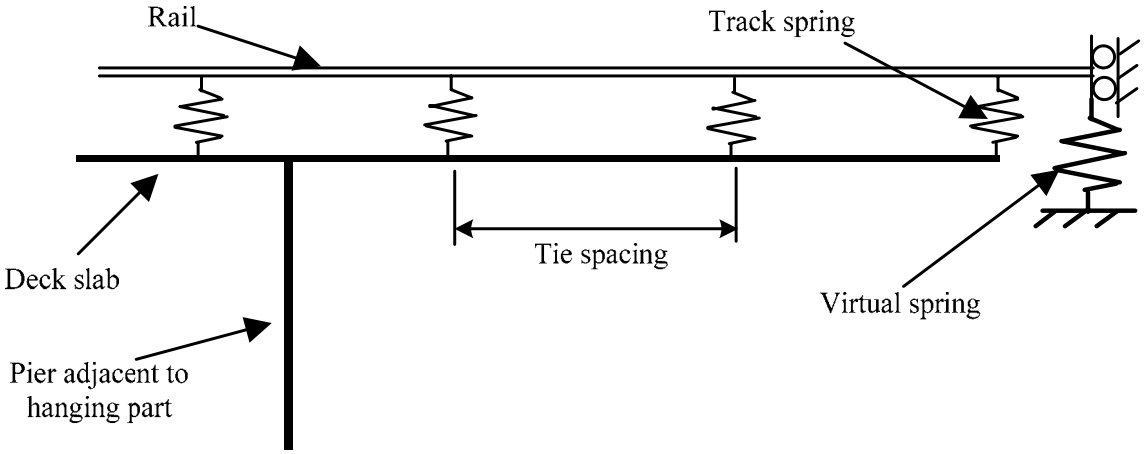

Fig. 3.8.2 Improved one span model of bridge

Table 3.8.1 Maximum acceleration and rms value of bridge

	Maximum acceleration (Gal)		rms value (Gal)	
	Experiment	With spring	Experiment	With spring
Point-1	239.4	296.0	79.8	80.7
Point-2	91.4	113.1	29.0	29.4
Point-3	43.1	51.4	14.9	17.9

Analytical acceleration responses of the case introducing double notes at the hanging parts and those due to 3-block bridge model simultaneously with experimental values are shown in **Fig. 3.8.3**. The maximum and rms values are shown in **Table 3.8.1**. The analytical responses of 1-block model are similar with those of the 3-block model by setting up double notes at the hanging part. The responses of Point-1 and Point-2 indicate relatively agreement with experimental ones. The reaction forces at the pier bottoms of both 1-block and 3-block models are shown in **Fig. 3.8.4**. The reaction forces due to the 1-block model are revised according to the ratio between the static reaction forces of the 1-block and 3-block models.

The problems of this technique are mainly thought of two points. One is that the criterion for determining the spring constants used in double notes is not certain and the other is that the damping effect of ballast is difficult to simulate. In addition, the reaction forces of piers are partly distributed by the double notes since one of them is assumed to be completely

restrained. To perform an accurate analysis with a 1-block bridge model, further efforts are demanded to solve these problems.

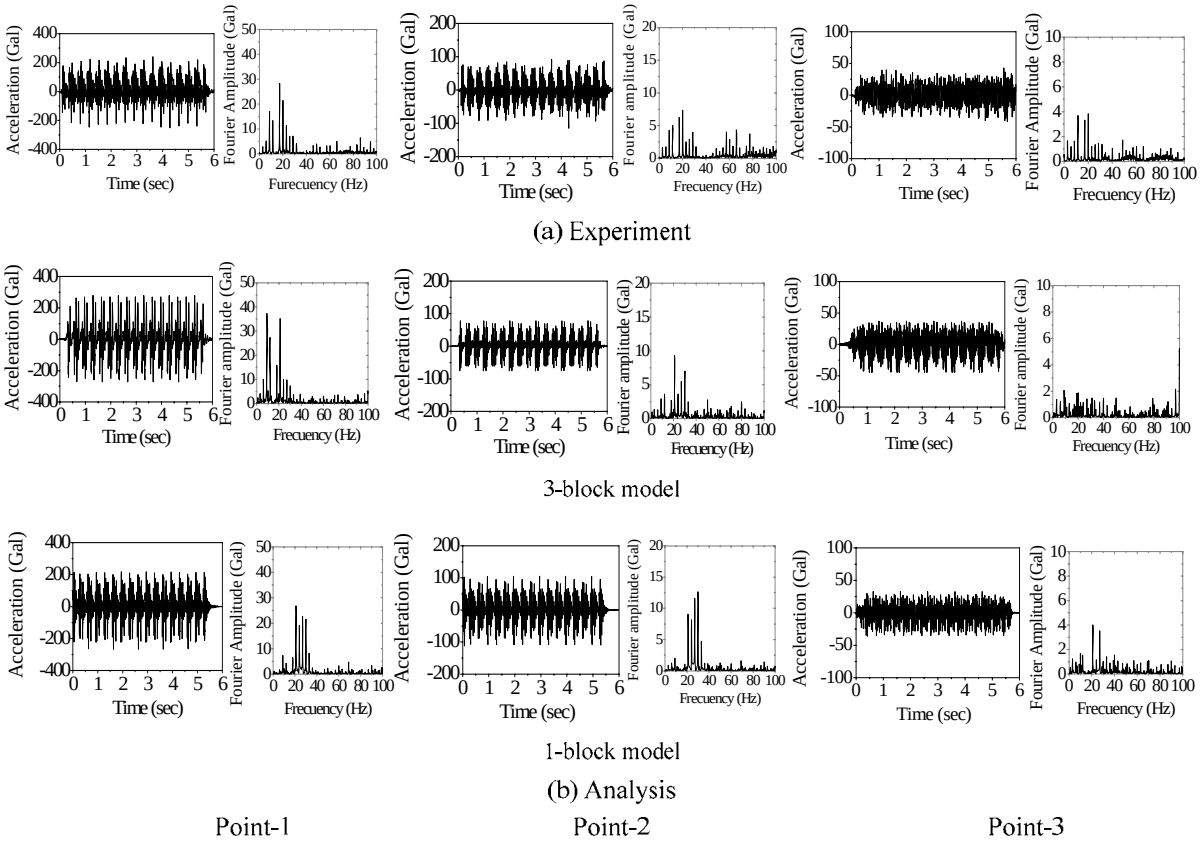

Fig. 3.8.3 Acceleration of bridge

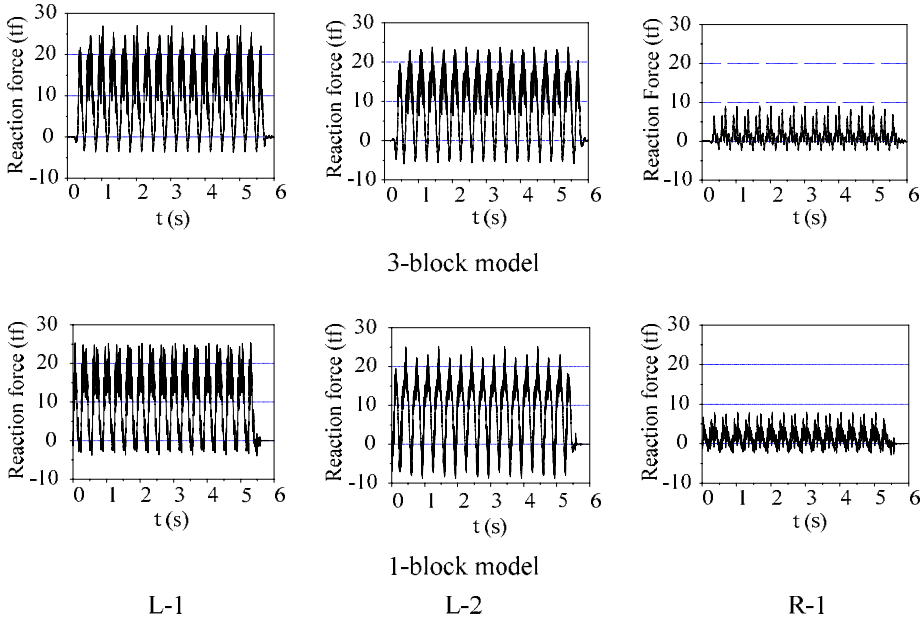

Fig. 3.8.4 Reaction forces

3.9 Conclusions

In this chapter, an analytical procedure to simulate the bridge-train coupled vibration problem considering their interaction as well as the effect of ground properties is established. Dynamic responses of a standard type of elevated bridge of reinforced concrete in the form of a portal rigid frame under moving bullet trains are analyzed in consideration of the wheel-track interaction with the rail surface roughness. The viaducts including the track structure are modeled as 3-D beam elements. The elastic effect of ground springs at the pier bottoms and the connection effect of the sleepers and ballast between the track and the deck slab are model with double nodes connected by springs. Bullet train models of two-, six- and nine-DOF dynamic systems developed in Chapter 2 are used for the analyses.

To demonstrate the validity of the finite element bridge model, eigenvalue analysis is carried out and the basic natural frequencies are investigated. The predominant frequency of the horizontal natural mode is showing good agreement with the value of filed test, through which the validation of bridge model is confirmed. For the validation of the developed bullet train models, the dynamic response analysis of the bridge-train interaction system was carried out and the analytical results using the nine-DOF train model indicate relatively good agreement with the experimental results, thereby validated the bullet train model and the analytical procedure developed can be considered effective.

Based on the simulation of bridge-train interaction, influences of train models on the dynamic responses of viaducts are discussed. The analytical results of six- and nine-DOF train models are showing better agreement with the experimental values, compared with the results of two-DOF model. Furthermore, the analytical results of nine-DOF model are considered indicating the best coincidence with the experimental ones, because it can take account of all the main factors that contribute to the vertical vibration of the bridge-train interaction system. Therefore the conclusion can be made that for more accurate investigation it is desirable to use the nine-DOF train model while the six-DOF model can used in preliminary discussions.

Based on the analytical results by nine-DOF train model, the predominant acceleration responses and frequencies of the bridge vibration are investigated and the dynamic characteristics of the viaducts are clarified. In particular, the analytical acceleration responses displayed larger amplitudes at hanging parts compared with experimental values. The main reason is considered as that the hanging parts of the viaducts are connected with neighboring ones by rail and ballast in the actual structures, but only the effects of the rail can be taken into account in the analysis, i.e. the damping effect of the ballast cannot be considered. The effect of train speeds on bridge response is also examined. The reaction forces at the pier bottoms, which can be used in further analysis of site vibration, are calculated using its

influence value matrix and the predominant components are estimated. Then the countermeasures to allay the undesirable vibration of the bridge are proposed. In this study, form the fact that the excessive vibration occurs at the hanging parts of the elevated bridge, which is elucidated by both dynamic response analysis and the experiment, countermeasures against the predominant vibration are proposed by reinforcing the hanging parts. The effect of the proposed countermeasures is demonstrated through dynamic analysis as well as the results from actual construction case. At last, the efforts are also made to improve the analytical efficiency by developing a one-block model of the bridge.

References

[1] Kawatani, M., He, X., Sobukawa, R., Masaki, S. and Nishiyama, S.: Dynamic Ground Reaction Forces at Pier Bottoms due to Running Trains on Viaducts, Proc. of Annual Conference of Civil Engineers 2003, JSCE Kansai Chapter, I-50, May 2003. (*in Japanese*)

[2] Kawatani, M., He, X., Sobukawa, R., Masaki, S. and Nishiyama, S.: Dynamic Ground Reaction Forces at Pier Bottoms due to Running Trains on Viaducts and Improvement of Analytical Efficiency, Proceedings of the 58th Annual Conference of the Japan Society of Civil Engineers, I-748, Sep., 2003. (*in Japanese*)

[3] Kawatani, M., He, X., Sobukawa, R. and Nishiyama, S.: Dynamic Response Analysis of Elevated Railway Bridges due to Shinkansen Trains and Influence of Train models, Proc. of International Workshop on Structural Health Monitoring Bridges / Colloquium on Bridge Vibration, pp.249-256, Kitami, Japan, Sept. 2003.

[4] Kawatani, M., He, X., Sobukawa, R. and Nishiyama, S.: Traffic-induced dynamic response analysis of high-speed railway bridges. *Proceedings of the Third Asian-Pacific Symposium on Structural Reliability and Its Applications*, Seoul, Korea, pp. 569-580, 2004.

[5] Kawatani, M., He, X., Shiraga, R., Masaki, S., Nishiyama, S. and Yoshida, K.: Dynamic response analysis of elevated railway bridges due to Shinkansen trains, *Journal of Struc-tural and Earthquake Engineering (Doboku Gakkai Ron-bunshuu A)*, JSCE, Vol. 62, No. 3, pp.509-519, 2006. (*in Japanese*)

[6] Yoshida, K. and Seiki, M.: Influence of improved rigidity in railway viaducts on the environmental ground vibration, Journal of Structural Engineering, JSCE, Vol. 50A, pp. 403-412, 2004. (*in Japanese*)

[7] Railway Technical Research Institute: Seismic design code for railway structures, MARUZEN Co., Ltd.: Tokyo, Japan, 1999. (*in Japanese*)

[8] Kobori, T. and Kubo, M.: A practical dynamic analysis method of continuous girder bridge with spring connections on spring supports, Proceedings of JSCE/Japan Society of Civil Engineers, No. 356/I-3, pp.395–403, 1985. (*in Japanese*)

[9] Railway Technical Research Institute: Design standard for railway structures (Foundation and soil pressure resistance structures), MARUZEN Co., Ltd.: Tokyo, Japan, 1997. (*in Japanese*)

[10] Agabein M.E.: The effect of various damping assumptions on the dynamic response of structure, Bulletin of International Institute of Seismology and Earthquake Eng., Vol. 8, pp. 217-236, 1971.

[11] Kito, M. and Nishimura, A.: Vibration test of viaducts, KOZOBUTUSEKKEISHIRYO,

No. 35, pp. 33-36, Sep., 1973. (*in Japanese*)

[12] Nishimura, A.: A study on integrity assessment of railway rigid frame bridge, RTRI Report, Vol. 4, No. 9, 1990. (*in Japanese*)

[13] Hara, T., Yoshioka, O., Kanda, H., Funabashi, H., Negishi, H., Fujino, Y. and Yoshida K.: Development of a new method to reduce Shinkansen-induced wayside vibrations applicable to rigid frame bridges: bridge-end reinforcing method, *Journal of Structural and Earthquake Engineering (Doboku Gakkai Ronbunshuu A)*, JSCE, Vol. 68, No. 766, pp.325-338, July 2004. (*in Japanese*)

Chapter 4

Site vibration around viaducts caused by bullet trains

4.1 Introduction

The bridge vibration caused by running trains propagates to the ambient ground via footing and pile structures of the viaducts, thereby causing some environmental problems related to site vibration around the viaducts and affects surrounding environments. Undesirable environmental vibrations should be eliminated as possible. However, only a few solutions against the wayside vibration have been practically developed due to its complexities. To find out more effective countermeasures against the traffic-induced environmental vibration problems, it is necessary to clarify the development and propagation mechanism of the site vibration caused particularly by running vehicles on viaducts.

Nevertheless, such site vibration phenomenon remains unclear because of its complicated nature. Without a clear grasp of the site vibration mechanism through analytical studies, environmental vibration problems are traditionally evaluated and predicted based on field test data. The efficiency of such a process is limited to particular cases. For more general cases, essential information and reliable evaluation of site vibrations are necessary to perform accurate predictions and develop effective countermeasures. For that purpose, a corresponding analytical approach to simulate the environmental vibration problems is anticipated.

Although a great deal of effort has been devoted to analytical studies of site vibrations induced by trains moving on the ground surface [1－3], little is known about the ground vibration caused by trains moving over viaducts because of its complicated nature: vibrations are transmitted to the ground via piers, footings and piles, i.e. the input motion of ground vibration is resulted form the running vehicles on bridge structures. Recently abroad, some efforts have been devoted to the train-bridge-ground interaction analysis. Xia et al [4] evaluated the vibration-related effects of light-rail train-viaduct system on the surrounding environment using a 2-D interaction model of a “train-bridge” system for obtaining the dynamic loads of moving trains on bridge piers and a 2-D dynamic model of “pier-foundation-ground” system for analyzing vibration responses of the ground. Wu et al [5] [6] attempted to establish a semi-analytical approach to deal with ground vibration induced by trains moving over viaducts. In Japan, environmental vibration problems caused by trains running along viaducts are mainly investigated and evaluated by RTRI based on empirical

knowledge from field test data [7] [8]. Recently, Hara et al [9] attempted to clarify the site vibration around Shinkansen viaducts by both experiments and analytical procedure, but in their analyses, the excitations of the trains are only treated as simple equivalent moving force based on the measured results. Such approach not only cannot directly take consideration of the interaction between the bridge and train, but is incapable to set the wheel loads without experimental results. Yoshida and Seki [10] indicated the necessities to consider the bridge-train interaction when discussing the environmental vibration problem around Shinkansen viaducts.

In this study, based on the analytical approach on train-induced vibration developed in previous Chapter 3, an approach [11－16] to simulate site vibration around the viaducts of the high-speed railway is established. In this approach, the dynamic interactions between the train and track and between the foundation and ground can be considered. The bridge-train interaction models established previously are conveniently used in this analysis. To obtain the dynamic reaction forces at the pier bottoms, the dynamic responses of viaducts are simulated taking account of the exact bridge-train interaction. Then, applying those reaction forces as input excitation forces in the foundation-ground interaction problem, the site vibration around the viaducts is simulated and evaluated using a general-purpose program. The dynamic acceleration responses of the ground are then evaluated. The effect of countermeasures against predominant bridge vibration on reduction of the environmental vibration is also confirmed.

The approach established in this research offers a new convenient analytical tool to investigate, evaluate and predict environmental vibration problems caused by bridge vibration under running train, either for existing viaducts or those in planning stages.

4.2 Analysis of soil-structure interaction system employing SASSI2000

In this research, the site vibrations around Shinkansen viaducts are simulated using a general program named SASSI2000 [17]. In this program, the soil-structure interaction problem [18] is conveniently analyzed using a substructuring approach, by which the linear soil-structure interaction problem is subdivided into a series of simple sub-problems. Each sub-problem is solved separately and the results are combined in the final step of the analysis to provide a complete solution. In particular for site response analysis, the 3-D thin layer element method is adopted in this approach. This method is an extension from the study of the 2-D problem that was originally developed by J. Lysmer [19], which can remove the limitation of half-space elastic theory of isotropic homogeneous media. The thin layer element method is expected to be widely applicable to different interaction problems and is studied by numerous researchers [20~22]. Theoretical procedure of this approach is briefly described as following.

4.2.1 Substructuring method of SSI analysis

The soil-structure interaction problem is most conveniently analyzed using a substructuring approach. In this approach, the linear soil-structure interaction problem is subdivided into a series of simpler sub-problems. Each sub-problem is solved separately and the results are combined in the final step of the analysis to provide the complete solution using the principle of superposition.

For the case of structures with surface foundations for which the structure and the foundation interface boundary is on the surface of the foundation medium, the substructuring method is relatively simple and many solution techniques are available. For structures with embedded foundations, the substructuring method becomes considerably more complicated. Conceptually, these methods can be classified into four types depending on how the interaction at the soil and structure interface degrees-of-freedom is handled [23], [24]. These four types are: 1) the rigid boundary method, 2) the flexible boundary methods, 3) the flexible volume method, and 4) the substructure subtraction method. Compared with the other two methods, the flexible volume method and the substructure subtraction method, because of the unique substructuring technique, require only one impedance analysis and the scattering analysis is eliminated. Furthermore, the substructuring in the subtraction method often requires a much smaller impedance analysis than the flexible volume method.

The SASSI computer program adopts both the flexible volume method and the substructure subtraction method of substructuring. For the limitation of pages, only the theory of flexible

volume method is presented here.

The flexible volume substructuring method is based on the concept of partitioning the total soil-structure system as shown in **Fig. 4.2.1** (a) into three substructure systems as shown in **Fig. 4.2.1** (b), (c) and (d). The substructure I consists of the free-field site, the substructure II consists of the excavated soil volume, and the substructure III consists of the structure, of which the foundation replaces the excavated soil volume. The substructures I, II and III, when combined together, form the original SSI system shown in **Fig. 4.2.1** (a). The flexible volume method presumes that the free-field site and the excavated soil volume interact both at the boundary of the excavated soil volume and within its body, in addition to interaction between the substructures at the boundary of the foundation of the structure. The theory and formulation that develop in the following sections are equally applicable to two- and three-dimensional SSI problems.

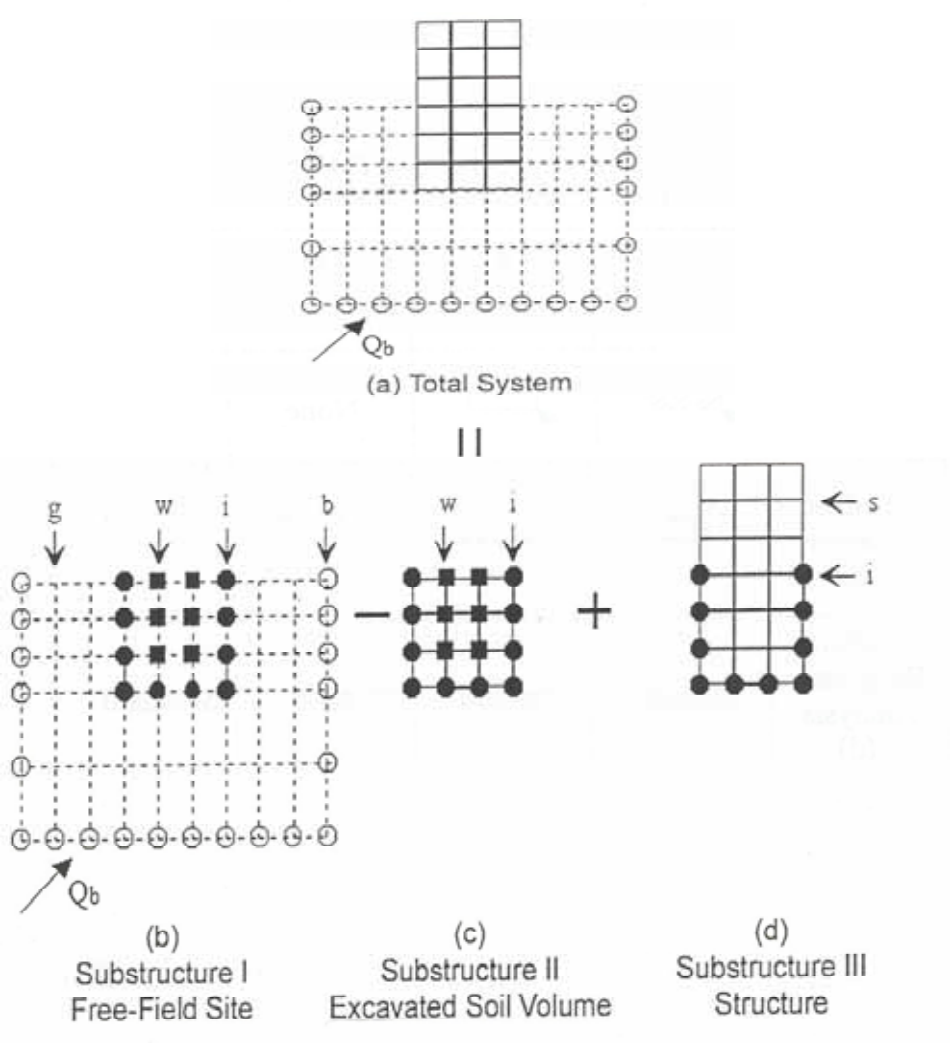

Fig. 4.2.1 Substructuring in flexible volume method

The equations of motion for the SSI substructures shown in **Fig. 4.2.1 (b), (c)** and **(d)** can be written in the following matrix form:

$$[\boldsymbol{M}]\{\ddot{\hat{\boldsymbol{U}}}\}+[\boldsymbol{K}]\{\hat{\boldsymbol{U}}\}=\{\hat{\boldsymbol{Q}}\} \tag{4.2.1}$$

where [***M***] and [***K***] are the total mass and stiffness matrices, respectively. $\{\hat{\boldsymbol{U}}\}$ is the vector of total nodal point displacements and $\{\hat{\boldsymbol{Q}}\}$ is the forces due to applied external dynamic forces or seismic excitations.

For the harmonic excitation at frequency ω, the load and the displacement vectors can be written as

$$\{\hat{\boldsymbol{Q}}\}=\{\boldsymbol{Q}\}\boldsymbol{exp}(i\omega t) \quad \text{and} \quad \{\hat{\boldsymbol{U}}\}=\{\boldsymbol{U}\}\boldsymbol{exp}(i\omega t)$$

where **{*Q* }** and **{*U* }** are the complex force and displacement vectors at frequency ω.

Hence, for each frequency, the equations of motion take the form

$$[\boldsymbol{C}]\{\boldsymbol{U}\}=\{\boldsymbol{Q}\} \tag{4.2.2}$$

where **[*C*]** is a complex frequency-dependent dynamic stiffness matrix:

$$[\boldsymbol{C}]=[\boldsymbol{K}]-\omega^2[\boldsymbol{M}]$$

Using the following subscripts, which refer to degrees of freedom associated with different nodes (see **Fig. 4.2.1**):

Subscript	Nodes
b	the boundary of the total system
i	at the boundary between the soil and the structure
w	within the excavated soil volume
g	at the remaining part of the free-field site
s	at the remaining part of the structure
f	combination of i and w nodes

The equation of motion for the system is partitioned as follows:

$$\begin{bmatrix} C_{ii}^{III} - C_{ii}^{II} + X_{ii} & -C_{iw}^{II} + X_{iw} & C_{is}^{III} \\ -C_{wi}^{II} + X_{wi} & -C_{ww}^{II} & 0 \\ C_{si}^{III} & 0 & C_{ss}^{III} \end{bmatrix} \begin{Bmatrix} U_i \\ U_w \\ U_s \end{Bmatrix} = \begin{Bmatrix} P_i \\ 0 \\ P_s \end{Bmatrix} \tag{4.2.3}$$

where superscripts: I, II and III, refer to the three substructures. The complex frequency-dependent dynamic stiffness matrix on the left of Eq. (4.2.3) simply indicate the stated partitioning according to which the stiftness and mass of the excavated soil volume are subtracted from the dynamic stiffness of the free-field site and the structure. The frequency-dependent matrix, $\begin{bmatrix} X_{ii} & X_{iw} \\ X_{wi} & X_{ww} \end{bmatrix}$ or $[X_{ff}]$, is called the impedance matrix, which is obtained from the model in substructure I using the methods which will be described later. ***P*** indicates the load vector has non-zero terms only where external loads are applied.

4.2.2 Eigenvalue problem and transmitting boundary matrices

The original site before the soil excavation to accommodate the structure is assumed to consist of horizontal soil layers overlying either a rigid base or an elastic halfspace using the techniques to simulate the halfspace boundary condition at the base as described later. The soil material properties for the soil layer system are assumed to be viscoelastic with the complex modulus representation of the stiftness and damping properties of the soil layers.
Based on the horizontally layered site model described above and the assumption of linear variations of displacement within each layer, Waas [25] formulated the eigenvalue problem for the system in the frequency domain. The eigenvalue problem can be subdivided into two uncoupled algebraic eigenvalue problems, one for generalized Rayleigh wave motion and another for generalized Love wave motions. A brief description of these two eigenequations, which are in effect a reduced form of the equation of motion for the site model, is presented as follows.

a) Eigenvalue problem for generalized Rayleigh wave motion

Using the discretized soil model shown in **Fig. 4.2.2 (a)**, the eigenequation for generalized Rayleigh wave motion may be written as

$$\left([A]\, k^2 + i[B]\, k + [G] - \omega^2 [M] \right) \{V\} = 0 \tag{4.2.4}$$

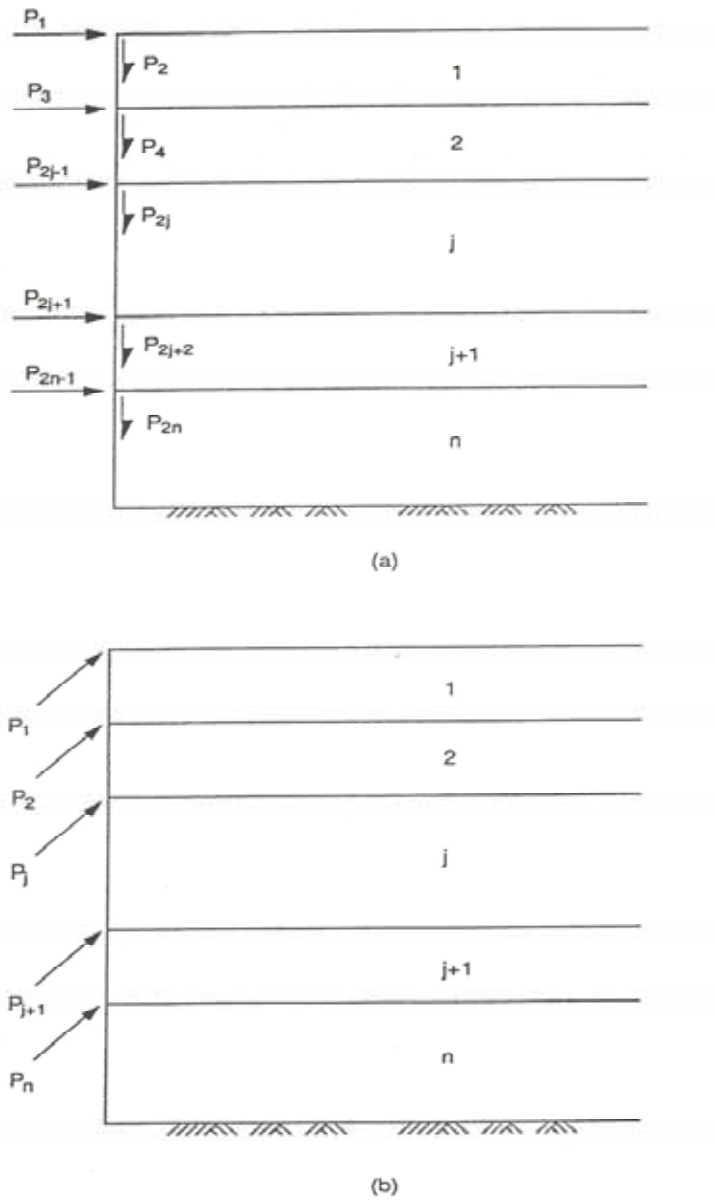

Fig. 4.2.2 Degrees of freedom: (a) Rayleigh wave, (b) Love wave

In this model, there are 2 degrees-of-freedom associated with each layer interface, with a total of 2n degrees-of-freedom for an n layer system. In the above equation, ω is the circular frequency, which is the frequency at which the model is excited; k is the eigenvalue known as the wave number; and $\{\boldsymbol{V}\}$ is the associated eigenvector with 2n components. The matrices [$\boldsymbol{A}$], [$\boldsymbol{B}$], [$\boldsymbol{G}$], and [$\boldsymbol{M}$] are of order 2n x 2n and are assembled from submatrices for the soil layers. Each submatrix corresponds to a soil layer. Denoting the thickness of the j^{th} layer from the top by h_j, the mass density by ρ_j, the shear modulus by G_j, and the Lame's constant by λ_j, these layer submatrices are:

$$[A_j]=\frac{h_j}{6}\begin{bmatrix} 2(\lambda_j+2G_j) & 0 & (\lambda_j+2G_j) & 0 \\ 0 & 2G_j & 0 & G_j \\ (\lambda_j+2G_j) & 0 & 2(\lambda_j+2G_j) & 0 \\ 0 & G_j & 0 & 2G_j \end{bmatrix}$$

$$[B_j]=1/2\begin{bmatrix} 0 & -(\lambda_j-G_j) & 0 & (\lambda_j+G_j) \\ (\lambda_j-G_j) & 0 & (\lambda_j+G_j) & 0 \\ 0 & -(\lambda_j+G_j) & 0 & (\lambda_j-G_j) \\ -(\lambda_j+G_j) & 0 & -(\lambda_j-G_j) & 0 \end{bmatrix}$$

$$[G_j]=\frac{1}{h_j}\begin{bmatrix} G_j & 0 & -G_j & 0 \\ 0 & (\lambda_j+2G_j) & 0 & -(\lambda_j+2G_j) \\ -G_j & 0 & G_j & 0 \\ 0 & -(\lambda_j+2G_j) & 0 & (\lambda_j+2G_j) \end{bmatrix}$$

$$[M_j]^{(c)}=\frac{\rho_j h_j}{6}\begin{bmatrix} 2 & 0 & 1 & 0 \\ 0 & 2 & 0 & 1 \\ 1 & 0 & 2 & 0 \\ 0 & 1 & 0 & 2 \end{bmatrix}$$

$$[M_j]^{(l)}=\frac{\rho_j h_j}{2}\begin{bmatrix} 1 & 0 & 0 & 0 \\ 0 & 1 & 0 & 0 \\ 0 & 0 & 1 & 0 \\ 0 & 0 & 0 & 1 \end{bmatrix}$$

The matnces $[M_j]^{(c)}$ and $[M_j]^{(l)}$ are the consistent and lump mass matrices, respectively. The mass matrix used in Eq. (4.2.4) is a combination of one-half lump mass matrix and one-half consistent mass matrix. Using the numerical techniques developed by Waas [25], the eigenvalue in Eq. (4.2.4) can be solved. The solution yields 2n Rayleigh modes and 2n wave numbers, which will be used in computing the transmitting boundary condition for the wave motions moving in the plane of the site model.

b) Eigenvalue problem for generalized Love wave motion

Based on the n horizontally layered soil model shown in **Fig. 4.2.2 (b)**, the eigenvalue problem for generalized Love wave motion may be written in the form

$$\left([\boldsymbol{A}]K^2+[\boldsymbol{G}]-\omega^2[\boldsymbol{M}]\right)\{\boldsymbol{V}\}=0 \tag{4.2.5}$$

In this wave mode, only one degree-of-freedom associated with each layer interface is required. The matrices [***A***], [***B***], [***G***], and [***M***] in Eq. (4.2.5) are assembled in a similar manner from the 2 x 2 Iayer submatrices defined below,

$$[A_j]=h_jG_j\begin{bmatrix}1/3 & 1/6\\ 1/6 & 1/3\end{bmatrix}, \qquad [G_j]=\frac{G_j}{h_j}\begin{bmatrix}1 & -1\\ -1 & 1\end{bmatrix},$$

$$[M_j]^{(c)}=\frac{\rho_j h_j}{6}\begin{bmatrix}2 & 1\\ 1 & 2\end{bmatrix}, \qquad [M_j]^{(l)}=\frac{\rho_j h_j}{2}\begin{bmatrix}1 & 0\\ 0 & 1\end{bmatrix}$$

The mass matrix used in Eq. (4.2.5) is similarly a combination of one-half lump mass matrix and one-half consistent mass matrix. The solution of the eigenequation of Eq. (4.2.5) yields n Love wave mode shapes with the associated wave n umbers which will be used in computing the transmitting boundary condition for the wave motions moving out of the plane of the site model.

c) Transmitting boundary matrix

Transmitting boundaries are formulated by using exact analytical solution in the horizontal direction and a displacement function consistent with the finite element representation in the vertical direction. These boundaries accurately transmit energy in horizontal directions. Development of these boundaries is central to the development of the impedance matrix which is presented next section. Formulation of these boundary matrices for two-dimensional problems only is described as following.

Using the eigenvalues and eigenvectors obtained for the generalized Rayleigh wave motion, and using the stress-strain relationship in each layer, Waas [25] formulated the force-displacement relationship in the frequency domain for the layered system as follows:

$$\{\boldsymbol{P}\}=\{\boldsymbol{R}\}\{\boldsymbol{U}\} \tag{4.2.6}$$

where {***U***} is the vector of 2n displacement and {***P***} are the associated forces and [***R***] is the dynamic stiffness of the semi-infinite layered region that can be obtained from

$$[\boldsymbol{R}] = \boldsymbol{i}[\boldsymbol{A}][\boldsymbol{V}][\boldsymbol{K}][\boldsymbol{V}]^{-1} + [\boldsymbol{D}] \tag{4.2.7}$$

In the above equation all matrices are of order 2n x 2n, matrix [***A***] is defined in Section 4.2.2 a), matrix [***V***] is the matrix containing 2n mode shapes, matrix [***K***] is the diagonal matrix containing the wave numbers (eigenvalues) of the generalized Rayleigh wave motion, and matrix [***D***] is assembled from the properties of each layer in the same manner as that described in Section 4.2.2 a).

The matrix for the j^{th} layer can be written as:

$$[D_j] = \frac{1}{2}\begin{bmatrix} 0 & \lambda_j & 0 & -\lambda_j \\ G_j & 0 & -G_j & 0 \\ 0 & \lambda_j & 0 & -\lambda_j \\ G_j & 0 & -G_j & 0 \end{bmatrix}$$

where G_j and λ_j are the shear modulus and Lame's constant as defined previously in Section 4.2.2 a); Matrix [***R***] is a symmetric full matrix and will be used for computation of the compliance matrix to solve for the impedance problem.

d) Modeling of semi-infinite halfspace at base

The approach described above was originally developed for layered sites resting on a rigid base. In many practical cases the site is a layered system which extends to such great depth that it becomes necessary to introduce an artificial rigid boundary at some depth. This boundary will reflect some energy back into the system and will cause the site to have some erroneous natural frequencies which will affect the overall response. This becomes especially critical for sites with low material damping.

To remedy this problem, in this approach, the two techniques, the variable depth method and viscous boundary at base are used to simulate the semi-infinite halfspace at the soil layer base. The details of these techniques can be found in the theoretical manual of SASSI2000 program [26].

4.2.3 Impedance analysis

The equations of motion of the SSI system based on the flexible volume and the subtraction substructuring methods used by SASSI include the impedance matrix [$\boldsymbol{X}_{ff}$] as shown in Eq. (4.2.3). In the flexible volume method, the impedance matrix needs to be computed for all the interacting nodes in the flexible volume, i.e., the excavated soil volume (i and w nodes in **Fig. 4.2.1)**. The calculation of the impedance matrix is achieved by inverting the dynamic flexibility (compliance) matrix for each frequency of analysis. The methods and analytical models used to compute the compliance matrix based on the model of substructure (b) shown in **Fig. 4.2.1** for two-dimensional problems only are described here. In the flexible volume method, two methods, namely, the direct method and the skin method, are used in SASSI for the impedance analysis. Depending on which method is used, the compliance matrix is computed for all or part of the interacting nodes. Herein, only the direct method of impedance analysis is described.

By definition of the compliance matrix, the components of the i^{th} column of the matrix are the dynamic displacements of the interacting degrees-of-freedom caused by a harmonic force

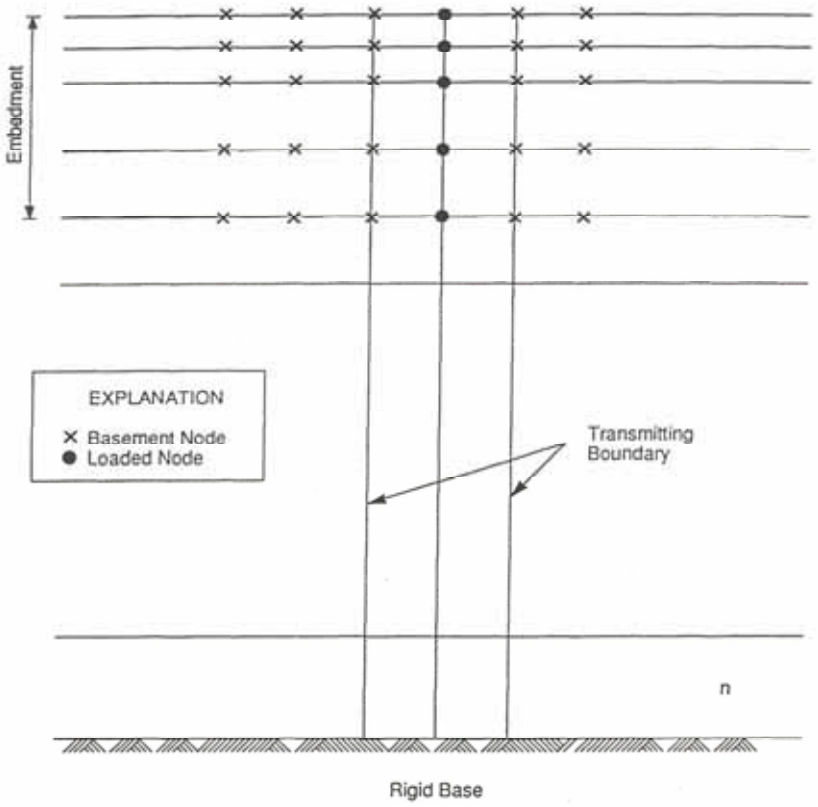

Fig. 4.2.3 Plane-strain model for impedance analysis

of unit amplitude acting at the i^{th} degree-of-freedom. Thus, the problem of determining the compliance matrix for two-dimensional problems is that of finding the harmonic response displacements of a layered halfspace to a harmonic line load. **Fig. 4.2.3** shows a layered system and the interaction nodes for which the matrix is to be determined. To obtain the compliance matrix, the basic problem is to determine the displacement responses of all the nodes subject to unit loads placed successively at one column of nodes shown as heavy dots in **Fig. 4.2.3**. Once this problem has been solved, solution corresponding to other nodes can be obtained simply by a shift of the horizontal coordinates.

The basic solution is obtained using a model which consists of a single column of plane-strain rectangular elements. This model, which takes advantage of symmetry, is shown in **Fig. 4.2.4** and is solved with different boundary conditions at the axis of symmetry depending on the direction of the applied forces at the loaded nodes. The existence of the semi-infinite layered region is simulated by applying the consistent transmitting boundary impedances as described in Section 4.2.2 on the nodes numbered n+1 to 2n, where n is the number of layers. The lower boundary may be fixed or a halfspace simulated using the variable depth method and the viscous boundary at base.

The equations of motion for the model are

$$\begin{bmatrix} \boldsymbol{C}_{cc} & \boldsymbol{C}_{c} \\ \boldsymbol{C}_{ll} & \boldsymbol{C}_{ll}+\boldsymbol{R} \end{bmatrix} \begin{Bmatrix} \boldsymbol{U}_{c} \\ \boldsymbol{U}_{l} \end{Bmatrix} = \begin{Bmatrix} \boldsymbol{Q}_{c} \\ 0 \end{Bmatrix} \tag{4.2.8}$$

where $\boldsymbol{C}$ indicates a dynamic stiffness matrix of the form ($\boldsymbol{C}$ = k-ω^2M) and $\boldsymbol{R}$ is the transmitting boundary impedance matrix described in Section 4.2.2. The indices *c* and *l* refer to degrees of freedom on the centerline and the lateral boundary, respectively; and $\boldsymbol{U}_c$ and $\boldsymbol{U}_l$ are the corresponding displacements. The load vector for each load case has only one non-zero element corresponding to a load of unit amplitude. Since the matrix in Eq. (4.2.8) is the same for all horizontal load cases (**Fig. 4.2.4 (a)**), only a single triangulation is required to find the solution vectors for these cases.

The unit horizontal harmonic loads are applied at the interacting nodes on the centerline of the model (see **Fig. 4.2.4 (a)**) successively. Solution to Eq. (4.2.8) yields displacement responses on the centerline and on the boundary of the model for each loading case. To compute the components of the flexibility matrix at interacting nodes outside the boundary of the model, the following relationship applicable to layered halfspace is used.

$$\{\boldsymbol{U}\} = \sum_{s=1}^{2n} \alpha_s \{\boldsymbol{V}\}_s \, exp(-ik_s x) \tag{4.2.9}$$

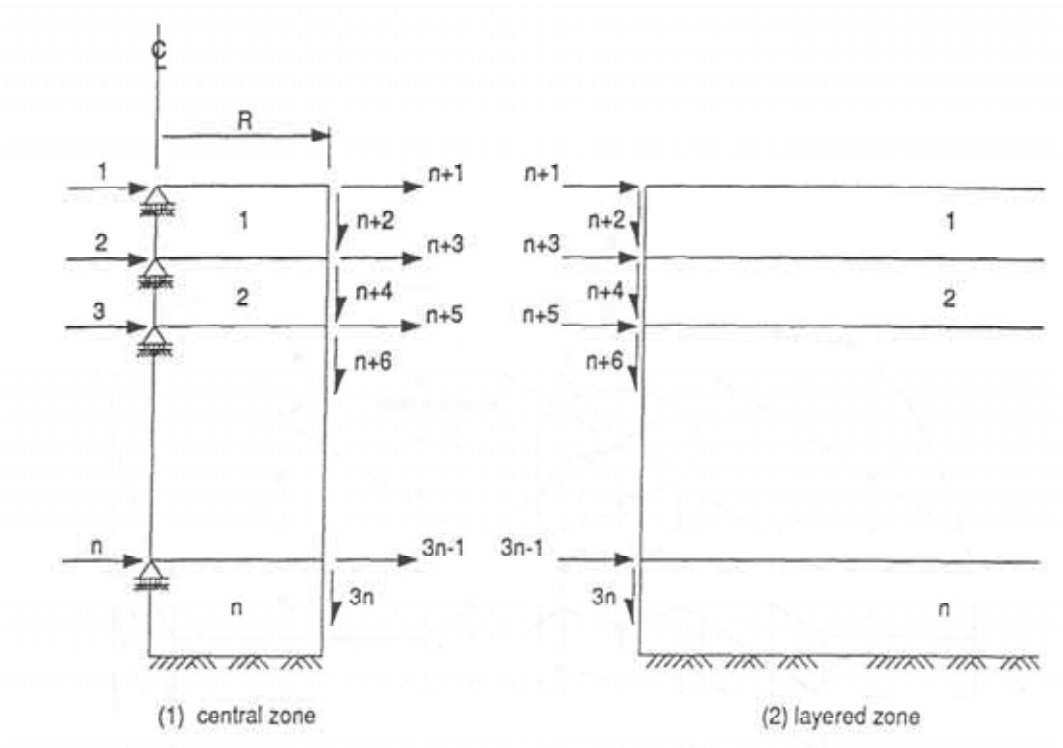

Fig. 4.2.4 (a) Boundary conditions for horizontal loading

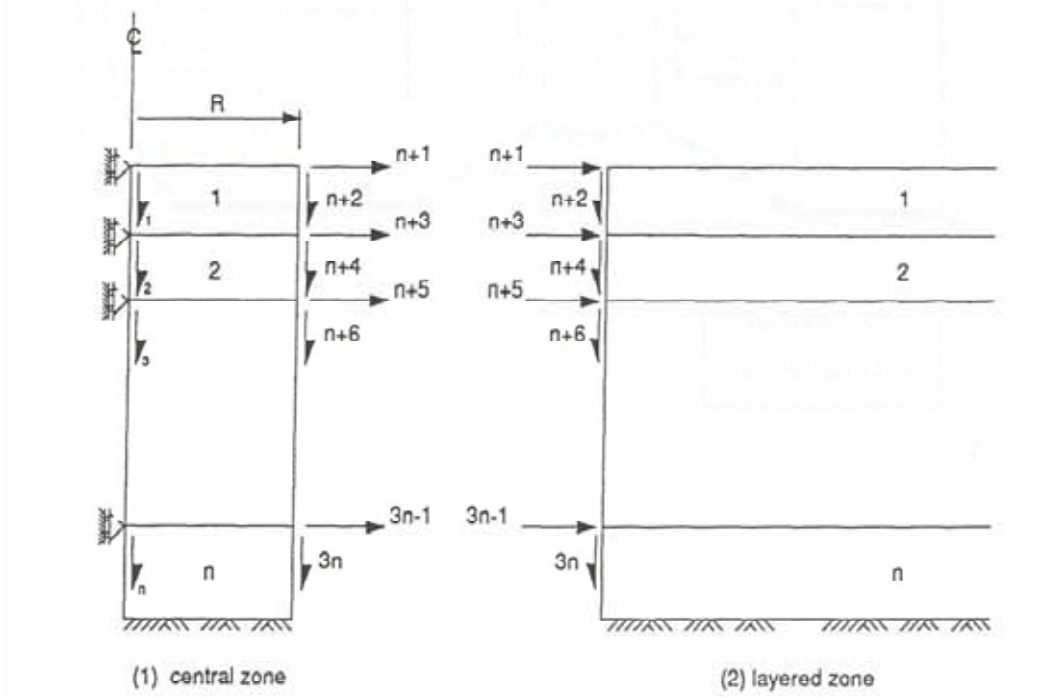

Fig. 4.2.4 (b) Boundary conditions for vertical loading

In this equation, x is the horizontal distance, $\{\boldsymbol{V}\}_s$, α_s, and k_s are the mode shapes, mode participation factors, and wave number associated with the soil layered system, respectively. As discussed in Section 5.2, there are 2n modes for a n layer soil system. The mode shapes and the associated wave numbers are obtained from the solution of the eigenvalue problem of a layered system as discussed previously. The mode participation factors are computed from Eq. (4.2.9) by letting x=0 and using the solution of Eq. (4.2.8) at the boundary nodes. Thus, by knowing the horizontal distance between the loaded nodes on the centerline and the interacting nodes outside the boundary, the displacements at all other nodes are computed from Eq. (4.2.9).

A similar technique is used for the vertical loading case. In this case the model shown in **Fig. 4.2.4 (b)** is used and the solution is obtained in a similar manner. Eq. (4.2.9) is then used to compute the displacement at other interacting nodes.

It should be noted, however, that the analytical models shown in **Figs. 4.2.4 (a)** and **Figs. 4.2.4 (b)** are analyzed only for one column of the interacting nodes as shown in **Fig. 4.2.3**. The same solution is successfully used for the remaining columns of interacting nodes and only the horizontal distance x in Eq. (4.2.9) needs to be computed to measure the horizontal distance between the new set of loaded nodes and the remaining interacting nodes.

Using the technique described above, a 2i x 2i compliance matrix associated with total of i interacting nodes is computed for each frequency of analysis.

In direct method of impedance analysis, the compliance matrix $[\boldsymbol{F}_{ff}]$ needs to be computed for all the interacting nodes using the methods described above. The impedance matrix $[\boldsymbol{X}_{ff}]$ is obtained by inverting the compliance matrix, i.e.,

$$\left[\boldsymbol{X}_{ff}\right] = \left[\boldsymbol{F}_{ff}\right]^{-1} \tag{4.2.10}$$

The impedance matrix as obtained is subsequently used in the assemblage of the equations of motion as described previously.

4.2.4 Structural analysis

In this section, computation of the structural and excavated soil properties used in the coefficient matrix of the equations of motion, namely, the components $\boldsymbol{C}_{ss}$, $\boldsymbol{C}_{si}$, and $\boldsymbol{C}_{ii}$, in Eq. (4.2.3) is described.

a) Modeling of structure

The structure, which consists of the superstructure and the basement, is modeled by finite elements. Several types of elements are included in the finite element library of SASSI. Basic theory for formulation of finite elements may be obtained from general finite element textbooks [27].

The material damping is incorporated in the stiffness matrix using the complex modulus representation. With this representation, the material damping ratio defined at the element level will be used to compute the complex stiffness of the element, thus allowing for variation of damping from element to element in the model. The mass matrices are either computed by the program by specifying the density for each element or assembled from the nodal lump mass input at the nodal points. When the mass matrix is computed by the program, the matrix consists of the summation of half lump mass and half consistent mass except for the plate and beam elements for which only lump mass and consistent mass matrices are computed, respectively.

b) Modeling of excavated soil and extended near field zone

The excavated soil is modeled using either plane-strain or three-dimensional solid elements for two- and three-dimensional problems, respectively. These elements are assigned two or three translational degrees of freedom per node. Thus, the moments from beam or plate elements are transferred to the soil through several common connecting nodes.

In some cases it may become necessary to include an additional volume of the soil in the immediate vicinity of the basement in the SSI model. This may be the case where the soil properties around the basement are different from those of the otherwise horizontal layered site or when the magnitude of the stress and strain in the soil around the basement is needed to measure the secondary nonlinear effects. For these cases, an additional soil volume is modeled with plane strain or brick elements and these elements are treated as structural elements. Subsequently, the excavated soil elements must cover the additional soil volume already modeled as structural elements.

c) Finite element size

The accuracy of a finite element analysis depends on the type of interpolation function used to represent the displacement field in the element and element sizes. The interpolation functions which are used for solid and plane strain elements vary linearly within the element.

It has been shown [28] that for such elements the accuracy of the solution is a function of the method used to compute the mass matrix and an accuracy better than 10 percent for wave amplitude is obtained if the element size h follows the relations shown below:

$h \leq 1/8\,\lambda_s$ for lumped mass matrix

$h \leq 1/8\,\lambda_s$ for consistent mass matrix

$h \leq 1/5\,\lambda_s$ for mixed mass matrix

In the above relation λ_s is the shortest wavelength which occurs in the volume represented by the elements. The shortest wavelength is obtained from

$$\lambda_s = V_s/f_{max} \tag{4.2.11}$$

where V_s is the shear wave velocity and f_{max} is the maximum frequency of analysis which must be transmitted through the finite elements. Thus, larger element size can be used in the zones with higher shear wave velocity.

In calculating the mass matrices for brick and plane-strain elements, combination of half consistent mass matrix with half lump mass matrix is used. Thus, the criterion of $h \leq 1/5\,\lambda_s$ need to be followed in selecting the finite element sizes.

These criteria along with the appropriate choice of f_{max} for the problem control the size of the model in terms of the degrees of freedom and subsequently the cost of analysis.

4.3 Analytical model of soil-structure interaction system

Based on the analytical theory for site vibration analysis described in previous section, and using the reaction forces obtained in the bridge-train interaction analysis in Chapter 3, the analytical models to perform site vibration analysis will be established in this section.

The site vibration around Shinkensen viaduct was measured simultaneously in the same actual field test [10] in Chapter 3. The field test was also conducted at the No. 1 Arasaki Viaduct of the Tokaido Shinkansen located in Ogaki, Gifu on November 1, 1999. While bullet trains composed of sixteen cars were running through the viaduct with its actual operational speeds of 270 km/h or 220 km/h, the site vibration was measured at different points around the viaduct during the bullet trains' passage using accelerometers. Then the acceleration responses of the viaduct were recorded on the data recorder from the accelerometers after being processed by amplifiers. The sampling rate of the data was also 512 Hz. Before the field test to measure the train-induced site vibration, the ground conditions [10] around the No. 1 Arasaki Viaduct were investigated, which will be used to establish the site model later.

Figure 4.3.1 indicates the positions of the piers and the surveyed points used in this analysis. In all, 24 footings of the three blocks of bridges used in previous bridge vibration analyses are adopted to be excited. Black rectangles in the figure indicate the footing positions. L and R denote the left and right sides of the bridge with respect to the moving direction of the train. The letters a–d and A–D and the numbers 1–4 respectively indicate the footing sequences in the three blocks of the bridge. The distances between the centers of neighboring footings on the same side are 6.0 m; those between the central lines of left and right footings are 5.2 m. Vicinity, 12.5 m and 25.0 m lying on the line passing through the centers of footings R-3 and L-3 denote the surveyed points at which the site vibration is measured in field test [10]. They are respectively 3.5 m, 12.5 m and 25.0 m distant from the longitudinal central line of the bridge. In this analysis, the site vibration response of a surveyed point is obtained from the superposition of those engendered by each of total 24 footings. Analytical results of these points are compared with experimental results.

Based on the conditions of the field test described above and the actual properties of the site and the substructures including footings and piles, the analytical models to perform site vibration analysis are established. Also here, there are many uncertainties in modeling either the site or the substructures. In addition to the uncertainties described previously in the bridge-train interaction model, it is conceivable to be more difficult to reproduce the accurate responses of the site vibration by the numerical approaches. However, it is beneficial enough to discuss the actual engineering problem if the amplitudes and main vibrational components can be approximately simulated.

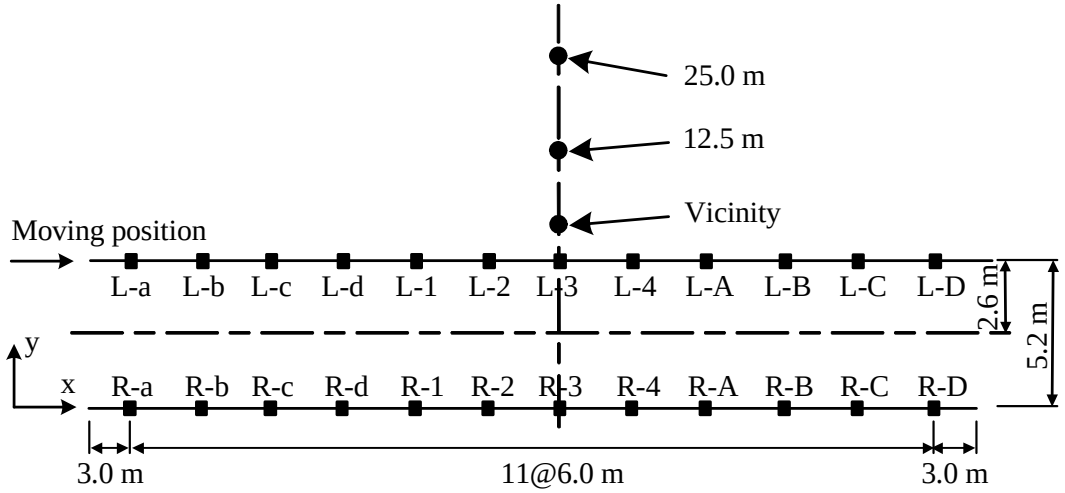

Fig. 4.3.1 Positions of piers and surveyed points of site vibration

Table 4.3.1 Ground properties

Depth of stratum (m)	0–6.8	6.8–17.2	17.2–
Unit weight (tf/m^3)	1.6	1.8	2.0
Shear modulus G(kN/m^2)	10400	66300	250000
Poisson's ratio ν	0.49	0.49	0.49
S wave velocity Vs(m/s)	80	190	350
Damping ratio	0.05	0.05	0.05

Table 4.3.2 Parameters of site model

Layer No.	Thickness (m)	Unit weight γ (tf/m^3)	S-wave velocity (m/s)	P-wave velocity (m/s)	S&P-damping ratio
1	0.26	1.6	80	570	0.05
2	0.54	1.6	80	570	0.05
2－12	0.60	1.6	80	570	0.05
13	0.60	1.6	80	570	0.05
14	1.00	1.8	190	1356.8	0.05
15－20	1.40	1.8	190	1356.8	0.05
21	1.60	2.0	350	2499.5	0.05
Halfspace	－	2.0	350	2499.5	0.05

4.3.1 Site model

Table 4.3.1 shows surveyed values of actual site properties and more detailed information is available in Reference [10]. The site mainly comprises three strata separated at depths of 6.8 m and 17.2 m. The velocity of an S-wave in the first stratum is 80 m/s, from which the soil can be considered as relatively soft. The damping constant is assumed as 5%, determined from experiential values. Analysis in the case of 3% damping constant is also performed later to investigate the influence of damping.

For analysis, the site model is divided further into 21 thin layer elements, whose profiles are shown in **Fig. 4.3.2**, and the parameters are shown in **Table 4.3.2.** The maximum thickness of each layer is determined in compliance with the criterion that it does not exceed 1/5 λs, where λs is the shortest S wavelength in that layer [26]. Layer elements are established down to the depth of 18.8 m, to which the structural model is embedded. The program then automatically adds some extra layer elements and the viscous boundary at the base to simulate the effect of half space.

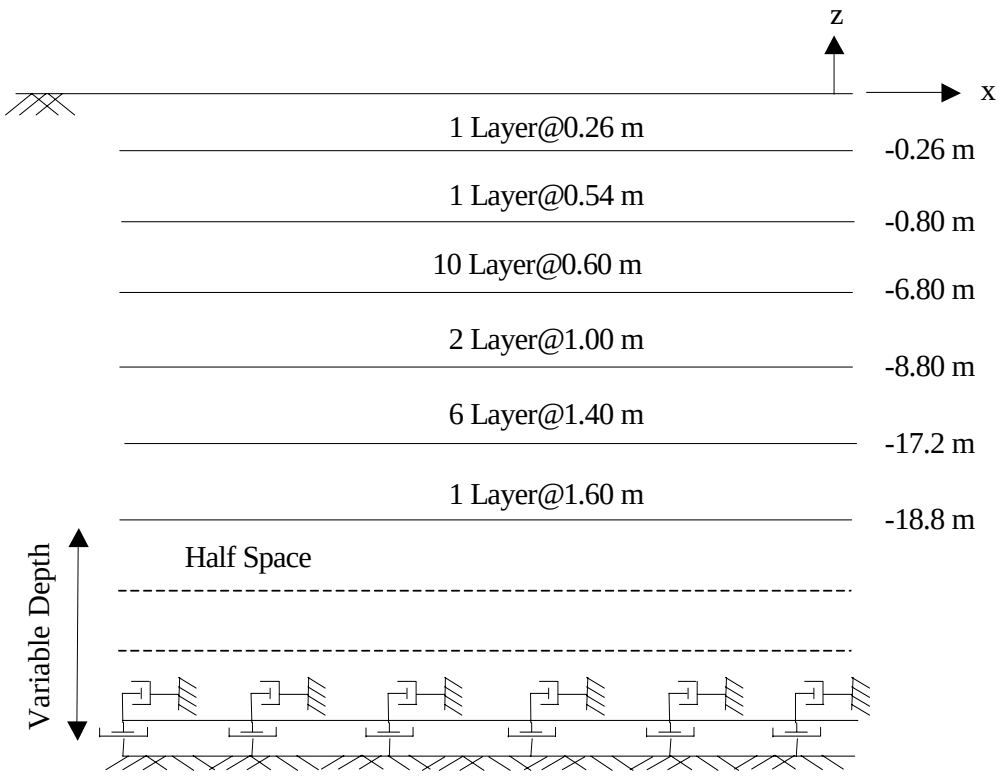

Fig. 4.3.2 Profile of the layer element site model

4.3.2 Structure model

One structural set consisting of one footing and seven piles is modeled as **Fig. 4.3.3**. Properties of the piles and the footing are shown respectively in **Table 4.3.3** and **Table 4.3.4**. The actual footing structure is in the shape of rectangular parallelepiped at the base and a trapezoid at the top. To simplify the analyses in this analysis, the footing is approximated as a rectangular parallelepiped divided into 36 solid elements according to the conversion of volume. The sizes of the solid elements also meet the criterion that they be less than 1/5 of the shortest S wavelength in the corresponding layer [26]. The upper footing surface is set to lie 0.26 m under the ground surface. The piles are divided into two types according to their length: Type 1 is 7 m long and Type 2 is 18 m. The ○ and × marks indicate the positions at which the piles are connected vertically to the footing. Herein, ○ represents 18-m-long piles and × represents 7-m-long piles. The piles are modeled as 3D beam elements. The ends of the beam elements are established at the soil layer interfaces.

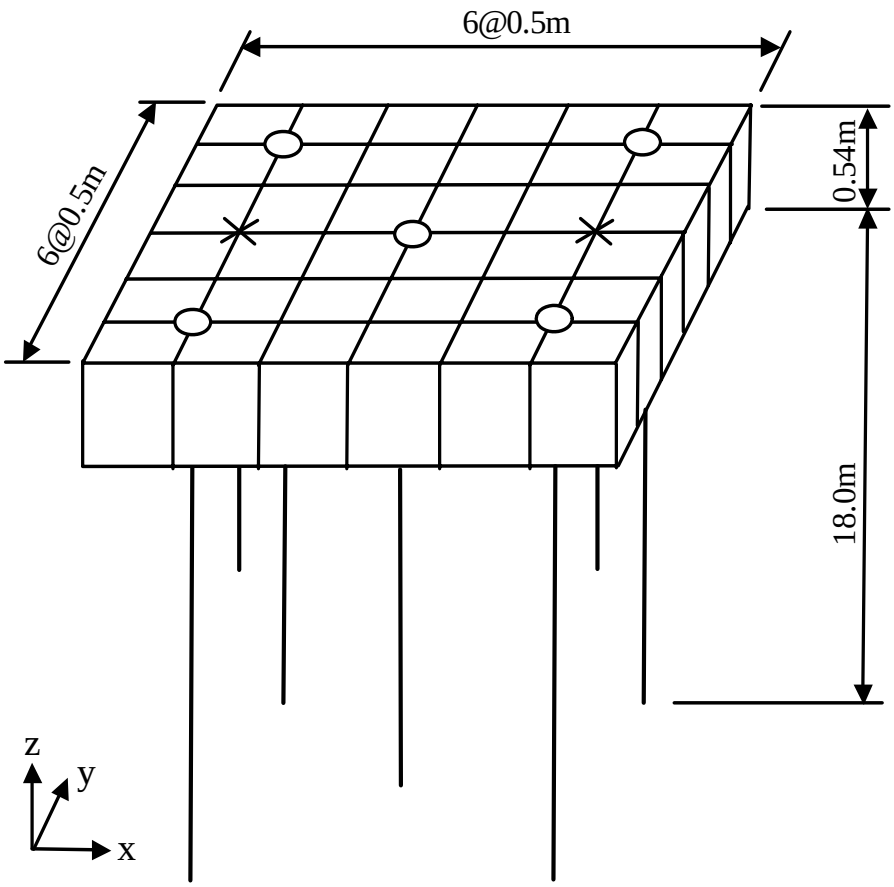

Fig. 4.3.3 Foundation model including footing and pile structure

Table 4.3.4 Properties of footing

Unit weight (kN/m^3)	24.5
Young's modulus E(kN/m^2)	2.50×10^7
Poisson's ratio ν	0.2
Damping ratio	0.05

Table 4.3.3 Properties of piles

Type	1	2
Unit weight (kN/m^3)	24.5	24.5
Cross-section area A (m^2)	0.058	0.045
Young's modulus E (kN/m^2)	3.5×10^7	3.5×10^7
Moment of inertia I (m^4)	6.2×10^{-4}	3.5×10^{-4}
Poisson's ratio ν	0.2	0.2
Damping ratio	0.05	0.05

4.3.3 Input excitations

The dynamic reaction forces (see **Fig. 4.3.4**) at the pier bottoms of the viaducts obtained in previous train-induced bridge vibration analysis are used as input motions for foundation-ground interaction system in time domain. Only the reaction forces of Piers L-1, L-2 and R-1 are indicated below.

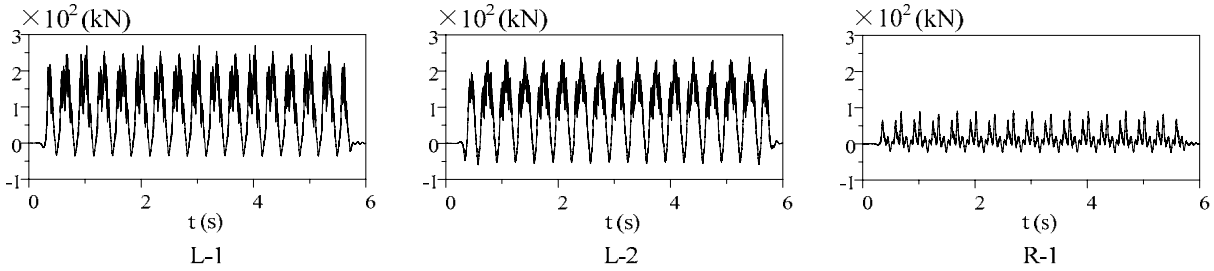

Fig. 4.3.4 Input motions for foundation-ground interaction system

4.4 Evaluation of site vibration by 9 DOF train model

4.4.1 Investigation on validity of SASSI

Prior to the site vibration analysis, validity of the program SASSI2000 is examined. The transfer function of the ground surface computed by SASSI2000 is compared with the exact analytical solution [29] under the same analytical conditions.

The comparison is shown in **Fig. 4.4.1**. The axes are generalized as dimensionless quantity. Exact analytical solution by exciting the ground with point load in vertical direction is indicated as W in **Fig. 4.4.1 (a)**. As kwon from the comparison, the solution obtained from SASSI2000 program shown in **Fig. 4.4.1 (b)** indicates good agreement with the exact analytical one. Thus the validation of the program can be confirmed.

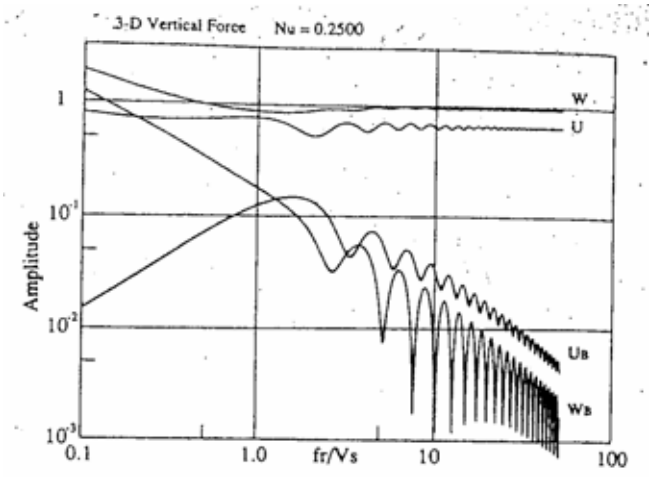

(a) Exact analytical solution

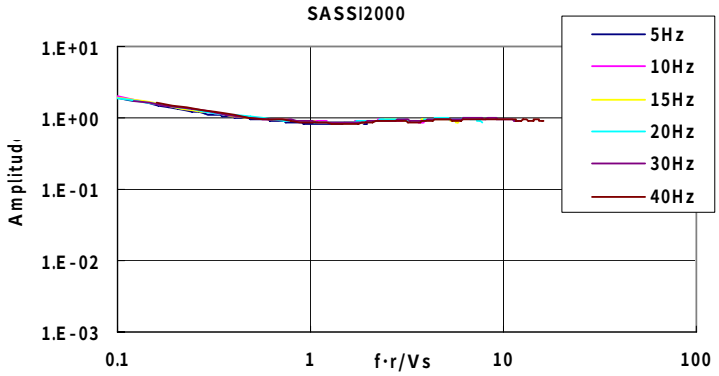

(b) SASSI2000 solution

Fig. 4.4.1 Validation of SASSI2000 program

4.4.2 Analytical results with 5% damping constant

Considering the predominant frequency components of the external forces that are confirmed within 15 Hz and the damping effect of the soil as well as efficiency of the analysis, the highest frequency taken into account in the analysis is selected to be 25 Hz. By applying the reaction forces obtained in elevated bridge vibration analysis at the footings, the site response analysis using the analytical models described in section 4.3 is carried out by program SASSI2000.

The analytical results of the points of Vicinity, 12.5 m and 25 m indicated in **Fig. 4.3.1** simultaneously with the experimental values are shown in **Fig. 4.4.2**. In the analysis, to investigate the influence of exciting manners on the total response, the results of five cases of only exciting footing L-1, exiting footings L-1 to L-4 (total 4 footings of middle block), exiting footings L-1 to R-4 (total 8 footings of middle block), exiting footings L-a to L-D (total 12 footings of left side) and exiting footings L-a to R-D (total 24 footings of three blocks) are calculated and shown in **Fig. 4.4.2**, respectively. The maximum and rms values of the site vibration corresponding both to experiment and analysis (exiting L-a to R-D) are shown in **Tables 4.4.1** and **4.4.2**.

As shown in **Fig. 4.4.2** and **Tables 4.4.1** and **4.4.2**, the analytical acceleration responses (with 5% damping constant) simultaneously with the Fourier spectra of the surveyed points by exciting all 24 footings are indicating relatively agreement with experimental values since they contain the main components of total response. The maximum errors remain within 30% of the experimental values. In spite of the complicated nature of the whole train-bridge-ground interaction system and the approximations or assumptions that have to be made in modeling the system, the analytical acceleration responses can reproduce the main tendencies of the actual ones. The amplitudes of the analytical results are considerably coincident with the experimental ones. The components of the Fourier spectra of the analytical results to a certain extent re-create the experimental ones. Thereby the validity of the analytical procedure can be confirmed.

Noticeable fact can be observed as that the results obtained by exciting 12 footings of L-a to L-D on the left side only are almost the same with that by exciting total 24 footings. The same phenomenon can be also confirmed in case 2 and case 3, which can lead to the conclusion that influences of the footings on the right side are extremely small and can be neglected. The reason is considered as follows. As indicated in the previous bridge vibration analysis, the predominant reaction forces occur at the piers of left side of the bridge since the bullet trains are assumed running along the left side. The amplitudes of the reaction forces of right piers are about only 1/3 of the ones of left piers. Furthermore, for the surveyed points in

this analysis the distances from the footings of the right side are 5.2 m far than those on the left side. Thus in site vibration evaluations as such cases, it is sufficient to excite the footings on the left side only, which can lead to a saving of computational cost.

In the case of exciting footing L-3 only, the response of point-1 is observed taking more than half component of total response since point-1 is lying at immediate vicinity of footing L-3. The responses of point-2 and point-3 take less proportion of the total responses, corresponding to their distances from the footing, from which the damping effect of the soil can be confirmed.

In addition, the responses calculated by exciting 12 footings of L-a to L-D only are observed to some extent larger than that obtained by exciting total 24 footings at some points. It is considered as the phenomenon that the waves interfere with each other according to different wave phases.

4.4.3 Analytical results with 3% damping constant

Since the damping constants of the soil layers used in the analysis is determined according to experience value, it is necessary to examine the influence of different damping constant on the analytical results. Analysis in the case of 3% damping constant is also carried out and the analytical results simultaneously with the experimental values are shown in **Fig. 4.4.3** with the same five cases of the 5% damping analysis. The maximum and rms values of the site vibration corresponding both to experiment and analysis (exiting L-a to R-D) are shown in **Tables 4.4.1** and **4.4.2**. As shown in **Fig. 4.4.3**, the analytical responses are indicating larger amplitudes compared with the analysis of 5% damping constant. The same tendencies of different cases of the results compared with those of 5% damping analysis can be confirmed. Both the maximum and rums values of the analytical results with 3% damping constant exceeded 60% errors compared with the experimental ones. Therefore, the damping constant of 5% is considered a proper one for the site model used in this analysis

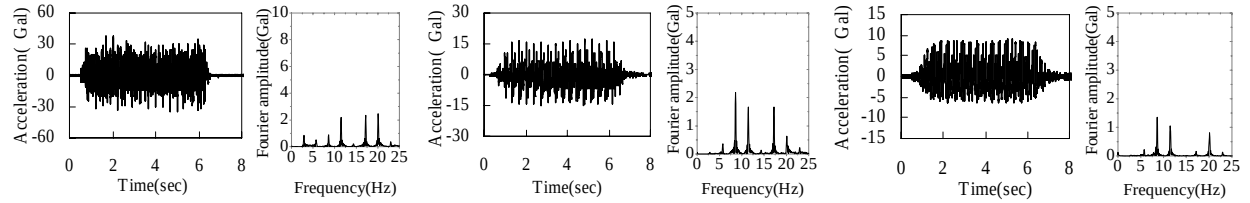

Experimental values

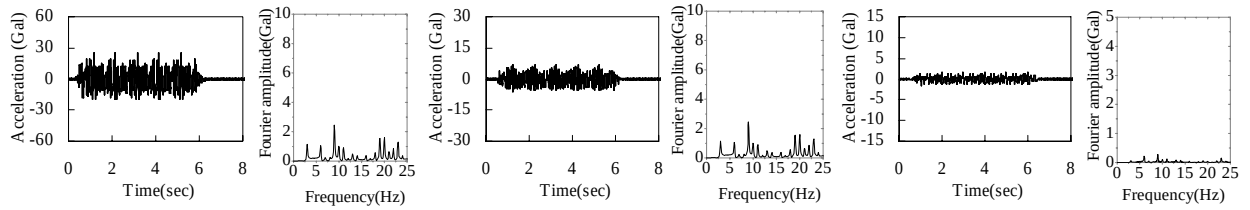

Case 1 (Exciting L-3 only)

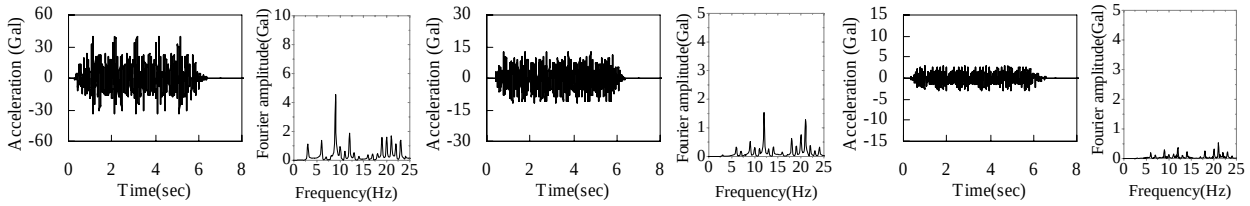

Case 2 (Exciting L-1 to L-4)

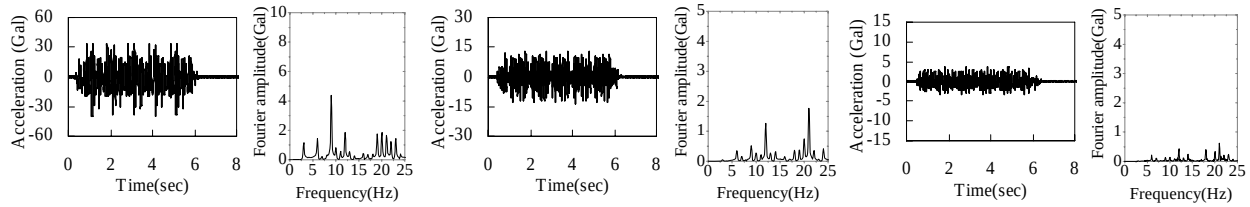

Case 3 (Exciting L-1 to R-4)

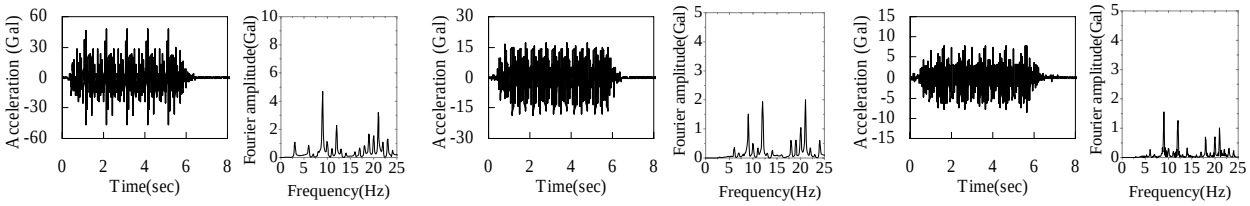

Case 4 (Exciting L-a to L-D)

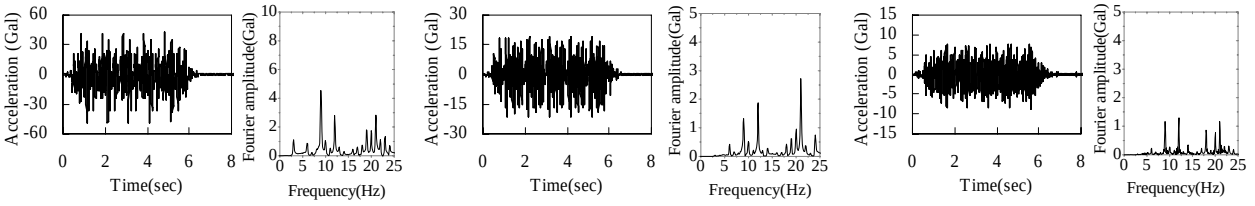

Case 5 (Exciting L-a to R-D)

Vicinity 12.5 m 25 m

Fig. 4.4.2 Evaluation on analytical results (5% damping)

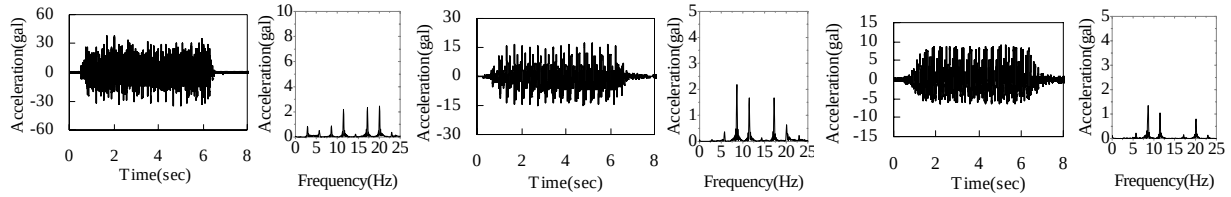

Experimental values

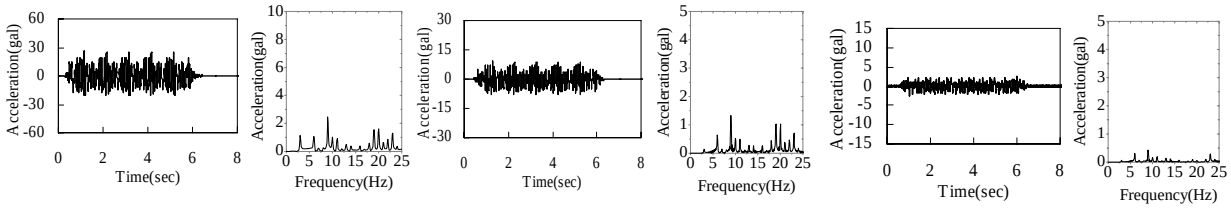

Case 1 (Exciting L-3 only)

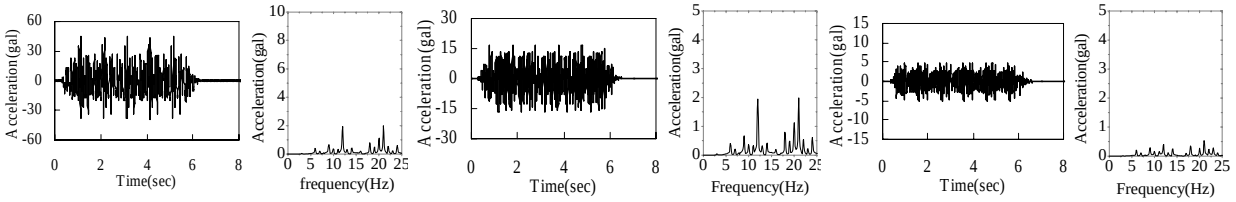

Case 2 (Exciting L-1 to L-4)

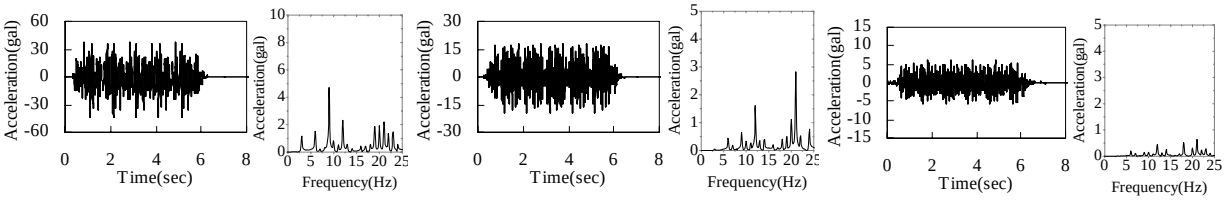

Case 3 (Exciting L-1 to R-4)

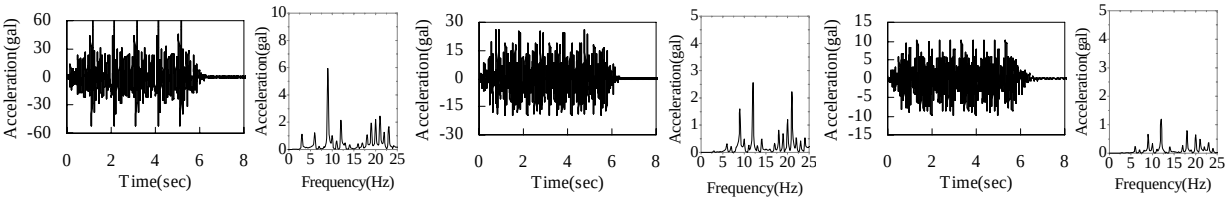

Case 4 (Exciting L-a to L-D)

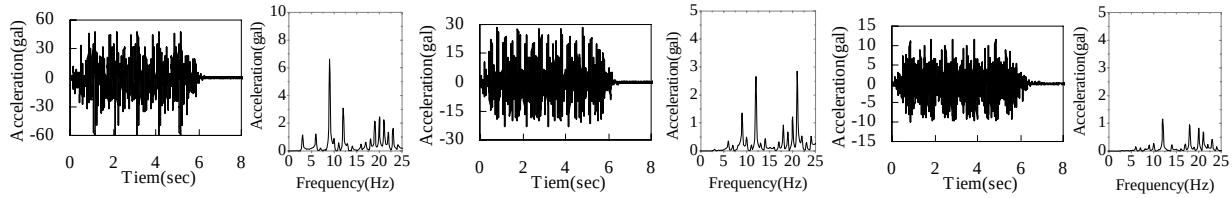

Case5 (Exciting L-a to R-D)

Vicinity 12.5 m 25 m

Fig. 4.4.3 Evaluation on analytical results (3% damping)

Table 4.4.1 Maximum accelerations of ground motion (v=270km/h)

Point No.	Maximum acceleration (Gal)		
	Experiment	Analysis (error)	
		5% damping	3% damping
Vicinity	37.7	48.8 (+29.4%)	60.7 (+61.0%)
12.5 m	17.3	21.7 (+25.4%)	28.8 (+66.5%)
25 m	9.1	8.9 (-2.2%)	11.5 (+26.4%)

Table 4.4.2 rms values of ground motion (v=270km/h)

Point No.	rms value (Gal)		
	Experiment	Analysis (error)	
		5% damping	3% damping
Vicinity	11.0	14.3 (+30.0%)	17.9 (+62.7%)
12.5 m	6.2	7.3 (+17.7%)	9.2 (+48.4%)
25 m	3.5	3.0 (-14.3%)	4.0 (+14.3%)

4.4.4 Analytical results of different output points

As shown in **Fig. 4.4.2**, the predominant frequency components in the analytical results differ somewhat from those of the experimental ones, especially at about the range of 20 Hz. In the actual field test, the surveyed points may differ slightly from those that are prearranged according to the local conditions. In turn, that difference might affect the predominant frequency component of the vibration because of the phase difference of the waves. To investigate such influences, the responses of the points which are 0.5 m, 1.0 m shifted from the points shown in **Fig. 4.3.1** in x direction on left or right side are simulated and the results simultaneously with the experimental values are shown in **Fig. 4.4.4**. In **Fig. 4.4.4**, (a) On straight line shows the results of the points in **Fig. 4.3.1**, (b) On +0.5 m side line indicates the results of the points determined by shifting the ones in **Fig.6.1** with +0.5 m in x direction and the others can be analogized.

As known from **Fig. 4.4.4**, the responses of the shifted points are similar with those of (a) but indicating some differences for the amplitudes. Especially for Point-2, the results of (b) and (c) are indicating better agreement with experimental ones. On the other hand, the predominant frequency components at about 10 Hz for point-1 and at about 20 Hz for point-2 are still indicating some disagreement with that of the experimental ones. The reason can be considered as that the discrepancies of the results come from the difference between the actual site properties and the idealized model. But for the frequency components in the range from 3 to 12 Hz which are mostly concerned in environmental problems, the analytical results is consider having acceptable accuracy to evaluate the site vibration.

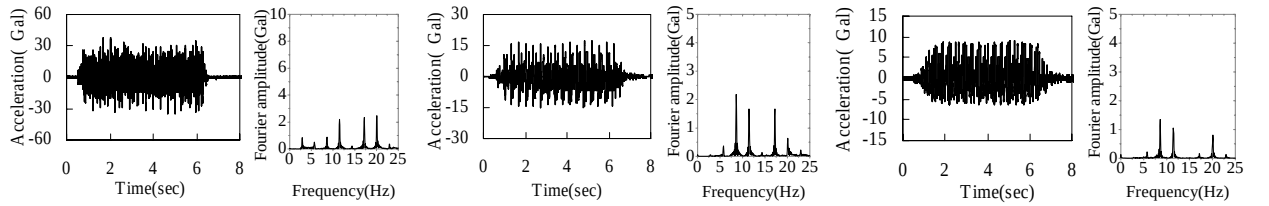

Experimental values

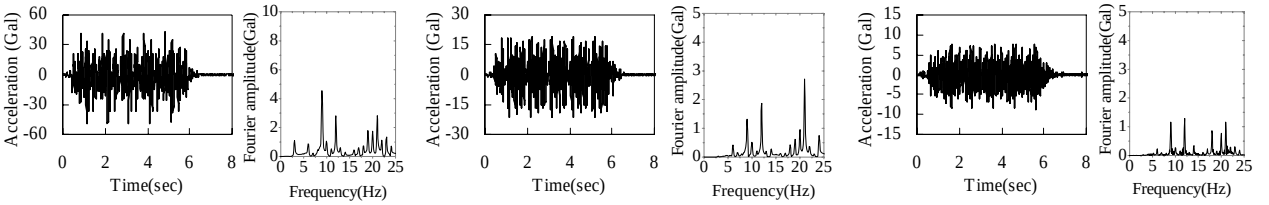

(a) On straight line

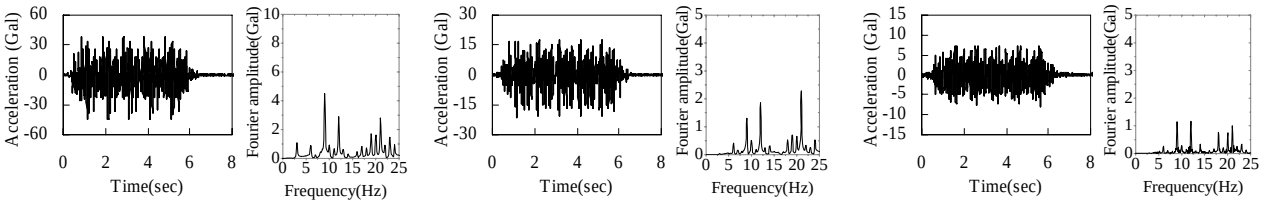

(b) On +0.5m side line

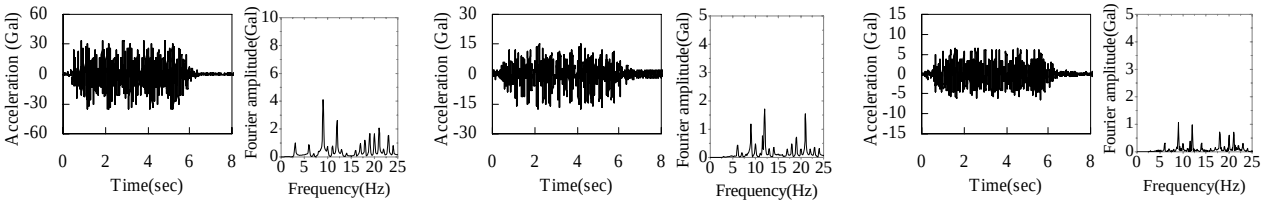

(c) On +1.0m side line

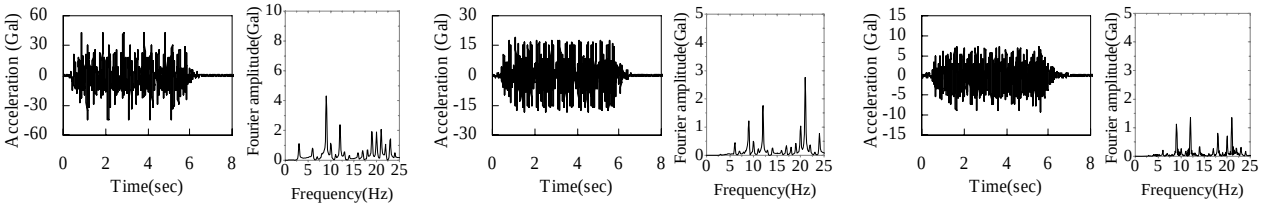

(d) On -0.5m side line

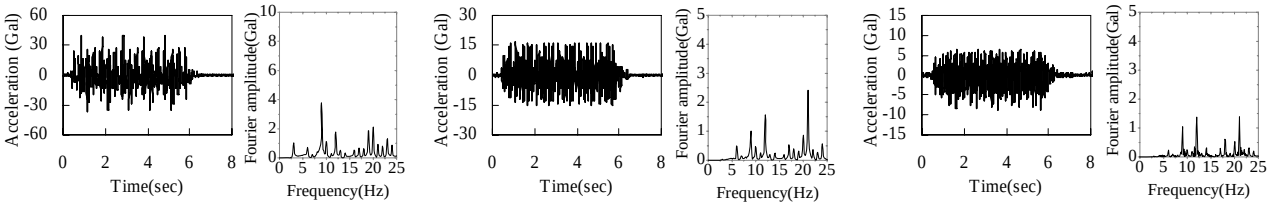

(e) On -1.0m side line

Vicinity 12.5 m 25 m

Fig. 4.4.4 Results of different output points

4.4.5 Responses under trains with different velocity

The analysis under the train with velocity of 220 km/h was also carried out and the analytical results composed by the components of total 24 footings are shown in **Fig. 4.4.5** simultaneously with the experimental values. The maximum and rms values of the site vibration corresponding both to experiment and analysis (exiting L-a to R-D) are shown in **Table 4.4.3**. The acceleration amplitudes especially the rms values of the analytical results indicated good agreement with the experimental ones. However, the frequency components of total three points between the analytical results and the experimental ones indicate considerable differences. Although the analytical conditions are difficult to be completely coinciding with the actual ones, further efforts are needed to discuss the predominant components of the site vibration.

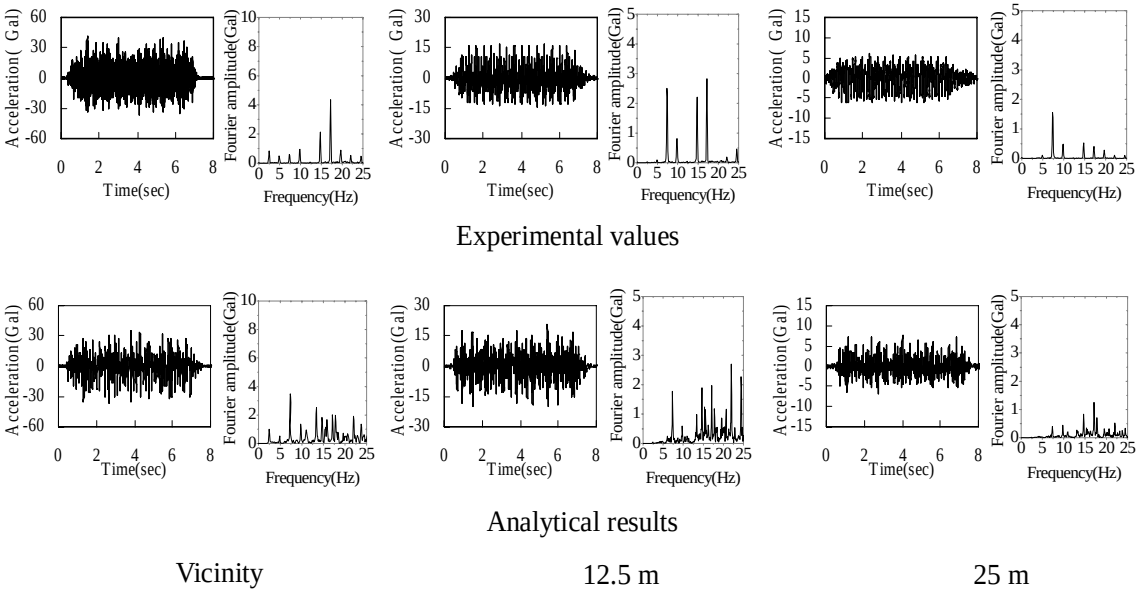

Fig. 4.4.5 Reponses of surveyed points (220 km/h)

Table 4.4.3 Maximum accelerations and rms values of ground motion (v=220km/h)

Point No.	Maximum acceleration (Gal)		rms value (Gal)	
	Experiment	Analysis (error)	Experiment	Analysis (error)
Vicinity	40.7	35.8 (-12.0%)	10. 9	10.8 (-0.9%)
12.5 m	16.5	20.4 (+23.6%)	6.0	6.0 (0.0%)
25 m	6.2	7.6 (+22.6%)	2.5	2.2 (-12.0%)

4.4.6 Vibration level of site vibration

The overall levels of the vibration simulated are also calculated and the values at Vicinity, 12.5 m and 25 m under different speeds of the train are shown in **Table 4.4.4**. The fact that both vibration level and vibration acceleration level decreased with the increase of intervals from the bridge as well as the slowdown of the train can be confirmed.

The 1/3-octave band analysis is also carried out to evaluate the site vibration. The vibration level and vibration acceleration level of the surveyed points computed from the analytical results are shown in **Fig. 4.4.6**. The same tendencies with that of the overall levels can be also confirmed for the 1/3-octave levels and the validation of the analytical procedure can be further confirmed. Such evaluation approach can be used in the actual investigations of site vibrations around the viaducts of high-speed railway system.

Table 4.4.4 Overall level

	270 km/h		220 km/h	
	VL (dB)	VAL (dB)	VL (dB)	VAL (dB)
Vicinity	81.7	85.2	78.8	82.8
12.5 m	74	79.1	71.8	77.6
25 m	67.2	71.7	63.4	69.1

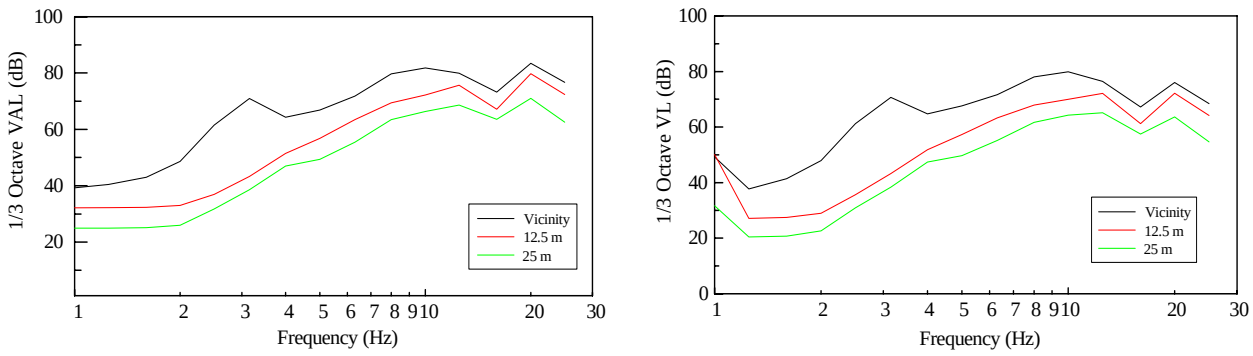

Fig. 4.4.6 Evaluation of VL and VAL (270 km/h)

4.5 Mitigation of site vibration by reinforcement of viaducts

The effect of the countermeasure (**Fig. 4.5.1**) described in Section 3.7 of Chapter 3 on site vibration is investigated in this section. As described in Chapter 3, the bridge model is established due to Hara et al's research [9]. The ground conditions and the properties of the substructures are also different from those used in the previous 3-block bridge model. The ground properties of the viaducts used by Hara et al are shown in **Table 4.5.1**. Based on the ground properties in **Table 4.5.1**, the layer element site model is shown in **Fig. 4.5.2**. The difference of the substructure is that there are only five piles under one footing in this viaduct and their length is 8 m. The other properties are the same with the substructure of previous 3-block model. The new substructural model of one set is shown in **Fig. 4.5.3**.

Using the analytical models established above, the site vibration analysis is carried out. The dynamic reaction forces before and after installing the countermeasure are shown in **Fig. 4.5.4**. The amplitudes of piers L-1 and R-1 which is easily affected by the vibration of the hanging part decreased due to the countermeasure. Then the analytical results and the experimental ones before and after the reinforcement at the point of the vicinity of pier L-1 are compared in **Fig. 4.5.5**. The analytical results indicate relative agreement with the experimental ones, though there are still some uncertainties in the analytical models. The analytical results of all three points of Vicinity, 12.5 m and 25 m before and after the reinforcement are shown in **Fig. 4.5.6**. Corresponding maximum and rms values are given in Table 4.5.2. From the results, the effect of the countermeasure can be fully confirmed.

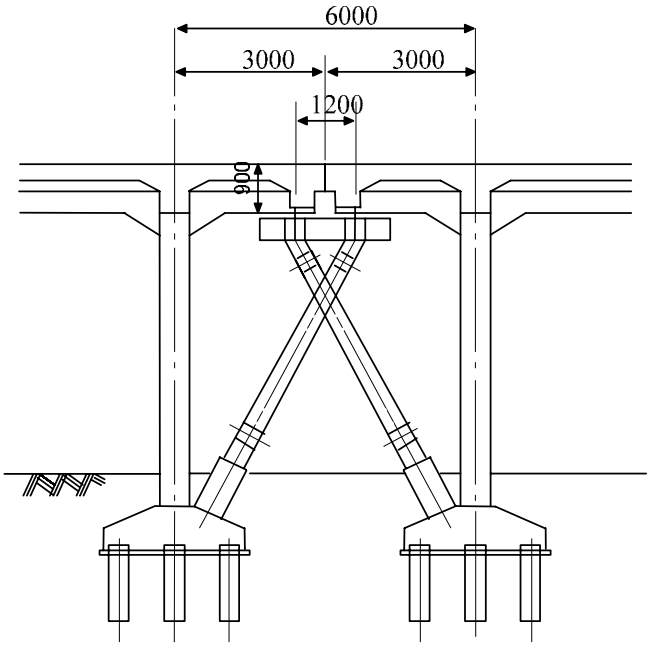

Fig. 4.5.1 Simple figure of reinforcement

Table 4.5.1 Ground properties

Depth of stratum (m)	0–4.6	4.6–8.0	8.0–
Unit weight (tf/m^3)	1.7	1.7	1.9
S wave velocity Vs(m/s)	115	183	295
Damping ratio	0.05	0.05	0.05

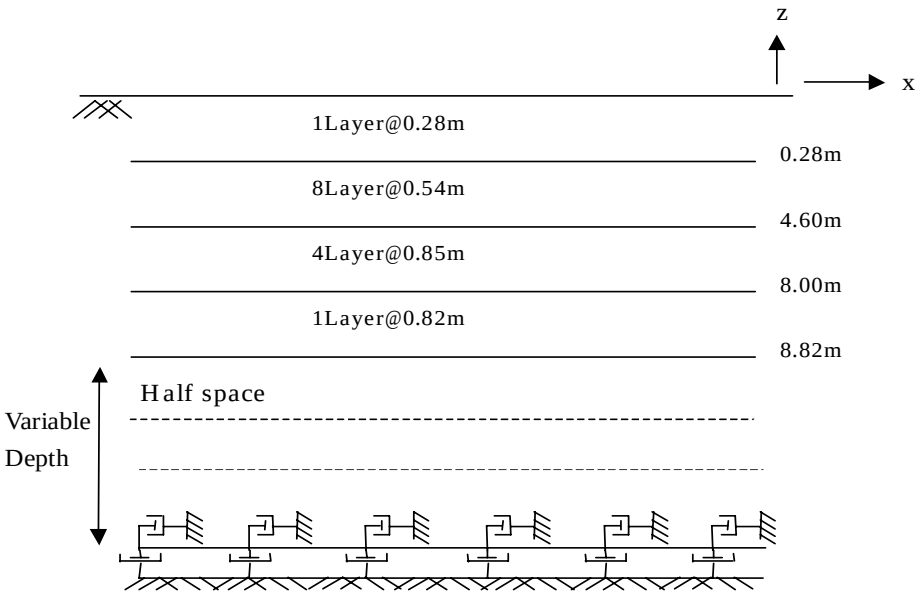

Fig. 4.5.2 Site model

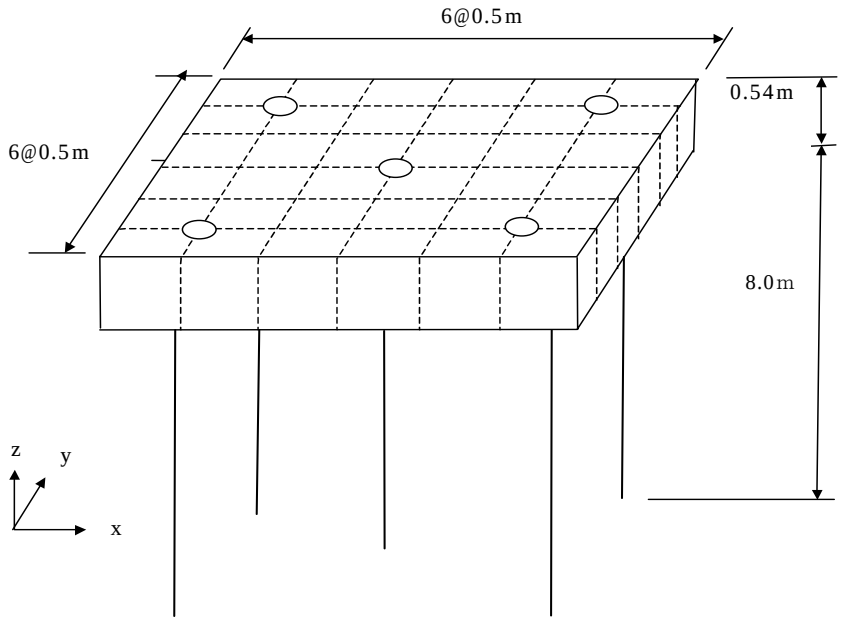

Fig. 4.5.3 Substructural model

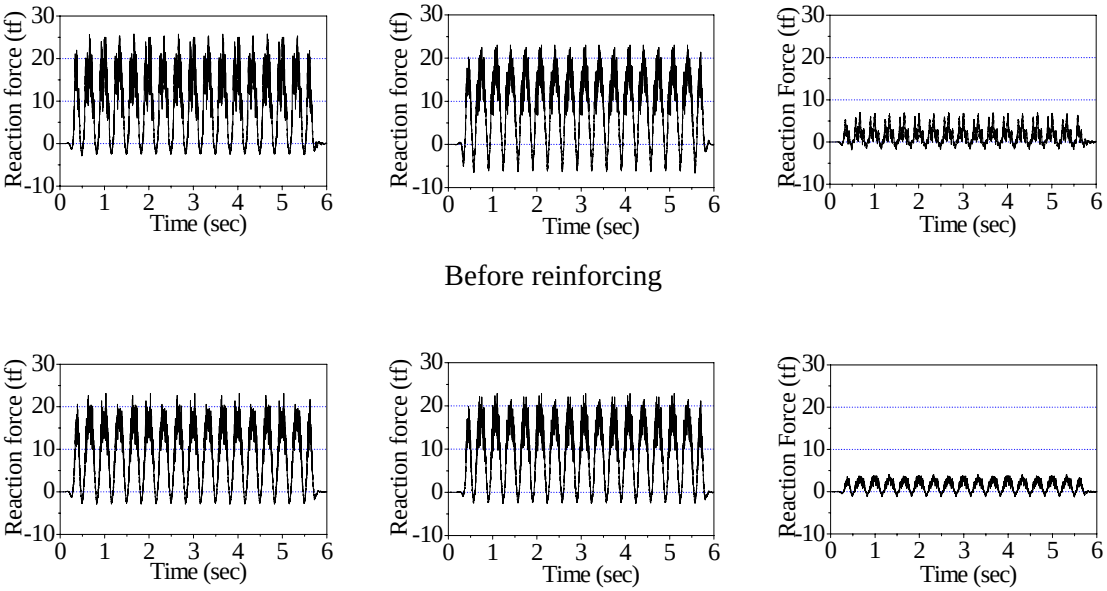

Fig. 4.5.4 Reaction forces before and after reinforcement

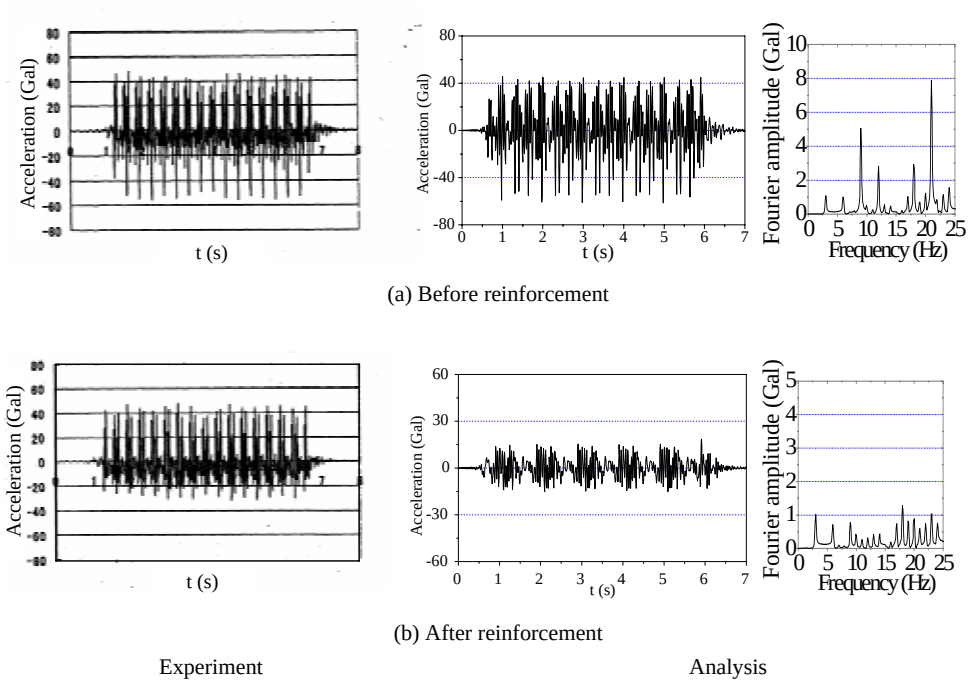

Fig. 4.5.5 Comparison of experimental and analytical responses

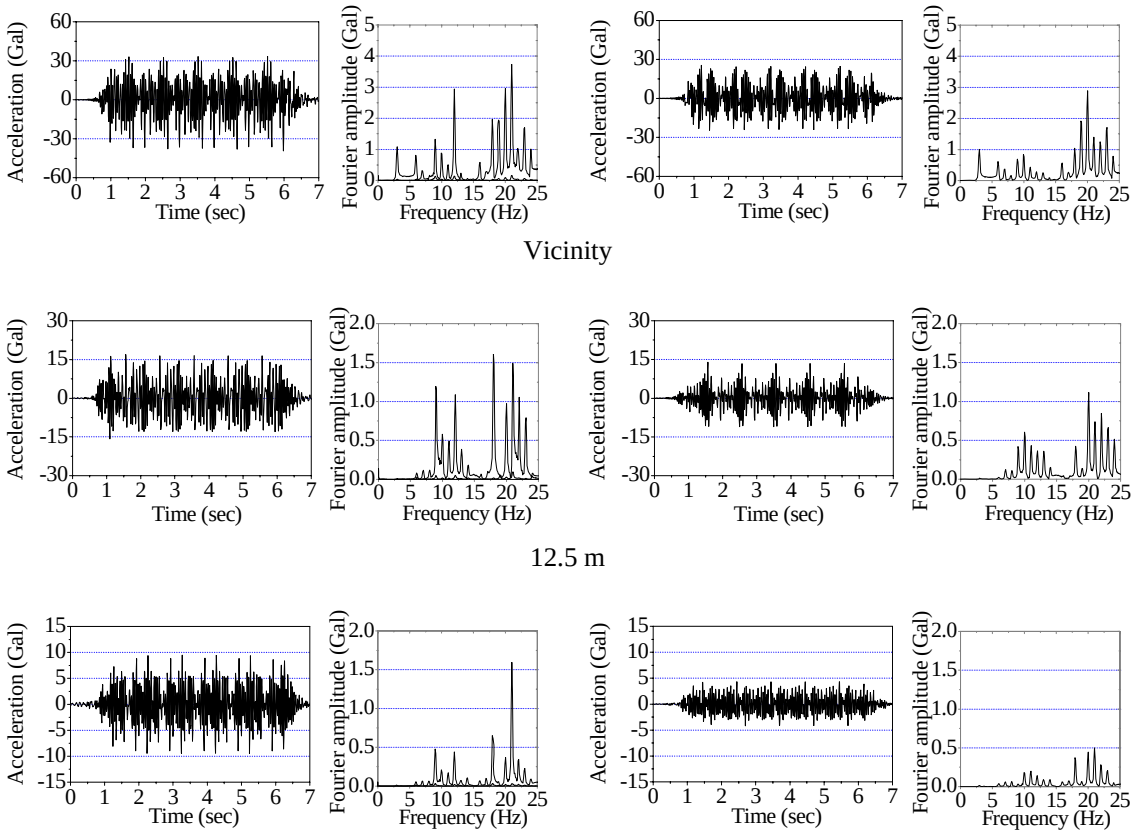

Fig. 4.5.6 Comparison of analytical responses before and after reinforcement

Table 4.5.2 Maximum and rms values of responses before and after reinforcement (Gal)

Point	Maximum acceleration (Gal)		rms value (Gal)	
	Before reinforcement	After reinforcement	Before reinforcement	After reinforcement
Vicinity	36.42	24.91	13.22	9.33
12.5 m	16.32	12.50	6.16	3.87
25 m	9.48	4.27	3.40	1.64

4.6 Evaluation of site vibration by 15 DOF train model

In the case of simulating the horizontal site vibration around the viaducts, it is desirable to use the horizontal dynamic reaction forces of the bridge simultaneously with the vertical ones. The horizontal response of the bridge may affect the site vibration especially in the ambient area around the viaducts. Therefore in this research, a 15-DOF car model is developed [16] based on the former described nine-DOF model by further taking account of the lateral translation and the yawing motion of the car body and bogies. This model can properly simulate not only the vertical motions but also the horizontal vibrations of the train, thus to obtain the lateral responses of the bridge. The applying both the horizontal and vertical dynamic reaction forces at the pier bottoms obtain by bridge-train interaction analysis, the site vibration of both directions can be simulated.

4.6.1 Train model

Bullet trains composed of 16 cars, modeled as 15 DOF system for each car described in Chapter 2, are employed for analysis. The properties of the train will be described in detail in the next chapter. The natural frequency of the bogies is higher than that of the train body, which can engender resonance in a higher-frequency field and contribute to high-frequency components of dynamic responses of the bridge. The train velocity is assumed to be 270 km/h, referring to the actual Shinkansen operational speed.

4.6.2 Dynamic responses of elevated bridge

The analytical acceleration responses and the experimental ones in vertical direction, of point-1 through point-3 of elevated bridges indicated in Chapter 3, are shown respectively in **Fig. 4.6.1**, and those in horizontal direction of point-3 are shown in **Fig. 4.6.2**. As shown in **Fig. 4.6.1** and **Fig. 4.6.2**, analytical results using the 15 DOF train model indicate good agreement with experimental results, thereby validating this analytical procedure.

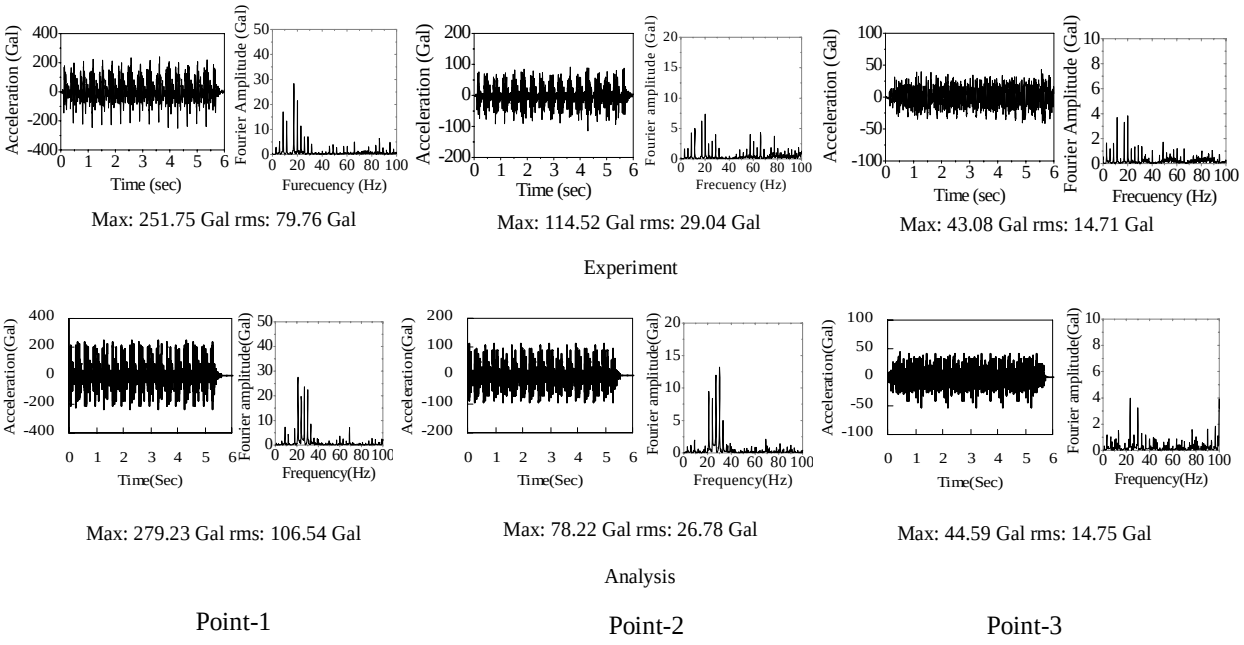

Fig. 4.6.1 Acceleration of bridge (vertical)

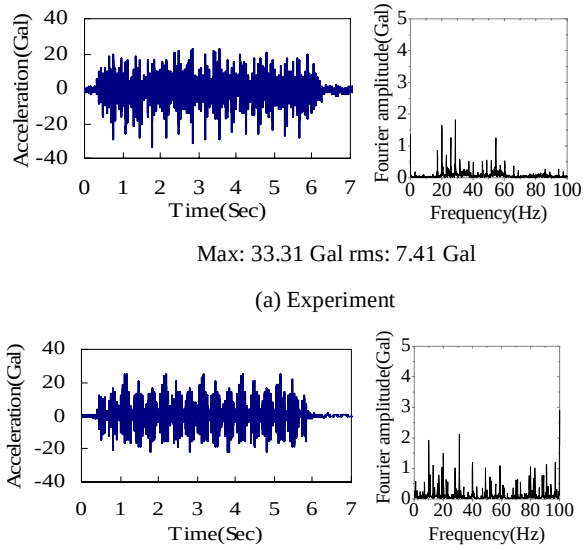

Fig. 4.6.2 Acceleration of bridge (Point-3, horizontal)

4.6.3 Dynamic reaction forces at bottoms of piers

Reaction forces at the bottoms of the piers in vertical and horizontal directions, as respectively shown in **Fig. 4.6.3**, are calculated using the influence value matrix of the reaction forces. As shown in **Fig. 4.3.1**, L-1 to L-4 and R-1 to R-4 respectively indicate the piers on the left and right sides of the middle block of the bridge, with respect to the train's direction.

The vertical reaction forces of the piers on the left side are much stronger than those on the right side because the trains are assumed to run along the left sides of the bridges. On the other hand, the reaction forces on the left and right sides in horizontal direction display similar amplitudes. In particular, for both directions in **Fig. 4.6.**, the amplitude at L-1 is larger than that of L-2. The reason is the same as described previously that the maximum acceleration response that engenders a larger inertia force appears at the hanging part of the bridge. Dynamic reaction forces obtained here are used as input external excitations in further analyses of site vibration problems.

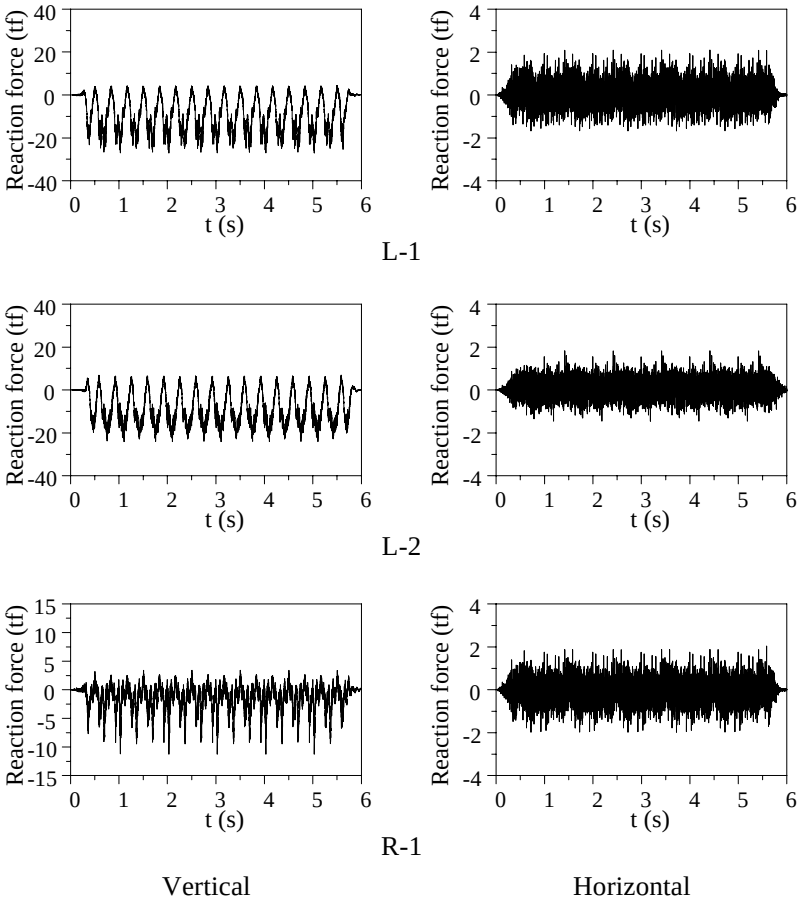

Fig. 4.6.3 Reaction forces

4.6.4 Analytical results of site vibration

Analytical results and experimental values in vertical and horizontal directions simultaneously with the maximum and rms values of the points of 12.5 m and 25 m are shown in **Fig. 4.6.4** and **Fig. 4.6.5**. For both vertical and horizontal directions, the amplitudes of analytical results show relative agreement with the experimental ones. On the other hand, the predominant frequency components, particularly in the horizontal direction, indicate somewhat disagreement with those of the experimental ones. The reasons can be considered as follows. First, since the wheel sets of the train are not modeled, the components of the analytical results are inevitable to have some differences with the actual responses especially for the horizontal direction. Furthermore, the discrepancies of the results arise from the difference between the actual site proper-ties and the idealized model. However, considering the complicated nature of the whole train-bridge-ground interaction system, the analytical results obtained here are considered good enough to evaluate site vibration around viaducts in the further studies.

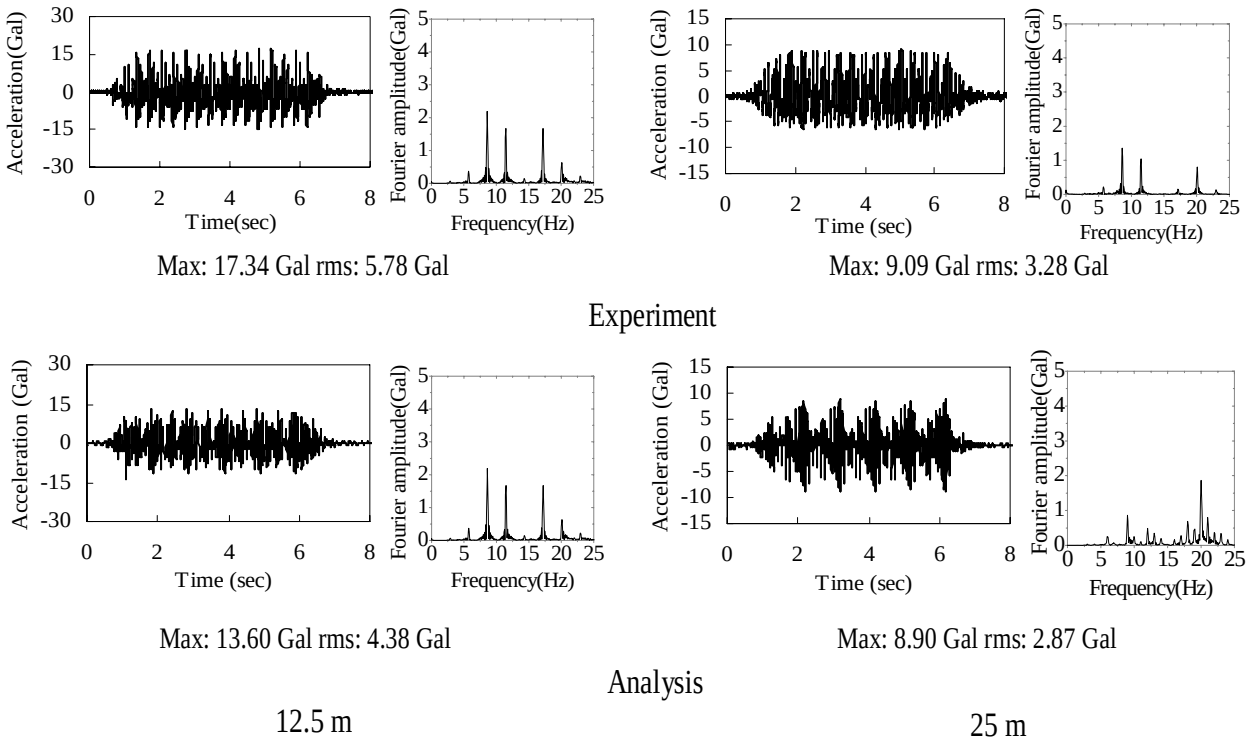

Fig. 4.6.4 Acceleration of ground (vertical)

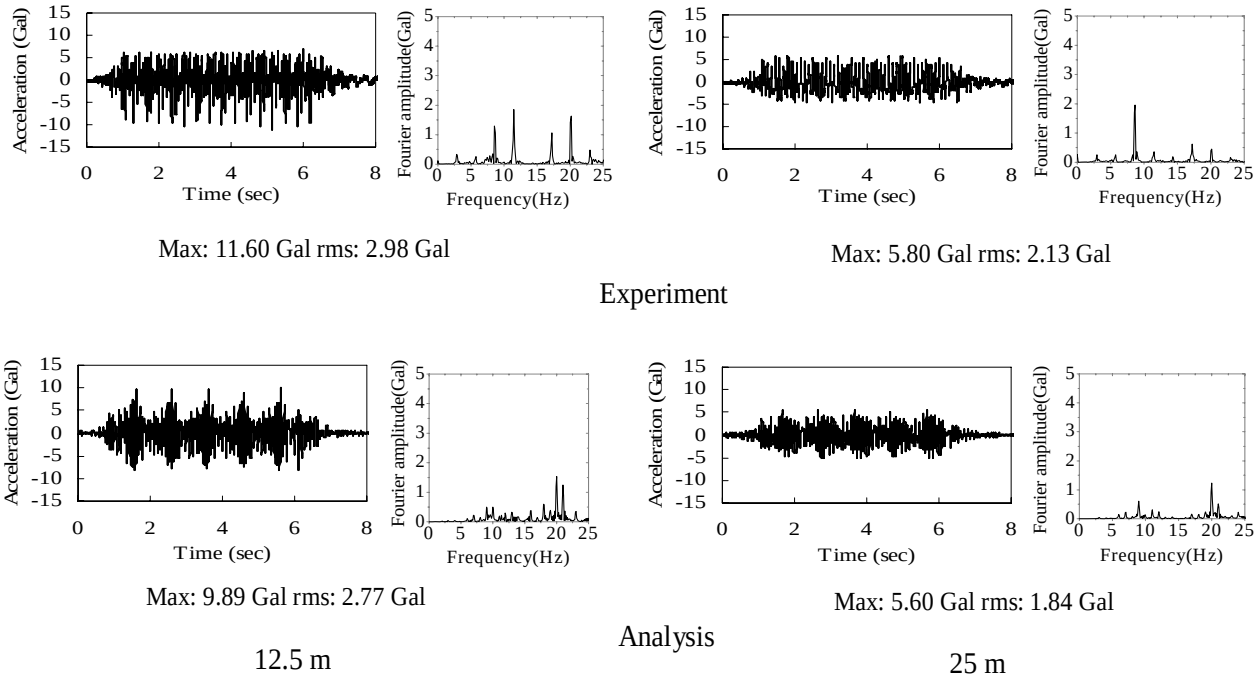

Fig. 4.6.5 Acceleration of ground (horizontal)

4.7 Conclusions

In this chapter, an approach to simulate site vibration around the viaducts of the high-speed railway is established. In this approach, the dynamic interactions between the train and track and between the foundation and ground are simultaneously considered. The entire train-bridge-ground interaction system is divided into two subsystems: train-bridge interaction and foundation-ground interaction. In the stage of the train-bridge interaction problem, the dynamic responses of viaducts are simulated to obtain the dynamic reaction forces at the pier bottoms. Then, applying those reaction forces as input excitation forces in the foundation-ground interaction problem, the site vibration around the viaducts is simulated using a general-purpose program named SASSI2000.

Based on the actual ground properties measured in field test, the site around the viaducts is modeled as layer elements down to the depth of which the structural model is embedded. The substructures of the viaducts including footings and piles are modeled with 3-D solid elements and beam elements. The reaction forces at the pier bottoms obtained in Chapter 3 are used as external excitations and inputted on the footing surfaces. Validity of the program SASSI2000 is examined by comparing the transfer function of the ground surface computed by SASSI2000 with the exact analytical solution given in reference. Then the site vibration around the viaducts is simulated by exciting each set of structural model and the final responses are obtained by means of superposition method.

In spite of the complicated nature of the whole train-bridge-ground interaction system and the approximations or assumptions that have to be made in modeling the system, the analytical acceleration responses can reproduce the main tendencies of the actual ones. The amplitudes of the analytical results are considerably coincident with the experimental ones. The components of the Fourier spectra of the analytical results to a certain extent re-create the experimental ones. Noticeable fact is observed as that in evaluating the overall tendencies of the site vibration it is sufficient to excite the footings only on the side of train running, which can lead to a saving of computational cost. It is found that due to the interference phenomenon of waves, the responses of the points that are shifted even a little to each other may differ significantly. The influence of damping constant of the ground is also investigated through analyses. The site vibration under different train velocity is also simulated and evaluated. The vibration levels of the site responses are also estimated. The effect of countermeasures against predominant bridge vibration on reduction of the environmental vibration is confirmed. At last, the horizontal site vibration analysis taking advantage of the 15-DOF train model is also carried out.

References

[1] Fujikake, T. A.: A prediction method for the propagation of ground vibration from railway trains, *Journal of Sound and Vibration*, Vol. 111, Issue 2, pp.289–297, 1986.

[2] Takemiya, H.: Simulation of track-ground vibrations due to a high-speed train: the case of X-2000 at ledsgard, *Journal of Sound and Vibration*, Vol. 261, Issue 3, pp.503–526, 2003.

[3] Yang, Y. B., Hung, H. H. and Chang, D. W.: Train-induced wave propagation in layered soils using finite/infinite element simulation, *Soil Dynamics and Earthquake Engineering*, Vol. 23, No. 4, pp.263–278, 2003.

[4] Xia, H., Cao, Y. M., Zhang, N. and Qu, J. J.: Vibration effects of light-rail train-viaduct system on surrounding environment, *International Journal of Structural Stability and Dynamics*, Vol. 2, No. 2, pp.227–240, 2002.

[5] Wu, Y. S., Hsu, L. C. and Yang, Y. B.: Ground vibrations induced by trains moving over series of elevated bridge, *Proc. of the 10th Sound and Vibration Conference*, Taipei, Taiwan, pp.1–7, 2002.

[6] Wu, Y. S. and Yang, Y. B.: A semi-analytical approach for analyzing ground vibrations caused by trains moving over elevated bridges, *International Journal of Soil Dynamics and Earthquake Engineering*, Vol. 24, Issue 12, pp. 949-962 2004.

[7] Yoshioka, O. and Ashiya, K.: Dependence of Shinkansen-induced ground vibration upon their influence factors, *QR of RTRI*, Vol. 29, No. 4, pp.176–183, 1988.

[8] Yoshioka, O.: A Dynamic Model for Generation and Propagation of Shinkansen-Induced Ground Vibrations and Its Applications to Vibration Reduction Measures, *RTRI Report*, Special No.30, Oct. 1999. (*in Japanese*)

[9] Hara, T., Yoshioka, O., Kanda, H., Funabashi, H., Negishi, H., Fujino, Y. and Yoshida K.: Development of a new method to reduce Shinkansen-induced wayside vibrations applicable to rigid frame bridges: bridge-end reinforcing method, *Journal of Structural and Earthquake Engineering (Doboku Gakkai Ronbunshuu A)*, JSCE, Vol. 68, No. 766, pp.325-338, July 2004. (*in Japanese*)

[10] Yoshida, K. and Seiki, M.: Influence of improved rigidity in railway viaducts on the environmental ground vibration, *Journal of Structural Engineering*, JSCE, Vol. 50A, pp. 403-412, 2004. (*in Japanese*)

[11] Kawatani, M., He, X., Sobukawa, R., Masaki, S., Nishiyama, S. and Sasakawa, T.: Analysis of Site Vibration around Shinkansen Viaducts due to Running Trains, Proc. of Annual Conference of Civil Engineers 2004, JSCE Kansai Chapter, I-73, May 2004. (*in Japanese*)

[12] Kawatani, M., He, X., Sobukawa, R., Masaki, S., Nishiyama, S. and Sasakawa, T.:

Evaluation on Ground Vibration around Shinkansen Viaducts due to Running Trains, Proceedings of the 59th Annual Conference of the Japan Society of Civil Engineers, I-431, Sep., 2004. (*in Japanese*)

[13] Kawatani, M., He, X., Yoshida, K., Sobukawa, R., Nishiyama, S. and Yamaguchi, S.: Countermeasures on Reducing Ground Vibration around Shinkansen Viaducts by means of Stiffening Rail Structure, Proc. of Annual Conference of Civil Engineers 2005, JSCE Kansai Chapter, I-35, May 2005. (*in Japanese*)

[14] Kawatani, M., Yoshida, K., He, X., Sobukawa, R. and Yamaguchi, S.: Analytical Evaluation of Effect on Reducing Site Vibration around Shinkansen Viaducts by Reinforcing Hanging Parts of Bridges, Proceedings of the 60th Annual Conference of the Japan Society of Civil Engineers, I-562, Sep., 2005. (*in Japanese*)

[15] Kawatani, M., He, X., Yoshida, K., Yamaguchi, S. and Nishiyama, S.: Soundness Investigation of Shinkansen Viaducts by means of analysis on ambient site vibration caused by bullet trains, Proc. of Annual Conference of Civil Engineers 2006, JSCE Kansai Chapter, I-65, Jun., 2005. (*in Japanese*)

[16] He, X., Kawatani, M., Yamaguchi, S. and Nishiyama, S.: Evaluation of Site Vibration around Shinkansen Viaducts under Bullet Train, Proc. of 2nd International Symposium on Environmental Vibrations (ISEV2005), Okayama, Japan, Sep. 20-22, 2005.

[17] Lysmer, J., Ostadan, F. and Chin, C.C.: SASSI2000 user's manual – A system for analysis of soil-structure interaction, Academic Version, University of California, Berkeley, 1999.

[18] Architectural Institute of Japan: An Introduction to Dynamic Soil-structure Interaction, 1996.4. (In Japanese)

[19] Lysmer, J. and Drake, J.A.: A finite element method for seismology, Method in Computational Physics, 198, Aca-demic Press Inc., 1972.

[20] Shimizu, N., Yamamoto, S., Koori, Y. and Minowa, N.: Three-dimensional dynamic analysis of soil-structure system by thin layer element method (Part 1. Outline of analysis method and formulation of layered zone), Trans. of A. I. J., No. 253, 1977.

[21] Shimizu, N., Yamamoto, S., Koori, Y. and Minowa, N.: Three-dimensional dynamic analysis of soil-structure system by thin layer element method (Part 2. Formulation of irregular zone and energy transmitting boundary), Trans. of A. I. J., No. 254, 1977.

[22] Yang, Y. B., Hung, H. H. and Chang, D. W.: Train-induced wave propagation in layered soils using finite/infinite element simulation, Soil Dynamics and Earthquake Engineering, Vol. 23, No. 4, pp.263–278, 2003.

[23] Chin, C.C.: Substructure subtraction method and dynamic analysis of pile foundations, Ph.D. Dissertation, University of California, Berkeley, 1998.

[24] Lysmer, J.: Analytical procedures in soil dynamics, Report No. EERC 78/29, Earthquake Engineering Research Center, University of California, Berkeley, Dec., 1978.

[25] Waas, G.: Earth vibration effects and abatement for military facilities – analysis method for footing vibrations through layered media, Technical Report 5-71-14, U.S. Army Engineer Waterways Experimental Station, Vicksburg, Mississippi, Sep., 1972.

[26] Lysmer, J., Ostadan, F. and Chin, C.C.: SASSI2000 theoretical manual – A system for analysis of soil-structure inter-action, Academic Version, University of California, Berkeley, 1999.

[27] Zienkiewicz, O.C., (1997): The Finite Element Method, 3rd edition, (McGraw-Hill).

[28] Lysmer, J. and Kuhlemeyer, R. L.: Finite dynamic model for infinite media, Journal of Engineering Mechanics Division, ASCE, Vol. 95, No. EM44, 859-877, 1969.

[29] Masanori SAITO: Branch Line Contribution in Lamb's Problem, BUTSURI- TANSA, Vol. 46 No. 5, pp. 372-380, 1993.

Chapter 5

Seismic performance of bridge-train interaction system

5.1 Introduction

After the Kobe earthquake and this Niigata earthquake, it came to be recognized that a high possibility exists to encounter an earthquake during rush hour. Therefore, it has become increasingly important to investigate and evaluate dynamic responses of bullet trains running on bridges under earthquake to ensure the train system's running safety. Nevertheless, discussion of the running safety of bullet trains on viaducts under Level-2 (L2) earthquake motion (earthquakes with low probability of occurrence during the service life of the structure, but which strike with high intensity) is not prescribed because of the complicated nature of its phenomenon, whereas that is designated for Level-1 (L1) earthquake motion (an earthquake of moderate intensity with recurrence probability of a few times during the service life of the structure) in the design standards for railway structures. Even without the danger of derailment, it is still necessary to evaluate the running characteristics and riding serviceability of the bullet train during an earthquake.

In both the Kobe earthquake and the Niigata earthquake, the bridge structures, especially the piers, were damaged severely over large distances. Although the live load of trains is considered in the Seismic Design Code for Railway Structuresin Japan, the trains are merely attached as an additional mass to the bridge structure. Nevertheless, it is not rational to treat the train merely as an additional mass because the train is a complicated dynamic system. To satisfy both safety and economy demands in seismic design, the dynamic effect of trains on the bridge structures subjected to ground motion should be investigated further. Therefore, a reliable and effective analytical procedure to simulate the dynamic response of the high-speed railway bridge-train-earthquake interaction system is expected.

In this chapter, an analytical approach to simulate bridge-train-earthquake interaction is established [1] [2], in which the bridge-train interaction models established previously are also conveniently used. The ground motions defined in seismic design codes and also actual measured ones downloaded from the Kyoshin Network (K-NET) of National Research Institute for Earth Science and Disaster prevention in Japan (NIED) are adopted as the seismic load. Newmark's β-method is also adopted here to solve the coupled differential equations of the bridge-train-earthquake interaction system. The accuracy of the seismic analysis algorithm is validated in comparison with a general program named MIDAS. The dynamic responses of

the bridge and the train are then simulated and evaluated. The seismic performance of the bridge is investigated by examining the cross-sectional forces of the pier with respect to the strength limits. To examine the running safety of the bullet train, the derailment coefficient defined as the lateral wheel load to the vertical one is simulated and examined.

To simulate the seismic performance of the bridge-train system subjected to violent earthquakes, it is necessary to establish the non-linear models of the bridge as well as the train, and the interaction between the bridge and train become extremely complicated. In this study, based on the results in the development of the linear bridge-train-earthquake interaction analysis, preparations to simulate the seismic performance of bridge-train system subjected to strong ground motion are also undertaken. The progress of the development is also introduced here.

5.2 Analytical models

5.2.1 Bridge model

The same bridge model used in Chapter 3 as shown in **Fig. 5.2.1** is also used in this study. Considering the ground motions are relatively weak, the damping constant of 0.03 is assumed for the first and second natural modes of the structure due to experimental results. The damping constant of 0.05 is also used to do comparison. The rail structure is also modeled as beam elements as the same in Chapter 3.

5.2.2 Train model

Figure 5.2.2 shows one car of the bullet train that is modeled as a 15-DOF system, assuming that the car body and the bogies are rigid bodies and that they are connected three-dimensionally by scalar spring and damper elements. In this train model, the sway, bouncing, pitching, rolling and yawing motions of the car body, and the sway, parallel hop, axle windup, axle tramp and yawing motions of the front and rear bogies are taken into account. In this stage of the study, assuming that the relative motion between the wheel and the track is small under a moderate earthquake, the motion of the wheel set is attached to the rail structure, considering the effect of rail surface roughness. The dimension and the dynamic properties of the moving train are shown in **Table 5.2.1** and **Table 5.2.2.**

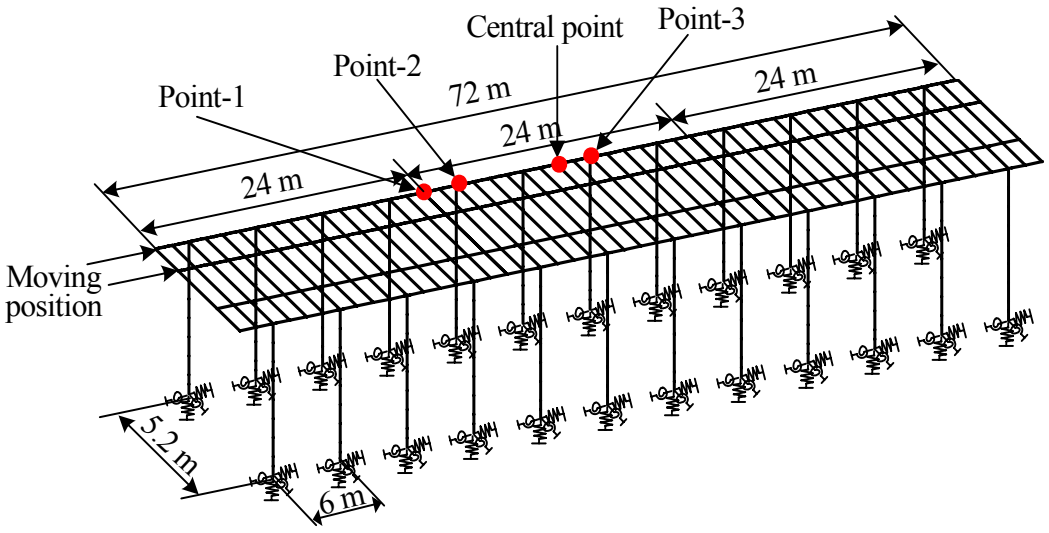

Fig. 5.2.1 Analytical model of the bridge (3-block model)

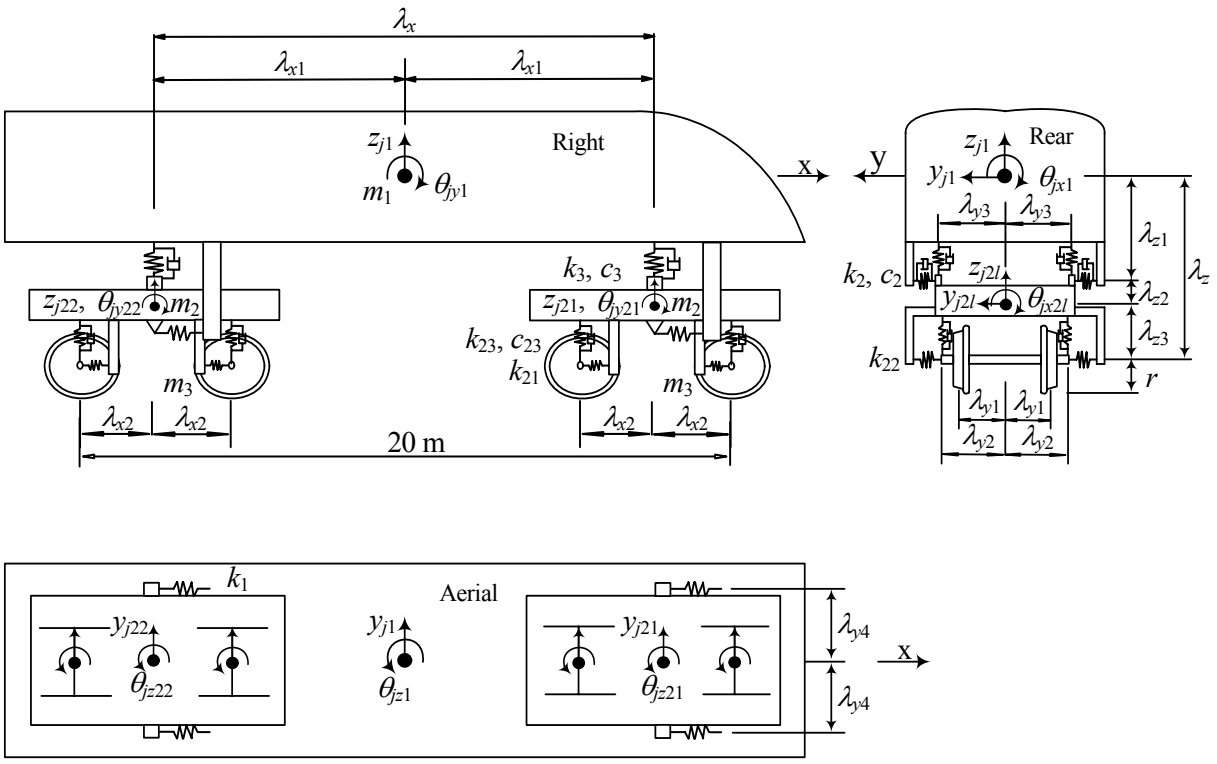

Fig. 5.2.2 15-DOF train model

Table 5.2.1 Dimension of bullet train

1/2 length of car body in x-direction	λ_c	12.50 m
Distance of centers of bogies in x-direction	λ_x	17.50 m
1/2 distance of centers of bogies in x-direction	λ_{x1}	8.75 m
1/2 distance of axes in x-direction	λ_{x2}	1.25 m
1/2 width of track gauge	λ_{y1}	0.70 m
1/2 distance of vertical lower springs in y-direction	λ_{y2}	1.00 m
1/2 distance of vertical upper springs in y-direction	λ_{y3}	1.23 m
1/2 distance of longitudinal upper springs in y-direction	λ_{y4}	1.42 m
Distance from centroid of body to axis in z-direction	λ_z	0.97 m
Distance from centroid of body to lateral upper spring in z-direction	λ_{z1}	0.50 m
Distance from centroid of bogie to lateral upper spring in z-direction	λ_{z2}	0.37 m
Distance from centroid of bogie to lateral lower spring in z-direction	λ_{z3}	0.10 m
Radius of wheel	r	0.43 m

Table 5.2.2 Properties of bullet train

Definition		Notation	Value
Weight	car body	w_1	321.616 kN
	bogie	w_2	25.862 kN
	wheelset	w_3	17.689 kN
Mass moment of inertia	car body	I_{x1}	49.248 kN·s^2·m
		I_{y1}	2512.628 kN·s^2·m
		I_{z1}	2512.628 kN·s^2·m
	bogie	I_{x2}	2.909 kN·s^2·m
		I_{y2}	4.123 kN·s^2·m
		I_{z2}	4.123 kN·s^2·m
	wheelset	I_{x3}	0.885 kN·s^2·m
		I_{z3}	0.885 kN·s^2·m
Spring constant	upper	k_1	5000.0 kN/m
		k_2	176.4 kN/m
		k_3	443.0 kN/m
	lower	k_{21}	17500.0 kN/m
		k_{22}	4704.0 kN/m
		k_{23}	1209.81 kN/m
Damping coefficient	lateral upper	c_2	39.2 kN/m
	vertical upper	c_3	21.6 kN/m
	vertical lower	c_{23}	19.6 kN/m

5.2.3 Natural modes and frequencies of train

Eigenvalue analysis of the car model is carried out and the total 15 modes and frequencies of the train are shown as follows. From the modes of the car, it can be seen that the natural frequencies of the bogies are much higher than those of the car body, which again proved the importance of the motions of the bogies.

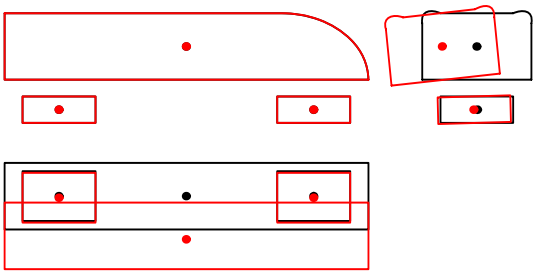

1st (0.811 Hz)
Sway and rolling of car body

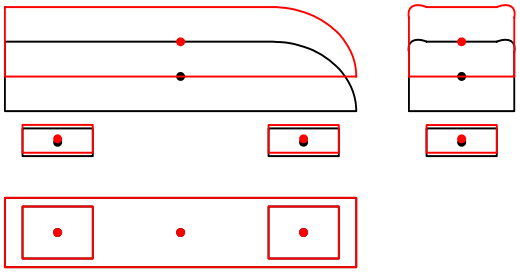

2nd (1.073 Hz)
Bouncing of car body

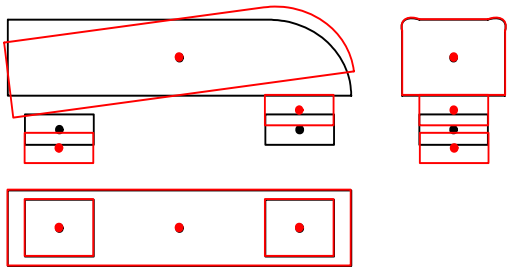

3rd (1.073 Hz)
Rolling of car body
and bouncing of bigies

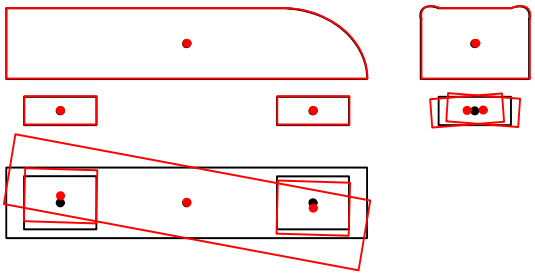

4th (1.169 Hz)
Yawing of car body
And rolling of bogies

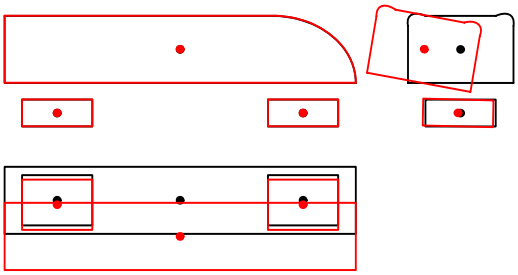

5th (1.304 Hz)
Rolling and sway of car body

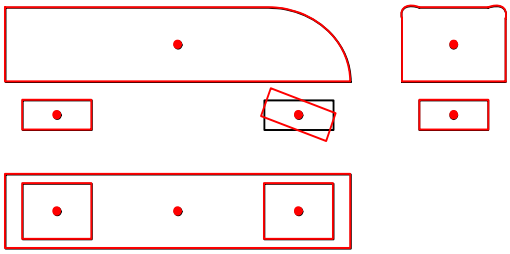

6th (6.816 Hz)
Pitching of bogie

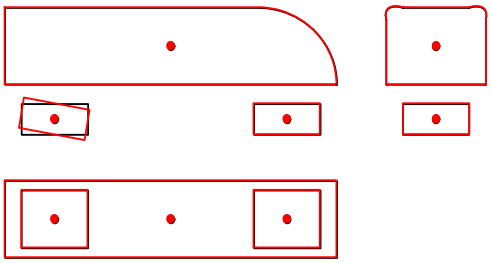

7th (6.816 Hz)-Pitching of bogie

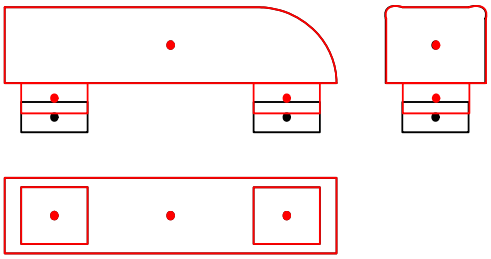

8th (7.428 Hz)-Bouncing of bogies

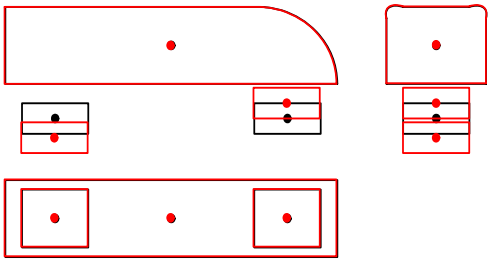

9th (7.428 Hz)-Bouncing of bogies

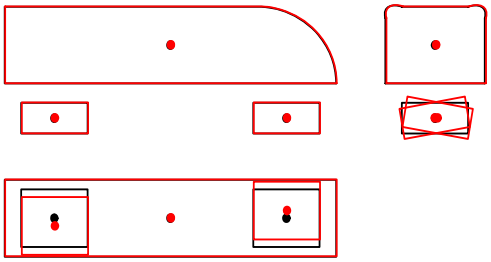

10th (7.670 Hz)-Rolling of bogies

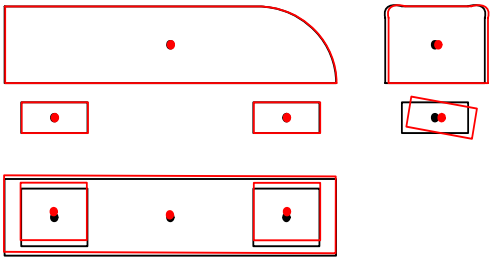

11th (7.684 Hz)-Rolling of bogies

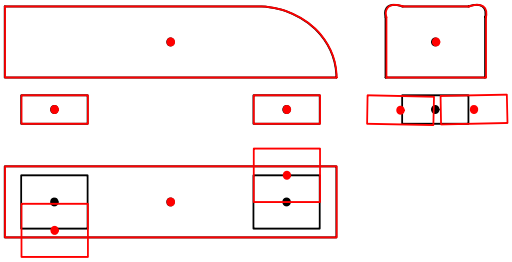

12th (13.752 Hz)-Rolling of bogies

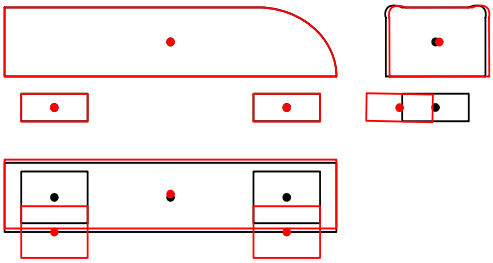

13th (13.753 Hz)-Sway of bogies

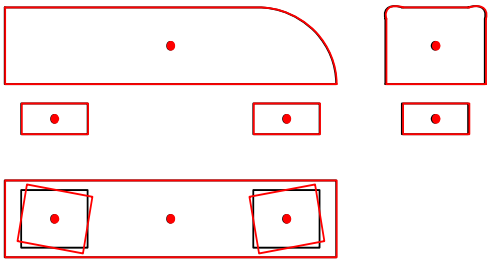

14th (27.904 Hz)-Yawing of bogies

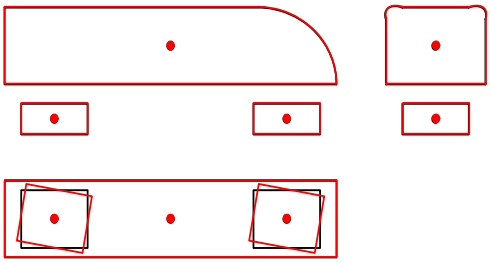

15th (27.905 Hz)-Yawing of bogies

Fig. 5.2.3 Modes and frequencies of 15-DOF train model

5.2.4 Adopted ground motions

Firstly, the Level 1 ground motion defined in "Standard Specifications for Concrete Structures (Seismic Performance Verification)" of JSCE [3], shown in **Fig. 5.2.4**, is adopted as the seismic load. Though total ground acceleration data of 80 seconds are supplied in this record, only the first 40 seconds of data are adopted in this analysis since the ground motion decreases after 40 seconds. The effects of the earthquake motion types referring to different ground conditions are not considered in this case.

Four actual measured moderate ground motions with different frequency components downloaded from the Kyoshin Network (K-NET) of National Research Institute for Earth Science and Disaster Prevention in Japan (NIED) [4], as shown in **Fig. 5.2.5**, are also adopted as the seismic loads. Ground motions 1 and 3 were recorded at Hobetsu, Yuuhutsu, Hokkaido on Sept. 26, 2003; Ground motion 2, Sakae, Saga, Saga Prefecture on Mar. 20, 2005, Ground motion 4, Shinyashiki, Okayama, Okayama on March 20, 2005. The designations of EW or NS and UD in the figures respectively indicate data channels of East-West or North-South and Up-Down directions.

For the seismic response spectra, the period of 0.455 s indicates the first horizontal natural period of the bridge, whereas that of 0.932 s is the bouncing natural period of the car body. As shown in **Fig. 5.2.5** although the maximum amplitudes of EW or NS (Horizontal direction) components of these ground motions are of a similar magnitude, the seismic response spectra of these four ground motions differ greatly. Especially for the UD component, Ground motion 1 has much smaller amplitude than Ground motion 2, but indicates a much larger value at the predominant period of the car body in the seismic response spectrum. Although total ground acceleration data of more than 100 s are supplied in these records, only 30 s of data are adopted in the analysis, considering the peak values of the motions.

As a criterion for selection of the ground motions, the ground properties of the measured points are chosen to be as similar as the actual ones under the viaducts. For the viaducts adopted in this analysis, the ground condition is inferior and is classified as G4 soil, which has the natural period of 0.5–0.75 s in surface ground and is defined as dense to soft soil in the Seismic Design Code for Railway Structures [5]. The phase difference of ground motion is ignored in this analysis.

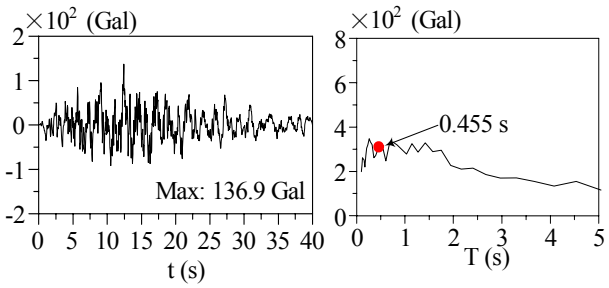

Fig. 5.2.4 Level1 ground motion

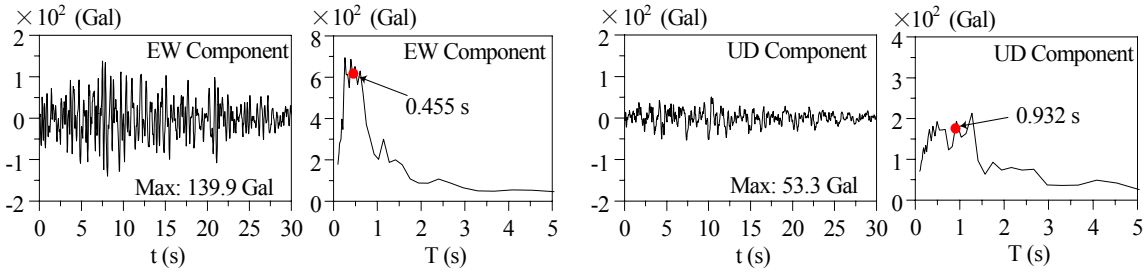

Ground motion 1

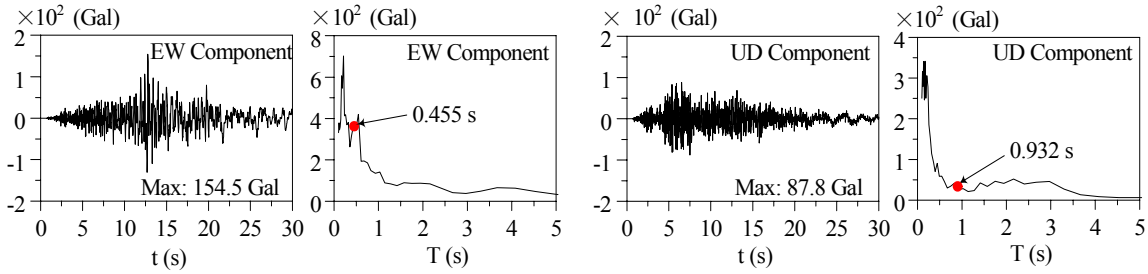

Ground motion 2

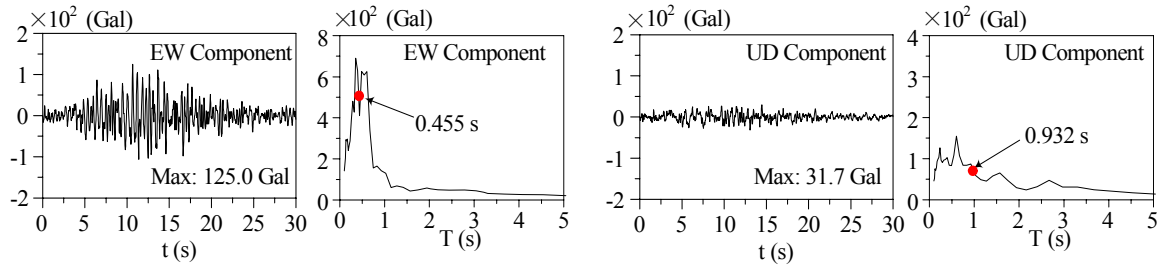

Ground motion 3

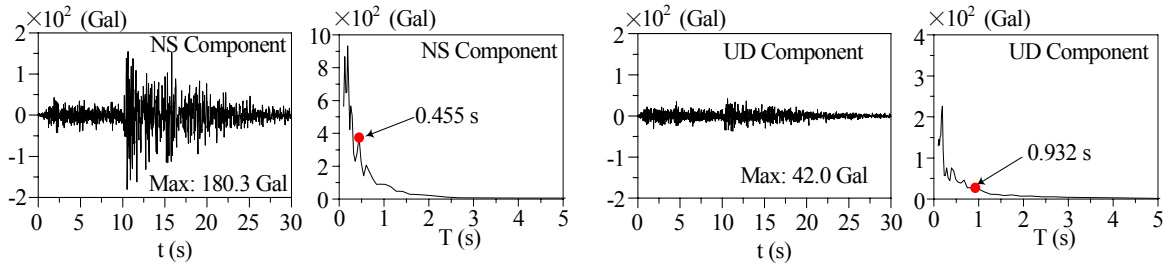

Ground motion 4

Fig. 5.2.5 Ground motions (Time history and seismic response spectrum)

5.3 Validation of seismic analysis algorithm

The developed seismic analysis algorithm is verified through comparison with the analytical results of the developed program and a general program named MIDAS. To simplify the analysis, the one-block bridge model shown in **Fig. 5.3.1**, in which the rail structure and the effect of ground spring are neglected, is employed. The eigenvalue analytical results of the developed program and the general program are compared in **Table 5.3.1**. Ground motion 2 is used as the seismic load. The EW and UD components of the ground motion are applied simultaneously. The dynamic acceleration responses in both directions of the examined point of the one-block bridge model indicated in **Fig. 5.3.1** are shown in **Fig. 5.3.2**. Both eigenvalues and the acceleration responses of the bridge show good coincidence of the developed program and the general program. Therefore, the validity of the seismic analysis algorithm can be demonstrated.

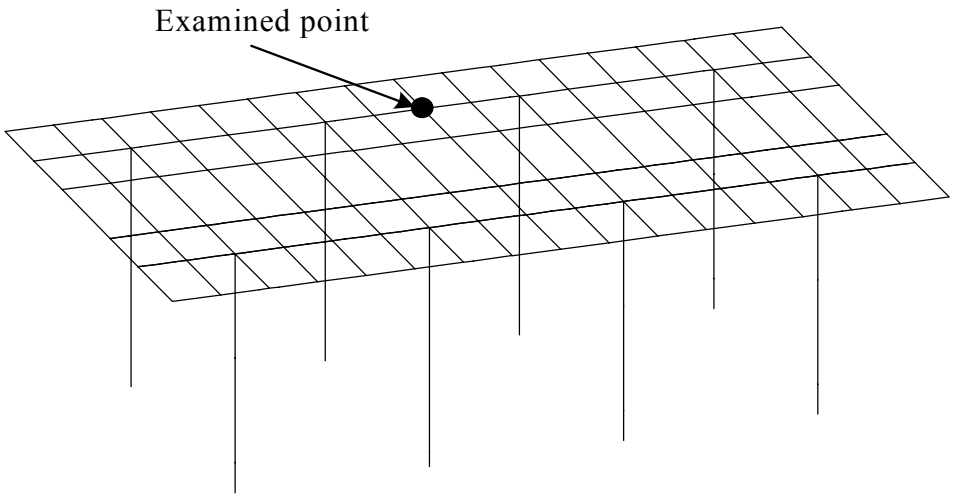

Fig. 5.3.1 One-block bridge model

Table 5 Eigenvalue analysis results

Mode No.	Frequency (Hz)		Mode No.	Frequency (Hz)	
	General program	Developed program		General program	Developed program
1	2.5362	2.5361	11	20.5450	20.5450
2	2.6362	2.6362	12	21.0001	20.9990
3	2.6626	2.6626	13	23.6505	23.6500
4	13.5977	13.5970	14	23.7205	23.7200
5	13.7933	13.7930	15	24.0413	24.0400
6	15.6291	15.6260	16	32.8912	32.8910
7	15.9561	15.9530	17	34.6777	34.6710
8	17.4441	17.4440	18	35.1380	35.1380
9	20.1617	20.1620	19	35.3290	35.3250
10	20.3215	20.3210	20	35.5419	35.5380

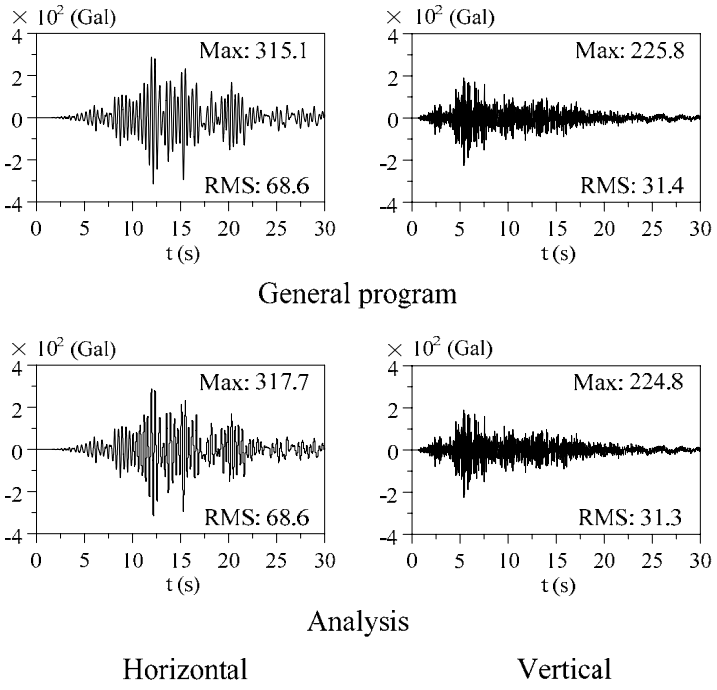

Fig. 5.3.2 Acceleration responses of examined point under Ground motion 2

5.4 Evaluation on seismic responses of bridge-train interaction system

In this section, employing the seismic analytical procedure of the bridge-train interaction system demonstrated in the preceding section, the dynamic response analyses are carried out using the analytical models and the ground motions described previously.

At first in the subsection 5.4.1, the seismic analysis of the bridge-train interaction system is conducted based on the actual operational conditions. Because of the limit of computational capacity, the 3-block bridge model has to be used. It is difficult currently to use more complicated structural model longer than the 3-block one. A train consist of actual number of cars are adopted for the analysis. However, the analytical results prove that it is difficult to fully consider the bridge-train interaction during the earthquake in such a case, because the train passes the 3-block bridge too rapidly.

In the subsequent subsections, in order to fully take account of the effect of ground motion on the responses of the bridge-train interaction system, a fictional running case is proposed. Then the seismic responses of the bridge as well as the train are evaluated for cases of Train running, Train standing and Train as mass. The influence of the excitation manner of the ground motion on the responses of the bridge-train interaction system is also investigated.

5.4.1 Effect of train velocities on seismic responses

The seismic analysis of the bridge-train interaction system is conducted based on the actual operational conditions. The ground acceleration defined in seismic design codes (**Fig. 5.2.4)** is used as seismic load. A train composed of 16 cars is assumed running through on the 3-block of bridges with the velocity of 270 km/h and 60 km/h under the ground motion. The seismic load is supposed only acting in the horizontal direction. Referring to the peak value of the ground motion, the train is set to enter the bridge at the 6th second after the seismic load starts.

The absolute acceleration responses in horizontal direction of Pint-1, Point-2 and Point-3 indicated in **Fig. 5.2.1** are shown in **Fig. 5.4.1**. The absolute acceleration responses of the train body of the second car are shown in **Fig. 5.4.2**. The parts between the dashed lines in **Fig. 5.4.1** indicate the responses of the observed points of the bridge during the period when the train is running on the bridge, and those in **Fig. 5.4.2** indicate the responses of the train body during the period when the second car is running on the bridge. As known from the comparison, the acceleration response of the bridge decreases with the speed-down, although the train passes through the 3-block of bridges within 7 seconds in the case of 270 km/h of

velocity while which is 28 seconds in the case of 60 km/h velocity. On the contrary, the body acceleration response of one car indicates no obvious difference in the two cases, if anything, the response of 60 km/h case to some extent shows lager amplitude and RMS value compared with that of 270 km/h case. The reason is considered as that one car passes through the bridge within 1 second in the 270 km/h case resulting that the interaction effect of the car and the bridge can not be adequately taken into account. So it is necessary to model the bridge long enough to discuss the runnability of the bullet train.

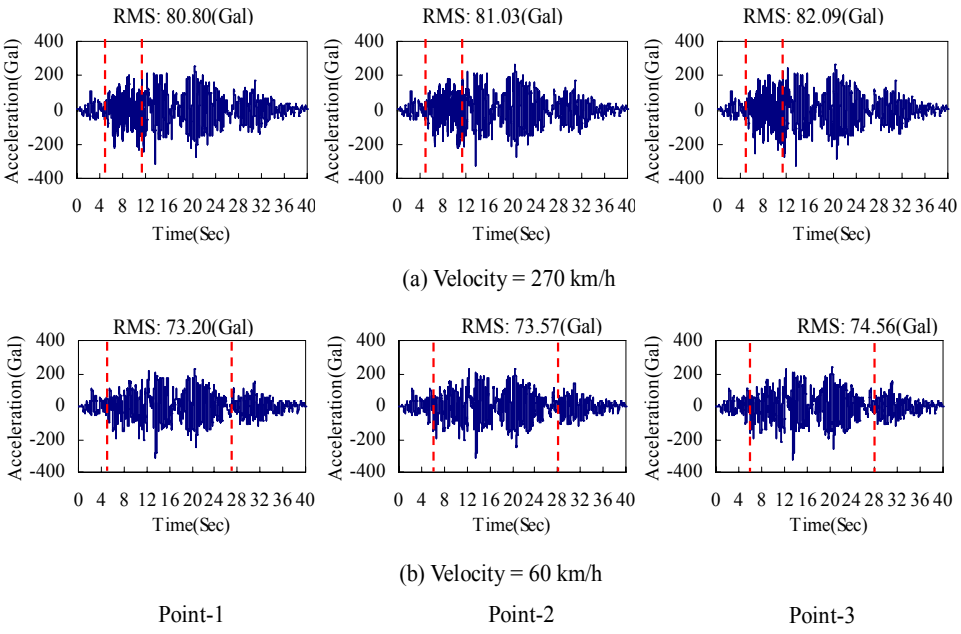

Fig. 5.4.1 Seismic responses of bridge

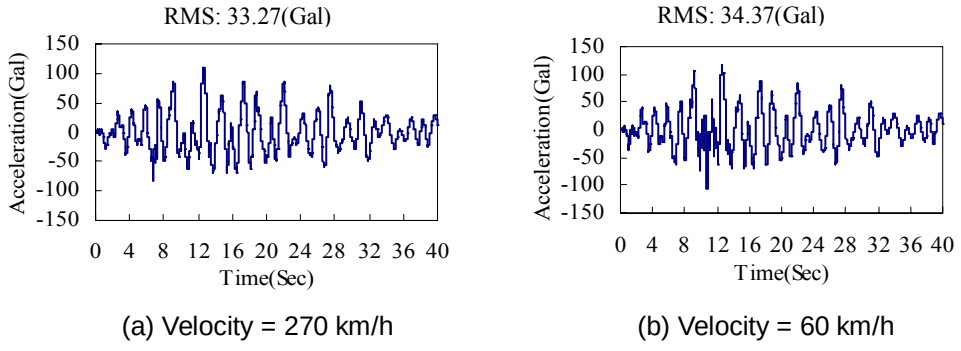

Fig. 5.4.2 Seismic responses of train body in the 2nd car

5.4.2 Evaluations on bridge response

In this subsection, to evaluate the dynamic responses of the bridge-train system fully considering their interaction, three cases are selected for seismic analyses. For all cases, both EW and UD components of Ground motions 1 and 2 are simultaneously applied.

Case 1: Considering the train as additional mass to the bridge model, just as used in seismic design codes. For the 3-block bridge model shown in **Fig. 5.2.1**, three cars of the train are presumed to stand on the middle of the bridge. Then, they are converted into mass and attached to the structural nodes at the wheel positions.

Case 2: Assuming the train as a vibrational system (15-DOF model) standing on the bridge. Similarly to Case 1, three cars are set standing on the 3-block bridge model at the same position in Case 1.

Case 3: The train is running through the bridge with the actual operation speed of 270 km/h. In this case, because its speed is very high, an actual train generally composed of 16 cars runs through the 3-block bridge model in a very short time. Therefore, it is difficult to evaluate the bridge-train interaction. Herein, to fully express the bridge-train interaction, the train is assumed to comprise an infinite number of cars that it can keep running on the bridge during the earthquake. One car runs through the bridge very quickly. Therefore, only the response of the car that is running on the middle block of the bridge will be evaluated. Consequently, the dynamic responses of the train shown in the results are actually the combination of those of all cars during the period that they are running through the bridge. To consider the initial train vibration, the train starting point is set as 75 m before the bridge.

Corresponding to the three cases described above, dynamic horizontal acceleration and displacement responses of the Central point of the bridge indicated in **Fig. 5.2.1** are respectively shown in **Fig. 5.4.3** and **Fig. 5.4.4**. Corresponding maximum and rms values are respectively shown in **Tables 5.4.1** and **5.4.2**. As described previously, because the seismic response spectra of the four ground motions are quite different, the dynamic response attributable to Ground motion 1 indicates the largest amplitude than others, while Ground motion 4 indicates the smallest one.

In the first three ground motions, for both acceleration and displacement responses, the case of Train-as-mass gives the largest maximum and root-mean-square (rms) values. This fact indicates that it might overestimate the seismic response of the bridge by considering the train as additional mass rather than as a vibration system. The train as a vibration system might act as a damper to the bridge during the earthquake. However for Ground motion 4, the largest maximum value appears in Train running. The reason can also be found in the seismic response spectra. The natural period of the bridge is predicted to increase somewhat due to the

additional mass of the train. Concurrently, the seismic response spectrum of Ground motion 4 decreases sharply with period increase, which lead to the apparent decrease of the dynamic responses. This phenomenon shows that the influence of the characteristics of the ground motion on the structural response is also important and should be fully considered. In such case, it may underestimate the dynamic response of the bridge and should be avoided in the seismic design codes.

For all ground motions, in the cases of Train-standing and Train-running, the dynamic responses of the bridge indicate little difference, but the responses of Train-running are larger than those of Train-standing. The reason can be attributed to the dynamic effect of the running train.

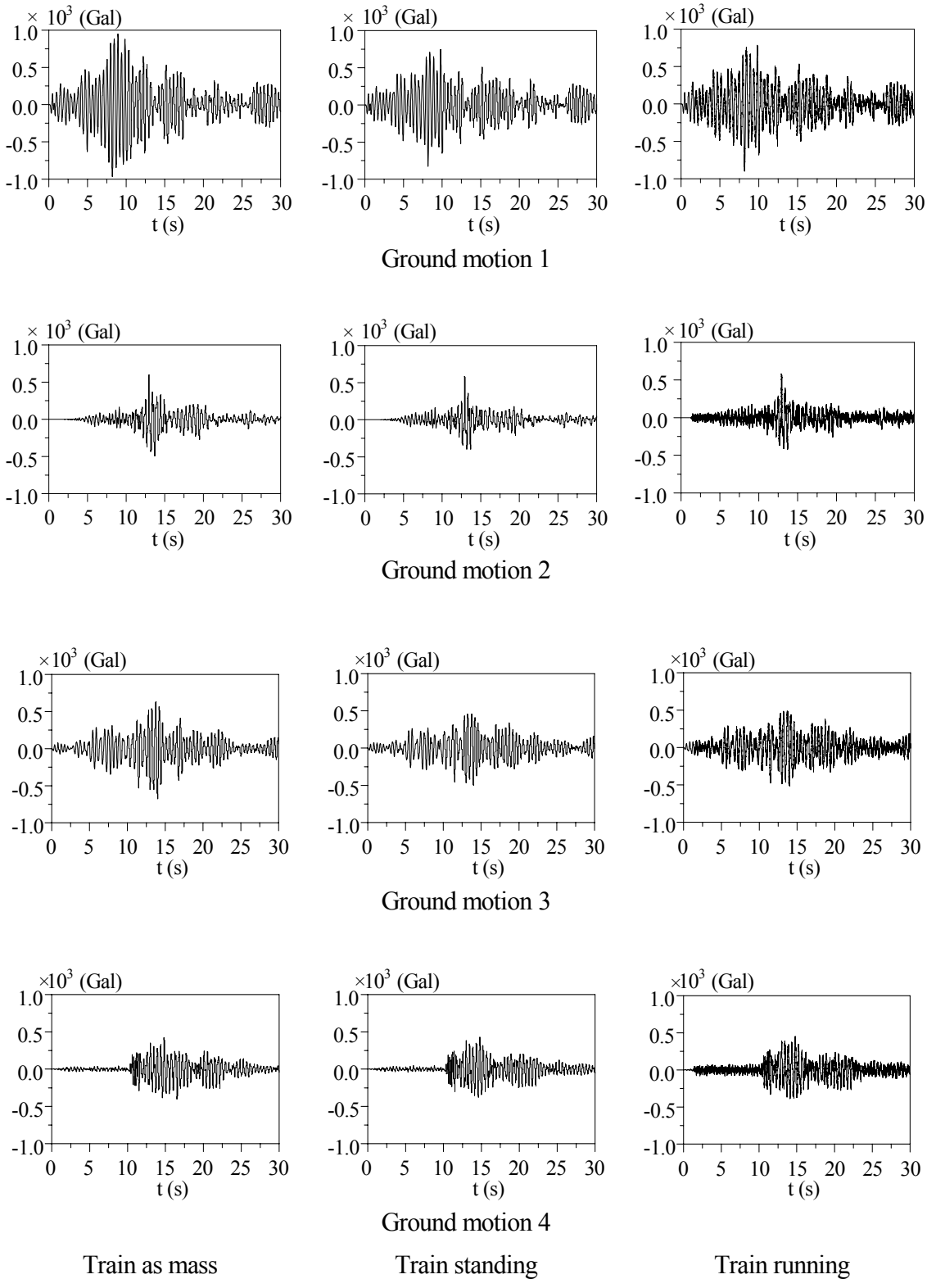

Fig. 5.4.3 Dynamic responses of bridge (horizontal acceleration)

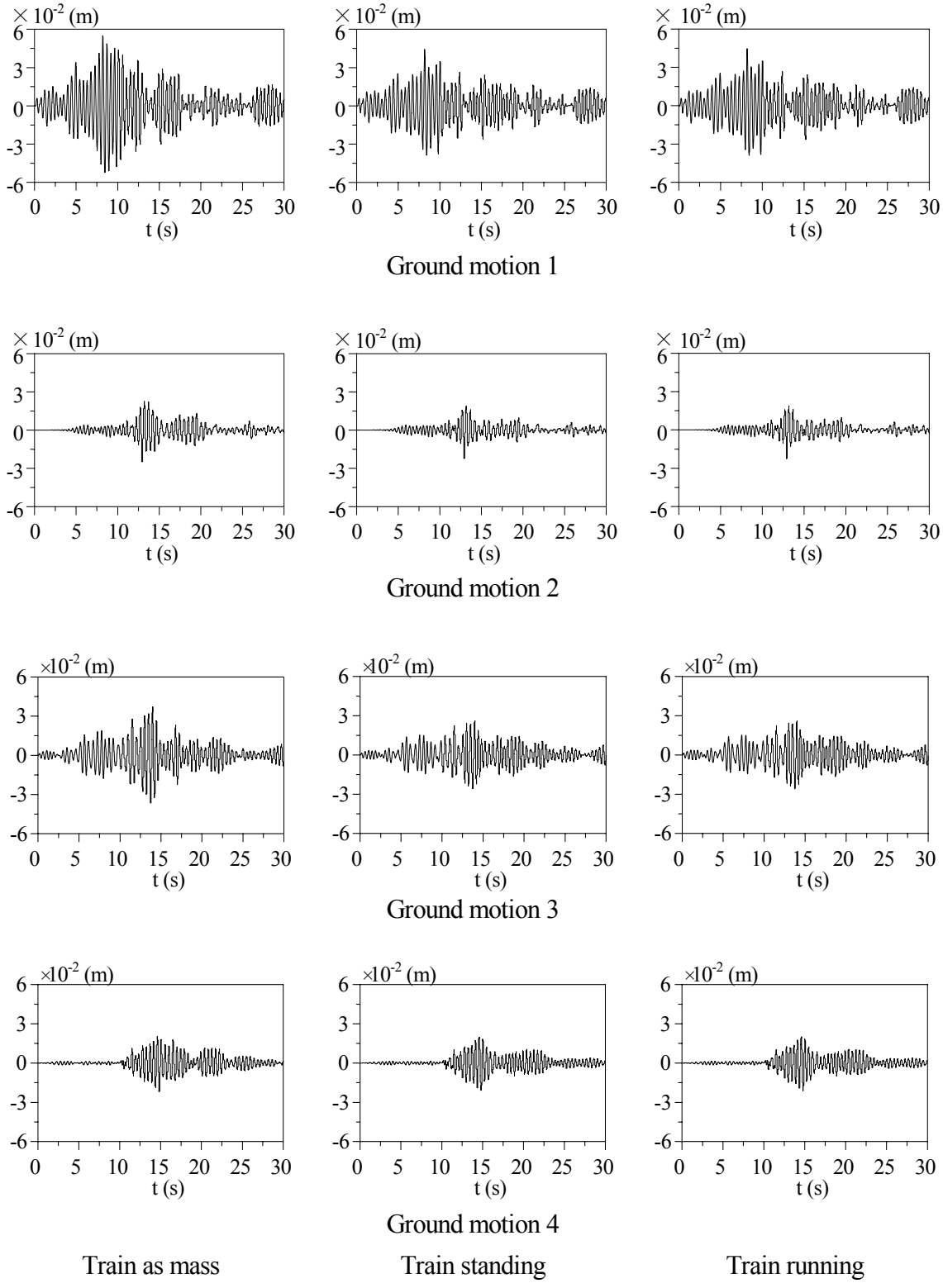

Fig. 5.4.4 Dynamic responses of bridge (horizontal displacement)

Table 5.4.1 Max and rms values of bridge acceleration (Gal)

Classification \ Case		Train as mass	Train standing	Train running
max	Ground motion 1	967.5	827.3	897.2
	Ground motion2	598.0	582.7	580.0
	Ground motion 3	675.7	502.2	512.2
	Ground motion 4	420.2	428.2	453.6
rms	Ground motion 1	275.7	218.4	221.8
	Ground motion2	92.7	78.0	80.0
	Ground motion 3	163.8	140.0	142.1
	Ground motion 4	102.8	99.6	101.8

Table 5.4.2 Max and rms values of bridge displacement (cm)

Classification \ Case		Train as mass	Train standing	Train running
max	Ground motion 1	5.491	4.428	4.460
	Ground motion2	2.481	2.235	2.240
	Ground motion 3	3.715	2.606	2.624
	Ground motion 4	2.180	2.082	2.105
rms	Ground motion 1	1.547	1.152	1.166
	Ground motion2	0.491	0.379	0.380
	Ground motion 3	0.920	0.737	0.743
	Ground motion 4	0.527	0.476	0.481

5.4.3 Seismic response of bullet train

Acceleration responses of the car body corresponding to the four ground motions in horizontal and vertical directions are shown respectively in **Fig. 5.4.6** and **Fig. 5.4.6**. Corresponding maximum and rms values are shown in **Table 5.4.3**. Herein, as described previously, the responses are the combination of those of all the cars running through the middle block of the bridge.

In agreement with the features of the seismic response spectra indicated in **Fig. 5.2.5**, the dynamic response of the car body caused by Ground motion 1 is much larger than those of others, just as that of the responses of the bridge. Dynamic responses of the case of Train-running are indicating somewhat larger rms values for all ground motions, which is considered due to the dynamic effect of the running train.

Table 5.4.3 Max and rms values of car body acceleration (Gal)

		Horizontal direction		Vertical direction	
Classification \ Case		Train standing	Train running	Train standing	Train running
max	Ground motion 1	361.0	374.2	108.7	106.4
	Ground motion2	158.8	156.2	21.5	25.9
	Ground motion 3	212.4	220.0	44.6	48.2
	Ground motion 4	151.7	157.8	19.0	21.5
rms	Ground motion 1	86.8	88.8	28.3	28.5
	Ground motion2	30.5	31.3	6.1	8.3
	Ground motion 3	55.1	56.6	12.1	13.1
	Ground motion 4	34.2	35.7	3.5	6.7

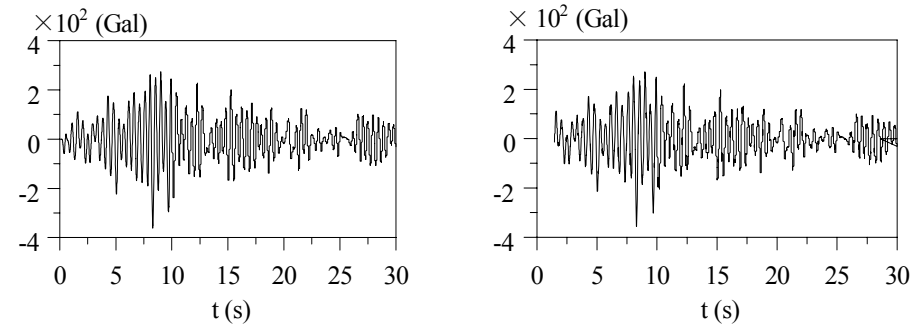

Ground motion 1

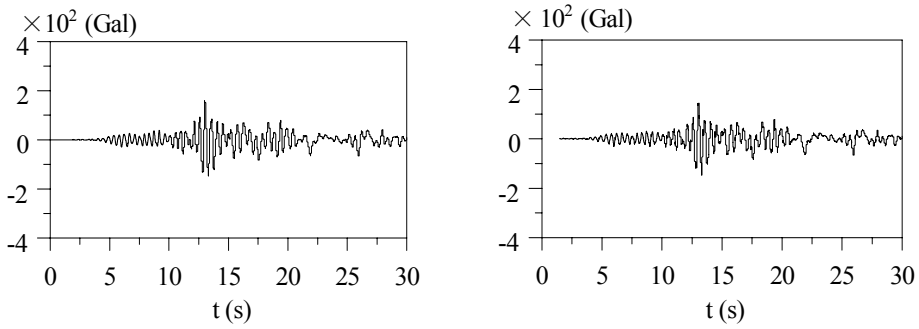

Ground motion 2

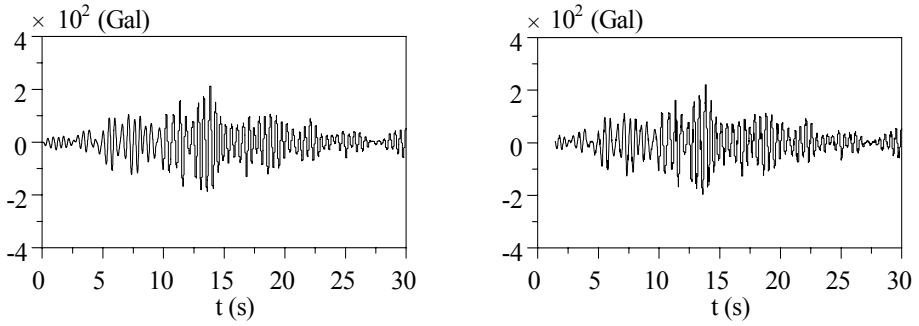

Ground motion 3

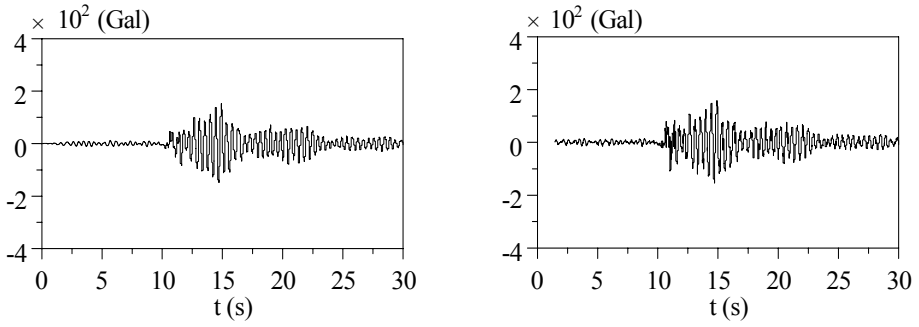

Ground motion 4

Train standing Train running

Fig. 5.4.5 Responses of car body (horizontal)

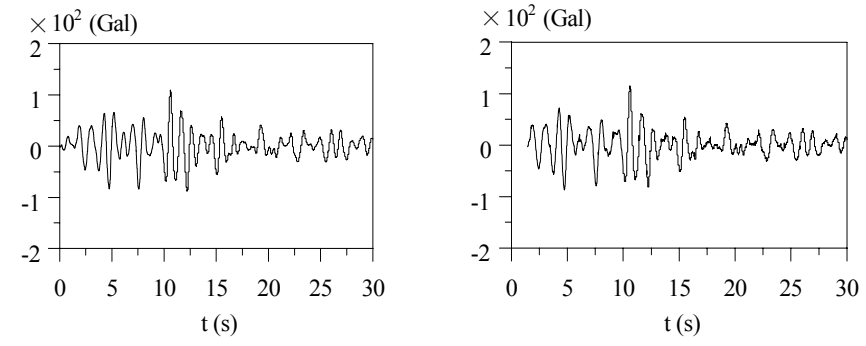

Ground motion 1

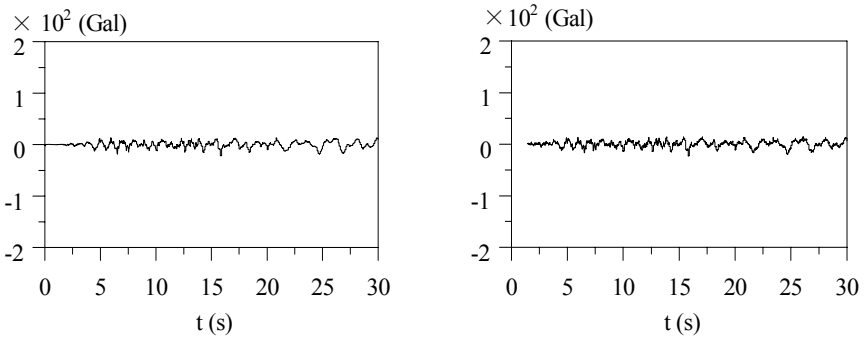

Ground motion 2

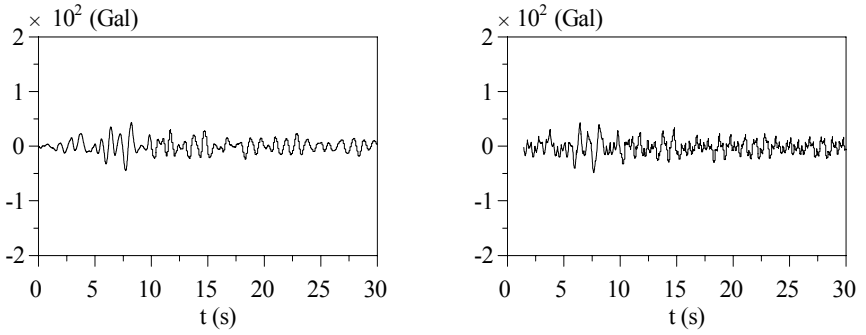

Ground motion 3

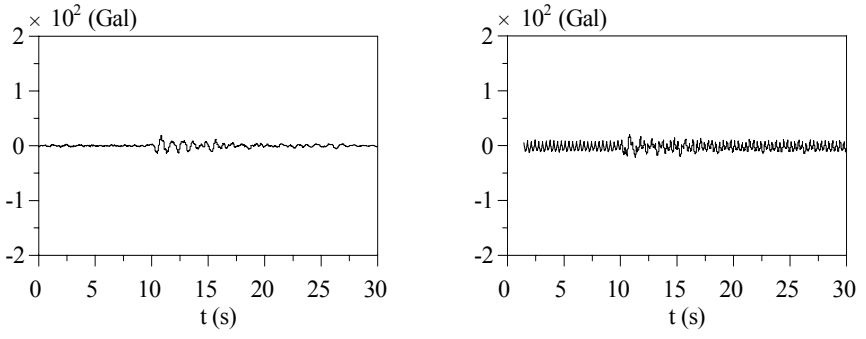

Ground motion 4

Train standing Train running

Fig. 5.4.6 Responses of car body (vertical)

5.4.4 Effect of UD component of ground motion

The effect of whether applying the UD component of the ground motion on the seismic responses of the bridge-train interaction system is investigated in this subsection. Here, the results only due to the case of Train standing are examined. Dynamic acceleration and displacement responses of the Central point of the bridge and the acceleration response of the car body all in horizontal direction are indicated **Figs. 5.4.7**, **5.4.8** and **5.4.9**. Corresponding maximum and rms values are respectively shown in **Table 5.4.4**.

From the results, no obvious differences between the two excitation manners are observed. This shows that in the case that the train stands motionlessly on the bridge, the earthquake motions of different directions do not affect corresponding dynamic responses distinctly. Further investigations should be made to examine the effect of excitation manners on the case of train running, in which the dynamic responses due to the bridge-train interaction itself exist and may be influenced by the UD component of the ground motion.

Table 5.4.4 Max and rms values of different excitation cases (Gal)

		Bridge acc. (Gal)		Bridge disp. (cm)		Car body acc. (Gal)	
Classification \ Direction excited		With UD	No UD	With UD	No UD	With UD	No UD
max	Ground motion 1	827.3	827.2	4.428	4.429	361.0	361.0
	Ground motion2	582.7	582.7	2.235	2.235	158.8	158.8
	Ground motion 3	502.2	502.2	2.606	2.606	212.4	212.4
	Ground motion 4	428.2	428.3	2.082	2.082	151.7	151.7
rms	Ground motion 1	218.4	218.5	1.152	1.152	86.8	86.8
	Ground motion2	78.0	78.0	0.379	0.379	30.5	30.5
	Ground motion 3	140.0	140.0	0.737	0.737	55.1	55.1
	Ground motion 4	99.6	99.6	0.476	0.477	34.2	34.2

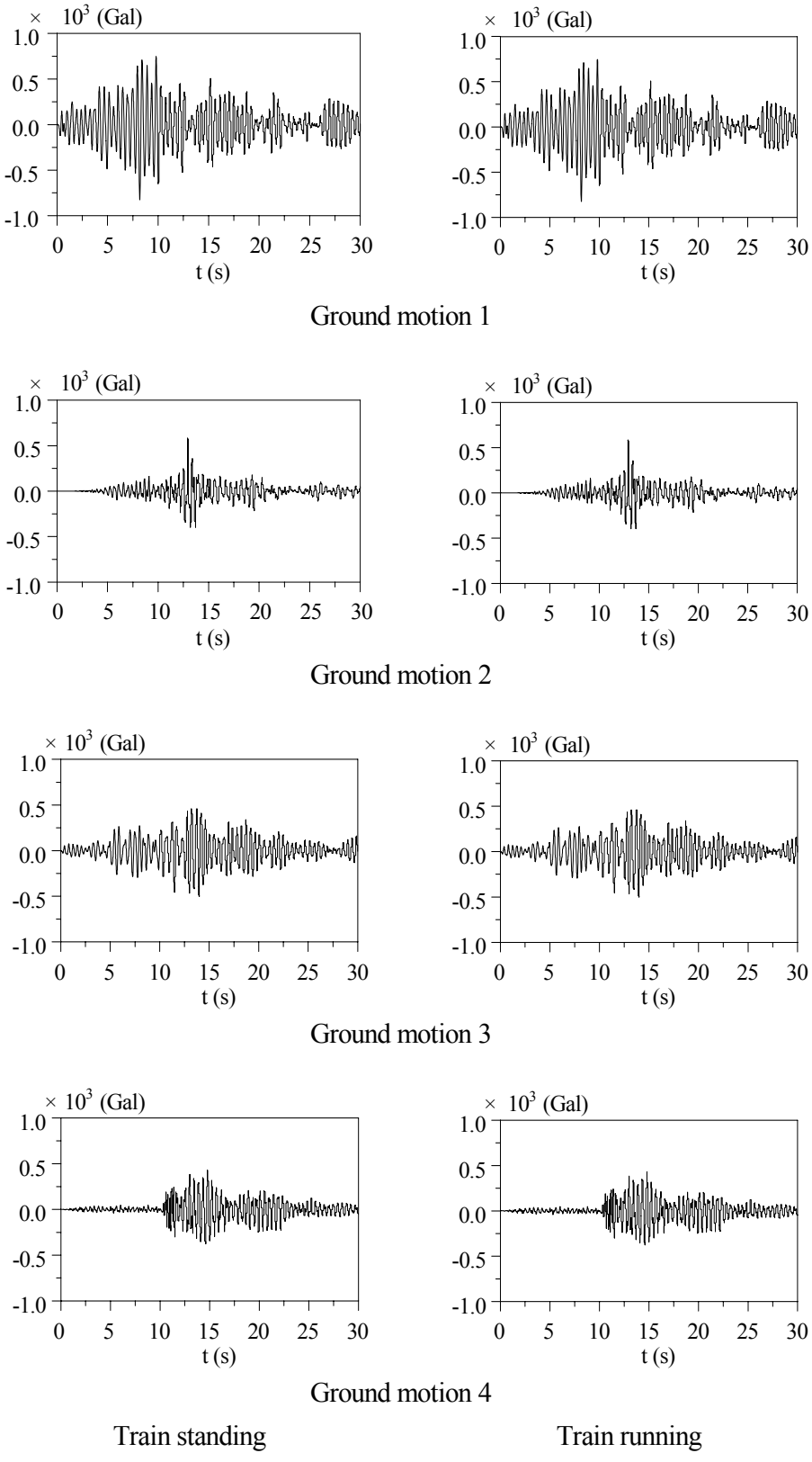

Fig. 5.4.7 Dynamic responses of bridge (horizontal acceleration)

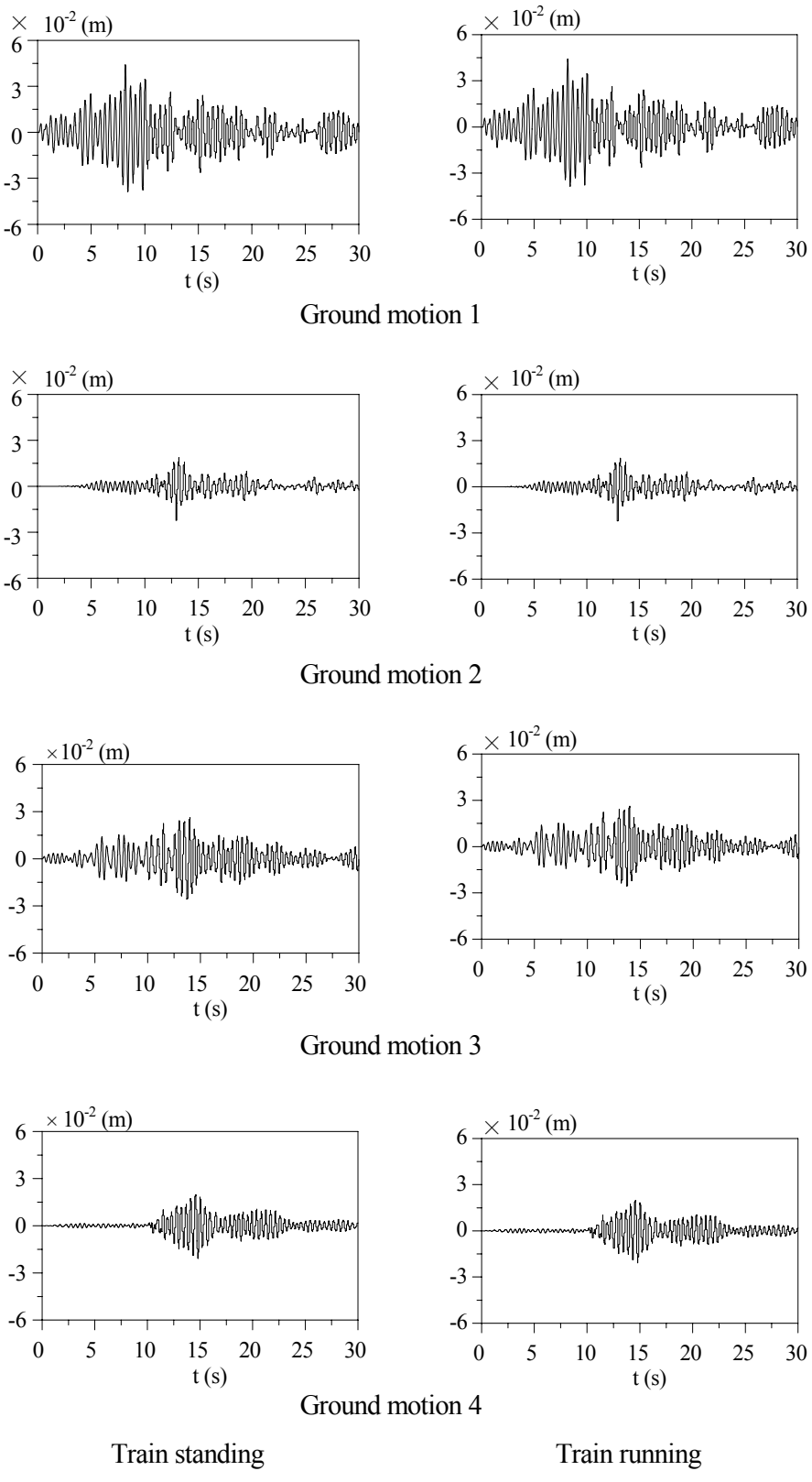

Fig. 5.4.8 Dynamic responses of bridge (horizontal displacement)

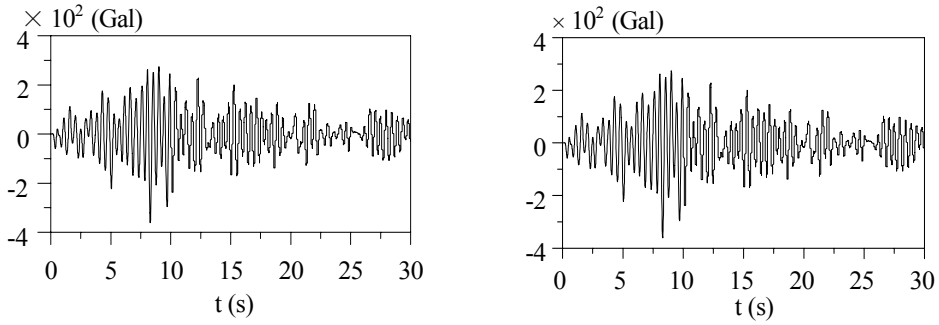

Ground motion 1

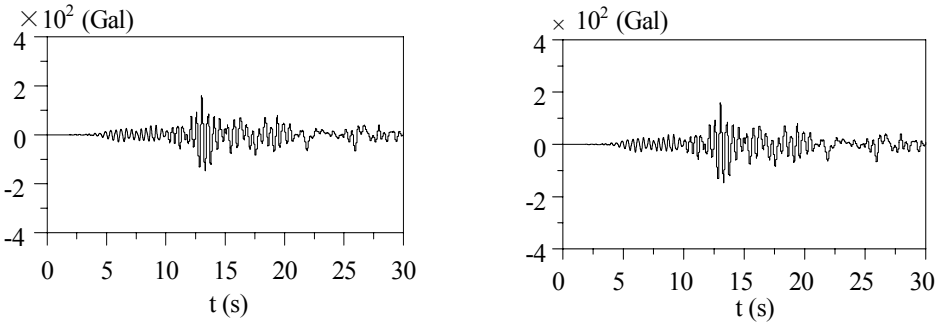

Ground motion 2

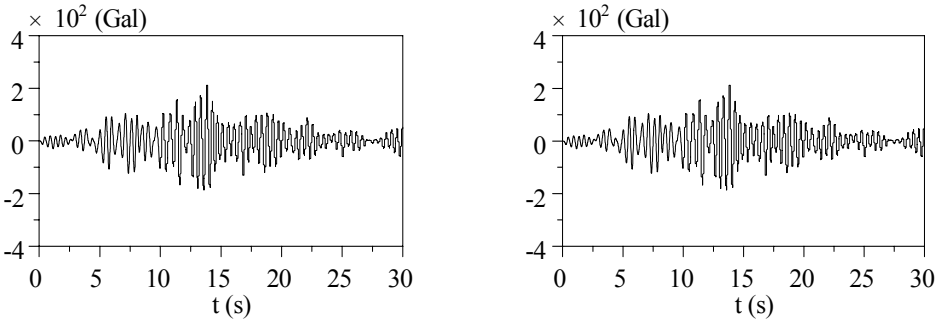

Ground motion 3

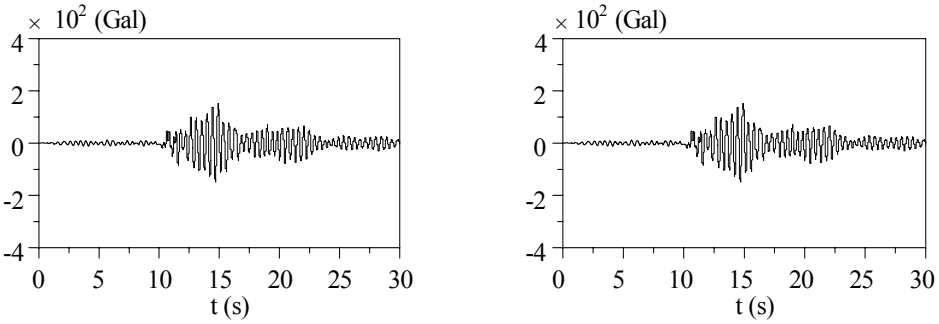

Ground motion 4

Train standing Train running

Fig. 5.4.9 Responses of car body (Horizontal)

5.5 Examination on seismic safety of bridge structure

In this section, the strength of the bridge pier under the seismic load is investigated. To examine the seismic performance, firstly the limit states for cracking of concrete and yielding of reinforcement bars are needed. The failure mode is defined [5] [6] by the ratio of the shear capacity resulting from the shearing force to that resulting from the bending moment. To examining the strength, the cross-sectional shearing force and bending moment of the pier obtained from dynamic response analysis will be compared with the limit states.

The sectional view of the pier is shown in **Fig. 5.5.1**. There are 12 axial reinforcing bars in the cross-section. **Fig. 5.5.2** shows the placement interval of the ties in the pier. The placement interval of the tie varies in different parts of the pier.

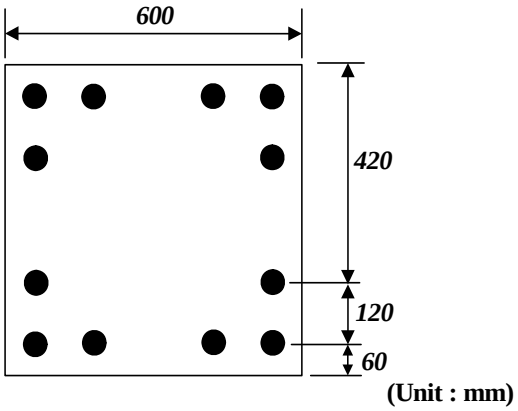

Fig. 5.5.1 Sectional view of the pier

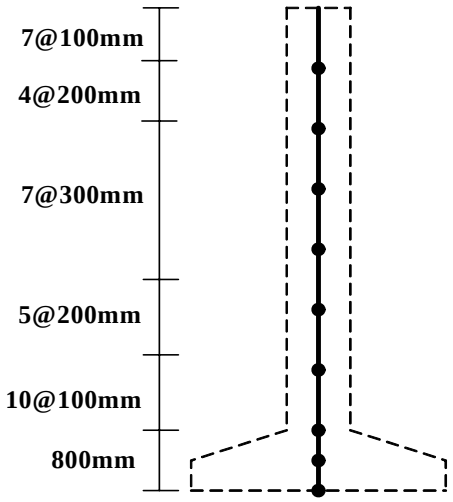

Fig. 5.5.2 Placement interval of the ties

5.5.1 Formula for seismic performance evaluation

a) Maximum capacity

The maximum capacity respectively for cracking of concrete and yielding of reinforcing bars are calculated by Eq. (5.5.1)-(5.5.3), which are defined in design codes [6]. M_c, M_{ud} and V_{yd} respectively denote the flexural capacity for cracking of concrete, the flexural capacity and shear capacity for yielding of reinforcing bars. To examine the flexural capacity, it is necessary to consider all axial reinforcements of the cross-section.

The flexural capacity for cracking is defined as the bending moment, when the stress at the edge of the pier reaches the flexural strength of concrete:

$$M_c = W_i(f_{bd} + N_i / A_i) \tag{5.5.1}$$

where W_i, f_{bd}, N_i and A_i are the section modulus considering of reinforcing bars, the flexural strength of concrete, axial compressive force at the cross-section and the sectional area considering of reinforcing bars, respectively.

The flexural capacity for yielding of reinforcing bars is defined as the bending moment of yielding of reinforcing bars. The bending moment is defined by the stress and the point of application. The stress is carried by the concrete and reinforcing bars.

$$M_{ud} = \{C' \cdot (d - e - \beta \cdot x) + T'_{sc} \cdot (d - e - d_c) + T_{st} \cdot e\} / r \tag{5.5.2}$$

Herein C', T'_{sc}, and T_{st} are the axial compressive force of concrete, the axial compressive force of reinforcing bars and the axial tensile force of reinforcing bars, respectively.

The shear capacity for yielding of the pier is the resultant force of shearing force carried by concrete and reinforcing bars. In order to calculate the shear capacity, both the effects of axial reinforcement and the ties should be considered.

$$V_{yd} = V_{cd} + V_{sd} \tag{5.5.3}$$

where V_{cd} and V_{sd} are the shear capacity carried by concrete and that carried by reinforcement bars, respectively.

b) The failure mode

In the Seismic Design Codes for Railway Structures in Japan [5], the failure mode should be classified into two categories, the flexural failure mode occurs under bending moment when the shearing failure mode occurs under shearing force. The categories are classified by the ratio defined as Eq. (5.5.4). When the ratio satisfies Eq. (5.5.5), the failure mode is the flexural failure mode and seismic performance of the pier should be examined by bending

moment. Otherwise, the failure mode is the shearing failure mode and seismic performance should be investigated by shearing force.

$$R = V_{yd} h / M_{ud} \tag{5.5.4}$$

$$R > 1.0 \tag{5.5.5}$$

where h is the length from pier to superstructure.

c) The dynamic cross-sectional forces

Employing the displacements at the finite element nodes obtained from the seismic analysis of the bridge-train interaction system, the cross-sectional forces are calculated. Using the global stiffness matrix of the element, the cross-section forces of the pier should be determined as Eq. (5.5.6).

$$\{\boldsymbol{f}_e\} = [\boldsymbol{K}_e][\boldsymbol{T}_e]\{\boldsymbol{w}_e\} \tag{5.5.6}$$

Herein $\boldsymbol{K}_e$, $\boldsymbol{T}_e$, and $\boldsymbol{w}_e$ respectively denote the local stiffness matrix of the element, transformation matrix, and global displacement vector of one element.

For examination of the seismic performance, the cross-section forces calculated by Eq. (5.5.6) are compared with the maximum capacities. The two cases of Train as mass and Train running described in previous section are selected for the evaluation. The dynamic effect of the train on the the seismic performance of the bridge will be shown with these two cases.

5.5.2 Evaluation of seismic performance

a) The failure mode

For this viaduct, the ratio defined in Eq. (5.5.4) is shown in **Fig. 5.5.3**. As shown in the figure, the failure mode is the flexural failure mode for the pier In the case of the flexural failure mode, seismic performance of the pier should be examined by bending moment. However, in this study the seismic performance is investigated by both the bending moment and the shearing force to see their tendencies.

b) Examination of dynamic cross-sectional force

The critical parts of the piers are adopted to be investigated. When the seismic performance is examined with the shearing force, the critical part is the central section of the pier where the interval of the tie is larger than the other parts. While examining with the bending moment, it is the basal section of the pier where is critical.

Under Ground motion 1: In the two cases, the shear force and the shear capacity of the most critical part of the pier L1 are shown in **Fig. 5.5.4 (a)**. The bending moment and the flexural capacity are shown in **Fig. 5.5.4 (b)**. In all cases under Ground motion 1, the cross-sectional forces are larger than the maximum capacities in the ultimate states. In particular, the bending moment in the case of Train as mass is most critical in all cases.

Under Ground motion 2: The shear force and the shear capacity of the most critical part of pier L1 is shown in **Fig. 5.5.4 (c)**. The bending moment and the flexural capacity are shown in **Fig. 5.5.4 (d)**. The shearing forces are much smaller than the limit states of yielding of reinforcing bars in both cases. The bending moment in the case of Train running is smaller than that in the case of Train as mass. The bending moment is slightly over the capacity in the case of Train as mass.

The reason for the difference due to the two ground motions is just as described previously that the seismic response spectra of Ground motions 1 and 2 are quite different. Because the spectra of Ground motions 1 predominated at the period of 0.455 s which is the first horizontal natural period of the bridge, the seismic performance under Ground motion 1 is more critical than that under Ground motion 2.

And also, dynamic response and the cross-sectional forces in the case of Train as mass is larger than those in the case of Train running. This fact also indicates that it might overestimate the seismic response of the bridge by considering the train as additional mass rather than as a vibration system.

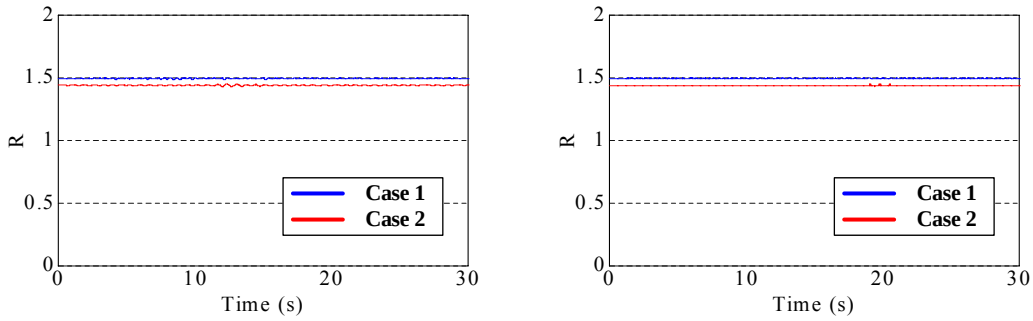

Ground motion 1 Ground motion 2

Fig. 5.5.3 The ratio for classifying the failure mode

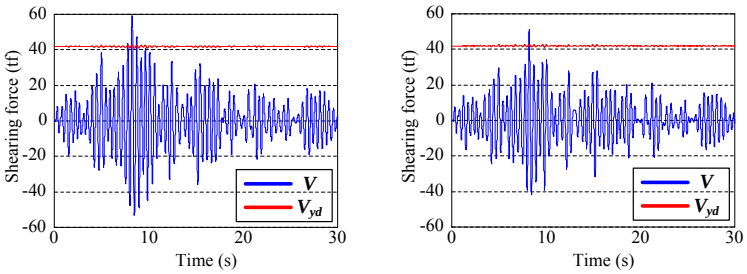

(a) Shearing force under Ground motion 1

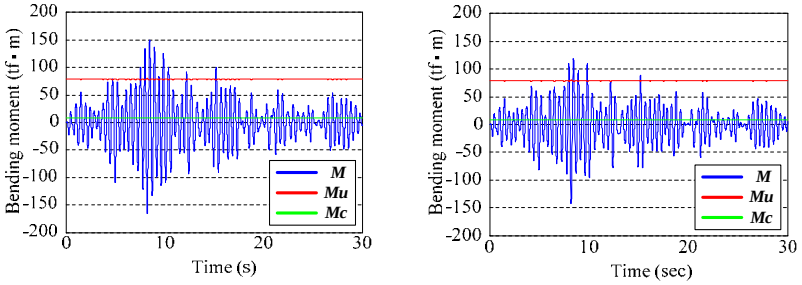

(b) Bending moment under Ground motion 1

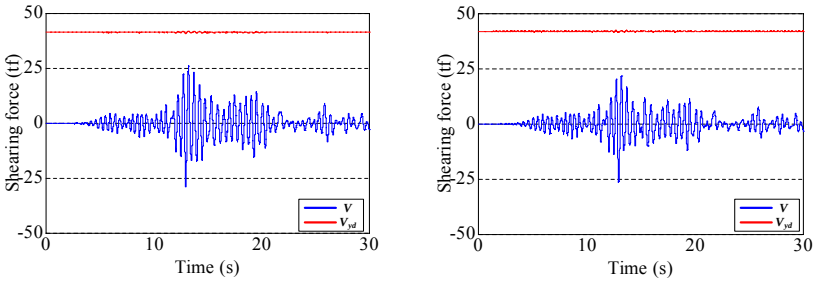

(c) Shearing force under Ground motion 2

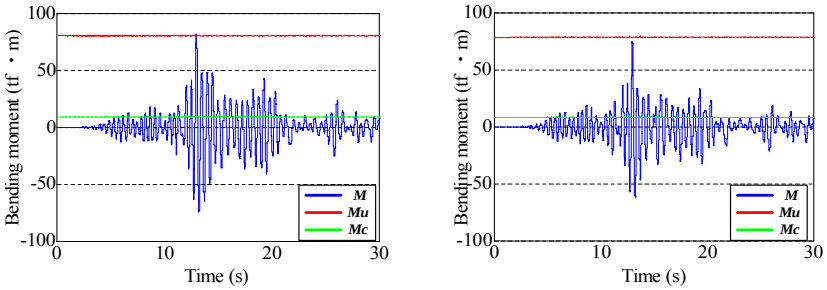

(d) Bending moment under Ground motion 2

Train as mass Train running

Fig. 5.5.4 Seismic performance of the bridge pier

5.6 Running safety of bullet trains

5.6.1 Evaluation of running safety by means of derailment coefficient [7－10]

Prevention of derailment accidents is a very crucial issue for a railway system because the resultant damage is directly connected to human life. For the train derailment due to a concurrence of causes (one particular factor cannot be specified as the cause for derailment, and multiple causes related to the car and track are combined to cause the derailment), some of the causes are not yet clarified and various types of research and development are required for their clarification. In 1968 the safety standard on derailment [7] was specified by RTRI based on enormous experiments and simulations.

Derailment assumed to be caused by multiple factors can be divided into four types according to the form [8] [9].

(1) Wheelclimb derailment accident

In this type of derailment, the attack angle (formed by the wheel and rail, see **Fig. 5.6.1**) is positive (the wheel flange climbs up the rail in the direction of motion), and transversal force is produced between the wheel and rail, with the result that wheel climbs up the rail.

(2) Slide-up derailment

In this type of derailment, the attack angle is negative, and the wheel is faced in the direction away from the rail, where force in the lateral direction is greater than that is applied, whereby the wheel slides up the rail.

(3) Jump-up derailment

In this type of derailment, abrupt force in the lateral direction is produced to cause the wheel to collide with the rail.

(4) Derailment due to decrease of the wheel load

In this type, the derailment occurs though the lateral pressure is not large, such as caused by the cant in a curve section, the centrifugal force, the wind pressure, the rolling motion of the car body and the deviation of the centroid, etc.

Of these four types of derailment, the wheelclimb derailment is most likely to occur. For the former three types of derailment, derailment coefficient described in the following is often used to evaluate the running safety of the trains.

In the railway car, the wheel travels along the rail. **Fig. 5.6.2** shows the force acting on the contact point between the wheel and rail. Force F acting on the contact point between the wheel and rail is divided into perpendicular component P (wheel load) and horizontal component Q (transversal pressure). Further, the force "f_y" of the contact point in the tangential direction is called lateral creep force.

As will be discussed later, this is assumed to affect the wheelclimb derailment. It should be noted that **Fig. 5.6.2** shows that the wheel flange is in contact with the rail. In this case, the contact angle forms flange angle α. From **Fig. 5.6.2** force acting on the contact point between the wheel and rail is kept in balance, we get the following using P and Q:

$$P\sin\alpha - Q\cos\alpha = f_y$$

$$P\cos\alpha + Q\sin\alpha = N$$

where N denotes the force acting in the normal direction of contact point.

Then the following relation can be obtained:

$$\frac{Q}{P} = \frac{\tan\alpha - f_y / N}{1 + (f_y / N)\tan\alpha}$$

This Q/P is called the derailment coefficient. The greater the Q/P is, the smaller the f_y will be. In other words, if one assumes that contact is made by the flange and balance is maintained, then the limit is approached at smaller Q/P as f_y is greater. It is said that, if the attack angle is increased, the f_y will also be increased, without exceeding the frictional force. Thus, the maximum value of f_y is substituted into frictional force μN (where μ denotes the friction coefficient). The minimum value of Q/P is given by:

$$\frac{Q}{P} = \frac{\tan\alpha - \mu}{1 + \mu\tan\alpha}$$

This is called Nadal's equation representing the limit value of derailment. Since the wheel load (P) and transversal pressure (Q) can be measured with comparative ease, the derailment coefficient has been used as an index for evaluating the traveling safety.

In Japan, the most critical upper limit of the derailment coefficient can be considered as 0.8. According to Ishida et al's research [10], when evaluate the running safety of the train, it is necessary to examine the max value of the derailment coefficient simultaneously with its duration. If the duration is within 0.015 sec, the train will not derail even with a rather greater derailment coefficient than 0.8. If the derailment coefficient continuously keeps greater than 0.8 over more than 0.015 sec, the possibility of derailment should be investigated.

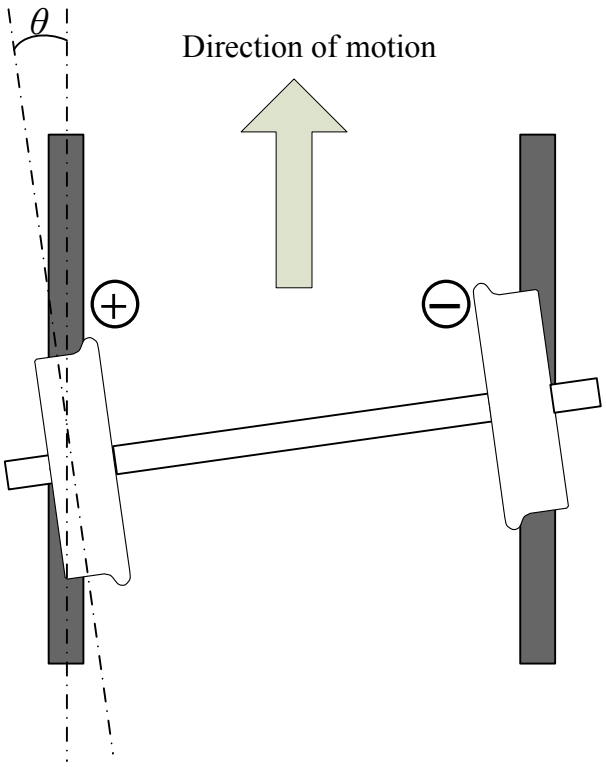

Fig. 5.6.1 Attack angle

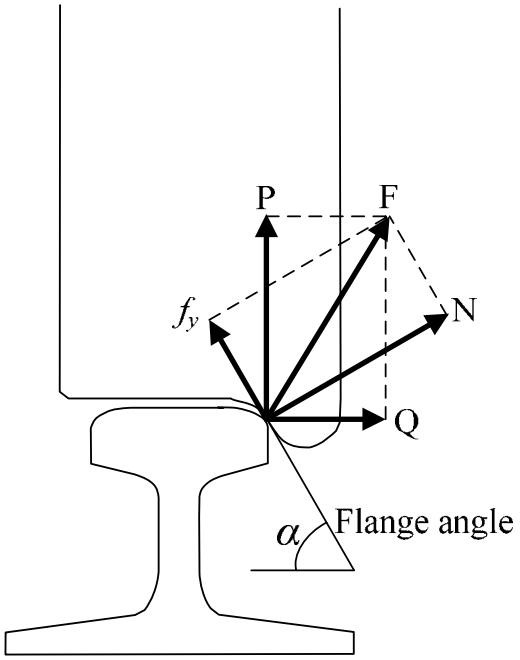

Fig. 5.6.2 Force acting on contact point between the wheel and rail

5.6.2 Analytical evaluation of the bullet train's running safety

In the present analytical models of this research, because the relative motion between the wheels and the track is neglected, the wheel load P and lateral pressure Q described in previous subsection can not be calculated through contact forces between the wheel tread and the rail surface. Therefore in this study, the wheel loads are derived based on the deformation of the springs between the bogies and wheel-sets. Then the derailment coefficient is defined as the ratio of the lateral wheel load to the vertical one. This evaluation is based on the assumption that the relative motion between the wheels and track is small and the vertical wheel loads do not decrease excessively. The dynamic effect of the car body and the bogies can be considered and the basic dynamic characteristics of the bridge-train interaction are obtainable. However, for some cases, the relative motion between the wheels and track is predominant such as subjected to violent ground motion, or the vertical wheel loads are extremely decreased. In such cases, it is difficult to evaluate the running safety of the train by derailment coefficient and the wheel-track contact model is necessary.

As a representative, only the derailment coefficients on the left and right sides of the front axle of the front bogie are indicated in **Fig. 5.6.3** because those of other wheels indicate no large differences. They are corresponding to Ground motions 1 to 4. It is also apparent that the derailment coefficient attributable to Ground motion 1 is larger those of the rest Ground motions because the dynamic responses of the train show that tendency. The safety limit of the derailment coefficient in Japan is set as 0.8. In the case that the derailment coefficient becomes greater than 0.8, the duration of the derailment coefficient will be examined to evaluate the train's running safety. In this analysis, little danger of derailment exists for any of the four ground motions because the derailment coefficients are much less than 0.8.

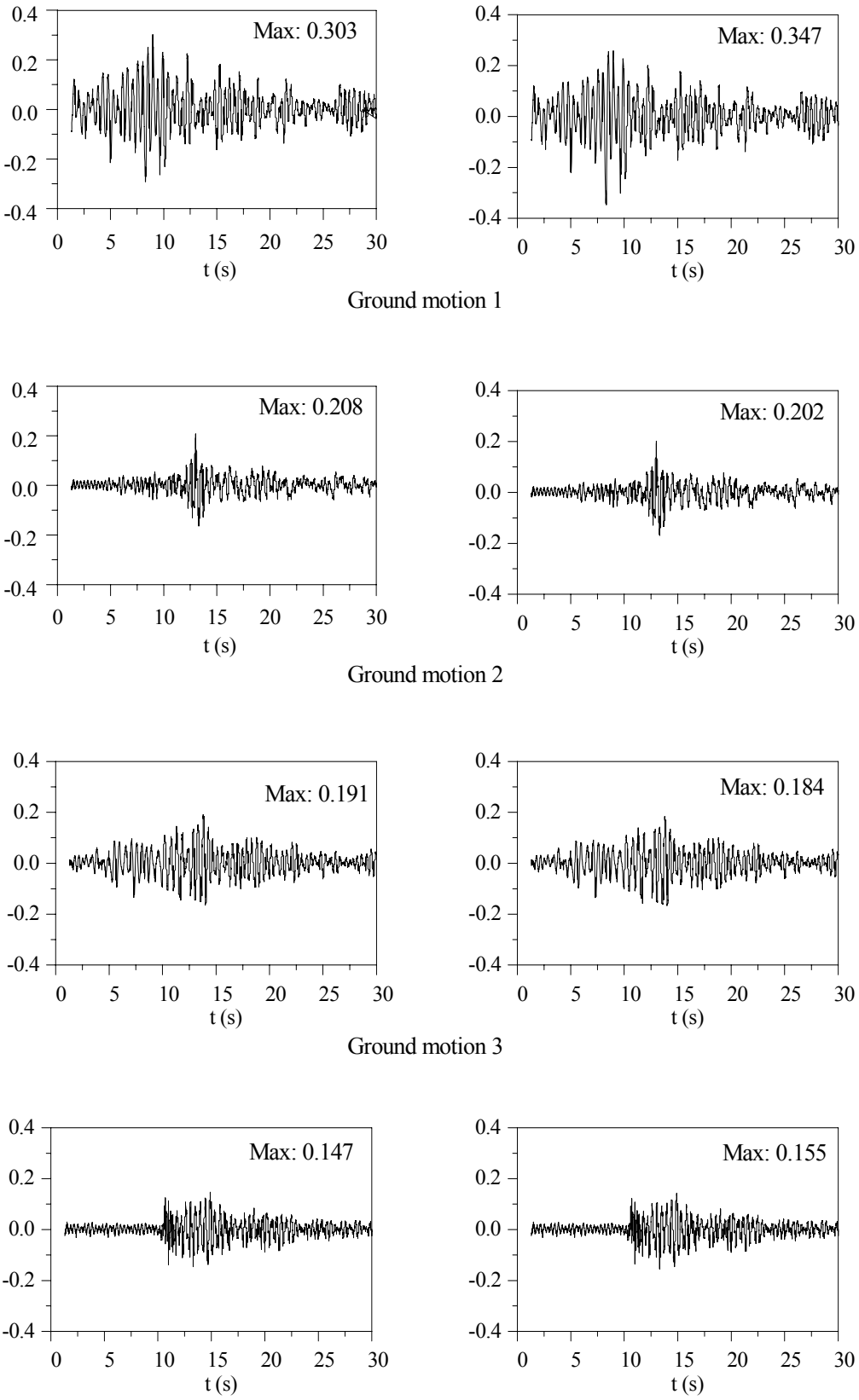

Fig. 5.6.3 Derailment coefficients

5.7 Urgent earthquake detection and alarm system [11] [12]

Urgent Earthquake Detection and Alarm System (UrEDAS), is an integrated real-time earthquake warning system using a single station with three-component seismometer. Detecting the initial P-wave of an earthquake, UrEDAS judges the destructive potential of the impending earthquake on the basis of the relation between magnitude and epicentral distance of earthquake, and issues a necessary warning within four seconds after the P-wave's arrival for a certain area which may sustain damage. At the arrival of S wave, it improves the estimates and updates the warning. UrEDAS is the fastest earthquake alarm system in the world, practically in use since 1988.

5.7.1 Analytical cases

In this section, the seismic response of the train, after it receives the warning from UrEDAS and executes speed-down operation, will be simulated. Because the upper limit of the acceleration of the brake system is around 3.6 km/h, 3.0 km/h of acceleration of the speed-down will be adopted in this study. Two cases are assumed to carry out the analyses.

Case-1:

In this case, the near-land interplate earthquake (Ground motion 1) is expected to occur and the distance between the epicenter and the viaducts is assumed relatively far. Since the velocity of P-wave propagates far more rapidly than the S-wave, there will be some time for the train to achieve speed-down after receiving the warning from UrEDAS system. Thus when the earthquake motion reaches the viaducts, the train has already been braked to a relatively low speed and the degree of danger can be reduced.

Concretely, the distance between the epicenter and the UrEDAS station is adopted as 40 km, and that between the epicenter and the viaducts is 200 km. Then, (1) it will be 5 sec for the P-wave to reach the UrEDAS station; (2) the UrEDAS system needs 3 sec to process data and send out the warning message; (3) after receiving the warning, the train use 1 sec to start the brake system; (4) the time for the S-wave to reach the viaducts is 50 sec. Therefore, the time that the train obtained to reduce the speed is 41 sec calculated as subtracting the time of (1), (2) and (3) from (4). With 3.0 km/h acceleration of speed-down, the train will reduce its speed down to 123 km/h from the operational velocity of 270 km/h when the S-wave of the earthquake arrives. Thus in the analysis, the initial velocity of the train is set as 147 km/h when the analysis starts.

Case-2:

In this case, the inland earthquake (Ground motion 2) is assumed as seismic load and the

distance between the epicenter and the viaducts is close. Thus the train does not have time to achieve speed down before the S-wave reaches. Here, the initial speed of the train is set as the operational velocity of 270 km/h. The train will start speed-down with 3.0 km/h acceleration in 1 sec (Operation time of brake system) after receiving the warning message from the UrEDAS system.

The responses and derailment coefficients of the train in these two cases will be compared with those of the case without speed-down to examine the effect of reducing speed.

5.7.2 Analytical results

The acceleration responses of the car body, Horizontal acceleration responses of the Central point of the bridge, and the derailment coefficient at the foremost left wheel corresponding to the Case-1, simultaneously with their maximum and rms values, are respectively shown in **Figs. 5.7.1**, **5.7.2** and **5.7.3**. Those corresponding to the Case-2 are respectively indicated in **Figs. 5.7.4**, **5.7.5** and **5.7.6**.

For Case-1, the maximum values of the car body acceleration in both horizontal and vertical directions are much smaller due to the speed-down in advance. Though the rms values indicate a contrary tendency, it is considered due to the initial conditions of the running train. The start position of the train was set at 75 m ahead of the bridge and the train took longer time to enter the bridge. For that reason, the rms values of the speed-down case are evaluated differently. It is conceivable that the rms values also decrease due to the speed-down. The responses of the bridge and the derailment coefficients indicate the same tendency. Therefore, through in advance speed-down, the fact that the running safety of the train is enhanced can be confirmed.

In Case-2, the effect due to the speed-down process is not obvious at that in Case-1 for the dynamic responses of both the train and the bridge. However, the derailment coefficient can also be confirmed apparently decreased due to the speed-down operation.

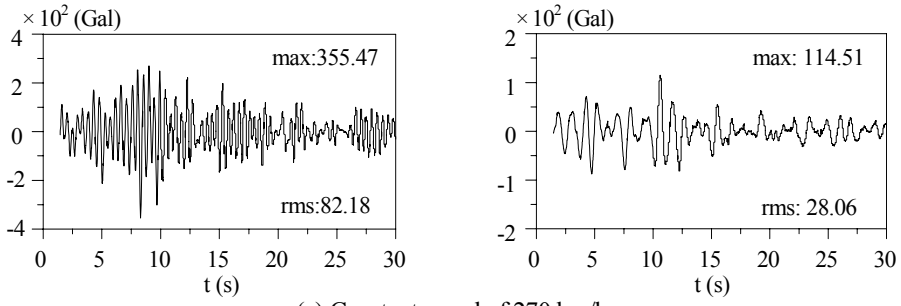

(a) Constant speed of 270 km/h

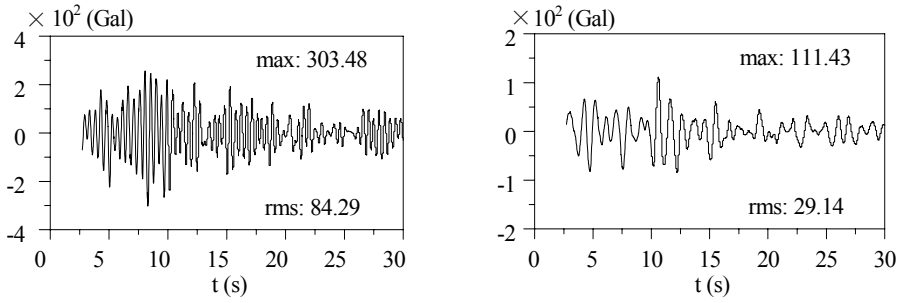

(b) Speed-down from 147 km/h

Horizontal Vertical

Fig.5.7.1 Acceleration responses of train body (Case-1)

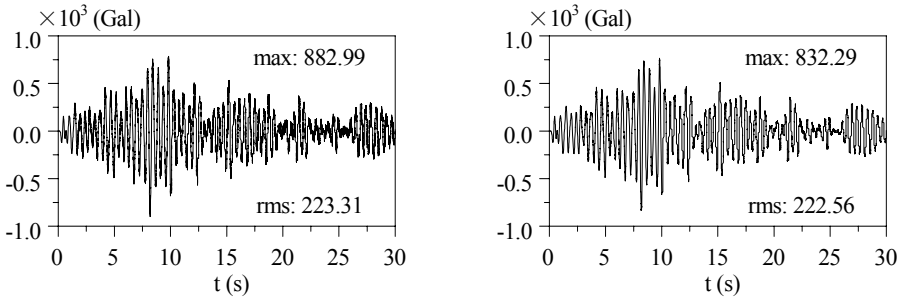

(a) Constant speed of 270 km/h (b) Speed-down from 147 km/h

Fig.5.7.2 Horizontal acceleration responses of Central point (Case-1)

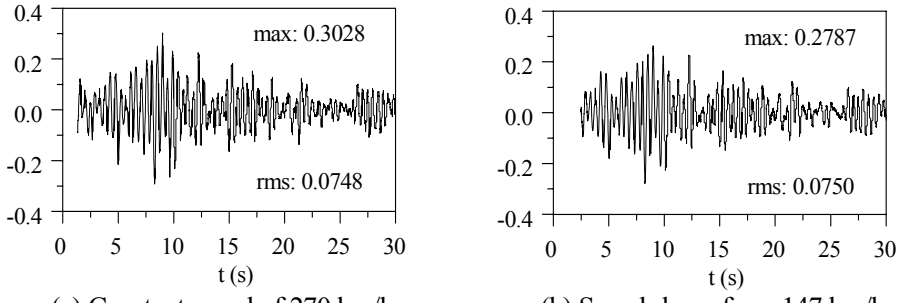

(a) Constant speed of 270 km/h (b) Speed-down from 147 km/h

Fig.5.7.3 Derailment coefficient (Case-1)

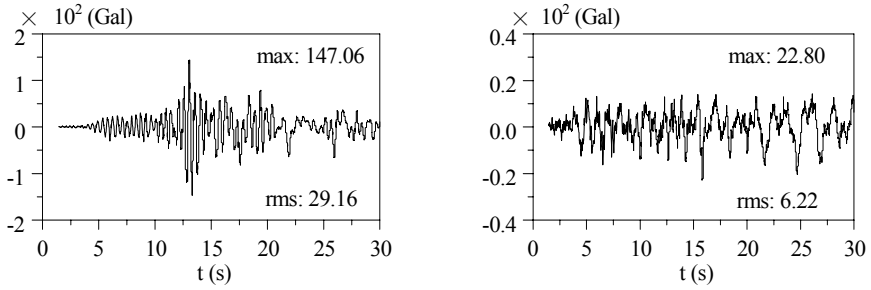

(a) Constant speed of 270 km/h

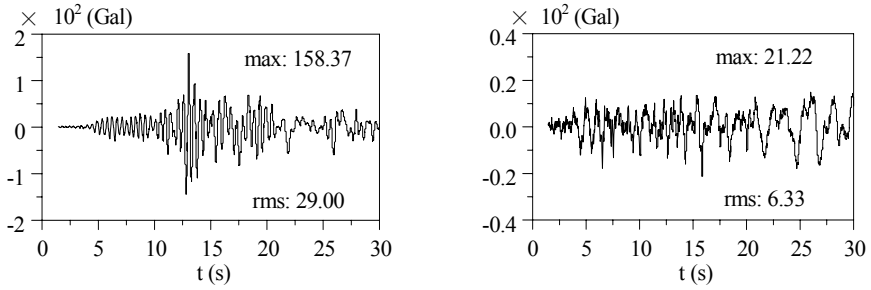

(b) Speed-down after 1 second

Horizontal Vertical

Fig.5.7.4 Acceleration responses of train body (Case-2)

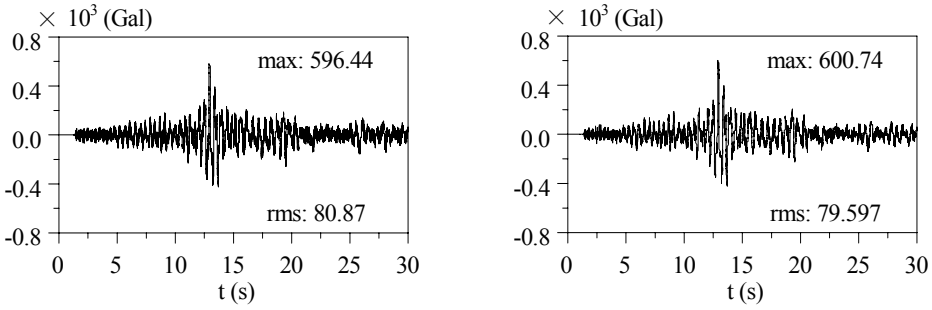

(a) Constant speed of 270 km/h (b) Speed-down after 1 second

Fig.5.7.5 Horizontal acceleration responses of Central point (Case-2)

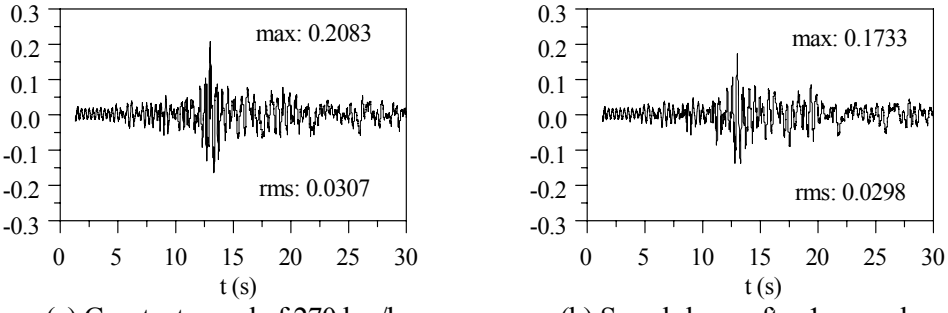

(a) Constant speed of 270 km/h (b) Speed-down after 1 second

Fig.5.7.6 Derailment coefficient (Case-2)

5.8 Seismic analysis of train-bridge interaction system by direct integration method

For the seismic performance of the bridge-train system subjected to strong ground motions, it is necessary to establish the non-linear models of the system. In such case, the interaction between the bridge and train become extremely complicated and the research on this kind problem is still in its early stage. In this study, based on the results of the linear bridge-train-earthquake interaction analysis, attempts to simulate the seismic performance of bridge-train system subjected to strong ground motion are also undertaken.

For strong ground motions, because the response of the bridge-train system is non-linear, modal analysis is no longer able to be applied. The dynamic differential equations should be solved by direct integration method. Moreover, in each integral time interval, convergent calculation is required because unbalance force occurs due to the non-linearity of the structural stiffness. Therefore, it is necessary to treat the train and the bridge as separated systems, while it is possible to treat the bridge and the train as an integrated system in linear analysis. In this study, the preliminary efforts on formulization of the bridge-train-earthquake interaction suitable for direct integration approach are devoted at first. For the direct integration approach, the independence of the train and the bridge systems is realized by considering their effects on each other as external forces.

Based on the formulization developed in Section 2.4.5, the analytical approach taking advantage of the direct integration method is developed. The flow chart of the direct integration approach is shown in **Fig. 5.8.1**. Then the validation of the approach is performed by comparing the analytical results by the direction integration approach and those of modal analytical approach.

Figure 5.8.2 shows the simplified 1-block bridge models of that used in Chapter 3 which is a 3-block model. Model (a) 260-node model is obtained by eliminating the rail structure from the middle block of the 3-block model. Model (b) 40-node model is further simplified from (a) by merging some beam elements.

At first, the analyses of the case that only the bridge is subjected to ground motions are carried out to confirm the validity of the seismic analytical algorithm in direction integration method. Ground motion 2 (Both EW and UD components) are used as seismic load. The analytical results at Point-1 shown in **Figure 5.8.2** of the 40-node model by both the direct integration method and the modal analytical approach, simultaneously with the results of the 260-node model by modal analytical approach, are shown in **Figure 5.8.3**. The results by the direct integration method indicate good agreement with those by modal analytical approach, thus the validity of the seismic analytical algorithm in direct integration method is confirmed.

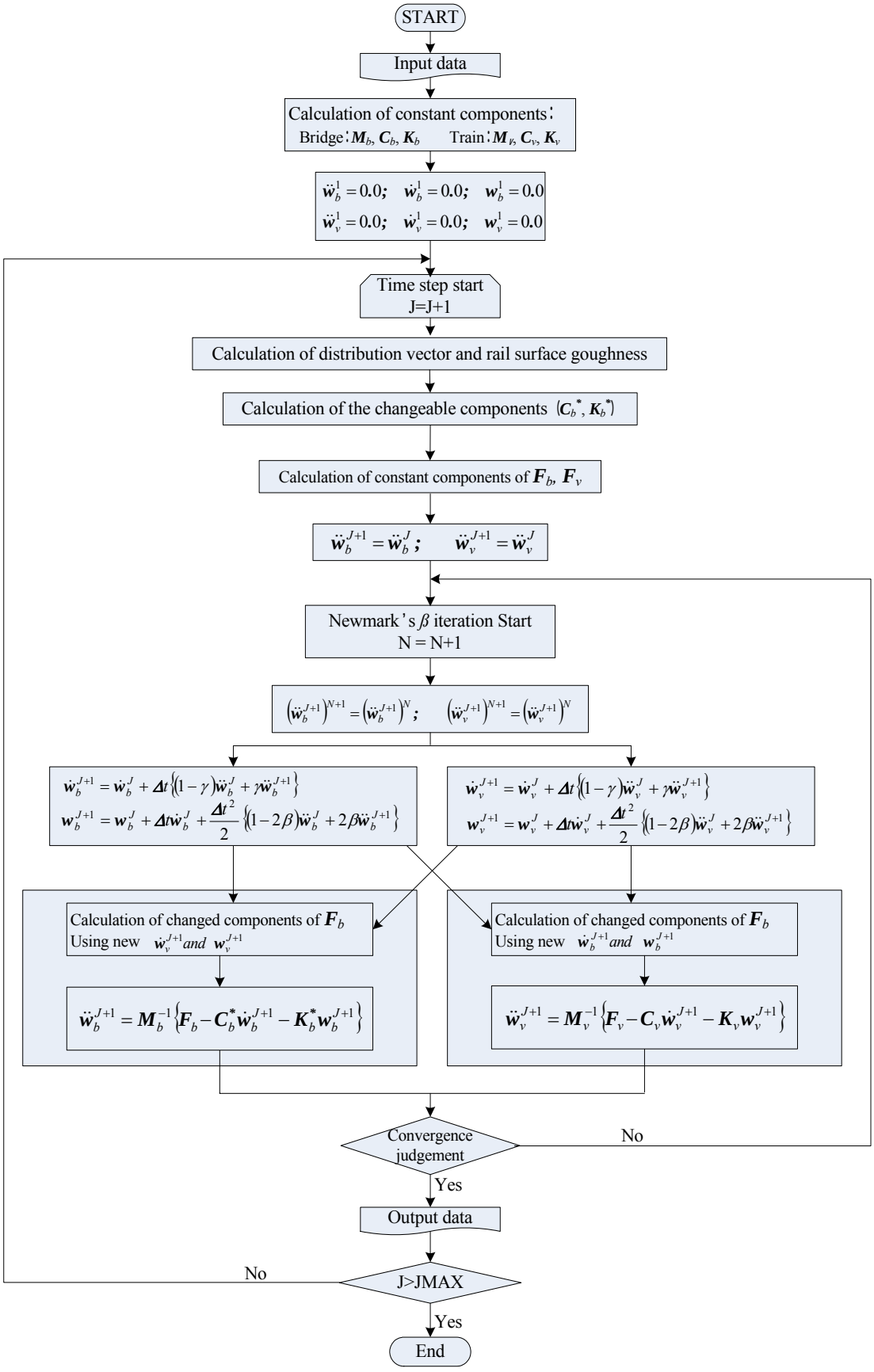

Fig. 5.8.1 Flow chart of direct integration method

The difference of the analytical results between the 260-node model and the 40-node model in the vertical direction indicated in **Fig. 5.8.3** can be considered caused by the difference of the two models that the nodal points in 40-node model are much less than those in 260-node model and the effect of the lumped mass system is different.

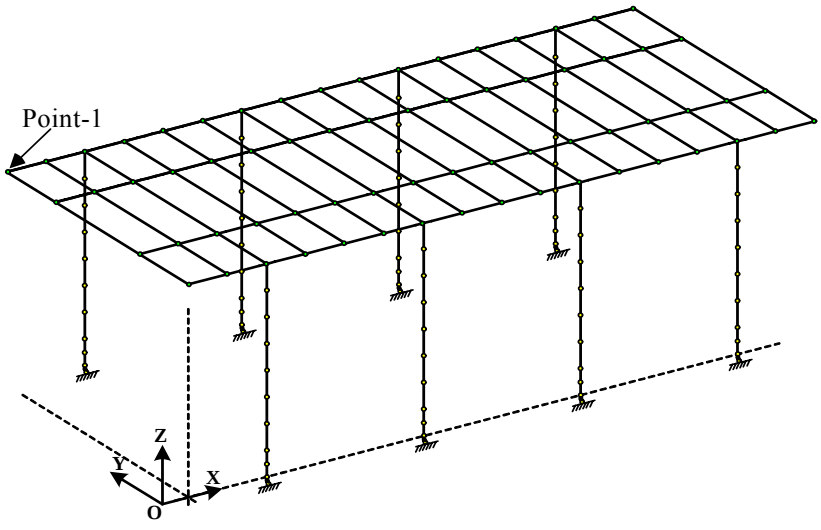

(a) 260-node model

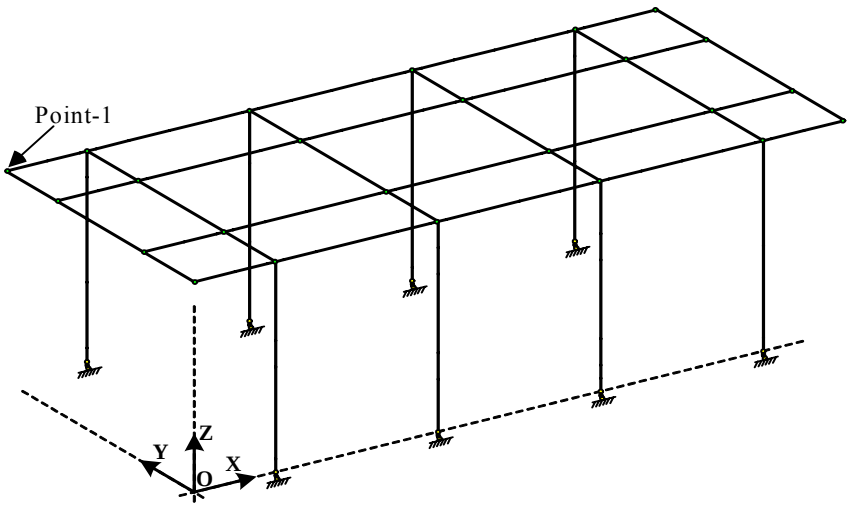

(b) 40-node model

Fig. 5.8.2 Simplified 1-block bridge models

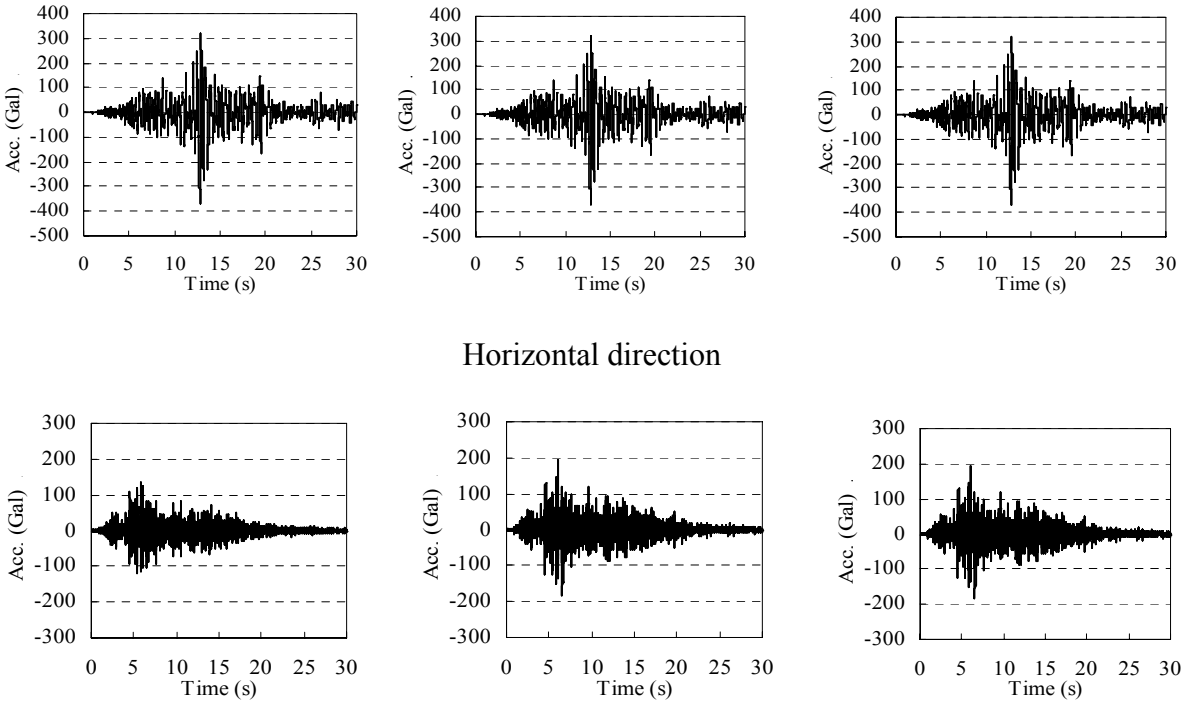

Fig. 5.8.3 Analytical results of different models and methods

To validate the bridge-train interaction procedure in direction integration method, the bridge responses of the 40-node model under running train without ground motion are simulated. The train composed of sixteen cars just the same as those in Chapter 3 are used for analysis. The velocity of the train is also set as actual operational speed of 270 km/h. Since there are no rail structures in the 40-node model, the train is assumed running on the slab deck on the lines of the rail. The acceleration responses of Point-1 in **Fig. 5.8.2** (b) by both the direct integration method and the modal analytical approach are shown in **Fig. 5.8.4**. The analytical results between the direct integration method and the modal analytical approach indicate complete agreement with each other; therefore the validity of the bridge-train interaction procedure in the direction integration form can be confirmed.

Since both the seismic analytical algorithm and the bridge-train interaction procedure are validated, the developed direct integration analytical procedure can be considered valid. Based on the direct integration procedure, non-linear bridge-train-earthquake interaction analytical approach can be developed.

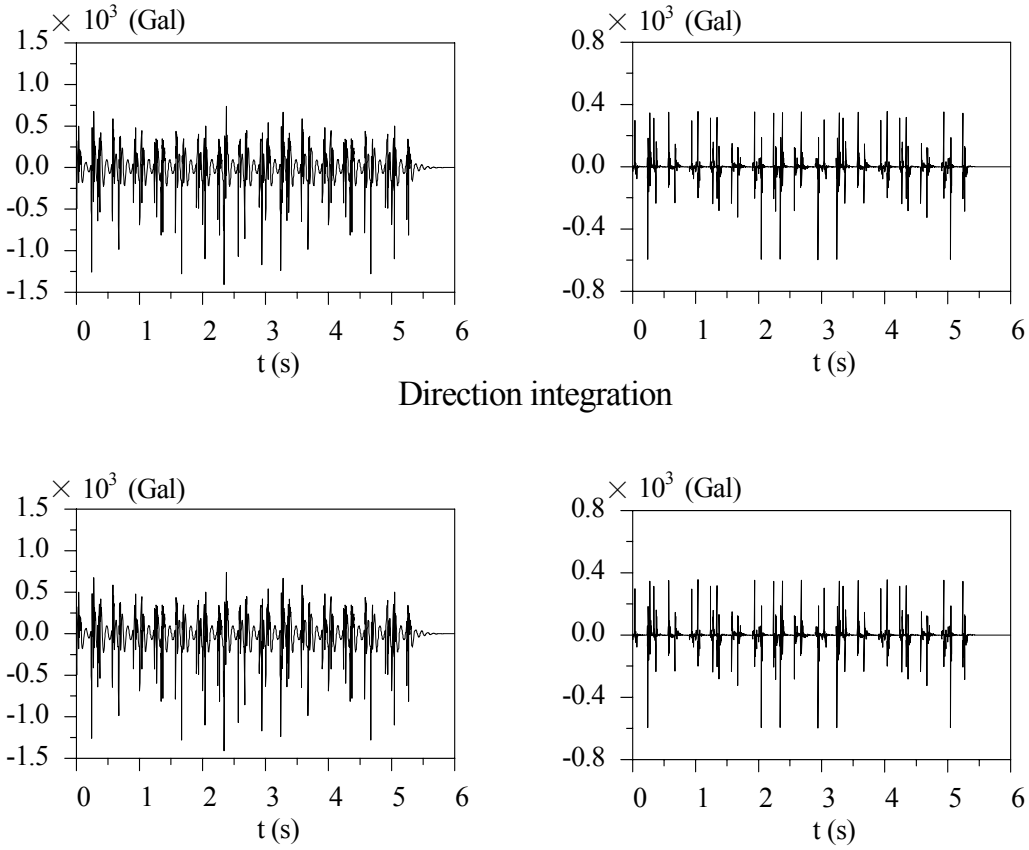

Fig. 5.8.4 Bridge responses under running train

5.9 Conclusions

The seismic analysis of bridge-train interaction is an important and difficult topic in bridge engineering. Especially for the seismic performance of the bridge-train interaction system under violent earthquakes, analytical researches are still in the early stage.

In this chapter, as the preliminary effort, an analytical approach to simulate dynamic response of the bridge-train interaction system subjected to moderate earthquakes is established. The deformation of the structure is assumed to remain in elastic domain during a moderate earthquake. In this stage of the analytical approach, considering the intensity of the ground motion and its complexity, the relative motion between the wheels and the track structure is neglected and the movement of the wheels is presumed dependent on the displacement of tracks.

The ground motions defined in seismic design codes and also actual measured ones downloaded from the Kyoshin Network of NIED are adopted as the seismic load. Newmark's β-method is also adopted here to solve the dynamic differential equations. The accuracy of the seismic analysis algorithm is validated in comparison with a general program named MIDAS. The dynamic responses of the bridge and the train are then simulated and evaluated.

Employing the ground motion define in seismic design codes, the case study, in which the dynamic responses of the elevated bridge and the train body are simulated assuming that the train composed of 16 cars runs through the 3-block bridge with the velocities of 270 km/h and 60 km/h, is carried out. From the evaluation of the results, the following problem is concluded. Considering the extremely high speed of the bullet train, the effort must be made to ensure that the bridge-train interaction is adequately taken into account in discussing the runnability of the train, such as by employing a bridge model with enough length or controlling the starting time for the train to enter the bridge of limited length.

For the ground motions downloaded from K-net, the dynamic responses of the elevated bridge and the car body were simulated assuming that the train was running through or standing on the bridge; the other case subsumed that the train was merely considered as additional mass to the bridge structure. Analytical results showed the damping effect of the train as a vibration system on the seismic response of the bridge. The seismic performance of the bridge is investigated by examining the cross-sectional forces of the pier with respect to the strength limits. To examine the running safety of the bullet train, the derailment coefficient is simulated and examined.

This analytical procedure is useful to perform various evaluations on the seismic response of the bridge-train system. It also laid a foundation to further research on the non-linear bridge-train-earthquake interaction problem.

References

[1] He, X., Kawatani, M., Sobukawa, R. and Nishiyama, S.: Dynamic response analysis of Shinkansen train-bridge interaction system subjected to seismic load, *Proc. of 4th International Conference on Current and Future Trends in Bridge Design, Construction and Maintenance*, Kuala Lumpur, Malaysia, pp. 1-12, 2005 (CD-ROM).

[2] Kawatani, M., He, X., Nishiyama, S., Yoshida, K. and Yamaguchi, S.: Dynamic Response Analysis of Shinkansen Train-Bridge Interaction System Subjected to Moderate Earthquake, Proceedings of the 61st Annual Conference of the Japan Society of Civil Engineers, I-502, 2006.9. (*in Japanese*)

[3] Japan Society of Civil Engineers, "Standard Specifications for Concrete Structures-2002, Seismic Performance Verification," Dec., 2002. (*in Japanese*)

[4] National Research Institute for Earth Science and Disaster Prevention. Kyoshin Network (K-NET), http://www.k-net.bosai.go.jp.

[5] Railway Technical Research Institute. Seismic Design Code for Railway Structures. Maruzen Co., Ltd.: Tokyo, Japan, 1999. (*in Japanese*)

[6] Railway Technical Research Institute: Design standard for railway structures (Concrete structures), MARUZEN Co., Ltd.: Tokyo, Japan, 2004. (*in Japanese*)

[7] Safety standard on derailment, *Railway Technical Research Report*, No. 914, Nov., 1968. (*in Japanese*)

[8] Maruyama, H. and Fukazawa, Y.: Railway engineering for civil engineers, MARUZEN Co., Ltd., Nov., 1981. (*in Japanese*)

[9] Maruyama, H. and Kageyama, N.: Railway engineering for civil engineers, MARUZEN Co., Ltd., Oct., 1981. (*in Japanese*)

[10] Ishida, H., Tezuka, K., Ueki, K., Fukazawa, K. and Matsuo, M.: Safety criteria for evaluation of the railway vehicle derailment, *RTRI REPORT*, Vol. 9, No. 8, Aug., 1995. (*in Japanese*)

[11] Nakamura, Y.: Research and development of intelligent earthquake disaster prevention systems uredas and heras, *Journal of Structural Mechanics and Earthquake Engineering*, JSCE, No.531/I-34, pp. 1-33, Jan., 1996. (*in Japanese*)

[12] Nakamura, Y.: Earthquake early warning and derailment of Shinkansen train at the 2004 Niigataken-Chuetsu Earthquake, Onging resport of Research Conference on Earthquake Engineering, JSCE, pp. 1-11, Aug. 23, 2005. (*in Japanese*)

Chapter 6

Concluding Remarks

6.1 Analytical approaches to dynamic issues related to high-speed railway bridge-train interaction system

6.1.1 Traffic-induced vibration analysis of high-speed railway viaducts

The dynamic interaction problems between the train and bridge as well as between the foundation and ground have been important topics in the filed of structural dynamics and numerous efforts have been made. For the high-speed railway system in Japan, considering the extremely high speed of bullet trains, the bridge vibration caused by bullet trains is concerned. The severe vibration over a long term may cause deterioration of the bridge structures, such as the cracking or exfoliation of concrete. In addition the investigation on the vibration characteristics of the viaducts by means of field tests, it is necessary to establish a reliable and effective analytical approach to simulate the bridge vibration caused by running trains. Such approach can offer convenient predictions and diagnoses to the vibration of either existing bridges or those in the planning stage, therefore effective countermeasures can be proposed.

In this research, an analytical procedure to simulate the bridge-train coupled vibration problem considering their interaction as well as the effect of ground properties is established. Dynamic responses of a standard type of elevated bridge of reinforced concrete in the form of a portal rigid frame under moving bullet trains are analyzed in consideration of the wheel-track interaction with the rail surface roughness. The viaducts including the track structure are modeled as 3-D beam elements. The elastic effect of ground springs at the pier bottoms and the connection effect of the sleepers and ballast between the track and the deck slab are model with double nodes connected by springs. Bullet train models of two-, six- and nine-DOF dynamic systems developed in Chapter 2 are used for the analyses.

To demonstrate the validity of the finite element bridge model, eigenvalue analysis is carried out and the basic natural frequencies are investigated. The predominant frequency of the horizontal natural mode is showing good agreement with the value of filed test, through which the validation of bridge model is confirmed. For the validation of the developed bullet train models, the dynamic response analysis of the bridge-train interaction system was carried out and the analytical results using the nine-DOF train model indicate relatively good

agreement with the experimental results, thereby validated the bullet train model and the analytical procedure developed can be considered effective.

Based on the simulation of bridge-train interaction, influences of train models on the dynamic responses of viaducts are discussed. The analytical results of six- and nine-DOF train models are showing better agreement with the experimental values, compared with the results of two-DOF model. Furthermore, the analytical results of nine-DOF model are considered indicating the best coincidence with the experimental ones, because it can take account of all the main factors that contribute to the vertical vibration of the bridge-train interaction system. Therefore the conclusion can be made that for more accurate investigation it is desirable to use the nine-DOF train model while the six-DOF model can used in preliminary discussions.

Based on the analytical results by nine-DOF train model, the predominant acceleration responses and frequencies of the bridge vibration are investigated and the dynamic characteristics of the viaducts are clarified. In particular, the analytical acceleration responses displayed larger amplitudes at hanging parts compared with experimental values. The main reason is considered as that the hanging parts of the viaducts are connected with neighboring ones by rail and ballast in the actual structures, but only the effects of the rail can be taken into account in the analysis, i.e. the damping effect of the ballast cannot be considered. The effect of train speeds on bridge response is also examined. The reaction forces at the pier bottoms, which can be used in further analysis of site vibration, are calculated using its influence value matrix and the predominant components are estimated. Then the countermeasures against to allay the undesirable vibration of the bridge are proposed. In this study, form the fact that the excessive vibration occurs at the hanging parts of the elevated bridge, which is elucidated by both dynamic response analysis and the experiment, countermeasures against the predominant vibration are proposed by reinforcing the hanging parts. The effect of the proposed countermeasures is demonstrated through dynamic analysis as well as the results from actual construction case. At last, the efforts are also made to improve the analytical efficiency by developing a one-block model of the bridge.

6.1.2 Evaluation on environmental vibrations caused by bullet trains

The bridge vibration caused by running trains propagates to the ambient ground via footing and pile structures of the viaducts, thereby causing some environmental problems related to site vibration around the viaducts and affects surrounding environments. Undesirable environmental vibrations should be eliminated as possible. However, only a few solutions against the wayside vibration have been practically developed due to its complexities. To find

out more effective countermeasures against the traffic-induced environmental vibration problems, it is necessary to clarify the development and propagation mechanism of the site vibration caused particularly by running vehicles on viaducts.

Nevertheless, such site vibration phenomenon remains unclear because of its complicated nature. Without a clear grasp of the site vibration mechanism through analytical studies, environmental vibration problems are traditionally evaluated and predicted based on field test data. The efficiency of such a process is limited to particular cases. To find out more effective countermeasures against the traffic-induced environmental vibration problems, it is necessary to clarify the development and propagation mechanism of the site vibration caused particularly by running vehicles on viaducts. In addition to empirical knowledge based on field test data, a corresponding analytical approach to simulate the environmental vibration problems is anticipated. Towards clarifying the site vibration caused by vehicles' running on viaducts, though some efforts were paid to simulate the site vibration numerically, few can appropriately handle the dynamic excitation on the foundation because the input motion is resulted form the running vehicles on bridge structures.

In this study, an approach to simulate site vibration around the viaducts of the high-speed railway is established. In this approach, the dynamic interactions between the train and track and between the foundation and ground are simultaneously considered. The entire train-bridge-ground interaction system is divided into two subsystems: train-bridge interaction and foundation-ground interaction. In the stage of the train-bridge interaction problem, the dynamic responses of viaducts are simulated to obtain the dynamic reaction forces at the pier bottoms. Then, applying those reaction forces as input excitation forces in the foundation-ground interaction problem, the site vibration around the viaducts is simulated using a general-purpose program named SASSI2000.

Based on the actual ground properties measured in field test, the site around the viaducts is modeled as layer elements down to the depth of which the structural model is embedded. The substructures of the viaducts including footings and piles are modeled with 3-D solid elements and beam elements. The reaction forces at the pier bottoms obtained in Chapter 3 are used as external excitations and inputted on the footing surfaces. Validity of the program SASSI2000 is examined by comparing the transfer function of the ground surface computed by SASSI2000 with the exact analytical solution given in reference. Then the site vibration around the viaducts is simulated by exciting each set of structural model and the final responses are obtained by means of superposition method.

In spite of the complicated nature of the whole train-bridge-ground interaction system and the approximations or assumptions that have to be made in modeling the system, the analytical acceleration responses can reproduce the main tendencies of the actual ones. The

amplitudes of the analytical results are considerably coincident with the experimental ones. The components of the Fourier spectra of the analytical results to a certain extent re-create the experimental ones. Noticeable fact is observed as that in evaluating the overall tendencies of the site vibration, it is sufficient to excite the footings only on the side of train running, which can lead to a saving of computational cost. It is found that due to the interference phenomenon of waves, the responses of the points that are shifted even a little to each other may differ significantly. The influence of damping constant of the ground is also investigated through analyses. The site vibration under different train velocity is also simulated and evaluated. The vibration levels of the site responses are also estimated. The effect of countermeasures against predominant bridge vibration on reduction of the environmental vibration is confirmed. At last, the horizontal site vibration analysis taking advantage of the 15-DOF train model is also carried out.

6.1.3 Seismic safety evaluations of bridge-train interaction system

After the Kobe earthquake and this Niigata earthquake, it came to be recognized that a high possibility exists to encounter an earthquake during rush hour. Therefore, it has become increasingly important to investigate and evaluate dynamic responses of bullet trains running on bridges under earthquake to ensure the train system's running safety. Nevertheless, discussion of the running safety of bullet trains on viaducts under Level-2 earthquake motion is not prescribed because of the complicated nature of its phenomenon, whereas that is designated for Level-1 (L1) earthquake motion in the design standards for railway structures. Even without the danger of derailment, it is still useful to evaluate the running characteristics and riding serviceability of the bullet train during an earthquake. In both the Kobe earthquake and the Niigata earthquake, the bridge structures, especially the piers, were damaged severely over large distances. Although the live load of trains is considered in the Seismic Design Code for Railway Structuresin Japan, the trains are merely attached as an additional mass to the bridge structure. Nevertheless, it is not rational to treat the train merely as an additional mass because the train is a complicated dynamic system. To satisfy both safety and economy demands in seismic design, the dynamic effect of trains on the bridge structures subjected to ground motion should be investigated further. Therefore, a reliable and effective analytical procedure to simulate the dynamic response of the high-speed railway bridge-train-earthquake interaction system is expected.

In this study, as the first effort to realize the final goal, assuming that the structures remain in elastic domain during a moderate earthquake, an analytical approach to simulate dynamic

responses of the bridge-train interaction system subjected to moderate earthquakes is established. In this stage of the analytical approach, considering the intensity of the ground motion and its complexity, the relative motion between the wheels and the track structure is neglected and the movement of the wheels is presumed dependent on the displacement of tracks. The ground motions defined in seismic design codes and also actual measured ones downloaded from the Kyoshin Network of NIED are adopted as the seismic load. Newmark's β-method is also adopted here to solve the dynamic differential equations. The accuracy of the seismic analysis algorithm is validated in comparison with a general program named MIDAS. The dynamic responses of the bridge and the train are then simulated and evaluated.

Employing the ground motion define in seismic design codes, the case study, in which the dynamic responses of the elevated bridge and the train body are simulated assuming that the train composed of 16 cars runs through the 3-block bridge with the velocities of 270 km/h and 60 km/h, is carried out. From the evaluation of the results, the following problem is concluded. Considering the extremely high speed of the bullet train, the effort must be made to ensure that the bridge-train interaction is adequately taken into account in discussing the runnability of the train, such as by employing a bridge model with enough length or controlling the starting time for the train to enter the bridge of limited length. For the ground motions downloaded from K-net, the dynamic responses of the elevated bridge and the car body were simulated assuming that the train was running through or standing on the bridge; the other case subsumed that the train was merely considered as additional mass to the bridge structure. Analytical results showed the damping effect of the train as a vibration system on the seismic response of the bridge. The seismic performance of the bridge is investigated by examining the cross-sectional forces of the pier with respect to the strength limits. To examine the running safety of the bullet train, the derailment coefficient is simulated and examined.

This analytical procedure is useful to perform various evaluations on the seismic response of the bridge-train system. It also laid a foundation to further research on the non-linear bridge-train-earthquake interaction problem.

6.2 Future works

In this study, analytical approaches to simulate the dynamic issues related to high-speed railway elevated bridge-train interaction system: the traffic-induced bridge vibration problem, the environmental vibration problem caused by bullet trains and the seismic performance of the bridge-train interaction system are established and case studies are carried out. In these approaches, the dynamic responses of the bridges, grounds and trains are simulated considering the bridge-train interaction. For general cases of discussion, the accuracy by these approaches is considered to some extent satisfied to apply on actual engineering problems. However, for more strict discussions of the dynamic responses, further improvements are necessary to elaborate the developed analytical approaches.

In the train-induced bridge vibration analysis, the interaction between the bridge and train is realized by attaching the motions of the wheels to the rail structure. However, this is a rather approximation. In fact, relative motions exist between the wheels and rail. For more accurate evaluations or detailed discussions of bridge-train interaction problems, it is desirable to employ the contact model of wheel-track interaction, which is rather complicated and needs proper presumptions.

On the other hand, in the analysis of site vibration around viaducts caused by running trains, it is desirable to model the train, bridge, foundation and ground as an integrated system to perform more accurate estimations. However, this is extremely complicated problem and also need enormous calculation capacities.

For the seismic analysis of the bridge-train interaction system, firstly it is also necessary to model the relative motion between the wheel and track, especially when discussing the derailment phenomenon caused by strong ground motion. In such cases, the contact between the wheels and the track becomes more complicated because derailment is expected to occur. In this research, the derailment coefficient is defined as the ratio of the lateral wheel load to the vertical one. This evaluation is based on the assumption that the relative motion between the wheels and track is small and the vertical wheel loads do not decrease excessively. However, for some cases, the relative motion between the wheel and track is predominant such as subjected to violent earthquake, or the vertical wheel loads are extremely decreased. In such cases, it is difficult to evaluate the train's running safety by derailment coefficient and the wheel-track contact model is necessary. Furthermore, in order to evaluate the seismic performance of the bridge and the running safety of the trains, it is necessary to carry out non-linear dynamic analysis of the interaction system, which includes not only the nonlinearity of the structures but also the trains.

Supplement

In this dissertation, a considerable number of references cited are written in Japanese. Some of the Japanese references have no exact corresponding titles in English, such as some book titles and some old literatures. Thus it may be difficult for readers to identify and search for a particular reference. For this reason, the exact titles of the Japanese references are listed here as follows, corresponding to each chapter.

Chapter 1

[1] 土木学会：2001 年制定コンクリート標準示方書（維持管理編），丸善株式会社，東京，2001.01.

[2] 鉄道総合技術研究所：鉄道構造物等設計標準・同解説（コンクリート構造物），丸善株式会社，東京，2004.04.

[3] 鉄道総合技術研究所 : 鉄道構造物等設計標準・同解説（変位制限），丸善株式会社，東京，2006.02.

[5] 環境庁長官：環境保全上緊急を要する新幹線鉄道振動対策について（勧告），1976.3.

[7] 吉岡　修 : 新幹線鉄道振動の発生・伝搬モデルとその防振対策法への応用，鉄道総研報告，特別第 30 号，1999.10.

[8] 鉄道総合技術研究所 : 鉄道構造物等設計標準・同解説（耐震設計），丸善株式会社，東京，1999.10.

[36] 松浦章夫 : 高速鉄道における橋桁の動的挙動に関する研究, 鉄道技術研究報告, No.1047, 1978. 3

[37] 松浦章夫 : 高速鉄道における橋桁の動的挙動に関する研究, 土木学会論文報告集, No. 256, 1978. 12

[38] 湧井　一 : 新幹線車両の走行性からみた長大吊橋の折れ角限度，鉄道技術研究報告，No. 1087, 1978. 7.

[39] 松浦章夫，湧井　一：鉄道車両の走行性からみた長大吊橋の折れ角限度，土木学会論文報告集，No. 291，1979. 11

[40] 涌井　一，松本信之，田辺　誠：鉄道車両と構造物の動的相互作用解析法に関する研究―力学モデルと実用解析法―，土木学会論文集，No.513/I-31，pp. 129-138，1995.4.

[41] 涌井　一，松本信之，松浦章夫，田辺　誠：鉄道車両と線路構造物の連成応答解析法に関する研究，土木学会論文集，No.513/I-31，pp. 129-138，1995.4.

[46] 川谷充郎，西山誠治：路面凹凸を考慮した道路橋の走行車両による動的応答特性，構造工学論文集，Vol.39A, pp. 733-740, 1993.3.

[47] 川谷充郎，山田靖則，嶽下裕一：三次元車両モデルによる桁橋の動的応答解析，土木学会論文集，No. 584/I-42, pp. 79-86, 1998.1.

[50] 川谷充郎・何興文・曽布川竜・関雅樹・西山誠治：高速鉄道高架橋の列車走行時の振動による地盤反力，土木学会関西支部年次学術講演会講演概要，I-50, 2003.5, 摂南大学.

[51] 川谷充郎・何興文・曽布川竜・関雅樹・西山誠治：高速鉄道高架橋の列車走行時の地盤反力および解析の効率化，土木学会 58 回年次学術講演会講演概要集，I-748，2003.9，徳島大学.

[54] 川谷充郎・何　興文・白神　亮・関　雅樹・西山誠治・吉田幸司：高速鉄道高架橋の列車走行時の振動解析，土木学会論文集Ａ Vol. 62, No. 3, pp.509-519, 2006, 07.

[61] 原　恒雄，吉岡　修，神田　仁，舟橋秀麿，根岸　裕，藤野陽三，吉田一博：新幹線走行に伴う沿線地盤振動低減のための高架橋補強工の開発, 土木学会論文集, No.766/I-68, pp. 325-338，2004.7.

[62] 吉田幸司，関　雅樹：RC ラーメン高架橋の柱剛性向上による鉄道振動への影響，構造工学論文集，Vol. 50A, pp. 403-412, 2004.3.

[63] 川谷充郎・何興文・曽布川竜・関雅樹・西山誠治・笹川剛：列車走行時の高速鉄道高架橋周辺地盤振動解析，土木学会関西支部年次学術講演会講演概要，I-73, 2004.5，立命館大学.

[64] 川谷充郎・何興文・曽布川竜・関　雅樹・西山誠治・笹川剛：高速鉄道高架橋の列車走行による周辺地盤振動評価，土木学会 59 回年次学術講演会講演概要集，I-431，2004.9，愛知工業大学.

[65] 川谷充郎・何興文・吉田幸司・曽布川竜・西山誠治・山口将：高速鉄道高架橋周辺の重軌条化による地盤振動低減対策, 土木学会関西支部年次学術講演会講演概要, I-35, 2005.5, 大阪工業大学.

[66] 川谷充郎・吉田幸司・何興文・曽布川竜・山口将：高速鉄道高架橋の張出部補強による周辺地盤振動低減の解析評価, 土木学会 60 回年次学術講演会講演概要集, I-562, 2005.9, 早稲田大学.

[67] 川谷充郎・何興文・吉田幸司・山口将・西山誠治：鉄道高架橋の列車走行時周辺地盤振動解析による健全度把握，土木学会関西支部年次学術講演会講演概要，I-65, 2006.6，神戸大学.

[75] 宮本 岳史・曽我部 正道・下村 隆行・西山 幸夫・松本 信之・松尾 雅樹：実台車加振実験による大変位車両運動シミュレーションの検証，鉄道総研報告，Vol. 17, No. 9, pp. 39-44, 2004.

[77] 川谷充郎・何興文・西山誠治・吉田幸司・山口将：高速鉄道高架橋－走行列車連成系の地震応答解析，土木学会 61 回年次学術講演会講演概要集，I-502，2006.9，立命館大学.

Chapter 2

[1] 川谷充郎・何　興文・白神　亮・関　雅樹・西山誠治・吉田幸司：高速鉄道高架橋の列車走行時の振動解析，土木学会論文集Ａ Vol. 62, No. 3, pp.509-519, 2006, 07.

[4] 鷲津久一郎・宮本博・山田嘉昭・山本善之・川井忠彦: “有限要素法ハンドブック・I 基礎編,” 培風館，1981.

[5] 鷲津久一郎・宮本博・山田嘉昭・山本善之・川井忠彦: “有限要素法ハンドブック・Ⅱ 応用編,” 培風館，1981.

[15] 戸川隼人：有限要素法による振動解析，サイエンス社，1975.

[18] 丸山弘志，深澤義朗：土木技術者のための鉄道工学，丸善株式会社，1981.11.

[19] 丸山弘志，景山允男：機械技術者のための鉄道工学，丸善株式会社，1981.11.

[20] 日本機械学会編:鉄道車両のダイナミクスー最新の台車テクノロジーー, 電気車研究会, 1994.12.

[21] 江島　淳：地盤振動と対策, pp. 146-154,吉井書店，1979.6.

[22] 吉岡　修：新幹線鉄道振動の発生・伝搬モデルとその防振対策法への応用，鉄道総研報告，特別第 30 号，1999.10.

[23] 川谷充郎，山田靖則，嶽下裕一：三次元車両モデルによる桁橋の動的応答解析，土木学会論文集，No.584/I-42, pp. 79-86, 1998.1.

[25] 涌井　一，松本信之，松浦章夫，田辺　誠：鉄道車両と線路構造物の連成応答解析法に関する研究，土木学会論文集，No.513/I-31，pp. 129-138，1995.4.

[26] 庄司朋宏，伊藤裕一，関　雅樹：高速列車の輪重分布と鋼桁部材の発生応力分布における研究，土木学会 59 回年次学術講演会講演概要集，I-078，2004.9.

[49] 土木学会：阪神淡路大震災の被害分析に基づくコンクリート構造物の耐震性能照査方法の検証―解析手法の適用と比較―，コンクリート技術シリーズ No. 49，2002.12.

Chapter 3

[1] 川谷充郎・何興文・曽布川竜・関雅樹・西山誠治：高速鉄道高架橋の列車走行時の振動による地盤反力，土木学会関西支部年次学術講演会講演概要，I-50, 2003.5, 摂南大学.

[2] 川谷充郎・何興文・曽布川竜・関雅樹・西山誠治：高速鉄道高架橋の列車走行時の地盤反力および解析の効率化, 土木学会 58 回年次学術講演会講演概要集, I-748, 2003.9, 徳島大学.

[5] 川谷充郎・何　興文・白神　亮・関　雅樹・西山誠治・吉田幸司：高速鉄道高架橋の列車走行時の振動解析，土木学会論文集Ａ Vol. 62, No. 3, pp.509-519, 2006, 07.

[6] 吉田幸司，関　雅樹：RC ラーメン高架橋の柱剛性向上による鉄道振動への影響，構造工学論文集，Vol. 50A, pp. 403-412, 2004.3.

[7] 鉄道総合技術研究所 : 鉄道構造物等設計標準・同解説（耐震設計），丸善株式会社，東京，1999.10.
[8] 小堀為雄，久保雅邦 : 弾性節点・弾性支点を有する連続桁橋の汎用的な動的解析法，土木学会論文集，No. 356/I-3，pp. 395-403，1985.4.
[9] 鉄道総合技術研究所 : 鉄道構造物等設計標準・同解説（基礎構造物・抗土圧構造物），丸善株式会社，東京，1997.
[11] 鬼頭　誠，西村昭彦 : 高架橋の振動試験，構造物設計資料，No. 35，pp. 33-36，1973. 9.
[11] 西村昭彦 : ラーメン高架橋の健全度評価手法の研究，鉄道総研報告，Vol.3，No.9，1990.9.
[13] 原　恒雄，吉岡　修，神田　仁，舟橋秀麿，根岸　裕，藤野陽三，吉田一博 : 新幹線走行に伴う沿線地盤振動低減のための高架橋補強工の開発，土木学会論文集，No.766/I-68，pp. 325-338，2004.7.

Chapter 4

[8] 吉岡　修 : 新幹線鉄道振動の発生・伝搬モデルとその防振対策法への応用，鉄道総研報告，特別第 30 号，1999.10.
[9] 原　恒雄，吉岡　修，神田　仁，舟橋秀麿，根岸　裕，藤野陽三，吉田一博 : 新幹線走行に伴う沿線地盤振動低減のための高架橋補強工の開発，土木学会論文集，No.766/I-68，pp. 325-338，2004.7.
[10] 吉田幸司，関　雅樹 : RC ラーメン高架橋の柱剛性向上による鉄道振動への影響，構造工学論文集，Vol. 50A, pp. 403-412, 2004.3.
[11] 川谷充郎・何興文・曽布川竜・関雅樹・西山誠治・笹川剛 : 列車走行時の高速鉄道高架橋周辺地盤振動解析，土木学会関西支部年次学術講演会講演概要，I-73, 2004.5, 立命館大学.
[12] 川谷充郎・何興文・曽布川竜・関　雅樹・西山誠治・笹川剛 : 高速鉄道高架橋の列車走行による周辺地盤振動評価，土木学会 59 回年次学術講演会講演概要集，I-431，2004.9, 愛知工業大学.
[13] 川谷充郎・何興文・吉田幸司・曽布川竜・西山誠治・山口将 : 高速鉄道高架橋周辺の重軌条化による地盤振動低減対策，土木学会関西支部年次学術講演会講演概要，I-35, 2005.5, 大阪工業大学.
[14] 川谷充郎・吉田幸司・何興文・曽布川竜・山口将 : 高速鉄道高架橋の張出部補強による周辺地盤振動低減の解析評価，土木学会 60 回年次学術講演会講演概要集，I-562，2005.9, 早稲田大学.
[15] 川谷充郎・何興文・吉田幸司・山口将・西山誠治 : 鉄道高架橋の列車走行時周辺地盤振動解析による健全度把握，土木学会関西支部年次学術講演会講演概要，I-65, 2006.6, 神戸大学.

Chapter 5

[2] 川谷充郎・何興文・西山誠治・吉田幸司・山口将：高速鉄道高架橋－走行列車連成系の地震応答解析，土木学会 61 回年次学術講演会講演概要集，I-502，2006.9，立命館大学.

[3] 土木学会 : 2002 年制定コンクリート標準示方書（耐震性能照査編），丸善株式会社，東京，2002.12.

[5] 鉄道総合技術研究所 : 鉄道構造物等設計標準・同解説（耐震設計），丸善株式会社，東京，1999.10.

[6] 鉄道総合技術研究所：鉄道構造物等設計標準・同解説（コンクリート構造物），丸善株式会社，東京，2004.04.

[7] 脱線に対する安全基準，鉄道技術研究報告，No. 914, 1968.11.

[8] 丸山弘志，深澤義朗：土木技術者のための鉄道工学，丸善株式会社，1981.11.

[9] 丸山弘志，景山允男：機械技術者のための鉄道工学，丸善株式会社，1981.11.

[10] 石田弘明，手塚和彦，植木健司，深沢香敏，松尾雅樹：脱線に対する安全性評価指標の研究，鉄道総研報告，Vol.9, No.8, pp.49-54, 1995.8.

[11] 中村豊 : 研究展望 : 総合地震防災システムの研究，土木学会論文集，No. 531/I-34, pp. 1-33, 1996.1.

[12] 中村豊：早期検知と脱線，地震工学研究発表会（報告），pp. 1-11, 2005.8.23.

Acknowledgments

This dissertation is the results of the past five years' work during my tenure as a master's and then a doctoral course student at the Kobe University. This work would never have been possible if it were not for the supports of many people. With this opportunity I would like to express my grateful acknowledgements to all of them.

First of all, I wish to express my full gratitude for the gentle but firm direction, eager support and kind encouragement provided by Professor Mitsuo Kawatani, my long-time advisor and committee chair. Professor Kawatani gave the author the opportunity to be involved in the research of structural dynamics. It is impossible to accomplish this work without his considerable mentoring.

I express special thanks to the members of my dissertation committee: Professor Shiro Takada, Professor Hidenori Morikawa, and Professor Koichi Osuka of Kobe University. Their support, patience and valuable advice are greatly appreciated. With their penetrating suggestions, I have been able to improve this dissertation remarkably.

I am also much indebted to Dr. Chul Woo Kim who has been giving precious help in my research life, especially from the point when I knew little about the professional knowledge.

The sincere thanks are due to the members of my research group, especially Dr. Seiji Nishiyama of Nikken Sekkei Civil Engineering, Ltd., Dr. Koji Yoshida and Dr. Seki Masaki of Central Japan Railway Company, and Mr. Ryo Shiraga of East Japan Railway Company, who have provided a great deal of useful advice and enriched my knowledge with their experiences. Mr. Ryo Sobukawa, Mr. Sho Yamaguchi, and Mr. Kohei Shinagawa et al have carried out the actual numerical analyses together with the author and achieved a remarkable work.

Special thanks go to Dr. Yasutoshi Nomura, assistant professor of the laboratory, who has enriched the author with the knowledge in different research field and has been a good friend. I would also like to give my thanks to Dr. Naoki Kawada of Asia Civil Engineering Co. Ltd. for his kind advice in the process of this work.

I would also like to express my sincere appreciation to all the members, present ones or alumni, of the Kawatani's Laboratory of Kobe University for their support and friendship.

I dedicate this thesis to my beloved family: my grandmother in heaven, my parents, my sisters, and my fiancée. Without their patience, understanding, support, and most of all love, the completion of this work would not have been possible.

Kobe, Japan, January 12, 2007

Xingwen HE